University of Bath

PHD

Photocrystallography

Savarese, Teresa

Award date:
2008

Awarding institution:
University of Bath

Link to publication

Alternative formats
If you require this document in an alternative format, please contact:
openaccess@bath.ac.uk

Copyright of this thesis rests with the author. Access is subject to the above licence, if given. If no licence is specified above, original content in this thesis is licensed under the terms of the Creative Commons Attribution-NonCommercial 4.0 International (CC BY-NC-ND 4.0) Licence (https://creativecommons.org/licenses/by-nc-nd/4.0/). Any third-party copyright material present remains the property of its respective owner(s) and is licensed under its existing terms.

Take down policy
If you consider content within Bath's Research Portal to be in breach of UK law, please contact: openaccess@bath.ac.uk with the details. Your claim will be investigated and, where appropriate, the item will be removed from public view as soon as possible.

Download date: 05. May. 2023

Photocrystallography

Submitted by Teresa Louise Savarese

for the degree of Doctor of Philosophy

University of Bath

Department of Chemistry

September 2008

Copyright

Attention is drawn to the fact that copyright of this thesis rests with its author. This copy of the thesis has been supplied on condition that anyone who consults it is understood to recognise that its copyright rests with its author and that no quotation from the thesis and no information derived from it may be published without the prior written consent of the author.

This thesis may be made available for consultation within the University Library and may be photocopied or lent to other libraries for the purposes of consultation.

Acknowledgements

Firstly I would like to start off by thanking my supervisors whose continued support and advice has been invaluable. Thanks to Prof. Paul Raithby for introducing me into the world of insomnia at Daresbury. If it wasn't for Paul's jokes (that most of the time only I seem to find funny) I think that the days spent on beam time would have gone much slower. Thanks also go to Dr. John Warren whose clever inventions and numerous ideas helped improve a number of the results obtained in this thesis. I am extremely grateful to you both.

I would also like to thank the members of both the Raithby and Johnson groups past and present who have helped me enormously. The tea breaks were always greatly received and I extremely value your continued support and friendship. I would particularly like to thank those who have joined me on many hours spent together on Station 9.8 on mammoth Daresbury trips.

The work carried out on this thesis would not have been possible without funding so I would like to express my gratitude to the STFC and States of Jersey for funding.

Finally to Mum, Dad, Fran and John who have been there for me through the highs and lows - hopefully I haven't caused too much stress! Your encouragement and support has helped to get me where I am now and I am extremely grateful. I love you all!

Teresa

-x-

Abstract

Photocrystallography is a relatively new and continuously developing technique used in the structure determination of metastable and transient species in the crystalline state. This thesis contains a description of investigations into photo-induced linkage isomerism reactions in the solid state with the use of single crystal and powder X-ray diffraction experiments to monitor structural changes at low temperature.

Chapter 1 provides a brief introduction to the concept of molecular electronics. A few examples of molecular switches are given before focusing on linkage isomerism as a potential switching property. Several successful photocrystallographic experiments on metal complexes that contain ambidentate ligands are described and the scene is set for the new research that is reported in this thesis.

Chapter 2 provides an introduction to some of the main principles of X-ray diffraction theory, as well as describing the experimental crystallographic techniques used in this thesis.

Chapter 3 is focused on the linkage isomerism of the sulphur dioxide ligand in two ruthenium complexes. The results of powder diffraction experiments and DFT calculations are described and compared to results obtained from single crystal diffraction experiments that have been reported previously.

Chapter 4 is concerned with the linkage isomerism of the nitrogen dioxide ligand. The results obtained from single crystal X-ray photocrystallography experiments on three related nickel compounds are discussed. Photocrystallographic temperature variation studies were performed and Slant Plane Fourier maps were generated to identify the temperature limitations of any metastable species obtained. An analysis of the bonding interactions is carried out and the packing of the molecules within the crystal lattice is discussed in relation to the isomeric conversion.

Chapter 5 contains a description of the use of crystal engineering to reduce the risk of crystal shattering during single crystal X-ray photocrystallographic experiments. Counterion exchange has been carried out on a number of compounds shown to exhibit photo-induced linkage isomerism and the structural results are reported.

Chapter 6 describes the experimental techniques and synthetic procedures used to provide the compounds discussed in the previous chapters.

The appendix contains crystallographic information obtained from the experiments presented in Chapters 3, 4 and 5 as well as details of the publication that has so far arisen from the work contained in this thesis.

Table of Contents

Chapter 2: Crystallographic Techniques and Methods

Chapter 3: Crystallographic Techniques and Methods

Abbreviations

Abbreviation	Definition
α	Alpha
Å	Ångstrom
ca.	Approximately
asu	Asymmetric unit
β	Beta
bipy	2,2’-bipyridine
I	Body centred
C	C centred
cm	Centimetre
cf.	Compare
conc.	Concentrated
CW	Continuous wave
°	Degrees
DFT	Density Functional Theory
DSC	Differential scanning calorimetry
OSSO	Dimethylbis(methylsulfinylmethyl)silane
DMSO	Dimethyl sulfoxide
eV	Electron volts
EXAFS	Extended X-ray absorption fine-structure spectroscopy
F	Face centred
γ	Gamma
HOMO	Highest occupied molecular orbital
h	Hour
Hbs	4-hydroxybenzene sulphonate
IR	Infrared
K	Kelvin

Abbreviation	Definition
τ	Lifetime
LED	Light emitting diode
LUMO	Lowest unoccupied molecular orbital
MLCT	Metal to ligand charge transfer
µs	Microsecond
hkl	Miller Indices (*hkl*)
ml	Millilitre
mm	Millimetre
ms	Millisecond
min	Minute
M_r	Molecular mass
Mol	Moles
nm	Nanometre
ns	Nanosecond
NMR	Nuclear Magnetic Resonance
PET	Photo-induced electron transfer
pm	Picometre
ps	Picosecond
h	Planck Constant
pmma	Poly(methyl methacrylate)
P	Primitive
py	Pyridine
R_1	*R*-factor
σ	Sigma
snp	Sodium nitroprusside
f_j	Structure factor
terpy	2,2':6',2-terpyridine

Abbreviation	Definition
i.e.	That is
θ	Theta
3D	Three dimensional
TRIR	Time-resolved infrared
Tos	Tosylate - ($C_7H_7SO_3$)
TEM	Transmission Electron Microscopy
2D	Two dimensional
UV	Ultraviolet
vis	Visible
V	Volume
λ	Wavelength
ν	Wavenumber
w*R*2	Weighted *R*-factor
XAS	X-ray absorption spectroscopy
YAG	Yttrium Aluminium Garnet

List of Tables and Figures

Chapter 1

Chapter 2

Chapter 3

Chapter 4

Chapter 5

Chapter 1

The Photocrystallography of Linkage Isomers - Materials for Molecular Switches in Molecular Materials

1.1 Introduction

1.1.1 Molecular Electronics

Over the past few decades the driving force behind modern electronic design is the miniaturisation of circuit components used within the information technology industry, with particular emphasis on data storage materials. However, these devices are facing very fundamental physical, chemical and materials limitations in terms of operation speed, density and sensitivity.[1] Methods are continually being developed in order to reduce the physical space required to store large amounts of data.

Traditionally a 'top down' approach has been employed to reduce the size of electronic components; however this process will eventually reach a physical limit.[2] Molecular electronics on the other hand, proposes an alternative - the 'bottom up' approach. This method starts with the smallest components of matter which have distinct shapes and unique properties - molecules, and builds them upwards.[3]

The use of a single molecule as a functional electronic device was first suggested in 1974.[4] Recent interest in the 'bottom up' approach has been focused on electronic computers integrated on the molecular scale.[5] Molecules have the potential to act as wires or switches and are approximately a million times smaller than components currently used on a conventional silicon microchip. The ability of molecules to act in this way allows the assembly of small computer logic circuits built from molecular-scale devices. Eventually in 2001, the assembly and demonstration of small computer logic circuits built from molecular-scale devices was achieved.[5] This is the ultimate goal in the quest for miniaturisation as a single molecule is the smallest conceivable entity that could have the required complexity.[6]

The simplest component of an electrical circuit is a wire. Molecular wires (figure 1.1[7]) consist of long, highly conjugated molecules with delocalised networks of π-orbitals providing a route electrons can travel along. Much research into the ability of molecules to behave as wires, has been conducted;[2] however the main focus of the work in this thesis looks at their ability to act as molecular switches.

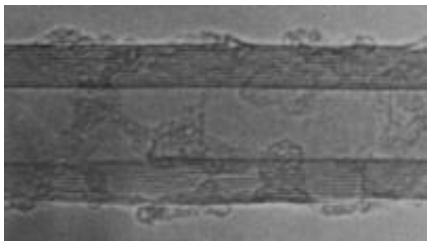

Figure 1.1 TEM of a carbon nano-tube capable of behaving as a molecular wire

1.1.2 Molecular Switches

This section gives a brief introduction to molecular switches with a few relevant examples. There are now thousands of papers on the subject and a comprehensive review is beyond the scope of this thesis. The term ‘molecular switch’ is a fairly general term used to describe any molecule which has a property that can be converted between two different states via the application of an external stimulus, i.e. the molecule has an ‘ON’ and ‘OFF’ state. In the ‘ON’ position the switch must perform some type of function or allow another device to perform its application. When ‘OFF’ the switch must totally hinder this function. Important properties for a molecular switch include that it must not spontaneously change between ‘ON’/’OFF’ states unless it has been activated to do so, that the switching phenomenon is almost instantaneous and fully reversible and that the switching process is repeatable many times.[8]

Many molecular attributes are amenable to switching, for example the structural, electronic and magnetic properties of a molecule. There are also a large number of external stimuli that can be used to induce the switching process. Examples of these include changes in pH, difference in temperature, application of an electric current and also the absorption of light. As a consequence, a large number of molecules can be classed as switches in some way or form.[2]

The example in figure 1.2 shows a molecular electronic catenane switch.[9] The switch closes when the linked molecular ring containing a tetrathiafulvalene unit, rotates as an oxidising potential is applied to the system. The switch can be subsequently re-opened by application of a reducing potential returning the ring to its original position.

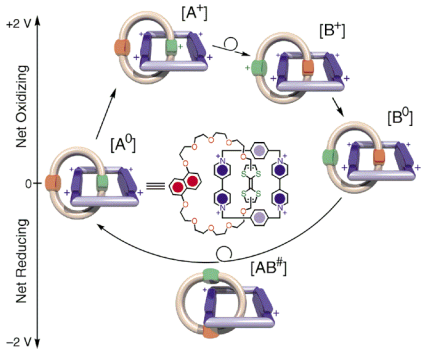

Figure 1.2 A catenane molecular switch[9]

Another class of molecules which can pose as molecular switches is rotaxanes. The first molecular shuttle was devised in 1991. A rotaxane with a tetracationic ring (cyclophane) demonstrated it was capable of moving back and forth between identical stations (two hydroquinol units). These units were grafted symmetrically into a polyether thread, terminated at the ends by large triisopropylsilyl groups. The bulky terminal groups act as stoppers to prevent the cyclophane rings falling off the chain. The shuttling process was confirmed by the use of NMR spectroscopy.[10]

The example shown in figure 1.3 has two potential docking stations for an electron donor macrocycle (bis-*para*-phenylene[34]crown10). The first is a strong primary π-electron acceptor (4,4'-bipyridinium) and the second a weak secondary π-electron acceptor (3,3'-dimethyl-4,4'bipyridinium). The switch can be activated via two mechanisms. The first mechanism involves photosensitisation of the $Ru(bipy)^{2+}$ complex using light of 532nm generating a MLCT excited state. This excited species undergoes PET reducing it to a radical cation, repelling the macrocycle and switching it to the other docking station. The process can be reversed by the oxidation of the radical cation. The second switching mechanism involves the use of a dual-action redox reagent which directly oxidises the photosensitiser unit allowing the macrocycle enough time to flip when the 4,4'-bipyridinium unit is reduced. Electronic recombination regenerates the 4,4'-bipyridinium di-cation, and completes the switching cycle.[11]

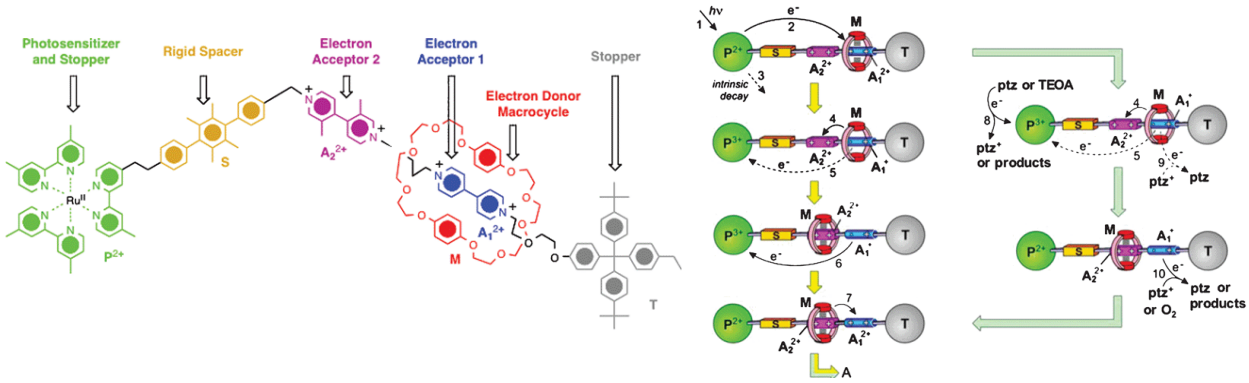

Figure 1.3 A rotaxane molecule with the potential to act as a molecular switch

A photo-activated switch can be seen below in figure 1.4. The molecule can be reversibly photo-isomerised to give a closed form - 'ON' using UV light of 365nm, or an open - 'OFF' state using light with a wavelength greater than 500nm, (visible light) where the conjugation of the system is broken. Upon irradiation the single crystal of 1,2-bis(2-ethyl-5-phenyl-3thienyl)perfluorocyclopentene not only changes colour from colourless to blue, but also undergoes a macroscopic deformation where the almost square crystal with angles of 88° and 92° changes to a more lozenge shape with angles of 82° and 98°.[12]

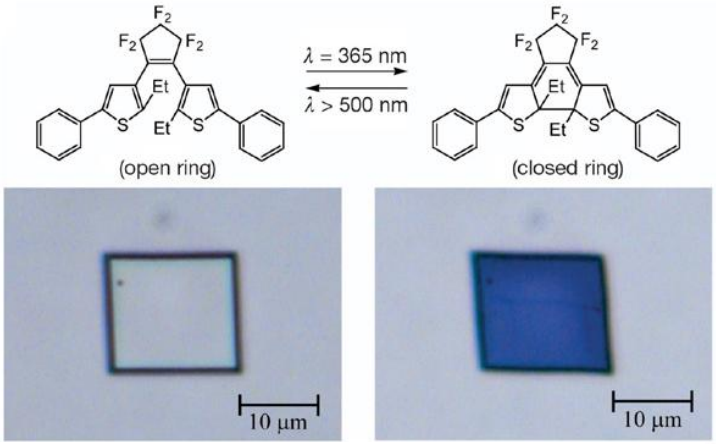

Figure 1.4 Photoinduced molecular switch

In recent years, interest has been shown in the use of linkage isomerism as a potential switching property and has been focused on photo-excitation of ambidentate ligands within metal complexes. The ground state isomer can act as one part of the switch, while the excited photo-isomer acts as the other. The switching between these two different states could be used as the basis of an information storage system, as information can be written and erased reversibly using light of two different wavelengths. The following sections detail the principles behind photocrystallography and excited state chemistry as well as examples of linkage isomers with the potential to act as switches.

1.2 Excited State Chemistry

1.2.1 Photocrystallography and Metastable States

A photo-induced compound is one formed by irradiation with light. Photo-induced species can occur in a number of environments such as chlorophyll in nature, through to technologically important materials such as LEDs.[13] Previously, identification of new photoactive species was carried out by DSC, UV absorption and emission as well as IR spectroscopy by investigating light-induced vibrational changes. Some of these methods are described at the end of this chapter. The term 'photocrystallography' is used to describe the field in which the techniques of crystallography and photochemistry are combined in single experiments to monitor the formation of light-induced metastable and transient species.[14] Photocrystallography is a relatively new, continuously developing method of characterisation in the identification of new photo-induced compounds and is discussed further in Chapter 2.

A species can be described as metastable if it exists without observable change even though it is thermodynamically unstable with respect to another state.[15] Metastable species generally have a longer lifetime than an ordinary excited state and usually a shorter lifetime than the lowest energy state, known as the ground state. Therefore a metastable state can be considered as a temporary energy trap or a fairly stable intermediate.

1.2.2 Photochemistry

Chemical reactions generally proceed via a transition state. Conventionally thermal energy is required to excite reactants to this intermediate state. The bond breaking and reorientation of atoms associated with reactions arise mainly as the result of thermal excitation of vibrational stretching and bending modes.[16]

In photochemistry the absorption of light can result in the production of an electronically excited species that exhibits different chemistry than the parent ground state. Electronic excitation of a molecule results in a redistribution of electrons from bonding HOMO orbitals to anti-bonding LUMO orbitals when

using a specific wavelength of light with the required energy.[16] These excited compounds are thermodynamically unstable and there are a number of ways in which an excited species can react or otherwise lose its excess energy. A few examples are dissociation, luminescence, charge transfer and isomerisation. The decay process adopted by the electronically excited species determines the lifetime of the excited state.[16, 17]

The stability of an electronically excited state is affected by its electronic configuration and several states are possible depending on the alignment of electron spin. A term symbol is used to describe its configuration and is defined as:

$$\text{Term symbol} = {}^{2S+1}L_J$$

S is the total spin angular momentum quantum number, and is obtained by the sum of the individual spin angular momentum quantum numbers. In a two electron system the electrons can align in one of two ways. If the electrons align anti-parallel to each other (↑↓) this results in a spin multiplicity of 2(½ - ½) + 1 = 1 which is a singlet state. If electron spins lie parallel (↑↑) the spin multiplicity then becomes 2(½ + ½) + 1 = 3 and forms a triplet state. S is the greatest contributor to the stability of the excited state species. L is the total orbital angular momentum quantum number and determines the total angular momentum of an electron about the nucleus. It is calculated by identifying the orbital angular momentum quantum numbers of electrons in the valence shell. Finally J is the total angular quantum number and is the sum of the orbit angular momentum (L) and the spin angular momentum (S).[18]

A spin selection rule determines if a transition is allowed or forbidden. The spin selection rule for molecular transitions is $\Delta S = 0$. This selection rule states that transitions are only allowed between states of the same multiplicity. Therefore transitions from S_0 to S_1 and T_1 to T_2 are spin allowed but transitions from S_0 to T_1 are spin forbidden. This has important consequences for the lifetimes of excited state species.[16]

The Jablonski diagram (figure 1.5) summarises various routes of decay for an electronically excited state. Firstly there are emissive processes such as fluorescence or phosphorescence. Fluorescence occurs as a result of decay from a singlet excited state by emission of a photon from the S_1 to S_0 singlet state. This process is spin allowed and singlet lifetimes of these excited molecules are very short due to fast vibrational relaxation. Phosphorescence is the decay of T_1 to S_0 by photon emission and is a spin forbidden process, resulting in triplet lifetimes being substantially longer than for a singlet species.[16] Absorption of radiation from a singlet to triplet transition is weak since it is also a spin forbidden process. Therefore excitation of phosphorescence by direct absorption of a photon is inefficient and is usually the

product of a triplet populated by intersystem crossing from an excited singlet state formed on absorption (figure 1.5).This process conserves the total electronic and vibrational energy during the transition. Since the T_1 state generally lies below the S_1 state (as triplet states have lower energies than singlet states) the transition corresponds to one from the ground vibrational state of S_1 to a higher vibrational state of T_1. Vibrational relaxation then occurs in the T_1 state. The other process which can occur is known as internal conversion. The electronic energy of S_1 may be transferred to produce a highly excited S_0 state without changing the total energy. The resulting excited vibrational state of S_0 relaxes rapidly to the Boltzmann distribution and the electronic excitation is lost in the form of heat. Internal conversion is also possible for higher singlet states e.g. from S_2 to S_1.[16, 17]

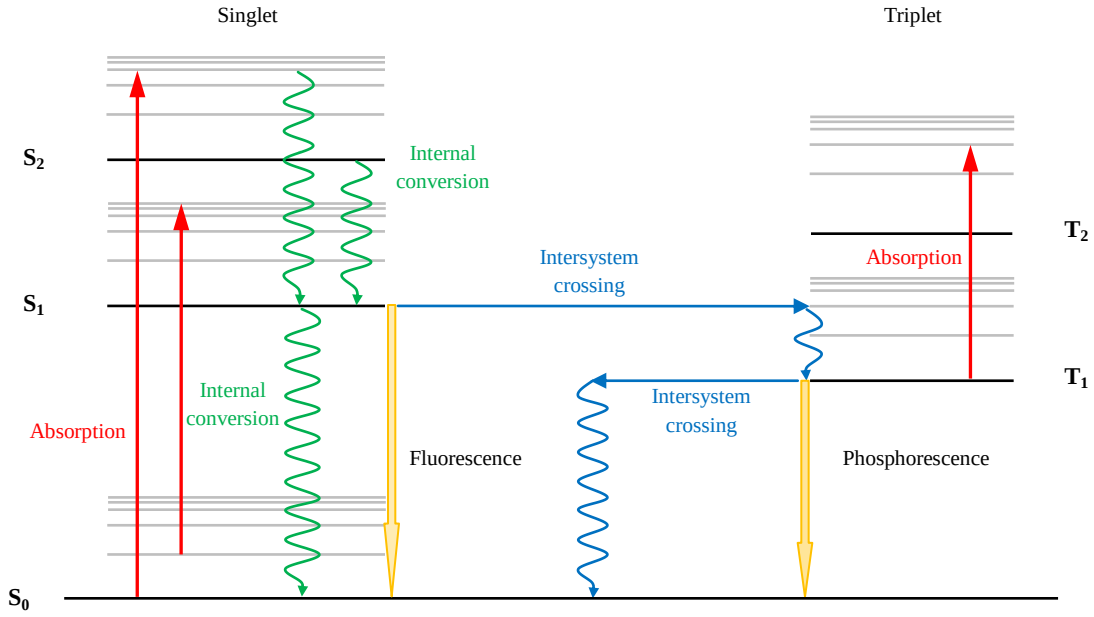

Figure 1.5 Jablonski diagram

This project is mainly concerned with the structural characterisation of the excited states of molecules. It is important that the excited species must exist without spontaneous decay despite being thermodynamically unstable (metastable). As mentioned previously metastable states can be thought of as fairly stable intermediates and considered as a local minimum on an energy level diagram (figure 1.6).

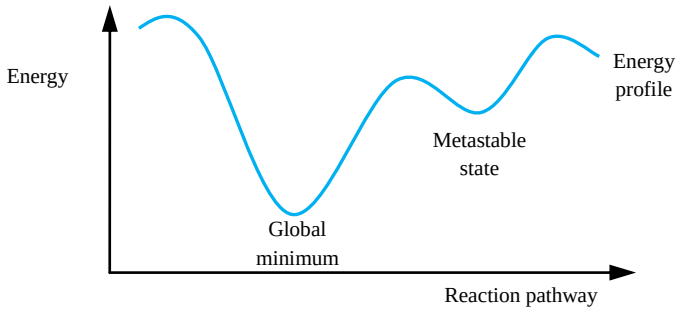

Figure 1.6 Energy level diagram showing position of metastable state

1.3 Excited State Experiments and Time-resolved Techniques

1.3.1 Introduction

Knowledge of the ground state structure of a molecule can help provide information to predict the reaction pathways and energetics for some photochemical reactions. The structures of short lived excited state molecules have remained largely unattainable due to the lack of suitable X-ray sources.[19] Previous approaches to obtain excited state structural information with the use of a synchrotron involved one of three methods:

- The use of gating detectors or chopping an X-ray pulse to obtain the required time resolution, i.e. pump-probe experiments.[20, 21]
- By cryogenically trapping an excited state species at low temperature for long periods of time in order to be examined via steady-state methods.[22, 23]
- Using energy dispersive X-ray absorption. The excited state structure is captured within the detector readout time.[24, 25]

Much early work on excited state molecules has been performed at μs time resolution. This unfortunately excludes many excited states, especially singlet excited states as they have significantly shorter lifetimes.[19] Over the past decade, three pulsed X-ray sources have been developed:

- Third generation synchrotron sources.
- Ultrafast laser-generated-plasma X-ray sources.
- Ultrafast laser-generated high harmonic soft X-rays.

As a result of the development of these pulsed X-rays a new era of time-resolved studies can be carried out.[19] New techniques such as photocrystallography (see Chapter 2) carried out on ps timescales[26] as well as more conventional methods are being constantly evolved to help identify new excited state molecules and metastable linkage isomers. Typically to identify the excited state structure of a molecule several techniques are used in conjunction with each other as different information can be yielded from different experiments. Some of these experimental methods are described briefly below.

1.3.2 XAS

Until the advent of synchrotron radiation, there was a shortage of suitable X-ray sources to undertake X-ray absorption spectroscopy (XAS) experiments. EXAFS is an extremely powerful technique that determines the environment of local structures in almost any mixture, independent of the samples physical state.[27] Chemical information can be obtained on the environment of a single element in a sample with high sensitivity and direct physical structural information can be obtained as in X-ray

diffraction experiments.[28] EXAFS is applied to a variety of very different problems and used more frequently to answer a variety of chemical questions. It is possible to obtain information about the local environments of two components in a binary system as well as monitor structural changes that result from a chemical reaction,[27] but the technique mainly provides information on electronic singlet states.

1.3.3 Mössbauer Spectroscopy

Mössbauer spectroscopy can provide information on the coordination number, chemical state and symmetry of the ligands of atoms with a Mössbauer nucleus. Spectra can be recorded by either transmission or by scattering (fluorescence) and hyperfine interactions in the Mössbauer spectrum have several features which provide information on the state of the atoms. The ionisation state and degree of covalency can be determined from isomer shift as well as the quadrupole splitting. The quadrupole splitting is also sensitive to the symmetry of the ligands surrounding the Mössbauer atom. The *f*-factor (the probability of the Mössbauer effect) determines the strength of atomic interactions, and this combined with the shift can infer the co-ordination number of the Mössbauer atom.[29] This is another very fast technique and is good for identifying linkage isomers (cf section 1.4.1 and work by Rusanov et al.[30-33]).

1.3.4 Time-resolved Vibrational Spectroscopy

Transient Raman and IR spectroscopy are being increasingly applied to molecular assemblies to study excited states formed following photo induced electron or energy transfer. Electronic excitation generally produces transient changes in IR absorption characteristic of the changes in electron density within the complex. The excited state species shifts to higher and/or lower energies which are observed in the vibrational bands (relative to the ground state) on the scale of its lifetime. These shifts can be interpreted in terms of structural or electronic changes that differ markedly from the ground state molecule. Technological advances made in TRIR make it possible to measure transient IR signals following laser excitation on many timescales (figure 1.7) up to a matter of nanoseconds. Limitations of the technique depending on the experimental strategy include source brightness and in some cases that the transient event must be repeated numerous times throughout the duration of the experiment.[34] This technique is generally used for studying singlet states with ps to ns lifetimes.

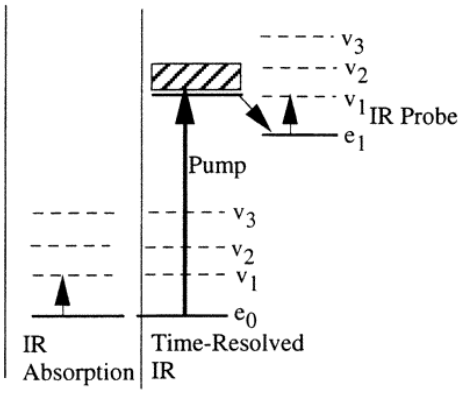

Figure 1.7 Comparison of IR absorption to transient IR absorption

1.4 Linkage Isomerism

Linkage isomers can occur when one or more of the ligands attached to a metal centre are able to coordinate to that centre in more than one way (i.e. the ligand has at least two donor atoms or binding sites available for coordination). These ligands are known as ambidentate.[15] There are many examples of ligands which can undergo linkage isomerism, specifically photo-induced isomerism and some examples are discussed in this section.

1.4.1 NO Linkage Isomers

Metastable isomers of transition-metal nitrosyl complexes first became apparent when light-induced changes were observed in crystals of sodium nitroprusside (snp) dihydrate during a Mössbauer spectroscopy study of iron containing photo-irradiated solids in 1977.[30-32] When snp was used during the experiment, a new low temperature species was observed with features notably different from those of the ground state structure.[21] Two light-induced metastable states were identified resulting from further research using DSC and characterised via photocrystallography (figure 1.8). The experiment concluded that the side bound η^2-NO MS2 isomer decayed at lower temperature than the isonitrosyl η^1-O MS1 isomer.[20]

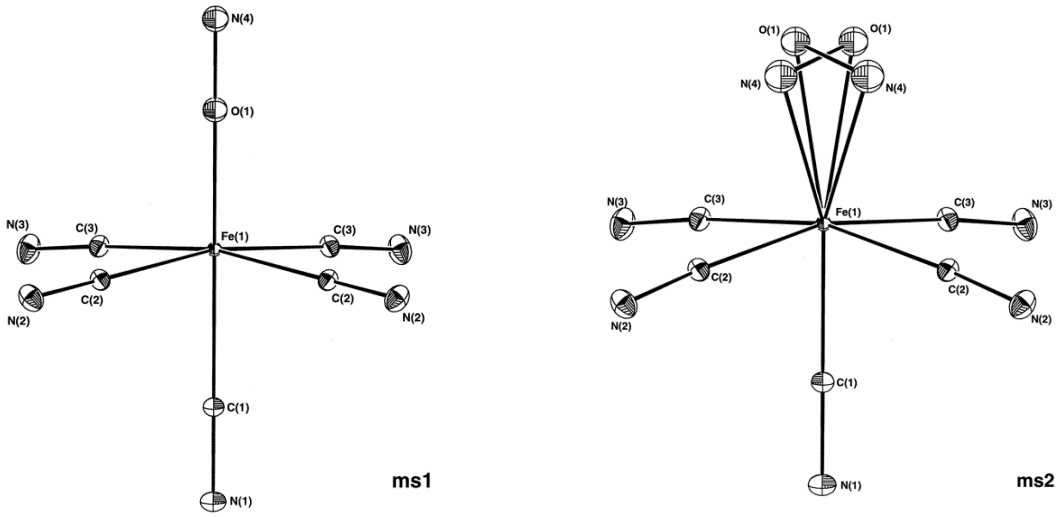

Figure 1.8 ORTEP representations of the MS1 and MS2 snp anion with 50% probability ellipsoids shown

Pressprich et al. provided the first indication that an atomic rearrangement was involved by a photocrystallographic investigation in 1994. Data was collected on a photo-excited crystal of snp and during a charge density refinement, more electrons were identified on the proximal atom than on the far atom of the NO group. This observation was also confirmed by the results of least-squares refinements, producing an anomaly in the atomic displacement parameters. When the N-bound conformation of the ligand was chosen, the terminal atom had mean-squares displacements up to 20 times larger than those of

the bonding atom which indicated an incorrect element assignment had been chosen. Further analysis using photo-difference maps illustrated the presence of MS1 being isonitrosyl (η^1-O) and MS2 side-bound (η^2-NO) both previously unknown for the nitrosyl group.[35] Similar results were obtained in 1996 in an investigation into the linkage isomerism of $K_2[Ru(NO_2)_4(OH)(NO)]$.[36]

In 1996 Carducci and co-workers performed a 50K X-ray diffraction study of the ground state and both metastable states of snp, having obtained suitable crystals from recrystallisation with water. In order to maximise the population of MS1 the sample was first warmed to 165K and irradiated at 488nm by an Ar^+ laser. The sample was kept at this temperature for approximately 5 minutes, before being re-cooled to 50K in order to eliminate the formation of the MS2 component. In order to populate the MS2 state the laser was exchanged for a Nd-YAG laser and irradiated at 1064 nm.[20]

For initial experimentation at 488nm, an increase in all cell axes lengths and therefore an increase in the cell volume was observed when compared to the ground-state species of snp. Changing the wavelength to 1064nm resulted in a noticeable contraction along the cell axis *a*, while the *c*-axis lengthened. When the *a*-axis reaches a minimum, the cell volume of MS2 is actually smaller than for the ground-state structure. The results indicated that not only was the ground state structure in agreement with other previous studies, but that the structure was in fact more accurate due to the lower temperature data collection and greater number of reflections collected during the study. A section of the ground state difference maps for MS1 and MS2 can be seen in figure 1.9.[20]

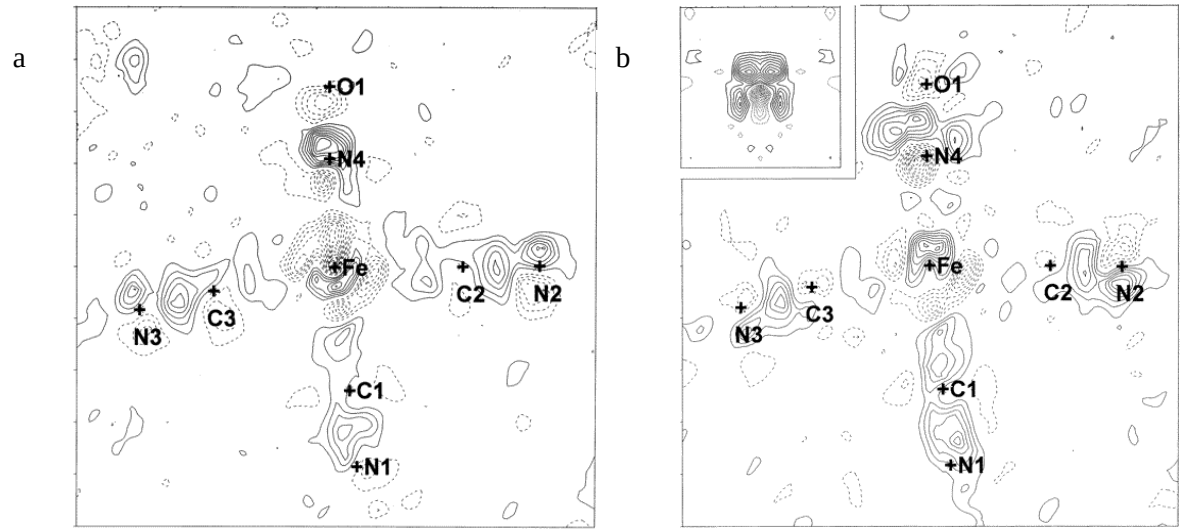

Figure 1.9 (a) ground state difference map of MS1 and (b) ground state difference map of MS2, crosses indicate the atomic positions of the ground state species

The key features in the difference map for MS1, indicate a shift of the Fe atom away from the NO group and bending of the ligands in equatorial positions toward the isonitrosyl group.[20] Previous

experimentation had only identified the M-O isonitrosyl bonding in two cases, both of which involve the NO fragment as a bridging ligand between multiple metal centres.[37] Results from this investigation along with others from a previous charge density study, suggest that the change in charge distribution can be attributed to an inversion of bonding in the NO fragment, and any distortions from tetragonal symmetry are no greater than those found in the ground state.[20]

For the MS2 anion the difference map shows a peak near the Fe atom, located in the direction of the nitrosyl group. There is also a trough in the other direction and peaks above each of the trans cyano ligands, displaced towards the metal centre. These results indicate the formation of a second metastable state where the Fe atom and the trans cyano groups are displaced in the direction toward the nitrosyl. The peaks beneath the equatorial cyano group N atoms suggest that the ligands in equatorial positions bend away from the nitrosyl ligand. The remaining features in the difference map indicate that the nitrosyl ligand is in the side-bound η^2-NO conformation.[20]

Formitchev et al. determined both a ground state and a light induced metastable state of [Ni(NO)(η^5-Cp*)] using X-ray diffraction. The metastable state was populated via irradiation of a suitable crystal at 25K for 3 hours using 458nm light. Upon irradiation a decrease in length of the *b*-axis, along which the nitrosyl ligand is oriented was observed, while the crystallographic *c*-axis lengthened to a lesser extent. The shortening of the *b*-axis was monitored along with changes in reflection intensities to ensure maximum conversion to the metastable state was achieved before commencing data collection. The metastable state observed was the η^2-NO isomer, and the Cp* ring is distorted as a result of the displacement of the metal centre from the symmetric position above the ring. ORTEP representations of the ground and the photo-excited state can be seen in figure 1.10.[38]

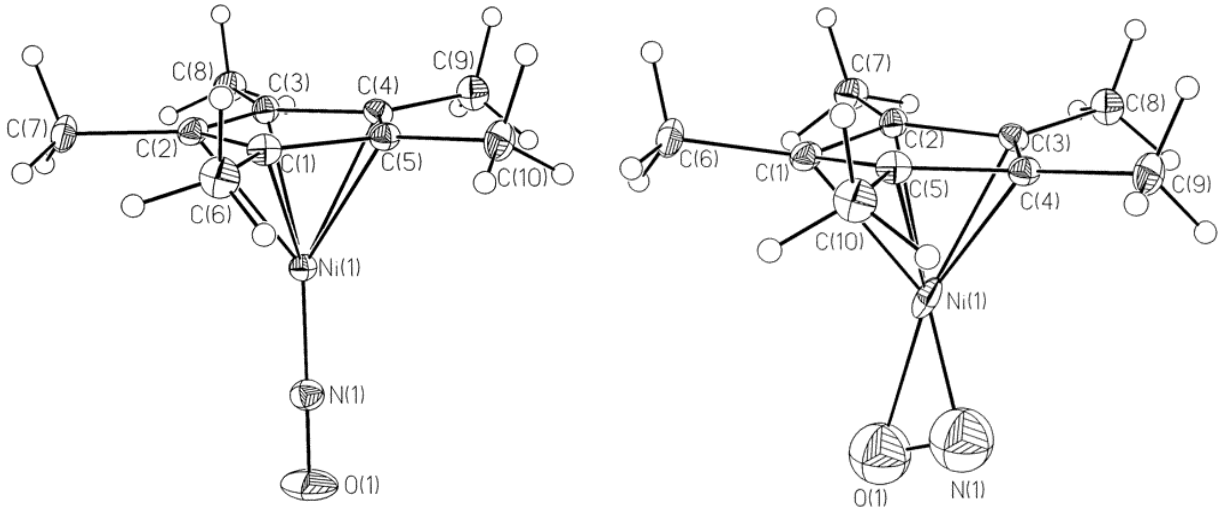

Figure 1.10 ORTEP representations of ground state (left) and light-induced metastable state (right) of [Ni(NO)(η^5-Cp*)] with 50% probability ellipsoids

More recently in 2007 two photo induced linkage isomers of $[RuCl(py)_4(NO)][PF_6]_2.½H_2O$ were identified and characterised using DSC, IR, absorbance spectroscopy and DFT calculations. Irradiation of the complex with light between 450-530nm (blue/green) generated the oxygen bound isonitrosyl isomer. Further irradiation using near infrared light (920-1100nm) resulted in a rearrangement of the isonitrosyl isomer to an η^2-NO side bound isomer at temperatures below 150K. A maximum population of 76% for the isonitrosyl isomer was achieved whereas only 56% could be converted into the η^2-NO form. These percentages were calculated by monitoring the decrease of the *ν*(NO) stretching absorption band in the IR spectrum of the ground state. The experimental observations were confirmed theoretically using DFT and found to be in good general agreement with the results obtained.[39]

1.4.2 NO_2^- Linkage Isomers

Linkage isomerism was first discovered by Alfred Werner during his studies on the metal complex - $[Co(NH_3)_5(NO_2)]Cl_2$.[40] The nitro (NO_2^-) ligand in this complex can coordinate to the cobalt metal centre either via the oxygen atom to form a nitrito complex, or via nitrogen to form a nitro complex. In the case of $[Co(NH_3)_5(NO_2)]^{2+}$ these linkage isomers can be distinguished using IR spectroscopy and also by a difference in colour. The ground state isomer is yellow and is N-bound, which on excitation with light, changes to the red O-bound complex. Further discussion of similarly related complexes can be found in Chapter 4.

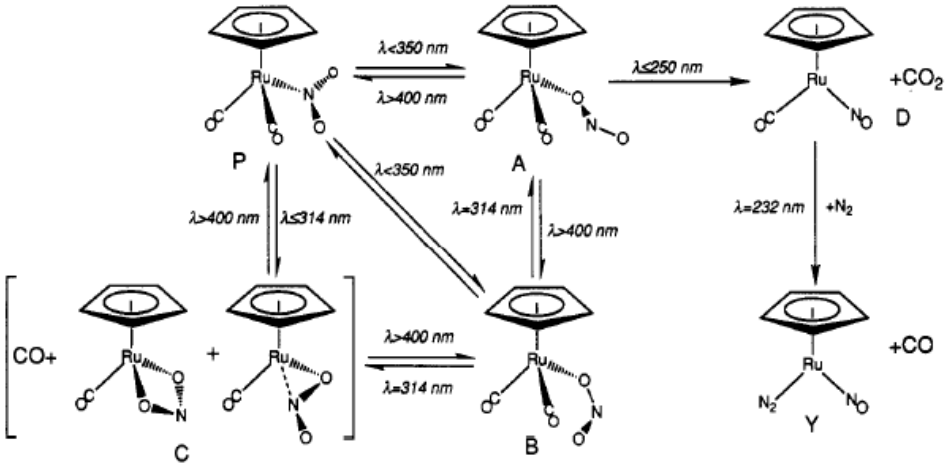

Figure 1.11 Matrix photochemistry of $[CpRu(CO)_2(NO_2)]$

A 13K matrix isolation study combined with FTIR was used to investigate the photochemical reactions of $[CpRu(CO)_2(NO_2)]$. UV photolysis at wavelengths greater than 350nm, was shown to produce two photoproducts A and B, assigned as two different O-bound isomers with the formula $[CpRu(CO)_2(ONO)]$ (one exo-nitrito and the other endo-nitrito, figure 1.11). This reaction was shown to be fully reversible. Photolysis using shorter wavelengths of 314 or 280nm, resulted in the loss of CO to

form compounds C. Despite the low product yield, there are indications that two isomers are formed at this lower wavelength, one where the nitro group is (N,O)-chelating to the ruthenium metal centre and the other (O,O)-chelating. Further photolysis at 254 and 229 nm was shown to form [CpRu(CO)(NO)] with the evolution of CO_2 via an oxygen transfer reaction.[41]

In 2005 Kovalevsky et al. reported on the photochemically-induced oxygen transfer in crystals of *cis*-$[Ru^{II}(bipy)_2(NO)(NO_2)](PF_6)_2$ where a double linkage isonitrosyl-nitrito isomer is formed and also provided crystallographic and infrared evidence for the oxygen transfer between the NO_2 and NO ligands at low temperature. The experimental data was also supported by DFT calculations.[42]

Single crystals of *cis*-$[Ru^{II}(bipy)_2(NO)(NO_2)](PF_6)_2$ were mounted on the diffractometer and cooled to 200K and 90K in two individual experiments. In each experiment a ground state structure was collected in the dark. Figure 1.12 shows the ground state structure of the ruthenium cation at 90K. The crystals were irradiated in situ while continually rotating with light of 458nm using an Ar^+ CW laser. At 200K the crystal was irradiated for a total of 5 mins and changed colour from orange to red. The sample was irradiated for 10 mins at 90K and also turned from orange to red however the colour after irradiation was much darker in the 90K experiment than at 200K. Over exposure of laser radiation resulted in the formation of powder lines.[42]

Figure 1.12 Ground state structure of the ruthenium cation at 90K without hydrogen atoms. An almost identical geometry was observed at 200K

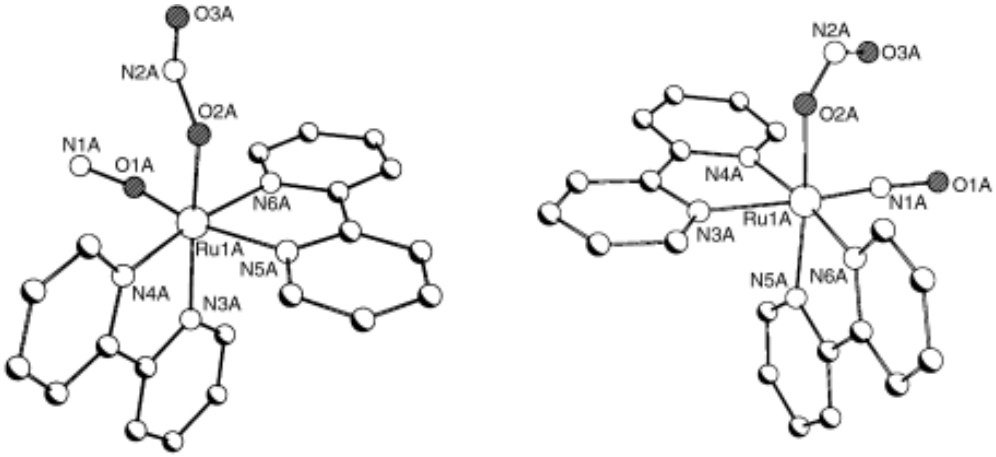

Figure 1.13 Photoinduced metastable state at 90K (left) and 200K (right)

Results from the photo-induced linkage isomerisation showed that at both temperatures residual electron density was found present in photodifference Fourier maps when the ground state coordinates were refined. The resulting peaks were in agreement with η^1-NO_2 nitro to η^1-ONO nitrito linkage isomerism in both experiments however at 90K a nitrosyl to isonitrosyl rearrangement was also observed and confirmed by anisotropic refinement of the NO ligand atoms. The structures of the metastable states are shown in figure 1.13.[42]

1.4.3 SO_2 Linkage Isomers

Another example of an ambidentate ligand is SO_2 which is isoelectronic with NO_2^-. It is a highly versatile ligand and is capable of forming a variety of complexes with metal ions due to its many different coordination modes.[43]

Johnson and Dew provided the initial evidence supporting the formation of metastable linkage isomerism in the late 1970s when investigating an IR study on the complex *trans*-$[Ru(NH_3)_4(SO_2)Cl]Cl$. Linkage isomerism can be photochemically induced using irradiation of 365nm, trapping any isomers formed by keeping the sample at low temperature. By varying the temperature used and the length of irradiation time, it was possible to isolate more than one photoproduct.[44]

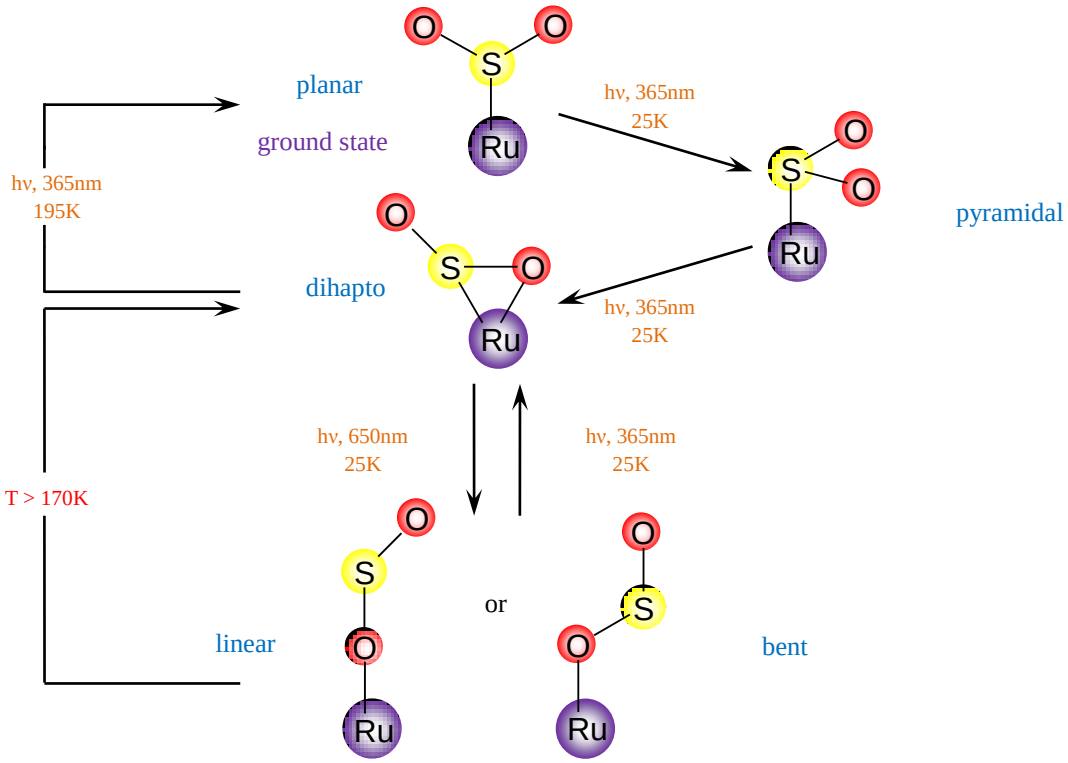

Figure 1.14 Postulated reaction scheme for *trans*-$[Ru(NH_3)_4(SO_2)Cl]Cl$

The IR spectrum for the ground state species has bands at 1255 and 1110cm^{-1} corresponding to asymmetric and symmetric S-O stretching modes respectively. Irradiation using 365nm light at 195K resulted in a change in the stretching frequencies relating to the SO_2 group. A decrease in the two bands in the ground state was observed as well as the formation of two new S-O absorption bands at 1165 and 940cm^{-1}. These results were observed using both KBr disks and Nujol mulls hence ruling out Br^- substitution in the former. Photolysis at 25K resulted in the presence of yet another absorption peak at 1180cm^{-1} suggesting a further product had been formed. Prolonged irradiation at this temperature also identified the presence of a third short lived intermediate, however they were unable to conclusively identify the exact structure of these isomers. It was postulated that spectral features were consistent with the formation of a S-bound pyramidal structure for the initial product and the isomer from prolonged irradiation was likely to be O-bound (either linear or bent). The results are summarised in figure 1.14.[44] Further discussion of SO_2 isomerism can be found in Chapter 3.

1.4.4 DMSO Linkage Isomers

DMSO, despite being larger in size than other ligands that undergo linkage isomerism, can also reorient itself in both the solid state and solution phase to form metastable isomers. DMSO is commonly found coordinated to a metal centre through the S atom, however, it is possible for complexes to occur where it is bound through the less stable O atom. Excited DMSO complexes exist as both S and O bound, however a metastable η^2-S,O complex can also exist.[45]

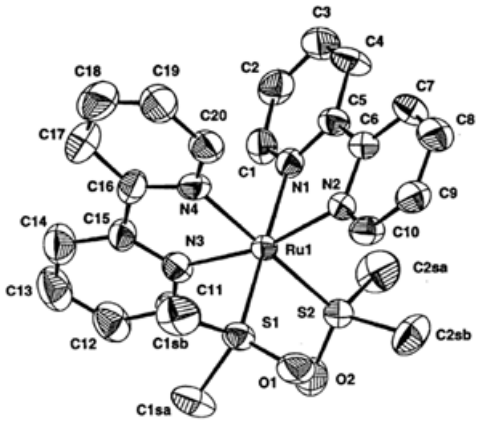

Figure 1.15 Structure of $[Ru(bipy)_2(DMSO)_2]^{2+}$

In 2000 both photochemical Ru-S to Ru-O and thermal Ru-O to Ru-S reactions were observed in DMSO solutions of $[Ru(Me_2bipy)_2(DMSO)_2]^{2+}$ and $[Ru(bipy)_2(DMSO)_2]^{2+}$ (the S-bound structure for one of the two molecules in the asu is illustrated in figure 1.15). On the basis of steric factors the authors commented that O-ligation would appear preferential in the *cis*-arrangement of the DMSO groups,

however electronic and bonding factors seem to be more important in the stability of the ground state structure which is why it adopts the S-bound coordination.[46]

The UV/vis absorption spectra can be seen for both the freshly synthesised yellow solution of $[Ru(bipy)_2(DMSO)_2](PF_6)_2$ in DMSO and the resulting red solution after irradiation (figure 1.16). The spectrum for the S-bound solution has λ_{max} = 348nm, $\varepsilon = 5760 M^{-1}cm^{-1}$. The spectrum for the irradiated solution has λ_{max} = 507nm, $\varepsilon = 3500 M^{-1}cm^{-1}$ as well as λ_{max} = 412nm, $\varepsilon = 5530 M^{-1}cm^{-1}$. This bathochromic shift is indicative of a coordination change from a 'soft' S-bound (high field) to a 'hard' O-bound (low field) ligand.[46]

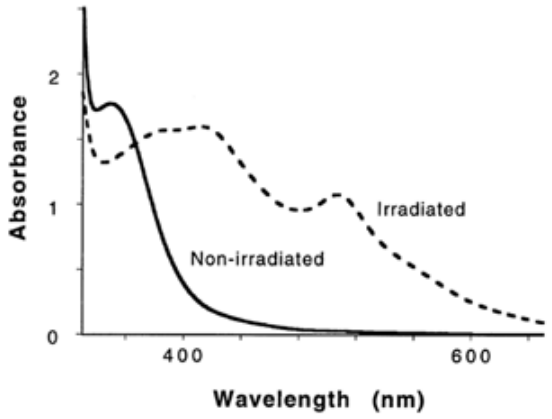

Figure 1.16 Absorbance spectra of $[Ru(bipy_2)(DMSO_2)](PF_6)_2$ in DMSO solution both before and after irradiation

A photochromic reaction of the complex- $[Ru^{II}(terpy)(bipy)(DMSO)](SO_3CF_3)_2$ from a Ru-S to Ru-O rearrangement of the attached DMSO ligand has been reported. Visible excitation was possible in single crystals, films and in solution. Upon irradiation at 442nm, a crystalline sample underwent an immediate colour change from yellow to red with the initial colour returning after several minutes. In both solutions of THF, DMSO or acetone and pmma films, irradiation between 430 and 450nm was shown to produce a new species which had an absorption maximum at 490nm.[45] This was very close to that reported for the product formed in the reaction of $(CH_3)_2S$ with $[Ru(O)(terpy)(bipy)]^{2+}$ and is consistent with the formation of O-bound Ru-DMSO. This suggests that the photochromism observed is due to the intramolecular isomerism from Ru-S to Ru-O of the DMSO ligand.[47]

Upon excitation, S-bound $[Ru^{II}(terpy)(bipy)(DMSO)](SO_3CF_3)_2$ produces a ^{1}MLCT state, which decays rapidly to form an emissive species on the ^{3}MLCT potential surface. Here the distorted η^2-DMSO state can either radiatively decay back down to the S-bound ground state, or rearrange itself to produce an electronically excited O-bound isomer, which luminesces at 720nm (figure 1.17).[45]

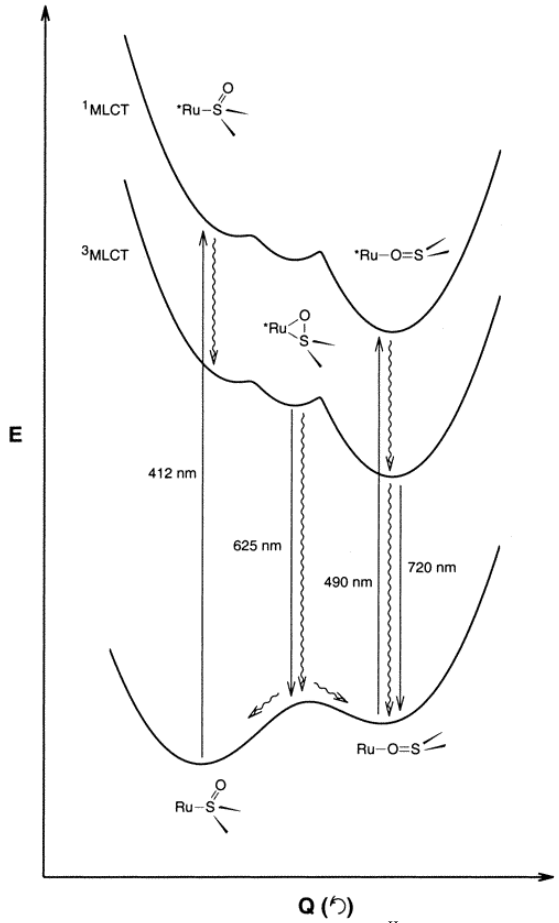

Figure 1.17 Formation of O-bound DMSO ligand in $[Ru^{II}(terpy)(bipy)(DMSO)](SO_3CF_3)_2$

A family of ruthenium complexes were investigated in pursuit of further mechanistic information. Compounds were designed which contained a metal capable of single electron redox chemistry ($Ru^{3+/2+}$), along with an ambidentate ligand capable of linkage isomerism (DMSO) and a ligand available for MLCT photochemistry. These compounds were of the form $[Ru(terpy)(L)(DMSO)]^{z+}$; where L was a variable bidentate ligand: bipy (**a**), pic (**b**), tmen (**c**), acac (**d**) or mal (**e**). The structures of these ligands can be seen in figure 1.18. Depending on which of these ligands is used, linkage isomerism can be either disfavoured or encouraged in response to the electronic nature of the bidentate ligand.[48]

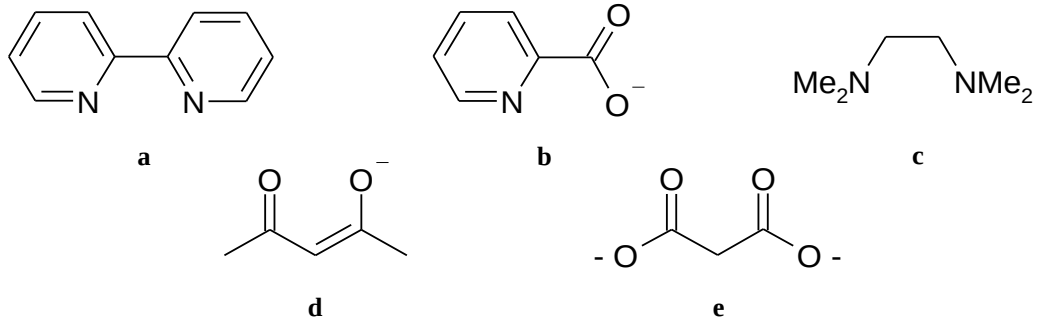

Figure 1.18 Structures of bidentate ligands used in complexes of $[Ru(terpy)(L)(DMSO)]^{z+}$

All complexes exhibit a S-bound DMSO ligand in the ground state, confirmed using electronic absorption, electrochemical data and IR spectra (see table 1.1). The lowest energy Ru dπ - terpy π* MLCT transition shifted to lower energy as the bidentate ligand changed from complex **a** (419nm) to **c** (429nm) to **e** (502nm). These trends were consistent with destabilisation of the t_{2g} dπ orbital set upon substitution of the strong-field π-acidic ligand (**a**) with a weak-field π-basic ligand (**e**) within the complex. The IR spectra of the aforementioned compounds showed ν(SO) stretching frequencies within the expected range of 1102-1066cm^{-1} for S-bound DMSO systems. In the analogous O-bound isomers, these frequencies are typically lower and found between 900-950cm^{-1}.[48]

Compound	λ_{max} (nm)		$E_{1/2}$ (V)		ν(SO)	ΔE_{abs}	ΔE_{ec}
	S[a]	O[a]	S[b]	O[b]	(cm^{-1})	(cm^{-1})	(cm^{-1})
(a) [Ru(terpy)(bipy)(DMSO)]$^{2+}$	419	490	1.67	1.10	1102	3860	4040
(b) [Ru(terpy)(pic)(DMSO)]$^{+}$	421	527	1.38	0.65	1089	4780	5890
(c) [Ru(terpy)(tmen)(DMSO)]$^{2+}$	429	530	1.65	1.03	1066	4230	4840
(d) [Ru(terpy)(acac)(DMSO)]$^{+}$	468	-	0.95	-	1088	-	-
(e) [Ru(terpy)(mal)(DMSO)]	502	-	0.82	-	1083	-	-

Table 1.1 Summary of analytical results for [Ru(terpy)(L)(DMSO)]$^{z+}$

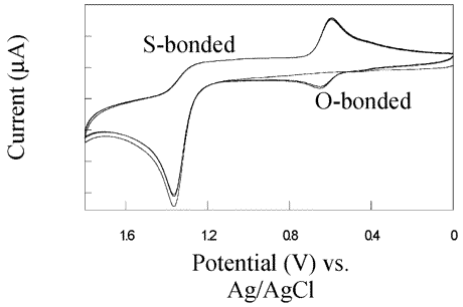

Figure 1.19 Cyclic voltammogram of [Ru(terpy)(pic)(DMSO)]$^{+}$

Cyclic voltammograms of **d** (z = 1) and **e** (z=0) are reversible one-electron couples, suggesting that these complexes do not undergo linkage isomerisation. Voltammograms of **a**, **b**, and **c** (z = 2 for complexes **a** and **c**, z=1 for **b**) however are irreversible (figure 1.19). Following the oxidation of S-bound Ru^{II} at 1.38V and reversing the scan polarity, the corresponding cathodic wave was not observed. Instead a new couple at 0.65V appeared suggesting that a new species formed following the oxidation of Ru^{II}-S around 1.4V which was indicative of an O-bound DMSO isomer.[48]

Irradiation of [Ru(terpy)(L)(DMSO)]$^{z+}$ when L = **a**, **b**, or **c** in DMSO solution, ionic liquids or polymer films resulted in dramatic shifts in the lowest energy visible MLCT transitions. The electronic absorption spectra of both S- and O-bound isomers of [Ru(terpy)(pic)(DMSO)]$^{+}$ in ionic liquid can be seen in figure 1.20 and the change in colour from yellow in its S-bound conformation to purple after irradiation is shown in figure 1.21. Similar results were also exhibited by the same complex in DMSO

solution and polymer films. After formation of the O-bound isomer, the S-form could be regenerated yielding the same original absorption spectrum after a period of a few minutes. Complexes **a** and **c** also demonstrated similar behaviour, however no change was observed in complexes **d** and **e**, which also indicated that S→O isomerisation is strongly disfavoured within these compounds. It has been postulated for **d** and **e** that the bidentate ligands used prevent the Ru^{III} metal centre from being hard enough to favour bonding from the hard O-donor atom over the soft S-donor.[48]

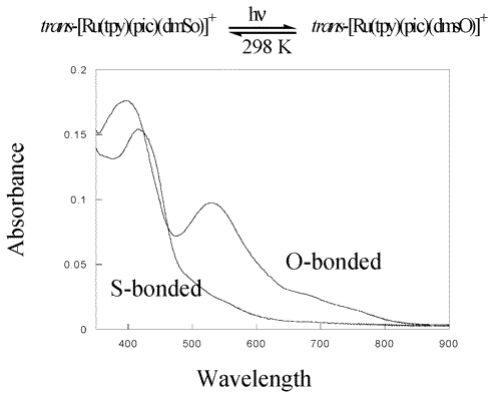

Figure 1.20 Electronic absorption spectra of S- and O-bound isomers of $[Ru(terpy)(pic)(DMSO)]^+$

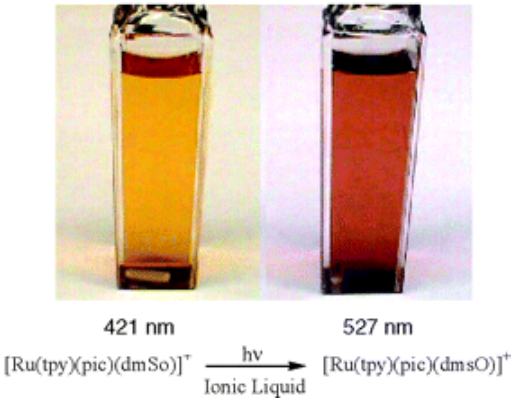

Figure 1.21 Solution of $[Ru(terpy)(pic)(DMSO)]^+$ before and after irradiation

1.4.5 Other systems

Many other ligands are also amenable to switching such as the cyano group and the thiocyanate ion.[43] A N-bound to S-bound isomerisation was observed in tetrahedrally coordinated samples of $M_2[Fe(NCS)_4]$ (where M = Me_4N^+, Et_4N^+ and K^+) when exposed to γ-rays at room temperature. Absorption and emission Mössbauer spectra were obtained suggesting the presence of S-bound isothiocyanate groups in irradiated samples. This evidence was supported by results from IR spectra.[49]

In 2008 Mockus et al. reported on a femtosecond isomerisation of the disulfoxide complex $[Ru(bipy)_2(OSSO)]^{2+}$. In its ground state this molecule has a S,S-bound geometry which undergoes a rearrangement using 355nm light to form a S,O-bound isomer. This species can further isomerise to give an O,O-bound complex (figure 1.22).[50]

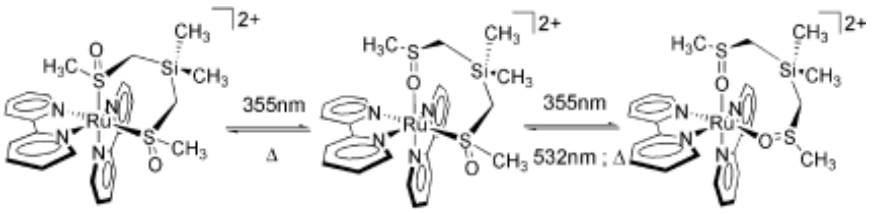

Figure 1.22 Isomerisation process of $[Ru(bipy)_2(OSSO)]^{2+}$

There are also examples of photochemical reactions forming excited state species that do not involve linkage isomerisation reactions. A combination of EXAFS studies and stroboscopic time resolved diffraction experiments on $[Pt_2(pop)_4]^{4-}$, (pop = pyrophosphate) showed that upon irradiation using a laser there was a shortening of the Pt-Pt bond by 0.28(9)Å. The photo-difference map in figure 1.23, illustrates the change in electron density before and after illumination with positive areas of electron density in red and negative areas in blue.[51]

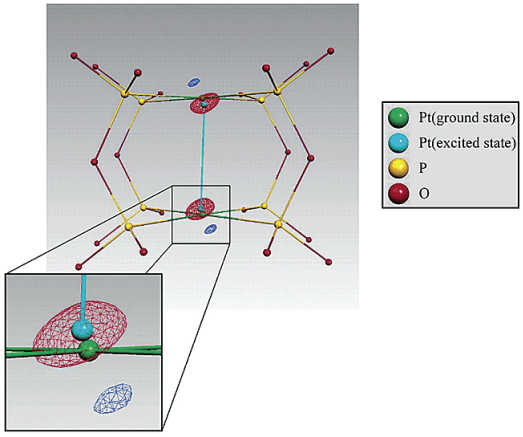

Figure 1.23 Photo-difference map of $[Pt_2(pop)_4]^{4-}$

Another example of bond contraction upon excitation is observed within crystals of $[Rh_2(dimen)_4]^{2+}$ (dimen = 1,8-diisocyano-*p*-menthane) studied by Coppens et al. In this complex a bond contraction of approximately 0.85Å is observed when irradiated within the range of 355-532nm at 17K.[52]

1.4.6 Conclusion

Intramolecular photochemical linkage isomerisation reactions are fairly uncommon with most examples involving metal nitrosyl complexes. Other ligands such as SO_2, DMSO, and NO_2 can also exhibit linkage isomerism and metal complexes using these ligands, could prove to be extremely important for use as information storage systems. There are more examples of linkage isomerism in solution, rather fewer in the solid state. However, for information storage devices the solid state reactivity is key. This thesis sets out to determine the structures of metastable linkage isomers via photocrystallographic techniques mainly focusing on those formed by SO_2 and NO_2 metal complexes.

1.5 References

[1] Y. Wada, M. Tsukada, M. Fujihira, K. Matsushige, T. Ogawa, M. Haga, S. Tanaka, *Jpn. J. Appl. Phys.* **2000**, *39*, 3835.
[2] M. D. Ward, *J. Chem. Ed.* **2001**, *78*, 321.
[3] V. Balzani, A. Credi, F. M. Raymo, J. F. Stoddart, *Angew. Chem. Int. ed.* **2000**, *39*, 3348.
[4] A. Aviram, M. A. Ratner, *Chem. Phys. Lett.* **1974**, *29*, 277.
[5] K. S. Kwok, J. C. Ellenbogen, *Materials Today* **2002**, *5*, 28.
[6] M. D. Ward, in *Chem. & Ind.*, **1997**, p. 640.
[7] H. J. Dai, E. W. Wong, C. M. Lieber, *Science* **1996**, *272*, 523.
[8] R. L. Carroll, C. B. Gorman, *Angew. Chem. Int. ed.* **2002**, *41*, 4379.
[9] A. R. Pease, J. O. Jeppesen, J. F. Stoddart, Y. Luo, C. P. Collier, J. R. Heath, *Acc. Chem. Res.* **2001**, *34*, 433.
[10] P. L. Anelli, N. Spencer, J. F. Stoddart, *J. Am. Chem. Soc.* **1991**, *113*, 5131.
[11] S. Saha, J. F. Stoddart, *Chem. Soc. Rev.* **2007**, *36*, 77.
[12] S. Kobatake, S. Takami, H. Muto, T. Ishikawa, M. Irie, *Nature* **2007**, *446*, 778.
[13] J. M. Cole, *Chem. Soc. Rev.* **2004**, *23*, 501.
[14] P. Coppens, *Chem. Commun.* **2003**, 1317.
[15] C. E. Housecroft, A. G. Sharpe, *Inorg. Chem.*, First ed., **2001**.
[16] L. M. Peter, *CH30074 Photochem.* **2004**.
[17] C. E. Wayne, R. P. Wayne, *Photochem.*, OUP, **2004**.
[18] P. Atkins, *The Elements of Physical Chemistry*, 3rd ed., OUP, **2001**.
[19] L. X. Chen, *Angew. Chem. Int. ed.* **2004**, *43*, 2886.
[20] M. D. Carducci, M. R. Pressprich, P. Coppens, *J. Am. Chem. Soc.* **1997**, *119*, 2669.
[21] P. Coppens, D. V. Fomitchev, M. D. Carducci, K. Culp, *J. Chem. Soc. Dalton Trans.* **1998**, 865.
[22] K. F. Bowes, J. M. Cole, S. L. G. Husheer, P. R. Raithby, T. L. Savarese, H. A. Sparkes, S. J. Teat, J. E. Warren, *Chem. Commun.* **2006**, 2448.
[23] L. X. Chen, M. K. Bowman, P. A. Montano, J. R. Norris, *J. Am. Chem. Soc.* **1993**, *115*, 4373.
[24] L. X. Chen, P. L. Lee, D. Gosztola, W. A. Svec, P. A. Montano, M. R. Wasielewski, *J. Phys. Chem. B* **1999**, *103*, 3270.
[25] S. Pascarelli, T. Neisius, S. De Panfilis, *J. Synchrotron Rad.* **1999**, *6*, 1044.
[26] G. Busse, T. Tschentscher, A. Plech, M. Wulff, B. Frederichs, S. Techert, *Faraday Discuss.* **2003**, *122*, 105.
[27] H. Bertagnolli, T. S. Ertel, *Angew. Chem. Int. ed.* **1994**, *33*, 45.
[28] G. Meitzner, *Catal. Today* **1998**, *39*, 281.
[29] J. A. Johnson, C. E. Johnson, *J. Phys. - Condens. Matter* **2005**, *17*, R381.
[30] U. Hauser, V. Oestreich, H. D. Rohrweck, *Z. Phys.* **1977**, *280*, 125.
[31] U. Hauser, V. Oestreich, H. D. Rohrweck, *Z. Phys.* **1977**, *280*, 17.
[32] U. Hauser, V. Oestreich, H. D. Rohrweck, *Z. Phys.* **1978**, *284*, 9.
[33] V. Rusanov, T. Woike, H. S. Kim, V. Angelov, T. Bonchev, S. Haussuhl, *Solid State Commun.* **2003**, *126*, 457.
[34] J. R. Schoonover, G. F. Strouse, *Chem. Rev.* **1998**, *98*, 1335.
[35] M. R. Pressprich, M. A. White, Y. Vekhter, P. Coppens, *J. Am. Chem. Soc.* **1994**, *116*, 5233.
[36] D. V. Fomitchev, P. Coppens, *Inorg. Chem.* **1996**, *35*, 7021.
[37] G. B. Richter-Addo, P. Legzdins, *Metal Nitrosyls*, OUP, **1992**.
[38] D. V. Fomitchev, T. R. Furlani, P. Coppens, *Inorg. Chem.* **1998**, *37*, 1519.
[39] D. Schaniel, B. Cormary, I. Malfant, L. Valade, T. Woike, B. Delley, K. W. Kramer, H. U. Gudel, *Phys. Chem. Chem. Phys.* **2007**, *9*, 3717.
[40] A. Werner, *Brt.* **1907**, *40*, 765.
[41] C. M. Gordon, R. D. Feltham, J. J. Turner, *J. Phys. Chem.* **1991**, *95*, 2889.
[42] A. Y. Kovalevsky, G. King, K. A. Bagley, P. Coppens, *Chem. Eur. J.* **2005**, *11*, 7254.

[43] P. Coppens, I. Novozhilova, A. Kovalevsky, *Chem. Rev.* **2002**, *102*, 861.
[44] D. A. Johnson, V. C. Dew, *Inorg. Chem.* **1979**, *18*, 3273.
[45] J. J. Rack, J. R. Winkler, H. B. Gray, *J. Am. Chem. Soc.* **2001**, *123*, 2432.
[46] M. K. Smith, J. A. Gibson, C. G. Young, J. A. Broomhead, P. C. Junk, F. R. Keene, *Eur. J. Inorg. Chem.* **2000**, 1365.
[47] L. Roecker, J. C. Dobson, W. J. Vining, T. J. Meyer, *Inorg. Chem.* **1987**, *26*, 779.
[48] J. J. Rack, A. A. Rachford, A. M. Shelker, *Inorg. Chem.* **2003**, *42*, 7357.
[49] H. H. Wei, L. Z. Ho, *Inorg. Chem.* **1984**, *23*, 624.
[50] N. V. Mockus, D. Rabinovich, J. L. Petersen, J. J. Rack, *Angew. Chem. Int. ed.* **2008**, *47*, 1458.
[51] I. V. Novozhilova, A. V. Volkov, P. Coppens, *J. Am. Chem. Soc.* **2003**, *125*, 1079.
[52] P. Coppens, O. Gerlits, Vorontsov, II, A. Y. Kovalevsky, Y. S. Chen, T. Graber, M. Gembicky, I. V. Novozhilova, *Chem. Commun.* **2004**, 2144.

Chapter 2

Crystallographic Techniques and Methods

2.1 Introduction

X-ray crystallography is a fundamental analytical technique used in the determination of crystal and molecular structure. The following chapter details a brief introduction into some crystallographic definitions as well as some of the basic principles of X-ray diffraction.

2.2 X-ray Crystallography

2.2.1 Crystallinity

Crystalline materials consist of regular arrays of atoms, ions or molecules in three dimensions, with interatomic distances of approximately 1Å (100pm). In order for diffraction to occur, the wavelength of the incident light has to be of the same order of magnitude as the spacings of the diffraction grating (i.e. the crystal). Because of the periodic nature of their internal structures, crystals (figure 2.1) can act as a three dimensional diffraction grating to radiation of a suitable wavelength (X-rays), and the resulting diffraction pattern generated can be interpreted to give the internal positions of atoms within a crystal very accurately.[1]

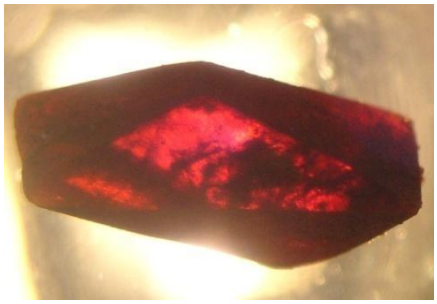

Figure 2.1 A single crystal

2.2.2 Historical Background of X-rays and Crystallography

X-rays were discovered by the German physicist Wilhelm Röntgen in 1895, however their nature remained unknown for several decades. Their wavelike properties were identified by von Laue in 1912. He suggested that on the basis of their wavelength, X-rays might be diffracted when using crystals as the diffraction grating.[2] This hypothesis was confirmed within the year by Friedrich and Knipping when the first diffraction photographs were produced, which lead to the development of X-ray crystallography.[3]

2.2.3 Bragg's Law

The discovery by von Laue was noted by W. L. Bragg and in 1913, with the help of his father W. H. Bragg, they solved the first crystal structure of NaCl. Subsequently they solved the structures of KCl, ZnS, CaF_2, $CaCO_3$ and diamond.[1] W. L. Bragg noted that diffraction was a consequence of reflections from the X-ray beam by various lattice planes belonging to the same family,[4] and only when the crystal

is in specific orientations with respect to the source, can X-rays be 'reflected' from these particular planes within the crystal.[1] This 'reflection' is therefore different to that of monochromatic light by a mirror, as this only requires the angle of incidence to equal the angle of reflection and this is possible for all angles.[5]

Bragg devised a model that details the geometrical conditions under which a diffracted beam can be observed. Figure 2.2 below shows X-rays being diffracted from a series of parallel planes. In order for constructive interference, and hence diffraction to occur, the path difference (MY+YN) must equal an integral value of wavelengths (n).[6] This leads to Bragg's law (equation 1), which is expressed as:

$$n\lambda = 2d_{hkl}\sin\theta \qquad \text{Equation 1}$$

where λ is the wavelength of the X-rays, d_{hkl} is the spacing between the adjacent planes within a parallel set in the crystal, and θ is known as the Bragg angle, at which reflections from these planes are observed.[1]

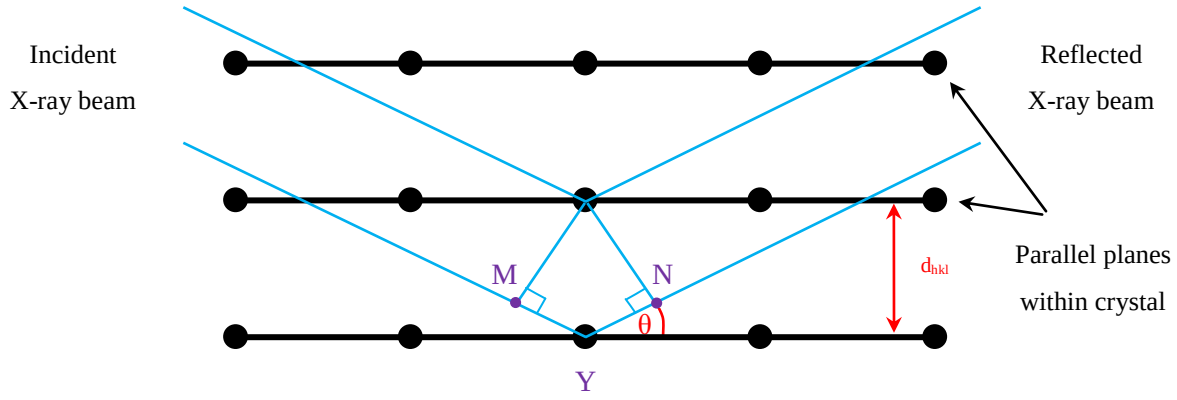

Figure 2.2 Bragg reflection from a set of planes with spacing d_{hkl}

It is important to note that Bragg's law is a simplification and cannot provide any information about the intensity of the reflected beam. The concept of reflection is also incorrect, as in practice X-rays are diffracted by the electron clouds surrounding atomic nuclei within a crystal.

2.2.4 Atomic Scattering Factors

In diffraction experiments, the X-rays are scattered by electron clouds surrounding the atomic nuclei. The amplitude of scattering for an atom is known as the atomic scattering factor and is given the symbol f_j.[5] This is proportional to the number of electrons in an atom. However, at low angle of incidence all the electrons are in phase, as 2θ increases, because the electron cloud is of a finite size, the

electrons around the nucleus stop scattering in phase and the intensity drops off.[4] The atomic scattering factors of some elements are illustrated in figure 2.3.[5]

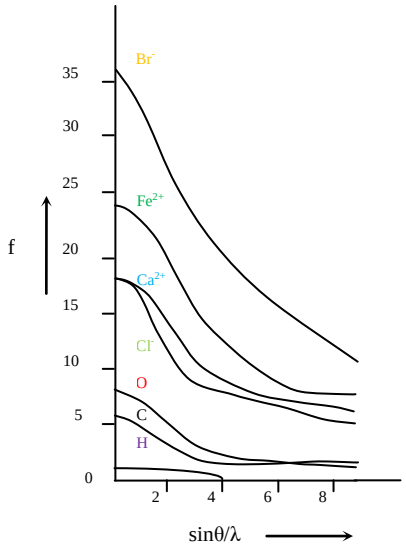

Figure 2.3 Atomic scattering factors as a function of sinθ/λ

2.2.5 Crystal Lattices, Unit Cells and Bravais Lattices

The repeating nature of ions, molecules or atoms within a crystal, generate the crystal lattice. This can be represented by a series of points, which are located at positions of identical environment by translation. The arrangement of these lattice points provides a description of how the repeating units occur. There are four different lattice types (figure 2.4); the primitive unit cell - P type, the body centred unit cell – I type, the all-face centred unit cell - F type and face centred unit cell - which can be labelled A, B, or C type.

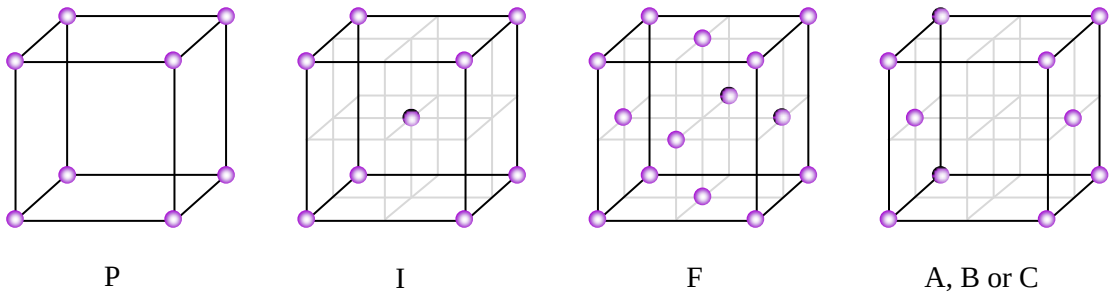

Figure 2.4 The four lattice types

The smallest repeating unit in a crystalline lattice is known as the unit cell, (figure 2.5) and when replicated by translation alone, generates the full symmetry of the crystal structure. Using standard convention, the three vector lengths of a unit cell are called *a*, *b*, and *c* and the angles α, β and γ (α is the angle between *b* and *c*, β is the angle between *a* and *c* and γ is the angle between *a* and *b*). These three lengths and angles are known as the unit cell parameters.[7]

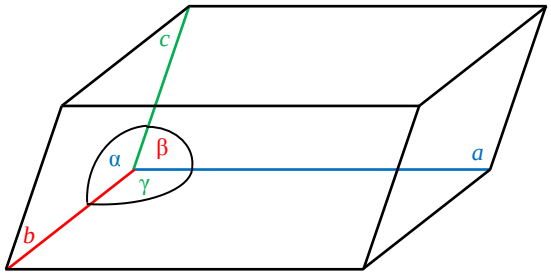

Figure 2.5 Unit cell diagram with cell dimensions and angles for a generic unit cell

There are a finite number of unit cells, which when stacked together will generate a crystalline array and fill all of a three dimensional space. The seven different geometric shapes are known as the seven crystal systems. The type of unit cell depends on the side lengths (*a*,*b*,*c*) and the angles between the sides (α, β, γ). The combination of the seven crystal systems along with one of the four lattice types, gives rise to fourteen unique Bravais lattices (illustrated below in table 2.1). These unit cell shapes are determined by their minimum symmetry requirements.[7]

Crystal System	Bravais Lattices	Unit Cell Parameters
Cubic	P I F	$a = b = c$ $\alpha = \beta = \gamma = 90°$
Hexagonal	P	$a = b \neq c$ $\alpha = \beta = 90°, \gamma = 120°$
Trigonal (Rhombohedral)	P	$a = b = c$ $\alpha = \beta = \gamma \neq 90°$
Tetragonal	P I	$a = b \neq c$ $\alpha = \beta = \gamma = 90°$
Orthorhombic	P C I F	$a \neq b \neq c$ $\alpha = \beta = \gamma = 90°$
Monoclinic	P C	$a \neq b \neq c$ $\alpha = \gamma = 90°, \beta \neq 90°$
Triclinic	P	$a \neq b \neq c$ $\alpha \neq \beta \neq \gamma \neq 90°$

Table 2.1 The Seven Crystal Systems and the distribution of the 14 Bravais Lattices attributed to each System

2.2.6 Symmetry Elements

For individual molecules a number of symmetry operations are possible which can relate one part to another, in a crystal however, only six symmetry elements are possible. These six symmetry elements can be broken down into two categories: non-translational symmetry elements which include rotations, inversions, reflections and rotary inversions, and translational symmetry elements which include screw axes and glide planes (figure 2.6).

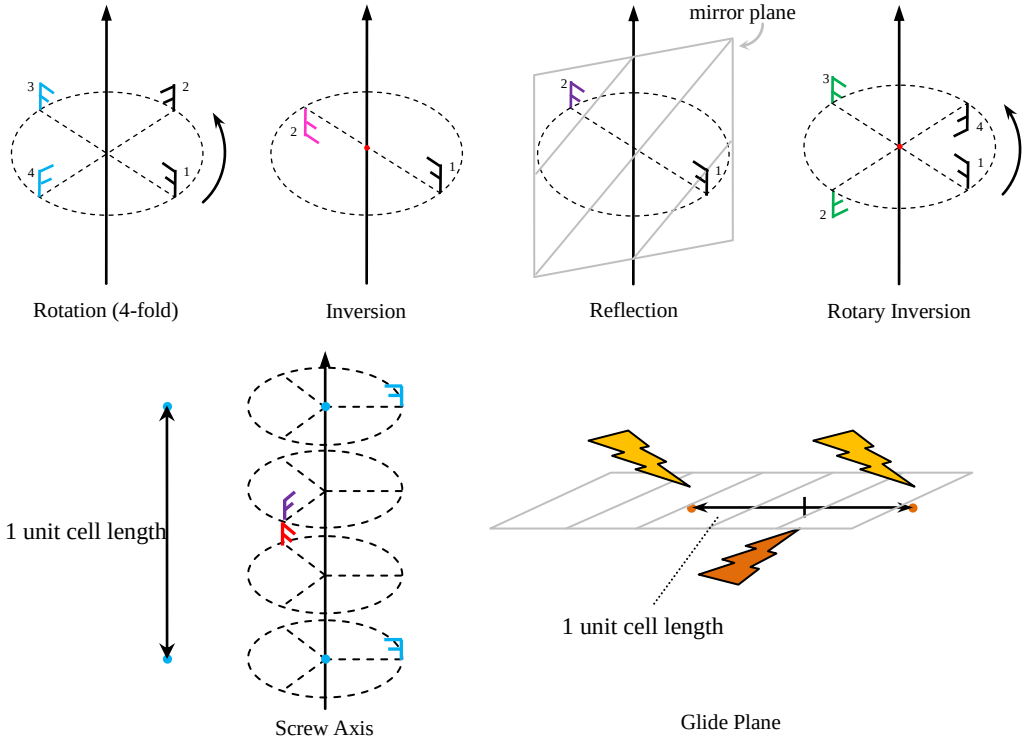

Figure 2.6 Illustration of the six symmetry elements possible in crystallography

A crystallographic rotation is when all the properties of the space remain unchanged after a rotation of $2\pi/n$ about an axis, where n can equal 1,2,3,4 or 6. An axis equal to 1 is trivial since a full 360° rotation of an object about an axis will always remain the same. Values of 2,3,4 and 6 (twofold, threefold, fourfold and sixfold) result in rotations of 180°, 120°, 90° and 60° about an axis respectively. In crystallography it is important to note that all rotations proceed in an anticlockwise direction.[4] Inversion centres result in an inversion about a point and reflections occur due to the presence of mirror planes. A rotary inversion is simply a rotation as described above followed by inversion about a point. The example given in figure 2.6 is a 4-fold rotary inversion.

A screw axis combines a translational element with a rotation and has the general notation n_i. Again n is the rotational order of the axis and the translational distance is given by the ratio of i/n. For example a 3_1 screw axis along the c axis is a rotation of 120° ($2\pi/n$ = 360/3) followed by a translation along the c axis of 1/3 of the total unit cell length.[1]

A glide plane involves a translation of 1/2 a unit cell length followed by a reflection. A *b*-glide perpendicular to *c* involves a translation of *b*/2 followed by a reflection in a plane normal to the *c* axis.[1]

2.2.7 Absences and Intensity Distributions

The intensity of each reflection in a diffraction pattern arises as a consequence of the interference of waves scattered from individual atoms in that particular direction. Absences in crystallographic data occur when the intensity of a reflection is systematically zero as a result of lattice centring (general absences - table 2.2) or as a consequence of transitional symmetry elements present (systematic absences - table 2.3). General absences affect the whole dataset while systematic absences only affect subsets of reflections. The presence or absence of non-translational symmetry elements cannot be detected from systematic absences as these symmetry elements have no translation components.[8]

Lattice type		Affected reflection	Condition for reflection to occur
Primitive lattice	P	*hkl*	none
Body-centred lattice	I	*hkl*	$h + k + l$ = even
Face-centred lattice	A	*hkl*	$k + l$ = even
	B	*hkl*	$h + l$ = even
	C	*hkl*	$h + k$ = even
Face-centred lattice	F	*hkl*	*h k l* all odd or all even

Table 2.2 General Absences due to lattice centring

Symmetry Element		Affected reflection	Condition for reflection to occur
Twofold screw, 2_1 along Fourfold screw, 4_1 along Sixfold screw, 6_1 along	*a*	*h00*	*h* = even
Threefold screw, 3_1,3_2 along Sixfold screw, 6_2, 6_4 along	*c*	*00l*	*l* divisible by 3
Fourfold screw, 4_1, 4_3 along	*a*	*h00*	*h* divisible by 4
Sixfold screw, 6_1, 6_5 along	*c*	*00l*	*l* divisible by 6
Glide plane perpendicular to Translation *a*/2 (*a* glide) Translation *c*/2 (*c* glide) *b*/2 + *c*/2 (*n* glide) *b*/4 + *c*/4 (*d* glide)	*b*	*h0l*	 *h* = even *l* = even *h* + *l* = even *h* + *l* divisible by 4

Table 2.3 Systematic absences due to translational symmetry elements

Although non-translational symmetry elements do not cause systematic absences, they do have an effect on the distribution of intensities within a diffraction pattern which can be analysed statistically. A number of approximations are made and the results indicate the likelihood a particular symmetry element is present in the crystal. Due to the unreliable nature of the statistics the only non-translational symmetry element routinely tested for in this manner is an inversion centre as the whole data set can be employed. When an inversion centre is present, atoms are in pairs related by the inversion. Their combined scattering tends to give a greater proportion of strong reflections and weak reflections so the data become centric and show more overall variation. When an inversion centre is absent from the solid state molecular structure fewer reflections in the dataset can be examined and hence is not very reliable. The normalized intensities do not vary greatly from the mean and the data are acentric (figure 2.7).[8]

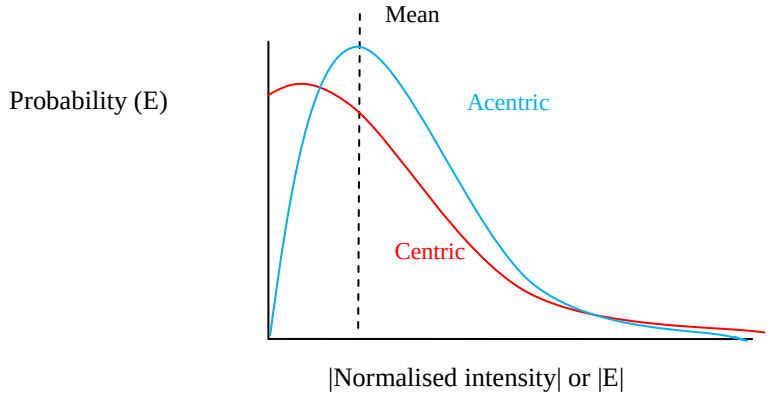

Figure 2.7 Distribution of intensities for model acentric and centric data

2.2.8 Space Groups

The combination of non-translational and translational symmetry elements combined with the fourteen Bravais lattices, generate 230 unique combinations of packing three-dimensional space known as space groups. These space groups are unequally distributed across the seven crystal systems, and determination of a space group from crystal data is achieved by looking at absences within the data.[9]

Space groups describe the positions of symmetry elements and several symmetry-equivalent objects can coexist within a single unit cell. The smallest part of a unit cell which will generate the whole cell when symmetry operations are applied is known as the asymmetric unit.[4] Equivalent position diagrams describe locations of the asymmetric unit, while space group diagrams provide information as to the position of all symmetry operators within a unit cell.

2.3 Single Crystal X-ray Diffraction

2.3.1 Introduction

Single crystal X-ray diffraction has become a routine analytical tool used to determine the solid state molecular structure of compounds. With the help of modern technological advances data collection times have been reduced from weeks to hours over the last couple of decades by the invention of area detectors. The information that can be obtained from these experiments is extremely valuable. Not only does it provide a 3D model of the structure under investigation, the technique also provides information on configuration, conformation, torsion and bond angles, bond lengths and bonding interactions. A brief description of the technique is described in the following section.

2.3.2 Experimental Set-up

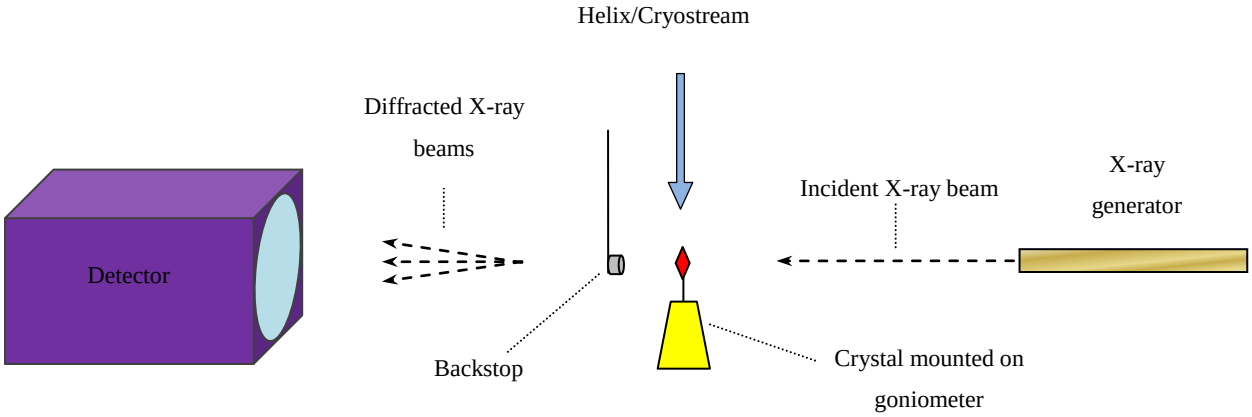

Figure 2.8 Schematic illustrating set-up for a single crystal X-ray diffraction experiment

The schematic in figure 2.8 illustrates the standard set-up used for single crystal X-ray structure determination experiments, while figure 2.9 shows the Nonius Kappa CCD diffractometer used for data collection at the University of Bath. X-rays are generated by firing high speed electrons at a metal target, which is typically made out of copper or molybdenum. When produced in this manner, the X-rays have variable wavelengths so they are typically run through a graphite monochromator to create a monochromatic beam of K_α radiation which is suitable for use during the experiment. The crystal (typically 0.2mm^3 and 0.4mm^3) is mounted on a fine glass fibre fixed on a goniometer head which can rotate during data collection. X-rays are fired toward the crystal where some are diffracted and recorded as a series of diffraction spots by the detector (each spot corresponds to diffraction from a set of Miller planes for which Bragg's law has been satisfied). A backstop is positioned immediately in front of the detector to absorb any X-rays not diffracted by the sample. The use of a cryostream or helix blows cooled

nitrogen or helium gas over the crystal and allows data to be recorded at low temperature. This helps reduce the thermal motion of atoms within the crystal.[5]

Figure 2.9 The Nonius Kappa CCD Diffractometer at the University of Bath

2.3.3 Collection Strategy

The general collection procedure for single crystal X-ray diffraction experiments can be seen in figure 2.10. The methods used for processing data and structure elucidation are discussed in the following section.

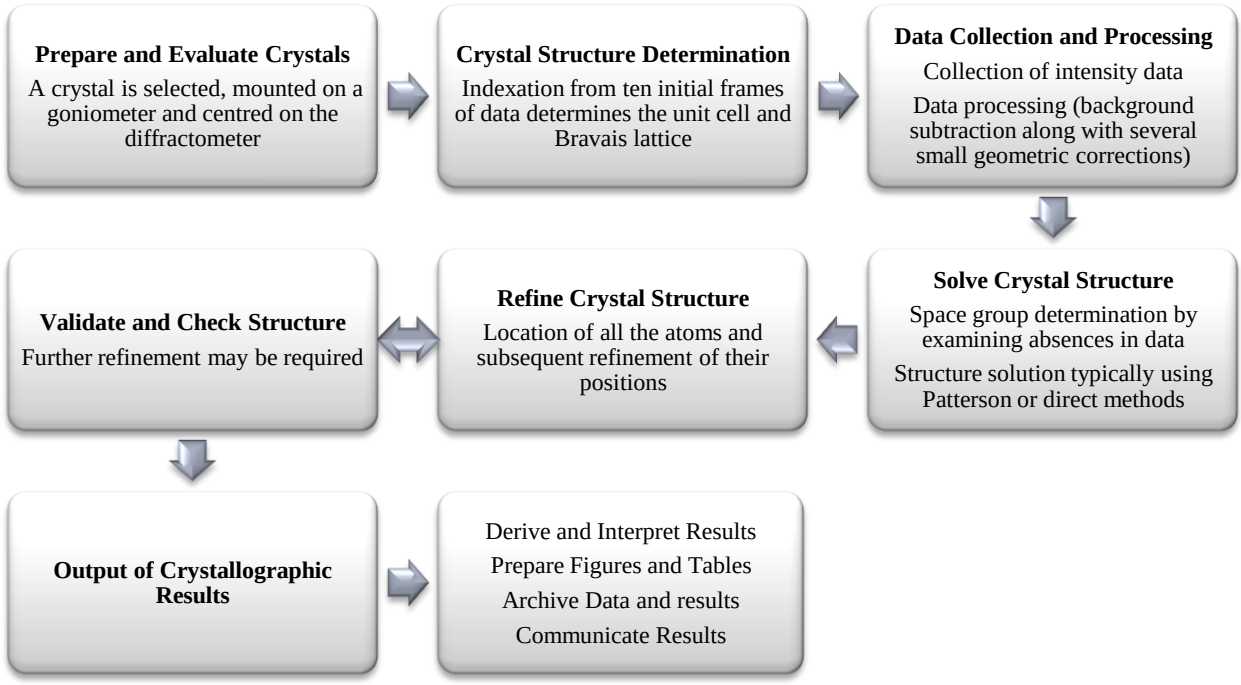

Figure 2.10 Procedure for a single crystal X-ray diffraction experiment

2.3.4 Structure Solution

Each spot on the diffraction pattern resulting from diffracted X-rays can be described by a structure factor 'F_{hkl}', which relates to atomic coordinates within the crystal by using equation 2 for N atoms in the unit cell:

$$F_{hkl} = \sum_{j=1}^{N} f_j \exp\left[2\pi i(hx_j + ky_j + lz_j)\right] \qquad \text{Equation 2}$$

The position of atom 'j' is given by coordinates x_j, y_j, and z_j and f_j is its atomic scattering factor. The integers h,k, and l are the indices pertaining to a particular reflection.[10]

X-ray diffraction experiments measure the intensity (I_{hkl}) of the diffracted X-ray beam from each Miller plane (hkl) within the crystal. The intensity is proportional to the square of the structure factor ($I_{hkl} \alpha F_{hkl}^2$) and despite being able to measure the value of the structure factor its phase cannot be determined. This is known as the phase problem in crystallography. In order to construct an electron density map for structure solution both the structure factor and its phase need to be determined. The relationship between electron density ($\rho(xyz)$) at point xyz in the unit cell and the structure factor is given in equation 3 below, where V is the volume and α is the phase angle[2]:

$$\rho(xyz) = (1/V)\Sigma_h\Sigma_k\Sigma_l |F_{hkl}| \cos\left[2\pi(hx + ky + lz) - \alpha\right] \qquad \text{Equation 3}$$

An appropriate method needs to be selected in order to overcome the phase problem. Crystal structures are solved by creating a set of trial phases for the structure factors. There are two main methods utilised to do this. The first is the Patterson method and relies on the presence of at least one heavy atom in the unit cell. This makes the technique useful for solving the structures of organometallic and inorganic compounds. The second strategy employed is known as direct methods and is used mainly to solve the structures of organic molecules and biological compounds.[1]

2.3.4.1 Patterson Methods[11]

Patterson identified that a Fourier synthesis using structure factor values as the coefficients produces a 3D electron density map (according to equation 4) however a similar Fourier synthesis using $|F_{hkl}|^2$ as the coefficients has peaks corresponding to all the interatomic vectors.[1]

$$P(u,v,w) = (1/V)\Sigma_h\Sigma_k\Sigma_l |F_{hkl}|^2 \cos\left[2\pi(hu + kv + lw)\right] \qquad \text{Equation 4}$$

The Patterson method performs a synthesis on the data set to create a 3D map of the unit cell from the values of $P(u,v,w)$ which correspond to vectors between all pairs of atoms in the unit cell. Take

two platinum atoms in a molecule that has crystallised in the space group *P*-1 as an example (figure 2.11). The atomic coordinates of Pt_1 and Pt_2 are *x,y,z* and *-x,-y,-z* respectively related to each other by an inversion centre. The direction of the vector (*u,v,w*) between the two platinum atoms is given in equation 5:

$$u,v,w = [(x,y,z)-(-x,-y,-z)] = 2x, 2y, 2z \qquad \text{Equation 5}$$

This vector appears in the Patterson map and allows the location of the two platinum atoms to be located by dividing the result by two.[1]

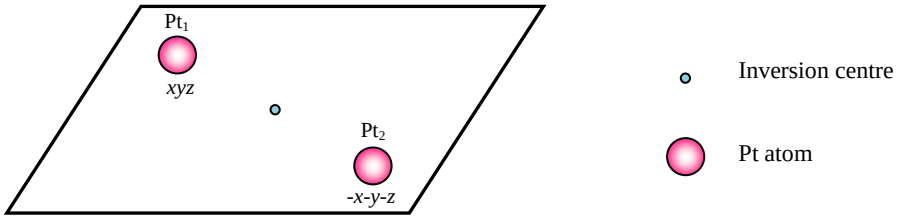

Figure 2.11 Cell projection diagram containing two platinum atoms related to each other by inversion symmetry

The reason that Patterson method work well for heavy atoms is because the size of the vector is proportional to the product of the atomic numbers of the atoms concerned. Once these heavy atoms have been identified and their phases determined, an electron density map can be constructed highlighting the positions of other lighter atoms in the unit cell.[1]

2.3.4.2 Direct Methods

Direct methods are used to combat the phase problem when all the molecules in the unit cell have similar atomic scattering factors. Direct methods calculate mathematical probabilities for phase values and use these to construct an electron density map for the unit cell directly from a single set of experimentally obtained X-ray intensities. The probabilities are calculated by making two main assumptions: that electron density in a structure cannot take any value, however it must always be positive, and that the structure consists of discrete spherically symmetric atoms evenly distributed throughout the unit cell.[1]

Structure factor amplitudes can be related to phases through a knowledge of the electron density. If the phases are known, amplitudes can be computed to conform to known information of the electron density, similarly if the amplitudes are known, phases can be determined from electron density data. Constraints on the electron density can be applied and as it is related to the structure factors by a Fourier transformation, constraints applied to electron density data impose corresponding constraints onto the

structure factors. As structure amplitudes are known, the majority of constraints restrict the values of structure phases and in favourable circumstances are enough to determine the phase values directly.[6]

Table 2.4 summarises some of the constraints used for direct method structure solution and the mathematical techniques that are applied to the constraint.[6]

Constraint	Mathematical Method of Application
Discrete atoms	Normalised structure factors
$\rho(\mathbf{x}) \geq 0$	Inequality relationships
Random distribution of atoms	Phase relationships and tangent formula
$\int \rho^3(\mathbf{x})\, dV = \max$	Tangent formula
Equal atoms	Sayre's equation
$-\int \rho(\mathbf{x}) \ln(\rho(\mathbf{x})/q(\mathbf{x}))\, dV = \max$	Maximum entropy methods
Equal molecules	Molecular replacement method
$\rho(\mathbf{x})$ = constant	Density modification techniques

Table 2.4 Electron density constraints for direct method structure solution and the mathematical techniques used for their application

In small molecule crystallography the key constraints used are:

- *Discrete atoms*: The effects of the atomic shape are removed from the observed structure factors and are converted to *E*'s – normalised structure factors. The *E*s are closely related to the Fourier coefficients of a point atom structure and when applied to a phase determining formula, strengthen the phase constraints so the electron density map should always contain atomic peaks. The assumption is made that all the peaks are the same shape and the deconvolution of peak shape is expressed in equation 6 below, where $\varepsilon_{\mathbf{h}}$ is a factor which accounts for the effect of the space group symmetry on the observed intensity.[6]

$$|E(\mathbf{h})|^2 = \frac{|F_o(\mathbf{h})|^2}{\varepsilon_{\mathbf{h}} \sum_{i=1}^{N} f^2}$$

Equation 6

- *Non-negative electron density*: This constraint imposes $\rho(\mathbf{x}) \geq 0$ (a site with a negative number of electrons is an impossibility) and gives rise to inequality among structure factors.[6, 12]
- *Random atomic distribution*: This constraint is more powerful than that used for non negative electron density which is only capable of restricting phases which make $\rho(\mathbf{x})$ negative for some value of the phase. This is less likely to occur in slightly larger structures and so a constraint is

therefore required which operates on the whole of the electron density no matter what its value (achieved by combining the constraints for discrete atoms and non-negative electron density). The structure is assumed to contain a random distribution of atoms and results in a probability distribution for the phases rather than allowed and disallowed values.[6]

- *Equal atoms*: This constraint assumes that in a large proportion of crystals the atoms can be considered approximately equal if hydrogen atoms are ignored. This constraint was developed by Sayre who came up with an equation which gives exact relationships among the structure factors.[13] If the electron density is squared, it will contain equal peaks in the same positions as the original density but the peak shapes will have changed.[6]

Direct methods are popular in structure determination due to the fact that they are fully automated which makes them easy to use, however the suitability of the constraints applied depends heavily on the nature of the crystalline sample.

2.3.5 Structure Refinement

Structural models obtained by Patterson methods and direct methods are often incomplete and usually represent a first approximation of the real structure. The final stage in single crystal X-ray diffraction experiments is refinement. Refinement is performed for a couple of reasons:

- *To improve phasing* - This ensures that the computed electron density maps more closely represent the actual electron density.
- *To obtain the 'best' values for the parameters in the model* – When the structure is fundamentally correct, weighted least squares refinement is used to optimise parameter values.[14]

Refinement is generally carried out using least squares analysis which aims to find a good description of the crystal structure in terms of numerical parameters that best fits the evidence of the observed diffraction pattern. Refinement is usually performed using the amplitudes of (F_{hkl}) or more generally using $(F_{hkl})^2$ as the phases of the observed structure factors are unknown.[4]

At the end of the refinement process a final residual index the *R*-factor (R_1) is computed for the structure which gives an indication as to how good the model is based on (F_{hkl}) or a weighted *R*-factor (w*R*2) based on $(F_{hkl})^2$. The *R*-factor is defined in equation 7 below, where F_o is the observed structure factor and F_c is the calculated structure factor.[6] The weighted *R*-factor is defined in equation 8 where w is a weighting factor and is always greater than the *R*-factor.

$$R_1 = \frac{\Sigma \, ||F_o|-|F_c||}{\Sigma \, |F_o|}$$

Equation 7

$$wR_2 = \frac{\Sigma\,[w(F_o^2 - F_c^2)^2]}{\Sigma\,[w(F_o^2)^2]}$$

Equation 8

In general the smaller the *R*-factor the better and solutions are considered acceptable if this value is between 2-7%. A good check is also an assessment of the estimated standard deviations on atom positions and bond parameters. The structure is deemed complete once all errors have been checked and the overall model makes chemical sense.

As there is no method to directly and unequivocally solve the structure from experimental data, there is always a possibility that the proposed structure is incorrect. Methods can be employed to check the validity of the model including comparison with other known properties of structures obtained from different analytical techniques. Further examination of the X-ray data may also be required as another solution may be possible that gives a similar goodness of fit for amplitudes, but a better fit for the unmeasured phases.

2.4 Powder Diffraction

A polycrystalline material consists of a large number of randomly oriented crystallites. When several crystallites are irradiated simultaneously by X-rays, they each generate their own diffraction pattern and are superimposed upon each other. As the sample is rotated diffraction is observed from planes in each of the individual crystallites which happen to be oriented at the correct angle to satisfy the Bragg equation (the Bragg angle and intensity will be the same in each case, but the direction of the diffracted beam will vary, while always being inclined at 2θ to the straight through direction).[1] This results in individual lattice spacings within the crystallite forming a cone of diffraction (figure 2.12). Each cone is comprised of a series of closely spaced spots arising from diffraction from a single crystallite within the bulk sample. The sheer quantity of these crystallites allows these diffraction spots to join together to form cones.[15] Thus the 2D diffraction pattern for a single crystal is compressed into one dimension for powder samples.

To obtain data in a form suitable for analysis the positions of the various cones need to be determined. This can be achieved using either photographic film in a Debye-Scherrer camera or with a detector sensitive to X-ray radiation. In both instances, the main principle is to determine the diffraction angle, 2θ, of the diffraction cones.[15]

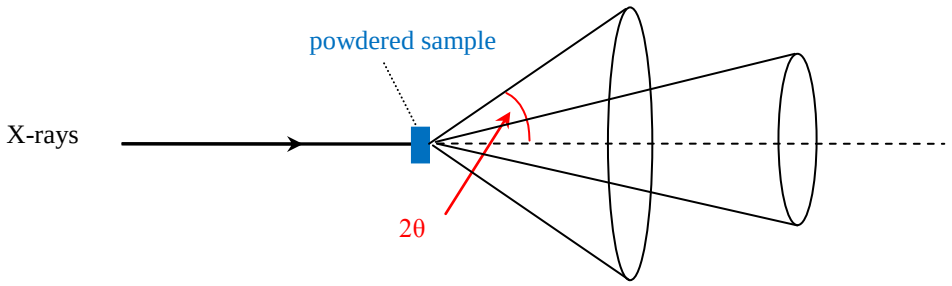

Figure 2.12 Diffraction cones generated from a polycrystalline sample

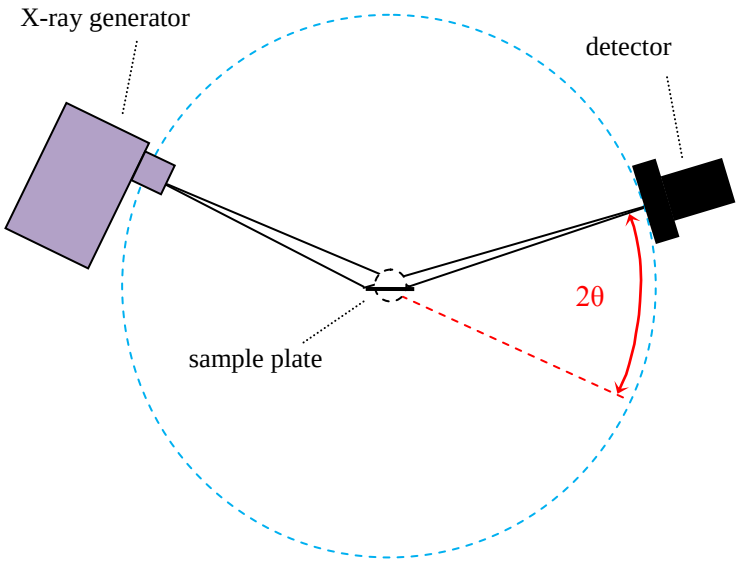

Figure 2.13 Schematic of a powder diffractometer

Powder diffractometers generally use X-ray detectors such as Geiger-Muller tubes or a scintillation detector to measure the positions of diffracted beams. By scanning the detector around the circumference of a circle, it cuts through each of the diffraction cones at the various maxima for the sample (figure 2.13). The intensity of X-rays are measured as a function of detector angle 2θ and this is presented as a powder diffraction pattern (figure 2.14).[1, 16]

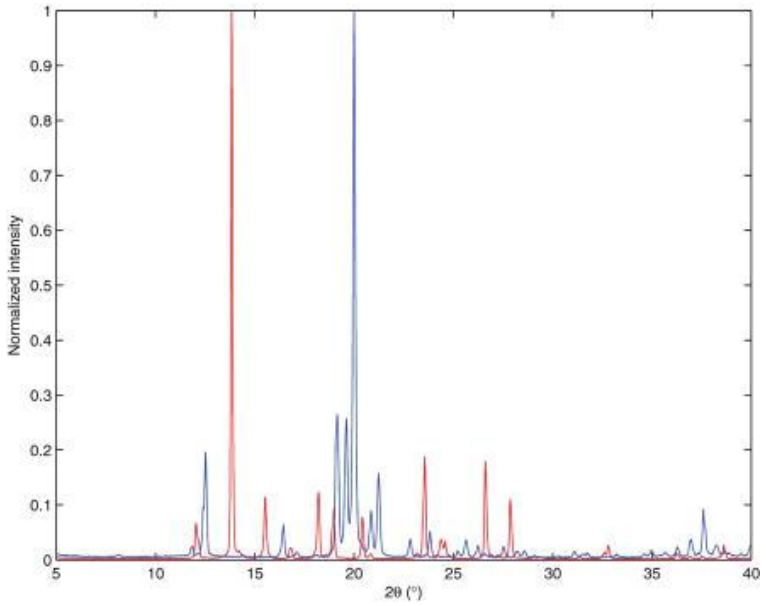

Figure 2.14 Powder diffraction patterns of paracetamol (red) and lactose (blue)[13]

The difficulty in powder diffraction is identifying which planes in the crystallites are responsible for each observed diffraction peak. This process is known as indexing and involves assigning the correct *hkl* index to each reflection. Although this is generally possible for simple compounds in high symmetry systems, it is extremely difficult for many larger/less symmetrical systems as the diffraction patterns become more complex due to the presence of a greater number of peaks. Overlap between reflections becomes problematic as it is harder to index the pattern and measure the intensities of reflections.[1] Most X-ray powder diffraction experiments are carried out using copper radiation, which has a longer wavelength than molybdenum that is often used in single crystal X-ray diffraction; this spreads the diffraction pattern over a larger 2θ range. This helps during the indexing process as the diffraction pattern is expanded and peak overlap is reduced. The development of new techniques such as Rietveld methods has made the solution and subsequent refinement of structures from powder diffraction experiments possible.[17]

X-ray powder diffraction is mainly used as finger-print tool to obtain information about the composition of a bulk material or to detect the presence of a known compound or phase in a product. The identification of compounds using powder diffraction methods can be useful for the qualitative analysis of a product and also as a rough check of its purity. However, powder diffraction will not detect amorphous products or detect impurities of less than 5 %. Another application of the technique involves using it for an analysis of unit-cell parameters as a function of temperature or pressure to determine phase diagrams.[1]

2.5 Photocrystallographic Techniques

Both single crystal and powder diffraction experiments can be modified in order to perform 'excited state' diffraction experiments. Photocrystallography as mentioned in the previous chapter is a technique used to monitor the formation of light-induced metastable and transient species.[18] It is possible to add the fourth dimension of time into these experiments in order to carry out light-induced reactions by time resolved X-ray diffraction.

The lifetime, τ_0, of the photoinduced state dictates the type of instrumentation required for structure determination. There are three principal methods that determine the type of experimental set-up, and these depend on the lifetimes of the material under study. The three techniques are known as: steady state methods, pseudo-steady state methods and stroboscopic methods which utilises pulsed X-rays. The experimental conditions for each of these methods are summarised in figure 2.15 below.[19]

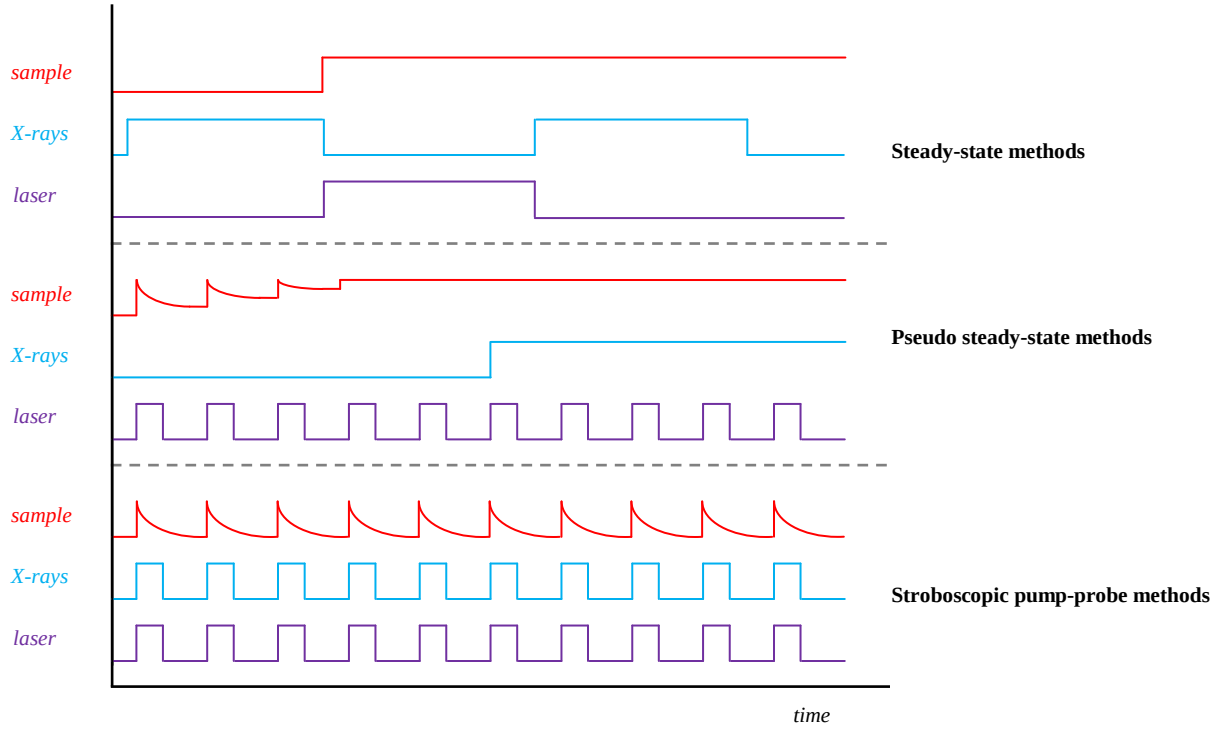

Figure 2.15 Schematic of experimental conditions for photocrystallographic experiments

The steady state method is employed for compounds with extremely long lifetimes or metastable structural changes. Here the photo-induced structure is obtained in three experimental steps. Firstly a ground state structure of the material is determined using normal crystal X-ray diffraction. Next the sample is irradiated with light typically using a laser or a broad-band light source. The light source is removed and the resulting structure re-determined using the same experimental conditions as before. The

resulting structure from the second data set will comprise of contributions from both the ground state structure and the excited state. This is due to the fact that 100% conversion is hard to achieve without compromising the crystal quality as the strains involved in the isomerisation process could cause it to crack.[19]

Pseudo steady-state methods are used for compounds with lifetimes between mins and ms. Here the excited state is maintained by continuously pumping the material with a light source that has a pulse frequency that repeats faster than the excited state lifetime. After a short cycling period, the maximum percentage conversion of the sample is observed for that particular optical source. The sample remains in its pseudo excited-state for the duration of the experiment provided that the light remains cycling at the necessary pulse rate. Again a ground state structure is obtained followed by another data collection to re-determine its structure once the material has reached its pseudo steady-state.[19]

For samples with lifetimes in the range of ms-µs, a mechanical chopper can be employed to produce pulsed X-rays. The length of each pulse is designed to be of the same magnitude as the lifetime of the photo-induced state of the sample. The repetition rate of the X-ray pulse is matched with that of the pulsed laser so that both the X-ray and optical pulses occur at the same time. The time when both pulses are "on" the light-induced structure is observed, however the times when these pulses are "off" the structure returns to its ground state. Intensity data is therefore only recorded when both pulses are "on" and the structure obtained via this approach is also a combination of both ground and excited states.[19] The experimental set-up for a stroboscopic experiment can be seen below in figure 2.16.[20]

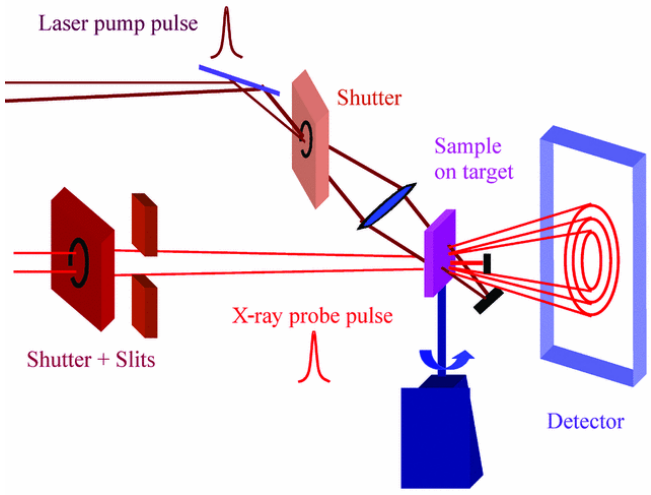

Figure 2.16 Set up for pump-probe excited state diffraction experiments[20]

2.6 Synchrotron Radiation

2.6.1 Generation of Synchrotron Radiation

Figure 2.17 Picture of Diamond - a synchrotron in Didcot, Oxfordshire, UK[18]

A synchrotron (figure 2.17)[21] is a type of particle accelerator consisting of a ring structure which is many meters in diameter.[6] Electrons are injected into a linac (linear accelerator) and are accelerated, before passing into a booster ring where they continue to gain energy. These accelerated electrons are then injected into a storage ring as beam of electrons. To constrain the particles in the chamber, superconducting external magnets are used which provide an inward acceleration and help the beam continue on its circular path. As a consequence of the constant change in direction and increasing speed of the electrons within the magnetic field, the electrons lose energy in the form of electromagnetic radiation, more specifically synchrotron light. This light is then captured by station beamlines where it can be tuned to a specific wavelength (ranging from IR to soft X-rays) depending on the type of experiment for which it is required. Modern synchrotrons are designed to maintain a beam of particles at high velocities for long periods of time and are known as storage rings (figure 2.18). Klystrons are used to

generate high power radiowaves which help sustain electron acceleration and replenish energy lost as a consequence of synchrotron radiation.[22]

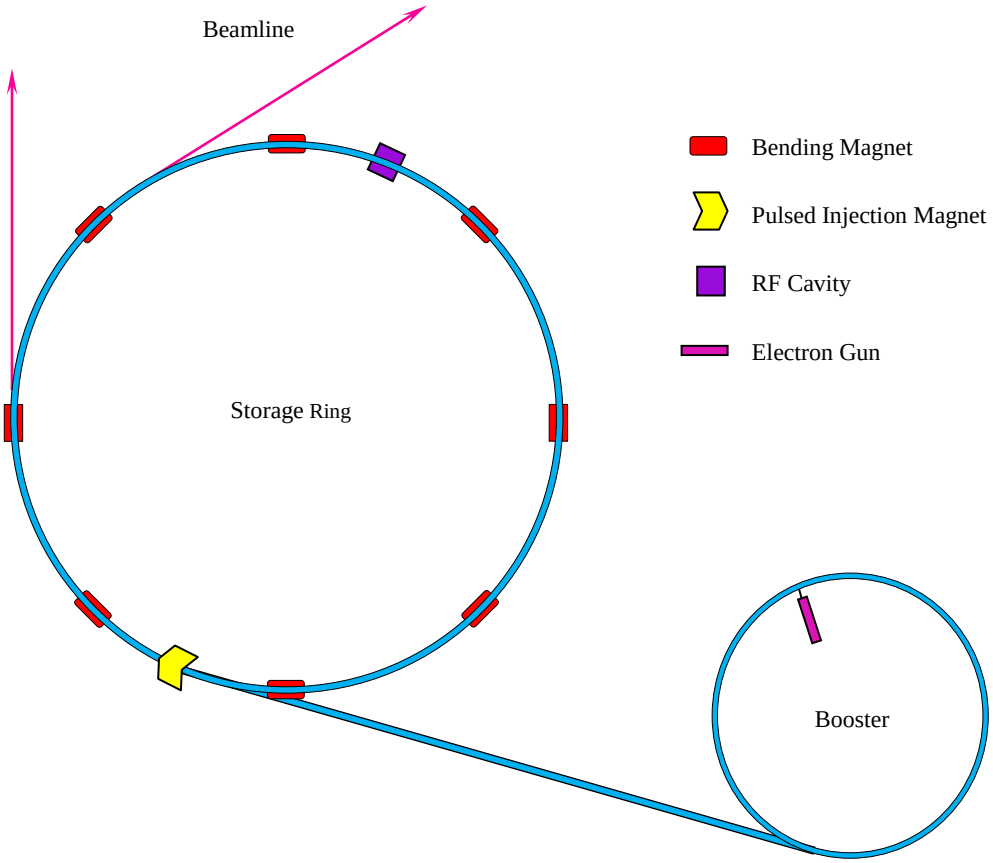

Figure 2.18 Schematic of a synchrotron with a storage ring

The electron beam is housed in an evacuated chamber, however it is impossible to obtain a perfect vacuum and eventually the strength of the electron beam is lost due to interactions with trace gas molecules present in the pipe. This means the synchrotron beam has a lifetime which depends heavily on the quality of the vacuum and makes continuous use of synchrotron light impossible.

There are a number of uses for the intense radiation provided from a synchrotron in the IR, visible, UV and soft X-ray regions however to generate the 'hard' X-rays needed for diffraction experiments additional magnetic components are required to extend the energy range and increase the intensity of synchrotron radiation. These magnetic components are known as wigglers and are comprised of a set of three magnets that deflect the electron beam through a straight section, send it around a curve then return it onto its original path. This results in extra emission of radiation, shifting it to a shorter wavelength required for diffraction experiments.[22]

2.6.2 Advantages of Synchrotron Radiation

There are many advantages to using a synchrotron X-ray source as opposed to a laboratory generated X-ray source. Due to the high flux and brilliance of X-rays generated from synchrotron radiation (this can be around a thousand times more intense than a laboratory K_α Cu or Mo source) structures can be elucidated for small weakly diffracting crystals, which would not be possible on a standard laboratory diffractometers.[6] This is a particular advantage for photocrystallographic experiments as during excitation of a sample by light, only the surface molecules tend to absorb the radiation. With a smaller sample it allows for better sample penetration depth and hence a greater percentage of the molecules within the sample will be exposed to the external light source, hopefully resulting in higher levels of excitation. Other advantages include the ability to freely select the wavelength required for experimentation with the use of a monochromator. This can be extremely useful for problematic samples.[22] Synchrotron light can also be pulsed allowing experiments to be performed on timescales that can monitor structural changes as a function of time.[23, 24]

The intensity that is achieved with a synchrotron and the continuing development of high speed area detectors allows for rapid data collections, whilst still maintaining an acceptable level of precision.[6] This is extremely important for unstable compounds, however, it is also valuable when collecting multiple data sets whilst varying sample conditions, such as monitoring the formation of isomers whilst being irradiated with light as a function of time.

2.7 References

[1] L. Smart, E. Moore, *Solid State Chemistry*, Second ed., **2001**.

[2] G. H. Stout, L. H. Jensen, *X-ray Structure Determination - A Practical Guide*, Second ed., John Wiley & Sons, **1989**.

[3] M. M. Woolfson, *An Introduction to X-Ray Crystallography*, 2nd ed., Cambridge University Press, **1997**.

[4] C. Giacovazzo, H. L. Monaco, G. Artioli, D. Viterbo, G. Ferraris, G. Gilli, G. Zanotti, M. Catti, *Fundamentals of Crystallography*, Second ed., OUP, **2002**.

[5] J. Pickworth Glusker, K. N. Trueblood, *Crystal Structure Analysis - A Primer*, Second ed., OUP, **1985**.

[6] W. Clegg, A. J. Blake, R. O. Gould, P. Main, *Crystal Structure Analysis Principles and Practice*, OUP, **2001**.

[7] W. Clegg, *Crystal Structure Determination*, OUP, **1998**.

[8] W. Clegg, in *Chapter 2: Space Group Determination - X-ray Structure Analysis 10th BCA/CCG Intensive School*, **2005**.

[9] W. Clegg, *Crystal Structure Determination*, OUP, **2002**.

[10] W. Clegg, in *Chapter 7: Fourier Synthesis - X-ray Structure Analysis 10th BCA/CCG Intensive School*, **2005**.

[11] A. L. Patterson, *Phys. Rev.* **1934**, *46*, 372.

[12] J. Karle, H. Hauptman, *Acta Crystallogr.* **1950**, *3*, 181.

[13] D. Sayre, *Acta Crystallogr.* **1952**, *5*, 60.

[14] D. Watkin, in *Chapter 12: Refinement of Crystal Structures - X-ray Structure Analysis 10th BCA/CCG Intensive School*, **2005**.

[15] M. T. Weller, *Inorganic Materials Chemistry*, OUP, **1994**.

[16] W. Dong, C. Gilmore, G. Barr, C. Dallman, N. Feeder, S. Terry, *J. Pharm. Sci.* **2008**, *97*, 2260.

[17] A. J. Florence, N. Shankland, K. Shankland, W. I. F. David, E. Pidcock, X. L. Xu, A. Johnston, A. R. Kennedy, P. J. Cox, J. S. O. Evans, G. Steele, S. D. Cosgrove, C. S. Frampton, *J. Appl. Cryst.* **2005**, *38*, 249.

[18] P. Coppens, *Chem. Commun.* **2003**, 1317.

[19] J. M. Cole, *Chem. Soc. Rev.* **2004**, *33*, 501.

[20] J. Davaasambuu, P. Durand, S. Techert, *J. Synchrotron Rad.* **2004**, *11*, 483.

[21] www.diamond.co.uk.

[22] W. Clegg, *J. Chem. Soc. Dalton Trans.* **2000**, 3223.

[23] C. Blome, T. Tschentscher, J. Davaasambuu, P. Durand, S. Techert, *J. Synchrotron Rad.* **2005**, *12*, 812.

[24] G. Busse, T. Tschentscher, A. Plech, M. Wulff, B. Frederichs, S. Techert, *Faraday Discuss.* **2003**, *122*, 105.

Chapter 3

Sulphur Dioxide Linkage Isomers

3.1 Introduction

Sulphur dioxide is an ambidentate ligand capable of adopting a wide range of coordination modes upon complexation as well as exhibiting changes in coordination upon excitation. Its versatility allows eight different metal-ligand arrangements, which can be seen below in figure 3.1. Just over half of these coordination geometries have been observed and structurally characterised, whereas the other bonding modes are currently only hypothesised.[1, 2]

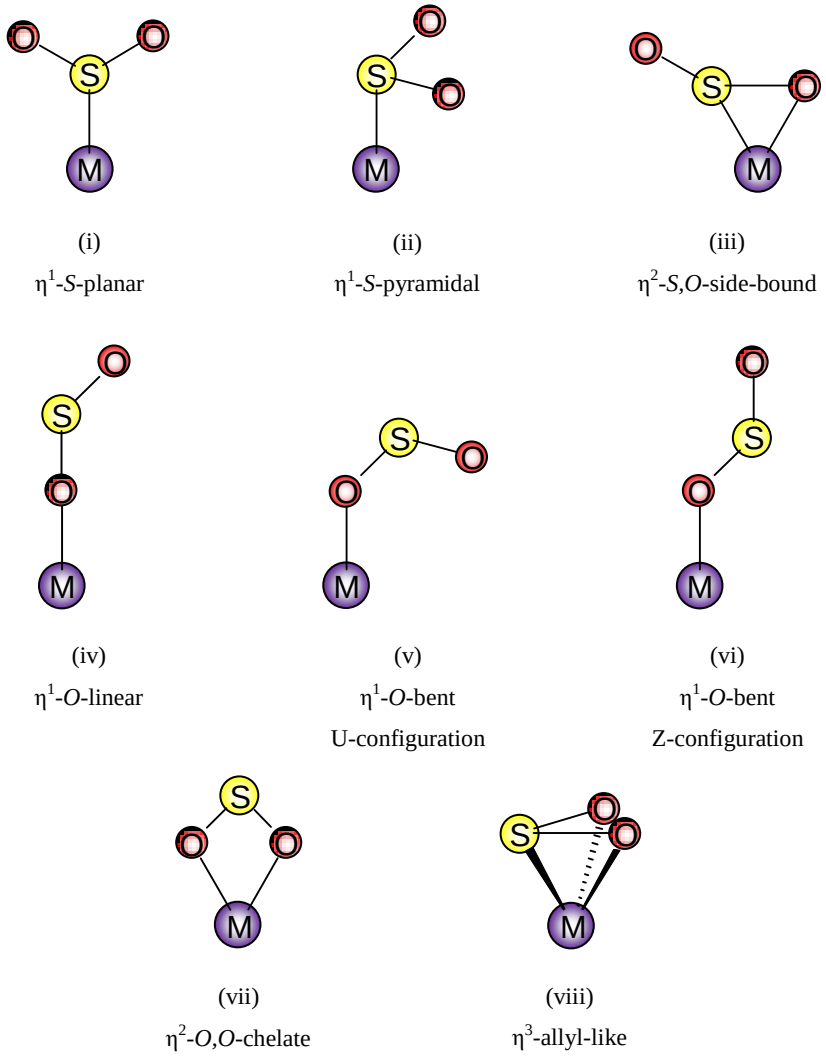

Figure 3.1 Coordination modes of the sulphur dioxide ligand

In 2002 the first photocrystallographic investigations were undertaken to monitor the formation/presence of linkage isomers of the sulphur dioxide ligand in the solid state, using the ruthenium complexes: *trans*-$[Ru(NH_3)_4(SO_2)Cl]Cl$ and *trans*-$[Ru(NH_3)_4(SO_2)(H_2O)](C_6H_5SO_3)_2$ following the spectroscopic work conducted by Johnson and Dew in 1979 (discussed in Chapter 1).[2, 3]

The experiments identified that the aforementioned complexes underwent an atomic rearrangement from a η^1-S-bound conformation ((i) in figure 3.1) to a η^2-S,O-side bound isomer ((iii) in figure 3.1) upon excitation. This isomer was observed for both of the ruthenium complexes under investigation with populations of this metastable state (known as MS2) refining to 10.0(1)% for *trans*-$[Ru(NH_3)_4(SO_2)Cl]Cl$ and 11.1(1)% for *trans*-$[Ru(NH_3)_4(SO_2)(H_2O)](C_6H_5SO_3)_2$ under the experimental conditions employed. Theoretical calculations performed on both ruthenium complexes also indicated the presence of another metastable state, MS1 (η^1-O-bent, U-configuration seen in figure 3.1 (v)), however, this isomer was not observed during the experiment using either spectroscopic or crystallographic methods.[2]

Further investigations into the linkage isomerism of sulphur dioxide in other ruthenium complexes were carried out using the following compounds: *trans*-$[Ru(NH_3)_4(SO_2)(H_2O)](Tos)_2$ and *trans*-$[Ru(NH_3)_4(SO_2)(CF_3C(O)O)]CF_3C(O)O.CF_3C(O)OH$.[4] Crystals of both complexes were cooled to 90K whilst being continuously irradiated with 488nm light. During this irradiation period the crystals appeared to darken and change from orange to a dark red/brown colour (figure 3.2).

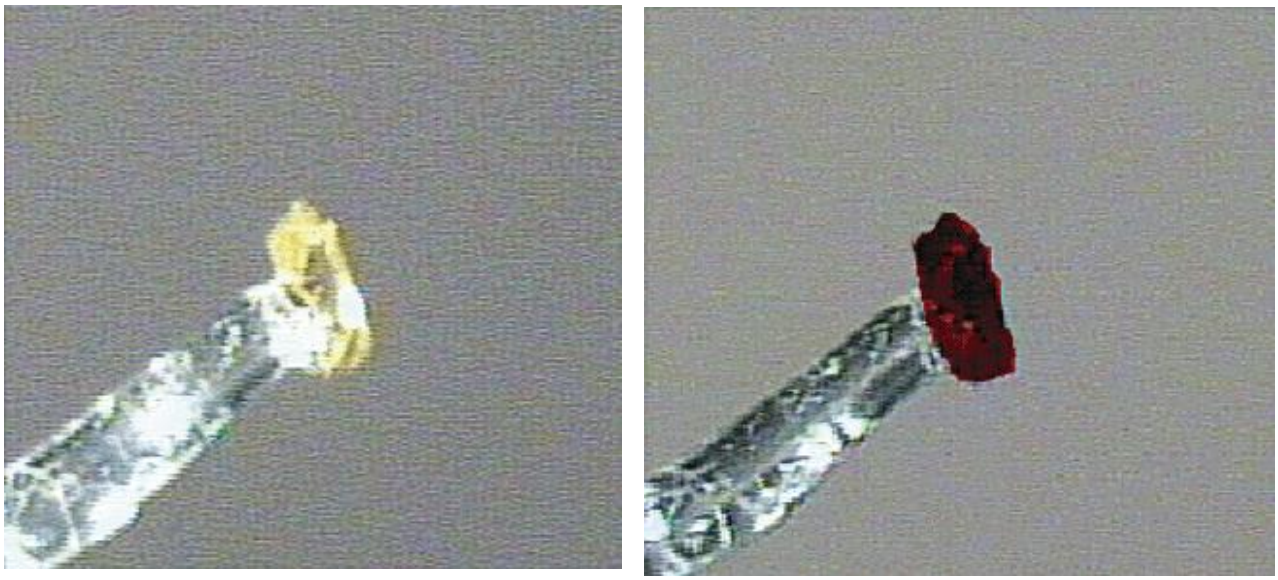

Figure 3.2 Colour change exhibited by trans-$[Ru(NH_3)_4(H_2O)(SO_2)](Tos)_2$ before (left) and after (right) irradiation with 488 nm light for 10 mins

Overexposure to light under the experimental conditions used resulted in a smearing of Bragg spots and caused the appearance of powder lines in the diffraction pattern. Therefore, irradiation was ceased and data collections were obtained after a delay of 10-20 mins in order to dissipate any heat accumulated in the crystal during the irradiation procedure. As with previous experiments the metastable isomer MS2 was achieved in both samples, however the populations achieved were considerably higher. The η^2-S,O-side bound linkage isomer of the sulphur dioxide ligand was accountable for 20.1(4)% of the solid state molecular structure of *trans*-$[Ru(NH_3)_4(SO_2)(H_2O)](Tos)_2$ and 37.3(5)% in *trans*-$[Ru(NH_3)_4(SO_2)(CF_3C(O)O)]CF_3C(O)O.CF_3C(O)OH$. The structures of the MS2 isomers can be seen in figure 3.3 below.[2, 4]

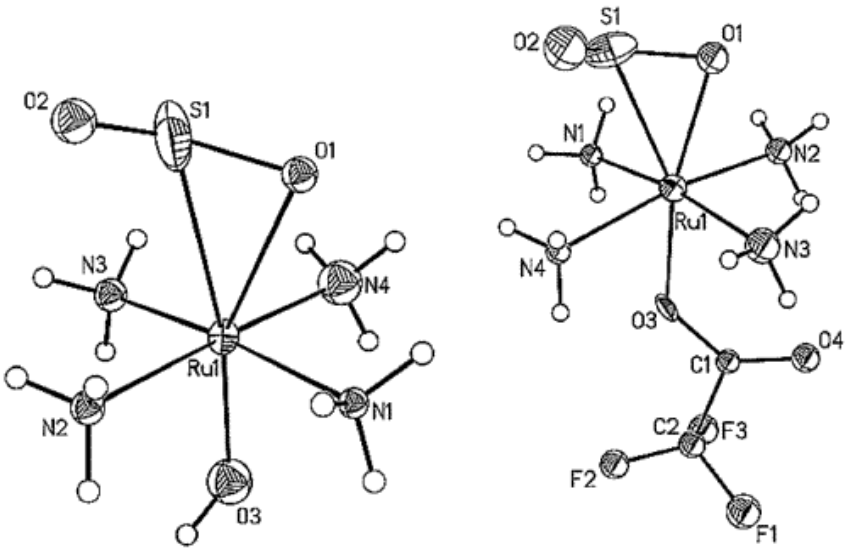

Figure 3.3 Solid state molecular structure of the ruthenium cation depicting the MS2 isomer in *trans*-$[Ru(NH_3)_4(SO_2)(H_2O)](Tos)_2$ (left) and *trans*-$[Ru(NH_3)_4(SO_2)(CF_3C(O)O)]CF_3C(O)O.CF_3C(O)OH$ (right)

From these two experiments it was apparent that metastable linkage isomerism is fairly common in complexes of Ru^{II} with sulphur dioxide ligands. It was postulated that the lifetimes of any metastable states formed could be lengthened by increasing the σ-donating ability of the trans ligand as well as by increasing the size of the counterion. There was also the indication from spectroscopic data that there was the presence of a the less stable MS1 species upon irradiation however the conclusion was made that the formation of this isomer was hindered by space restrictions in the crystal matrix.[2, 4]

This theory was disproved in 2006 by Bowes et al. who structurally characterised the MS1 isomer in crystals of *trans*-$[Ru(NH_3)_4(SO_2)(H_2O)](Tos)_2$ at 13K.[5] This was the first time that the η^1-OSO bonding mode had been observed in ruthenium coordination chemistry and was achieved using irradiation from a 200W tungsten lamp. The electron density difference map when modelled with the ground state coordinates showed residual electron density which corresponded to components of both MS1 and MS2

(figure 3.4). Both isomers were in fact disordered over two positions due to the C_{2v} symmetry of the ligated complex, and an overall total of *ca*. 44% excitation was achieved - 36% for the MS1 component and 8% for MS2. The separate components of the structure can be seen in figure 3.5 along with the complete overall structure.[5]

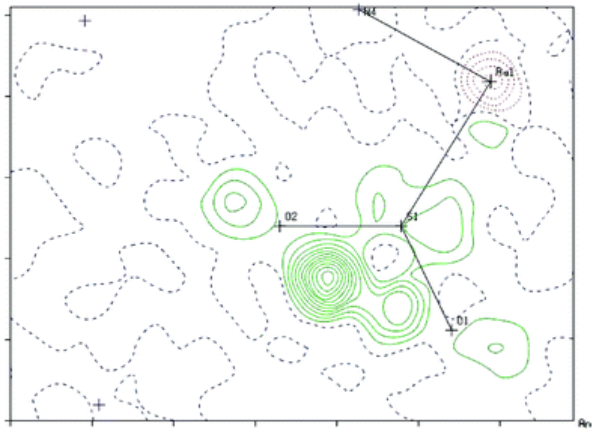

Figure 3.4 Electron density difference map with residual electron density owing to both MS1 and MS2 linkage isomers

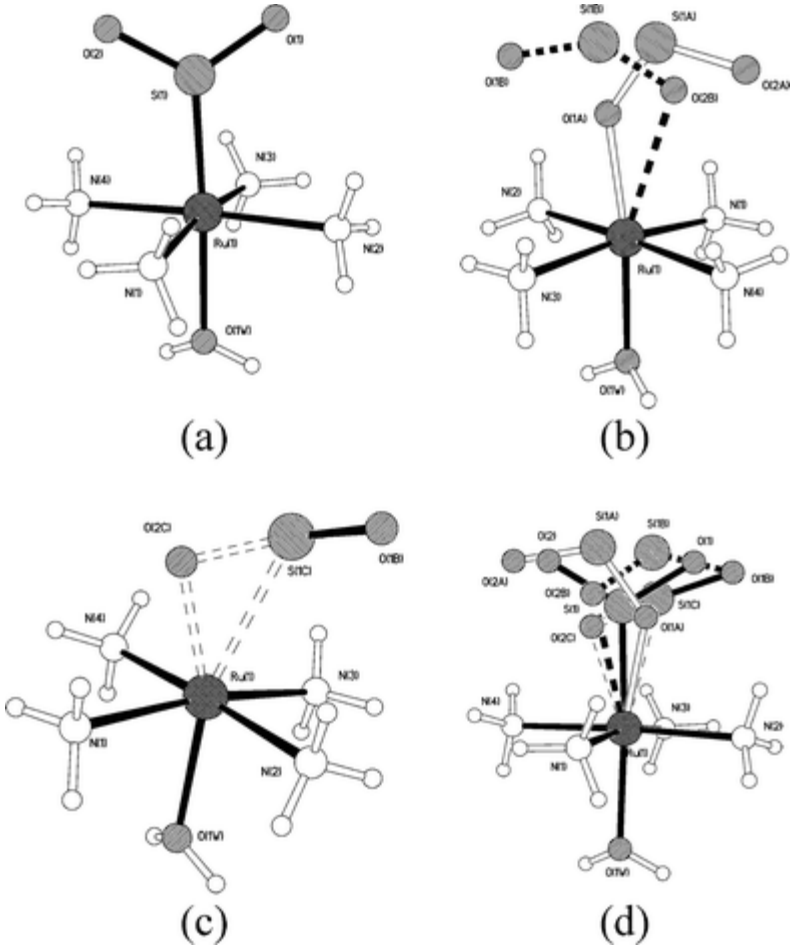

Figure 3.5 Structure of cationic component of *trans*-$[Ru(NH_3)_4(SO_2)(H_2O)](Tos)_2$ (a) ground state η^1-S bound SO_2 accounting for 56% of the structure (b) MS1 η^1-OSO with a total occupancy of 36% (c) main component of MS2 η^2-SO with 6% occupancy (d) overall structure showing all five contributions from the ground state, two from MS1 and two from MS2

3.2 Experimental Aims

The experiments within this chapter investigate the light induced linkage isomerism of the sulphur dioxide ligand within complexes of *trans*-$[Ru(NH_3)_4(SO_2)Cl]Cl$ and *trans*-$[Ru(NH_3)_4(SO_2)(H_2O)](Tos)_2$.

The main objectives are as follows:

- *To investigate and obtain evidence of linkage isomerism of the sulphur dioxide ligand in both complexes using powder diffraction.* Due to the restrictions involved in single crystal photocrystallographic experiments, particularly the risk of crystal fracture upon over excitation, powder diffraction experiments were attempted to see whether excitation was possible and if a higher percentage conversion would be observed.

- *To use DFT calculations to see whether theoretical results were in agreement with experimental observations.* From the results previously obtained in single crystal photocrystallographic experiments[5] and those published in the literature,[2, 4] DFT calculations were carried out to determine whether theoretical results reached the same conclusion as those obtained experimentally. If theoretical results were in good general agreement, this knowledge could then be applied for molecular design for future excitation experiments and also as a screening process to identify samples which may or may not isomerise.

3.3 Photocrystallography

3.3.1 Experimental

3.3.1.1 Data Collection

X-ray powder diffraction data were collected on Station 2.3 at the STFC Daresbury Laboratory synchrotron source. The details of hardware, software and equipment used are discussed in Chapter 6. The powder diffraction data was collected over three experimental allocation periods for a total of 8 days.

3.3.1.2 General Collection Procedure

Single crystals of the required sample were ground up into a fine powder. Grease was coated onto the outside of a capillary and then the capillary was rolled in the finely crushed sample to obtain an even coating. The decision to coat the sample on the outside of the capillary was made to obtain maximum percentage conversion upon irradiation in case the capillary tubes absorbed any of the radiation used to excite the sample. For ground state data collections a cover was placed over the sample in order to

eliminate as much light as possible and obtain an accurate ground state structure. Slits were carefully cut in the cover to allow X-rays through and the cryostream in to maintain the low temperature needed for data collection. The sample was then cooled to 150K and multiple scans set up between 2θ values of 5° and 60° using 0.01° steps at 2sec/step in order to obtain good quality data. The data was then combined and normalised to obtain a powder diffraction pattern.

To generate the metastable species, the cover was removed and a broadband white light source was employed to irradiate the sample as used in previous single crystal photocrystallography experiments.[5] The sample was irradiated for half an hour whilst being continuously rotated before the data collection was commenced. Again multiple scans between 2θ values of 5° and 60° using 0.01° steps at 2sec/step were set up and once these were completed three further scans between 2θ values of 30° and 60° were collected. The data was combined and normalised and then compared to the data obtained for the ground state to identify any differences.

3.3.1.3 Experimental Set-up

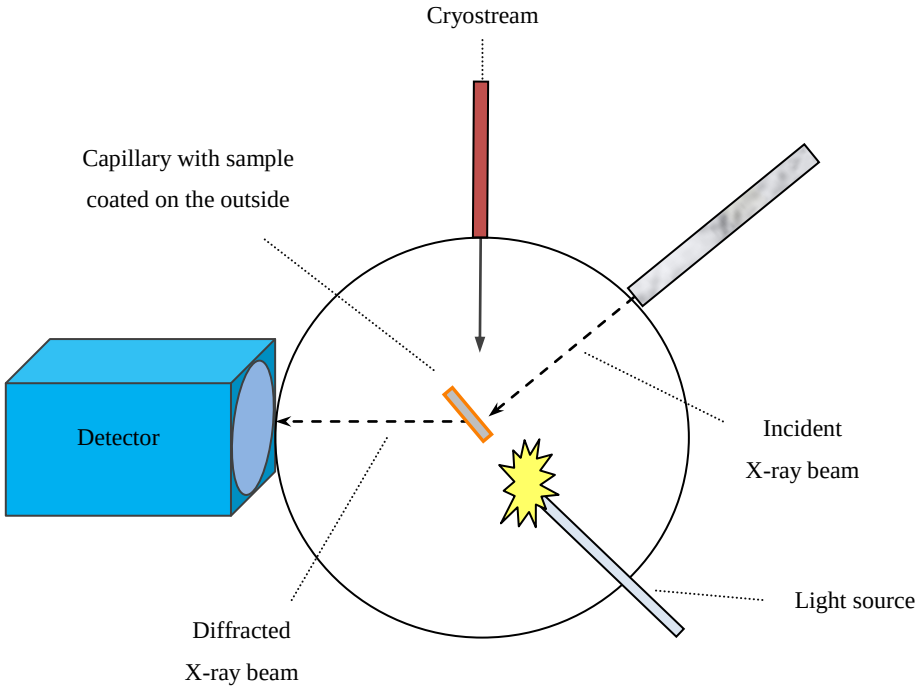

Figure 3.6 Schematic of experimental set-up

The general set-up for the photocrystallography experiment can be seen in figure 3.6. In order to generate the metastable state a broadband white light source was used and focused onto the sample. A cryostream was also in place to maintain the low temperatures required to populate the excited state species.

3.4 Results

Although the main focus of this chapter is to monitor metastable structures using powder diffraction and to compare experimental data with theoretical DFT calculations, it is important to obtain single crystal X-ray diffraction data to be used as a model.

3.4.1 *trans*-[Ru(NH$_3$)$_4$(SO$_2$)Cl]Cl

3.4.1.1 Single Crystal Data

A number of data collections were performed on red needle shaped crystals of *trans*-[Ru(NH$_3$)$_4$(SO$_2$)Cl]Cl using a Kappa CCD diffractometer. The crystals synthesised appear to be twinned and repeated recrystallisation attempts were unsuccessful in producing single crystals. Attempted refinements of the structure resulted in residual peaks of approximately 4.3Å^3 and 2.3Å^3 in the electron density map which were positioned near the metal centre. The solid state molecular structure as well as could be obtained from is shown below in figure 3.7 and a summary of crystal data can be seen in table 3.1. The metal cation has a distorted octahedral geometry with the sulphur dioxide ligand η^1-S coordinated to the ruthenium centre.

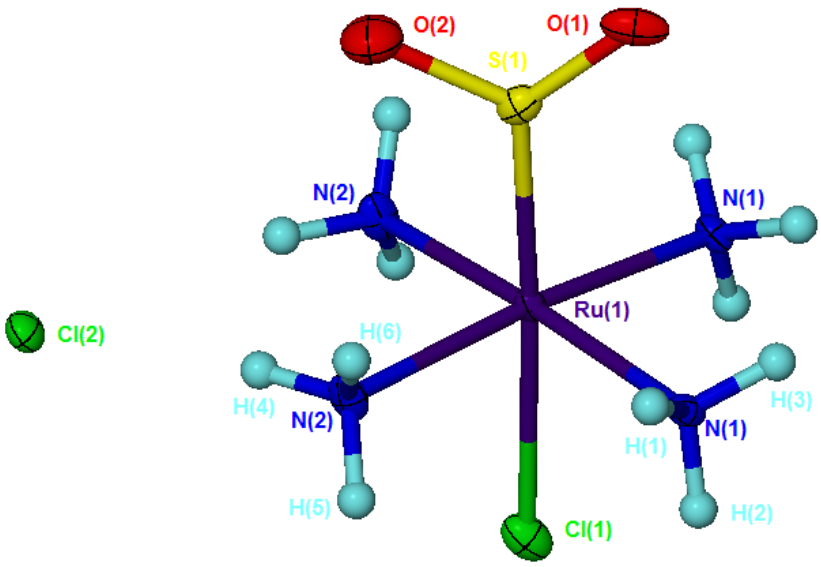

Figure 3.7 Solid state molecular structure of *trans*-[Ru(NH$_3$)$_4$(SO$_2$)Cl]Cl obtained from twinned data with 30% probability ellipsoids shown

Empirical Formula	$H_{12}\ Cl_2\ N_4\ O_2\ Ru\ S$
M_r	304.17
Temperature (K)	150(2)
Crystal System	Orthorhombic
Space Group	*Pmcn*
Wavelength (Å)	0.71073
***a* (Å)**	7.2430(4)
***b* (Å)**	9.2710(5)
***c* (Å)**	13.9710(8)
α (°)	90
β (°)	90
γ (°)	90
V ($Å^3$)	938.15(9)
Z	4
Absorption coefficient (mm^{-1})	2.421
Reflections collected	14661
Independent reflections	1164
R_{int}	0.1637
R_1, w*R*2	0.0597, 0.1400
***R* indices (all data)**	0.1209, 0.1656

Table 3.1 Summary of crystal data for *trans*-$[Ru(NH_3)_4(SO_2)Cl]Cl$

As a result of being unable to grow suitable crystals for single crystal photocrystallographic experiments, the decision was made to try and excite the sample as a powder.

3.4.1.2 Powder Diffraction Data

There are a few noticeable differences between the ground (blue) and excited state (black) powder patterns of *trans*-$[Ru(NH_3)_4(SO_2)Cl]Cl$ (figure 3.8). Upon excitation the powder diffraction pattern showed the formation of three new peaks at 2θ values of 17.5°, 20° and 31°. These new peaks could be due to the formation of a new product. There is also a change in the intensities of the 4 peaks that are present between the 2θ values of 26° and 27°.

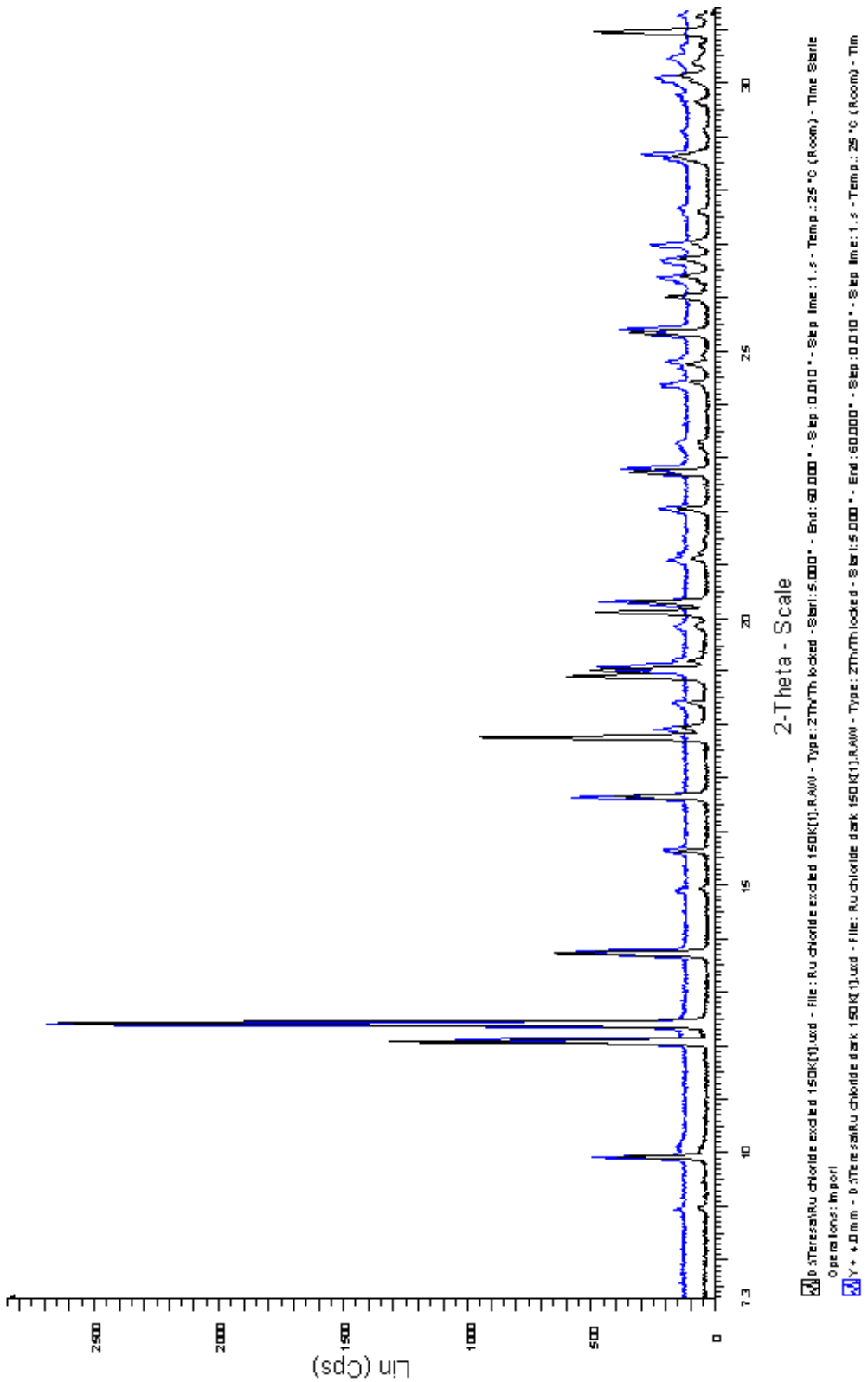

Figure 3.8 Ground state (blue) and excited state (black) powder patterns of *trans*-$[Ru(NH_3)_4(SO_2)Cl]Cl$

3.4.2 *trans*-$[Ru(NH_3)_4(SO_2)(H_2O)](Tos)_2$

3.4.2.1 Single Crystal Data

Single crystal X-ray diffraction measurements were made on an orange block shaped crystal of *trans*-$[Ru(NH_3)_4(SO_2)(H_2O)](Tos)_2$ (structure number h07prr14) with dimensions 0.09 x 0.05 x 0.03mm at 150(2)K on a Kappa CCD diffractometer. A summary of the crystal data can be seen in table 3.2 and the solid state molecular structure can be seen in figure 3.9.

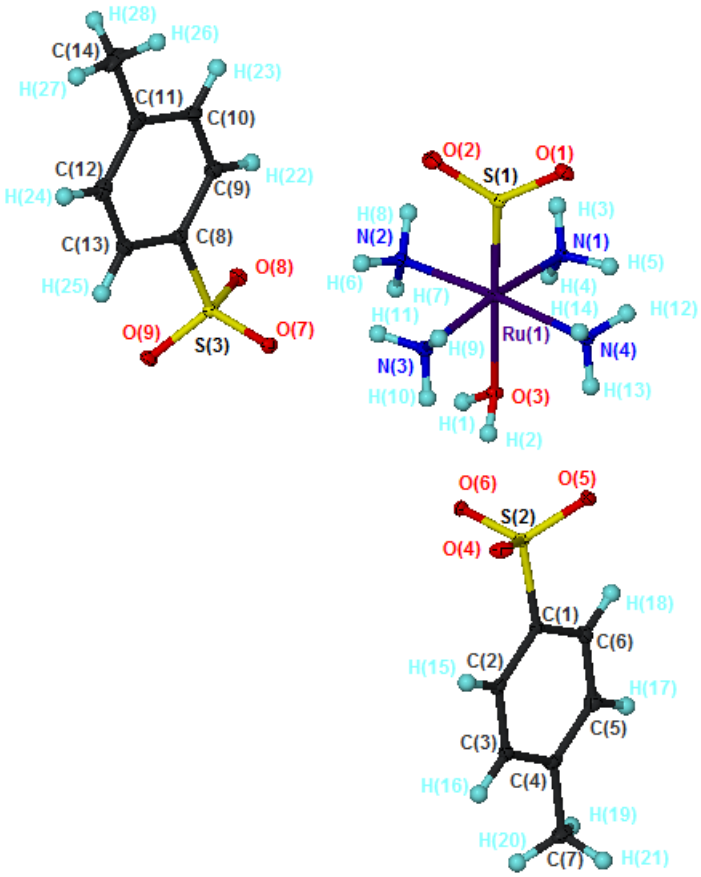

Figure 3.9 Solid state molecular structure of *trans*-$[Ru(NH_3)_4(SO_2)(H_2O)](Tos)_2$ with 30% probability ellipsoids shown

The solid state molecular structure consists of a ruthenium metal cation with two anionic tosylate groups. The ruthenium metal centre has an octahedral geometry with four ammine groups coordinated in equatorial positions. There is a sulphur dioxide group which is η^1-S bound and a water molecule coordinated in axial positions. The O_1-S_1-O_2 bond angle is 116.08(15)° with S_1-O_1 and S_1-O_2 bond distances are 1.440(2)Å and 1.441(2)Å respectively.

Hydrogen bonding is observed between the hydrogen atoms on the coordinated water molecule of the ruthenium cation and oxygen atoms on neighbouring SO_3 groups of the tosylate anions. There are also hydrogen bonds between protons on the ammine groups and the oxygen atoms of the SO_3 groups on

tosylate groups. The hydrogen bonding between adjacent cations and anions forms a sheet like structure (figure 3.10). These hydrogen bonds are of weak to moderate strength with distances between donor and acceptor atoms varying from 2.67Å and 3.29Å. The results obtained are in agreement with those reported in the literature.[4, 5]

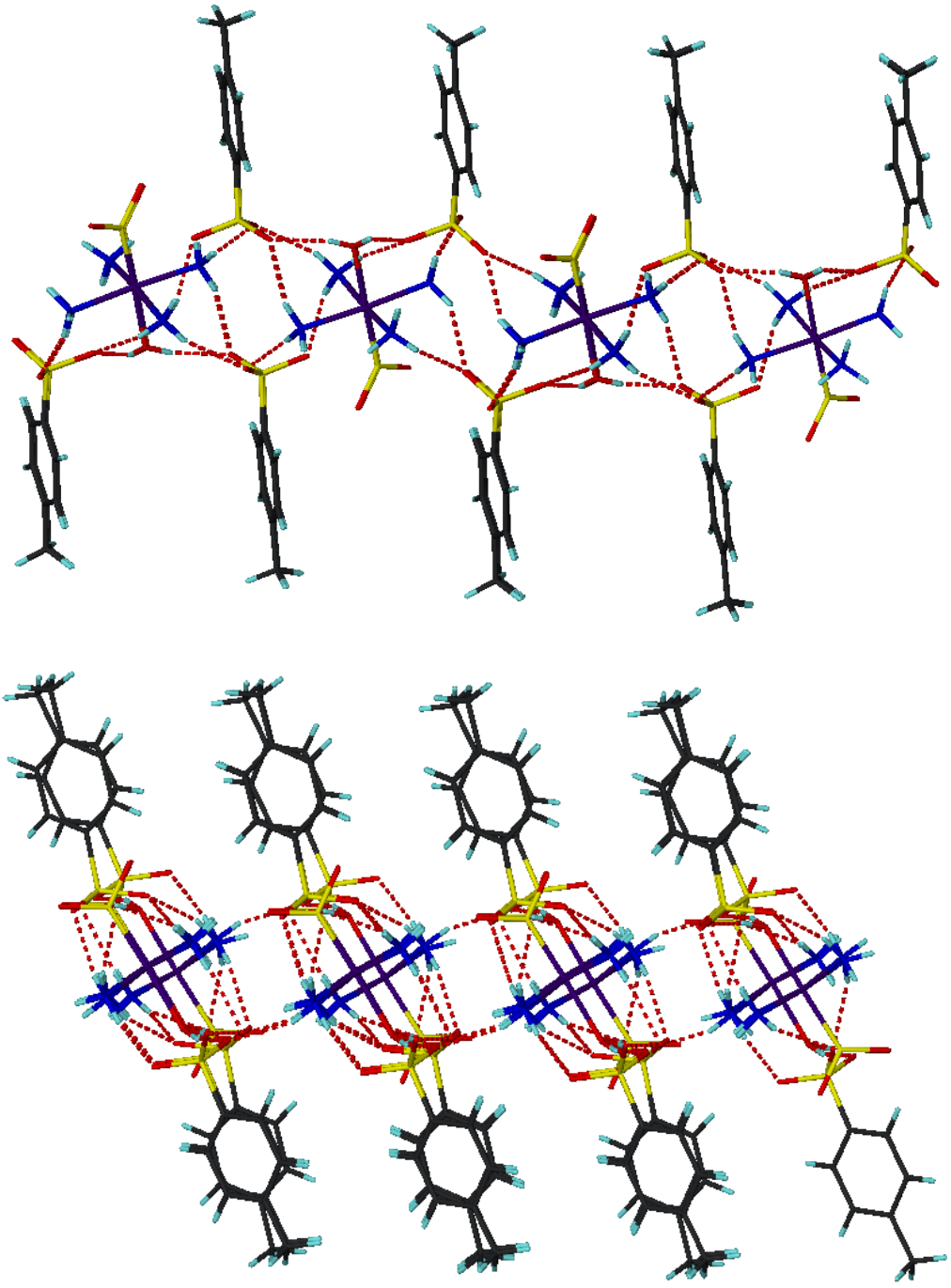

Figure 3.10 Hydrogen bonding of sheet layers in *trans*-$[Ru(NH_3)_4(SO_2)(H_2O)](Tos)_2$ from two different orientations

Empirical Formula	$C_{14}\ H_{28}\ N_4\ O_9\ Ru\ S_3$
M_r	593.65
Temperature (K)	150(2)
Crystal System	Triclinic
Space Group	*P*-1
Wavelength (Å)	0.71073Å
***a* (Å)**	6.6950(2)
***b* (Å)**	13.1000(5)
***c* (Å)**	13.6240(5)
α (°)	94.531(2)
β (°)	92.848(2)
γ (°)	103.542(2)
V (Å^3)	1155.17(7)
Z	2
Absorption coefficient (mm^{-1})	1.002
Reflections collected	14721
Independent reflections	6021
R_{int}	0.0681
R_1, w*R*2	0.0460, 0.0881
***R* indices (all data)**	0.0909, 0.1008

Table 3.2 Summary of crystal data for *trans*-$[Ru(NH_3)_4(SO_2)(H_2O)](Tos)_2$

3.4.2.2 Powder Diffraction Data

The ground (red) and excited (black) powder patterns for *trans*-$[Ru(NH_3)_4(SO_2)(H_2O)](Tos)_2$ are shown in figure 3.11. There does not appear to be any new peak formation upon excitation of the sample, however, there does appear to be slight shifts in peak positions and intensities; in particular for the peaks at 2θ positions of 20.5° and 22.5°. These minor changes in peak position are expected due to the small changes that are observed in the unit cell that occur when single crystals of *trans*-$[Ru(NH_3)_4(SO_2)(H_2O)](Tos)_2$ are excited.[4, 5]

Using the excited state structure of *trans*-$[Ru(NH_3)_4(SO_2)(H_2O)](Tos)_2$ obtained from previous experiments[5, 6] and the ground state structure (h07prr14) simulated powder patterns were generated and illustrated in figure 3.12. As well as generating a powder pattern for the ground state (green) and complete excited state structure (black), powder patterns were also simulated to look at the differences

between different excited state isomers by removing features pertaining to different conformers and refining the metastable state with 100% occupancy. The powder pattern in red relates to the metastable isomer which is η^2-S,O side bound to the ruthenium metal centre and the pattern in blue is the pattern for the endo η^1-O bound sulphur dioxide conformation.

What can be observed from the simulated patterns is that there does not appear to be any major differences present between the different powder patterns when moving from one conformer to the next. However, as shown for the photocrystallographic powder experiment, there are shifts in peak positions and intensities of some peaks.

Unfortunately so far it has not been possible to index the powder patterns obtained to confirm the change in unit cell and hence the change in coordination of the sulphur dioxide ligand.

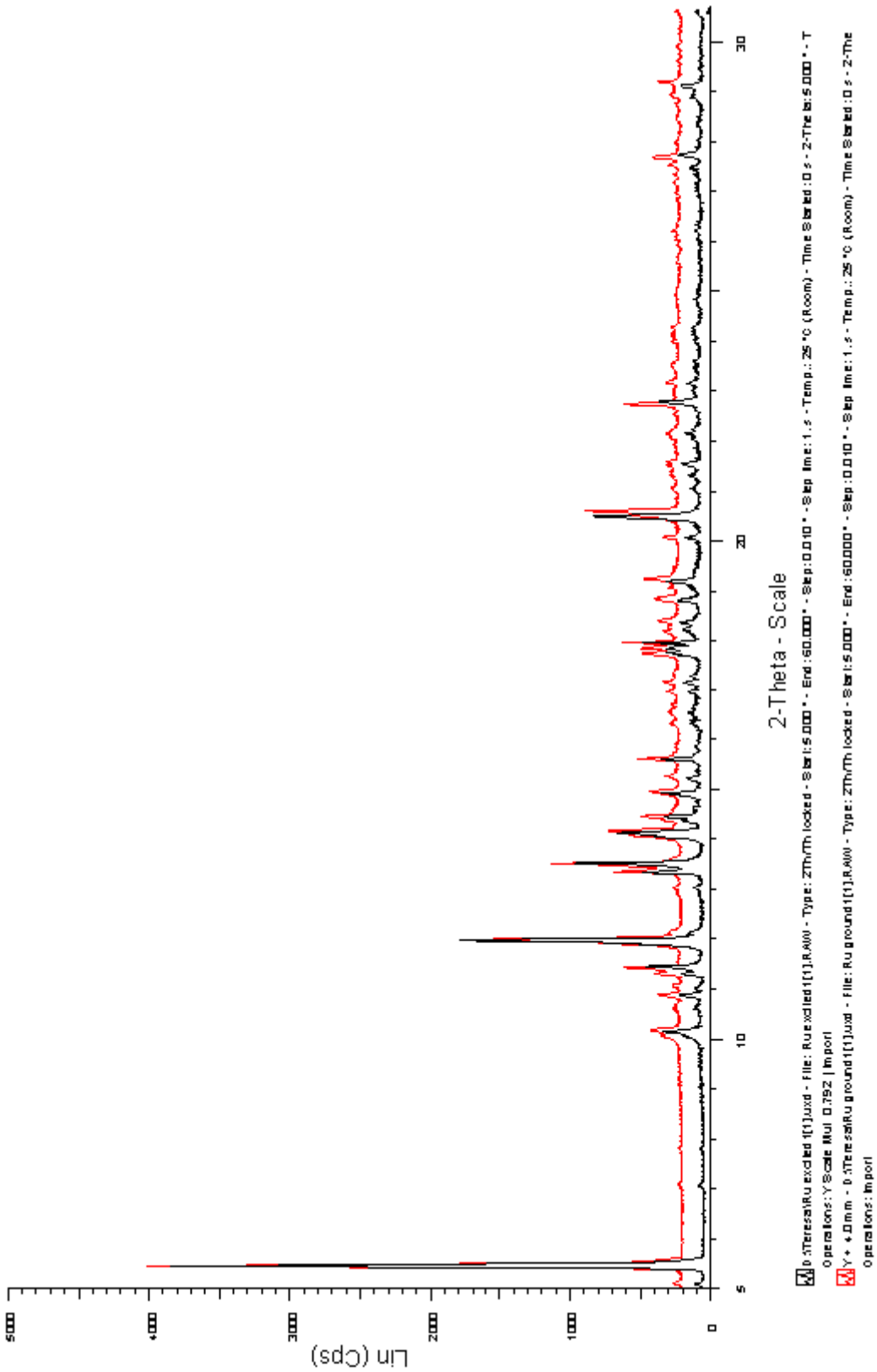

Figure 3.11 Ground state (red) and excited state (black) powder patterns of *trans*-$[Ru(NH_3)_4(SO_2)(H_2O)](Tos)_2$

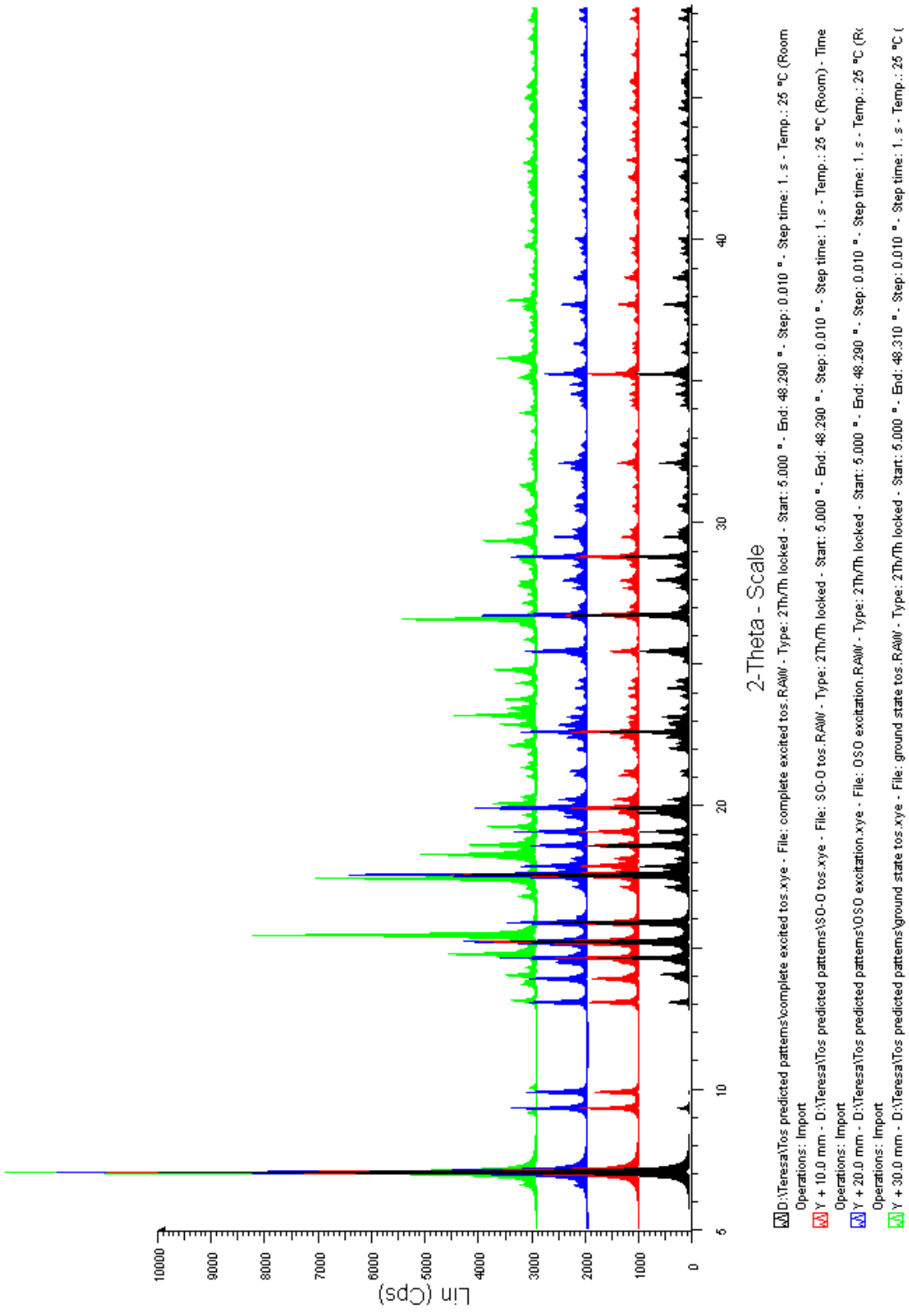

Figure 3.12 Simulated powder patterns for different conformers of *trans*-$[Ru(NH_3)_4(SO_2)(H_2O)](Tos)_2$

3.5 DFT Calculations

DFT calculations were performed to examine the electronic structural behaviour of compounds which undergo linkage isomerisation transformations of the sulphur dioxide ligand. The experimental process follows that described here in this section and further experimental details can be found in Chapter 6.4. Geometry optimisation was performed on the cation - $[Ru(NH_3)_4(SO_2)(H_2O)]^{2+}$ **(A)** (Figure 3.13), using the coordinates from the solid state molecular structure of the complex $[Ru(NH_3)_4(SO_2)(H_2O)](Tos)_2$,[4] as a starting point. Selected bond lengths and angles for **A** are summarised in table 3.3, which can be compared to the corresponding solid state molecular structure determined using single crystal X-ray crystallography.

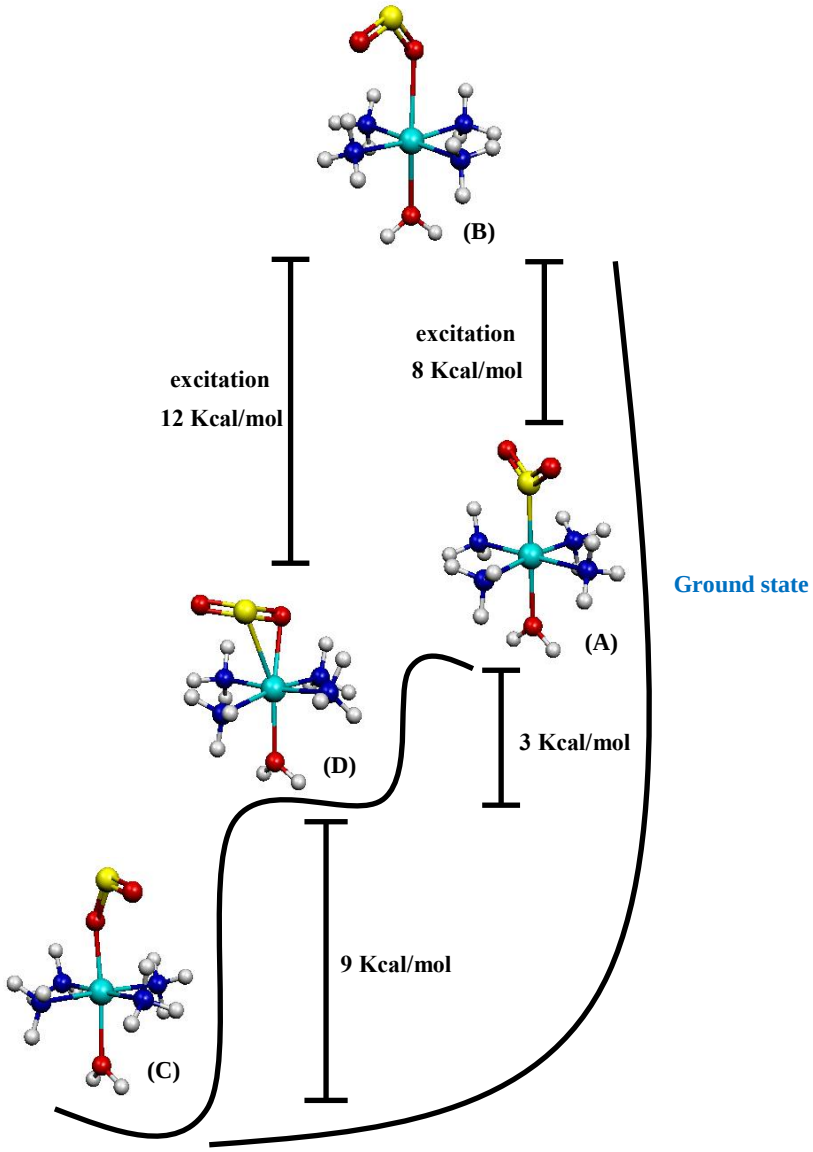

Figure 3.13 Relative energies of the different states of $[Ru(NH_3)_4(SO_2)(H_2O)](Tos)_2$

While quantitative agreement between the observed and calculated data is not expected due to the nature of the calculations and structural approximations involved, the optimised geometry of **A** is in good general agreement with the experimentally observed structural trends which allows for a high degree of confidence in the accuracy of the computations, and the conclusions drawn from them.

The geometry optimised structure of **A** presented the same gross structure as the experimentally determined structure,[4] with the Ru-N bonds having an average of 2.195Å (c.a. 2.141Å for the crystallographically determined structure). The angle between O_7-S_5-O_6 was found to be 121.7° which is slightly larger to that found in the solid state structure which has an angle of 116.06(9)°.

An analysis of the orbital structure of **A** reveals a metal based orbital for the HOMO, while the LUMO consists of an orbital with contributions from the metal centre as well as a major contribution arising from the sulphur dioxide ligand (figure 3.14). Interestingly the orbitals lower in energy than the HOMO all consist of interactions between the metal centre and the sulphur dioxide ligand.

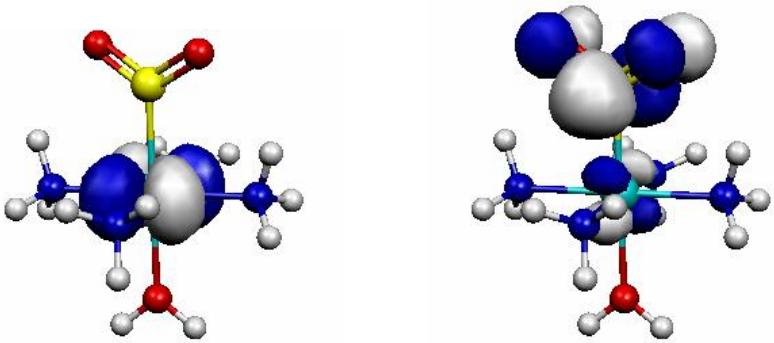

Figure 3.14 Molecular orbitals of **A**

In order to simulate the excitation events of the single crystal X-ray photocrystallography experiments, the multiplicity of **A** is increased from the ground state singlet to the excited state triplet (i.e. from 1 to 3) and the structure geometry re-optimised, resulting in the formation of $[Ru(NH_3)_4(OSO)(H_2O)]^{2+}$ - **(B)** (figure 3.13). This ruthenium metal centre is bonded to the sulphur dioxide ligand via the oxygen atom and is found to be 8 Kcal/mol higher in energy than **A**. The angle between O_7-S_5-O_6 is 114.4° which is a decrease to that found in **A**, while the angle between S_5-O_6-Ru_1 was found to be 138.7°.

When **B** is relaxed back to the ground state and the structure optimised again, a new structure, $[Ru(NH_3)_4(OSO)(H_2O)]^{2+}$ **(C)** (figure 3.13) is obtained. The structures of **B** and **C** are very similar, however they differ in energy by approximately 20Kcal/mol. There are also differences in the bond lengths of the two isomers (c.f. table 3.3). The Ru-N bond lengths for **C** average out at 2.19Å, while those

for **B** average out at 2.21Å. The most significant geometrical differences are found for the angle S_5-O_6-Ru_1 which is only 128.3° for **B** but 138.7° for **C** and the bond length Ru_1-O_6 which is 2.655Å in **B** and 2.076Å in **C**.

An analysis of the molecular orbital structure of **C** reveals a LUMO (figure 3.15) which is virtually identical to that found for **A** (cf. figure 3.14). The HOMO of **C** consists of an orbital interaction between the metal centre and a minimal contribution arising from the sulphur dioxide ligand, though there is no contribution from the oxygen atom bound to the ruthenium metal centre.

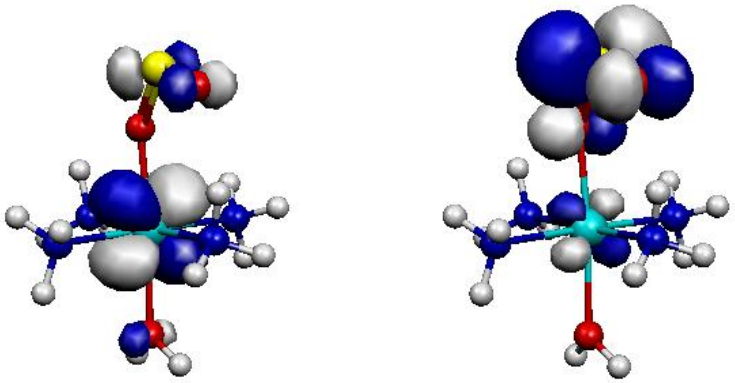

Figure 3.15 Molecular orbitals of **C**

The structures of **B** and **C** correspond to coordination mode (v) (figure 3.1) of the sulphur dioxide ligand.[2] The change in structure with the change in multiplicity is also in accordance with the postulated reaction scheme based on photochemical experimental results (figure 1.14 Chapter 1).[3]

A transition state structure calculation was carried out, to determine whether there was a reaction pathway between **A** and **C**, due to their difference in energy (ca. 12Kcal/mol). The transient species $[Ru(NH_3)_4(\eta^2\text{-}SO_2)(H_2O)]^{2+}$ **(D)** was identified. **D** exhibits the η^2-S,O side bound geometry, where both the sulphur and one of the oxygen atoms of the sulphur dioxide ligand are bonded to the ruthenium centre (figure 3.13) The structure obtained for **D** is 3Kcal/mol lower in energy compared to **A**, but approximately 9Kcal/mol higher in energy than **C**.

The optimised structure of **D** is very similar to a geometry optimised structure of the partial solid state molecular structure obtained during single crystal photocrystallography experiments on $[Ru(NH_3)_4(SO_2)(H_2O)](Tos)_2$,[2, 5]. When the multiplicity of **D** is increased from one to three and the geometry optimised, the structure obtained is **B** which is 12Kcal/mol higher in energy than **D**. When the multiplicity of **B** is relaxed back from three to one and the structure re-optimised, this again resulted in the structure obtained for **C**.

Table 3.3 Bond lengths(Å) and angles(°) for $[Ru(NH_3)_4(SO_2)(H_2O)]^{2+}$

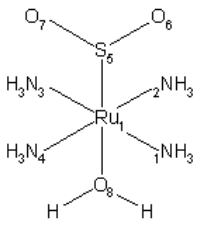	**Solid state molecular structure**	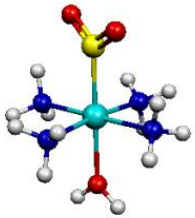 **A**	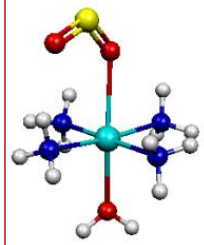 **B**	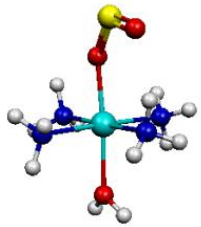 **C**	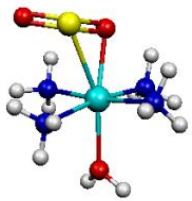 **D**
Ru_1-N_1	2.213	2.190	2.215	2.196	2.210
Ru_1-N_2	2.114	2.201	2.214	2.203	2.215
Ru_1-N_3	2.120	2.189	2.208	2.185	2.199
Ru_1-N_4	2.117	2.201	2.214	2.198	2.196
Ru_1-S_5	2.085	2.209	-	-	2.311
Ru_1-O_6	-	-	2.655	2.076	2.435
Ru_1-O_8	2.101	2.220	2.494	2.185	2.201
S_5-O_6	1.448	1.460	1.482	1.515	1.411
S_5-O_7	1.446	1.460	1.463	1.465	1.525
O_7-S_5-O_6	116.06	121.7	114.7	114.4	125.3
S_5-O_6-Ru_1	-	-	128.3	138.7	83.5

3.6 Discussion and Conclusion

The photocrystallographic powder diffraction experiments resulted in some changes between ground and excited state patterns. For *trans*-$[Ru(NH_3)_4(SO_2)Cl]Cl$ the formation of some new peaks were observed upon excitation as well as a few changes in peak intensity. Unfortunately as there was no single crystal X-ray photocrystallographic experiments performed on the sample, (due to the fact that crystals synthesised were all twinned) no simulated powder patterns could be obtained to see what changes may occur upon excitation and hence determine whether excitation was successful.

For *trans*-$[Ru(NH_3)_4(SO_2)(H_2O)](Tos)_2$ no new peak formation was observed upon irradiation of the crystalline sample, however there were some slight shifts in positions and intensities of peaks. Predicted powder patterns generated from solid state molecular structures obtained on previous experiments however, also demonstrated that upon excitation that only minor changes were observed in powder diffraction patterns. It is highly possible that excitation of the powder sample has been successful, however without being able to index the patterns it is not possible to determine to what extent excitation has occurred.

The samples for powder experiments were coated on the outside of capillaries in order to try and maximise the percentage conversion achieved upon excitation. The only downside to this methodology is that the samples are water soluble so some slight impurities may occur as a result of formation of ice on the sample. Samples were therefore monitored regularly to guarantee no ice build-up ensued.

From these experiments it can be concluded that linkage isomerism could be monitored with the use of powder diffraction as it can be seen that changes occur upon irradiation of the samples by the changes in intensities and peak positions going from ground to excited state. This is encouraging and with further developments it may be possible to use powder diffraction as a method of determining metastable state structures. As a negative point however, with samples that do not isomerise 100% from ground to excited state, any changes in unit cell may go unnoticed via powder diffraction methods as only a minor change in percentage of the overall powder pattern will occur. For example a sample that excites to around 20% upon irradiation would have 80% of features pertaining to the ground state species and the powder pattern may appear unchanged overall.

From the DFT results obtained, it can be concluded that changes observed in theoretical calculations are in good agreement with solid state molecular structures determined experimentally.[2, 5] As mentioned previously, quantitative agreement between the observed and calculated data is not expected due to the nature of the calculations as computations are performed on systems in the gas phase and generally speaking molecules tend to behave differently depending on their physical states. The results

obtained also confirm the postulated reaction scheme proposed by Johnson and Dew,[3] as seen in Chapter 1, figure 1.14.

The DFT calculations however show **C** which is η^1-O bound to the ruthenium metal centre to be the most thermodynamically stable product, however there is no evidence for this. This may reflect the limitations of the energies calculated in the DFT program as energies might have errors of $\pm$ 2Kcal/mol.

As this technique seems to be accurate in identifying linkage isomerism reactions, it would be sensible to screen suitable candidates for photocrystallographic experiments prior to synthesis to test their suitability. DFT could also aid in identifying isomers that may form in preference over others. This may help in the identification process when more than one isomer forms in a single crystal X-ray photocrystallographic experiment and residual peaks in the electron density map are not very strong.

3.7 References

[1] P. Coppens, I. V. Novozhilova, A. Y. Kovalevsky, *Chem. Rev*. **2002**, *102*, 861.
[2] A. Y. Kovalevsky, K. A. Bagley, P. Coppens, *J. Am. Chem. Soc.* **2002**, *124*, 9241.
[3] D. A. Johnson, V. C. Dew, *Inorg. Chem.* **1979**, *18*, 3273.
[4] A. Y. Kovalevsky, K. A. Bagley, J. M. Cole, P. Coppens, *Inorg. Chem.* **2003**, *42*, 140.
[5] K. F. Bowes, J. M. Cole, S. L. G. Husheer, P. R. Raithby, T. L. Savarese, H. A. Sparkes, S. J. Teat, J. E. Warren, *Chem. Commun.* **2006**, 2448.
[6] H. A. Sparkes, *Solid State X-Ray Structural Studies*, University of Bath, Dept. of Chem., **2005**.

Chapter 4

Nitrite Linkage Isomers

4.1 Introduction

The ambidentate nature of the nitro group has been well established for over a century. As discussed in Chapter 1, linkage isomerism was initially discovered by Alfred Werner when he studied the various coordination modes of the nitro ligand. There are several possible coordination modes for the nitro group as seen below in figure 4.1.[1] Of these coordination modes only structures (v) and (vi) have not been conclusively identified; all others have been characterised using X-ray diffraction techniques.[1]

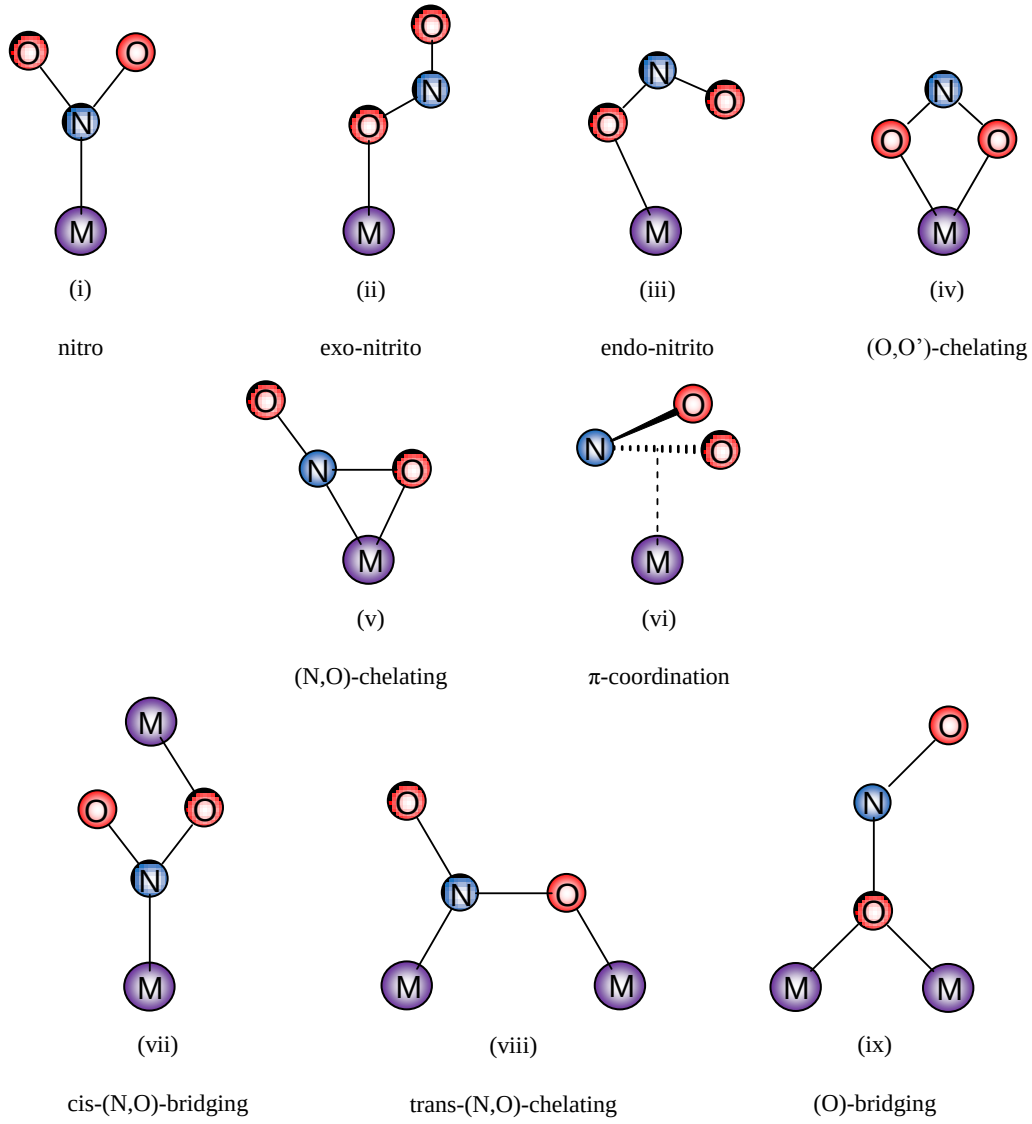

Figure 4.1 Coordination modes of the nitro group

Jørgenson later identified that nitrito isomers could be synthesised not only directly in solution, but also by irradiation of the analogous solid nitro isomers.[2] This research was confirmed by Adell in 1955, by demonstrating that the yellow nitro complex of $[Co(NH_3)_5(NO_2)]Cl_2$ would transform into the red nitrito *O*-bound isomer when left exposed in sunlight for a substantial period of time (figure 4.2).[3] Since these discoveries a vast amount of research has been undertaken into understanding the properties of nitrite photo-induced isomers.[4]

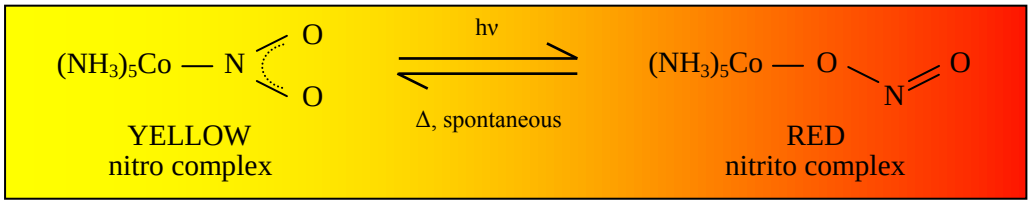

Figure 4.2 Isomerisation reaction of $[Co(NH_3)_5(NO_2)]Cl_2$

An investigation into the differences between chemically synthesised $[Co(NH_3)_5(ONO)]Cl_2$,[5] with samples obtained via irradiation of the corresponding nitro isomer using a tungsten lamp concluded that these nitrito complexes could be synthesised directly, however had the tendency to isomerise both in solution and in the solid state to the more stable nitro form. Prior to this study, nitrite complexes had only been observed via the synthetic route with Cr^{III} complexes, due to its preference for O-donor atoms.[6]

Powder diffraction patterns (figures 4.3a and b) illustrate a gradual shift in peak positions as well as a difference in peak intensities, hence confirming a change in cell dimensions over time.[5] Both the thermal nitrito to nitro and the reverse reaction occur with the retention of crystallinity, however the powder pattern for the photo-induced product differs to that of the chemically synthesised crystals. This lead to the hypothesis the thermal reaction occurred via a two-step process.[5]

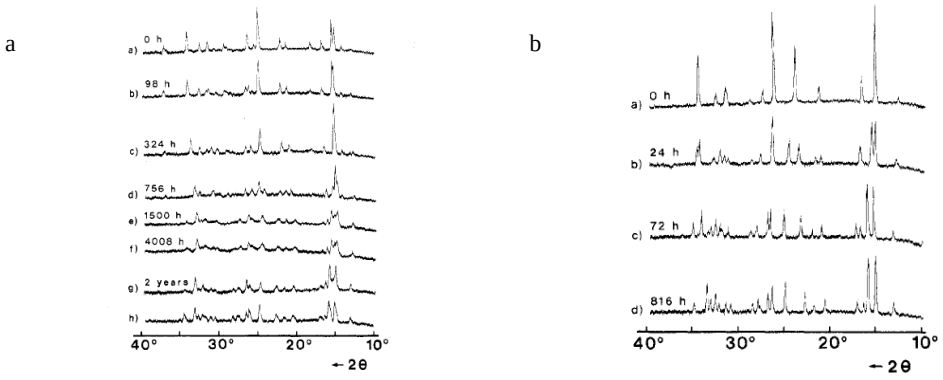

Figure 4.3 Powder diffraction patterns illustrating reactions:
(a) $[Co(NH_3)_5(ONO)]Cl_{2(s)}$ (synthetic product) →$[Co(NH_3)_5(NO_2)]Cl_{2(s)}$ (unstable) → $[Co(NH_3)_5(NO_2)]Cl_{2(s)}$ (stable)
and (b) $[Co(NH_3)_5(ONO)]Cl_{2(s)}$ (photochemical product) →$[Co(NH_3)_5(NO_2)]Cl_{2(s)}$[5]

A low temperature single crystal diffraction study was also performed on $[Co(NH_3)_5(NO_2)]Cl_2$ as a method used to identify the nature of the nitrito group. The nitro complex was irradiated using an unfiltered 150W Xe lamp, and the photo-activation achieved a population of approximately 15% of the nitrito complex seen below (figure 4.4).[7]

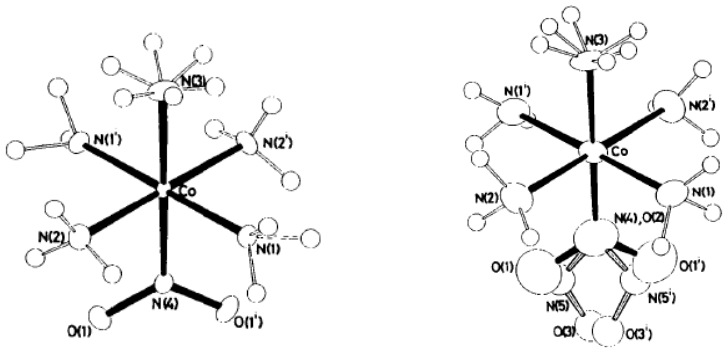

Figure 4.4 ORTEP diagrams of nitro and combined nitro and nitrito $[Co(NH_3)_5(NO_2)]^{2+}$ with 50% probability ellipsoids

Balzani et al. carried out a study on a related complex – $[Co(NH_3)_5(NO_2)](NO_3)_2$ in order to clarify some of the experimental and theoretical aspects of its photochemistry.[8] Results confirmed that solid state irradiation using a broadband light source at room temperature, converted the metal complex from the nitro to the nitrito isomer. IR spectra from irradiated Nujol mulls showed bands present at 1430, 1315 and 825cm^{-1}, all underwent a progressive decrease in peak intensity, while new bands appeared at 1460 and 1065cm^{-1}, corresponding to the *O*-bound isomer. Upon irradiation of the Nujol mulls, almost 100% conversion of nitro to nitrito was achieved; however the nitrito complex did not appear to be thermodynamically stable. When the nitrito form was placed in the dark at room temperature, a back reaction occurred resulting in a final IR spectrum which looked identical to that of the nitro complex.[8]

The first reported evidence of synthesis and characterisation by single crystal X-ray diffraction of linkage isomers of both nitro and nitrito complexes of nickel(II) was in 1998.[9] Previous evidence of the existence of these isomers had been postulated for a few nickel(II) nitrite amine complexes with bulky substituents. Further investigation however, concluded that these complexes were more likely to contain a chelating and a non bonding nitrite.[10, 11] Das et al. successfully synthesised and characterised stable forms of monodentate nitro and nitrito isomers of nickel(II) complexes with 1-(2-aminoethyl)piperidine.[9] As both isomers crash out of solution together, it suggested a delicate equilibrium between steric and electronic factors to allow both nitro and nitrito forms to be isolated in the solid state.[12] They have since reported on a series of related complexes where various nitro isomers (including complexes where the nitro ligand is chelating) have been identified, although not always characterised by single crystal X-ray diffraction experiments.[9, 12-15]

4.2 Experimental Aims

The experiments within this chapter investigate the light induced linkage isomerism of the nitrite ligand within complexes of $[Ni(L)_2(NO_2)_2]$ where L = 1-(2-aminoethyl)piperidine (aep), 4-(2-aminoethyl)morpholine (aem) and 1-(2-aminoethyl)pyrrolidine (aepy).

The main objectives are as follows:

- *To investigate and obtain evidence of linkage isomerism of the nitrite ligand within* $[Ni(aep)_2(NO_2)_2]$. Due to the delicate equilibrium noted in the synthesis of isomeric forms of $[Ni(aep)_2(NO_2)_2]$[9] a small energetic difference between both nitro and nitrito species is expected. Photocrystallographic experiments will be undertaken in order to identify whether the isomerisation process from nitro to nitrito is possible in the solid state using a light source to convert between various forms. If any linkage isomers are shown to be present experiments to see whether the species are metastable will be carried out.

- *To obtain evidence of linkage isomerism in related systems* $[Ni(aem)_2(NO_2)_2]$ *and* $[Ni(aepy)_2(NO_2)_2]$. It is feasible that closely related structures will behave in a similar if not identical fashion upon photo excitation. The analogous aem and aepy complexes to the $[Ni(aep)_2(NO_2)_2]$ species will be investigated for photocrystallographic evidence of linkage isomerism upon excitation. Again if isomerisation is successful, the isomers will be tested to see if they are metastable.

- *To investigate the temperature range of metastable states*. If metastable states are identified data collections will be performed in order to determine the temperature limitations of the metastable states present in the complexes.

4.3 Photocrystallography

4.3.1 Experimental

4.3.1.1 Data Collection

Single crystal X-ray diffraction data were collected on Station 9.8 at the STFC Daresbury Laboratory synchrotron radiation source (SRS). The details of hardware, software and equipment used are discussed in Chapter 6. The data presented within this chapter was collected over several experimental allocation periods for a total of around 40 days. Approximately 220 data sets were collected and analysed. The structures were sequentially numbered using the form Bath 123 where 123 represents the structure number. A summary of the crystallographic data for each of ground and ‘excited’ structures discussed in

this chapter are included in tables 4.15, 4.16 and 4.17 at the end of this chapter. A list of bond lengths and angles for all structures discussed can be found in Appendix 7.2.

4.3.1.2 General Collection Procedure

A low temperature data set is collected in the dark, eliminating as much external light as possible, to obtain an accurate initial 'ground state' structure. The crystal is subsequently irradiated at the appropriate wavelength whilst continually rotating and being maintained at low temperature. This allows the metastable state to build up gradually. The amount of time required to generate the transient species varies from sample to sample and so during the excitation period several datasets are collated using the same experimental conditions as for the ground state. Once the excitation appears to have reached a maximum the light source is removed while maintaining the same low temperature conditions. A further data collection is performed on the sample, again using the same strategy as for the ground state collection so that heating effects can be eliminated. Using the combined data, refinement is carried out using the ground state coordinates, and additional features should appear in the electron density map which correspond to the metastable structure. The crystal is then flash warmed to ensure the metastable state is quenched, and a further ground state collected to confirm all excitation has dissipated.

It is important to note that this methodology only works if the metastable state lasts without appreciable decay over the lifetime of the data collection, which can be anywhere between 40 mins to 1½h.

4.3.1.3 Experimental Set-up

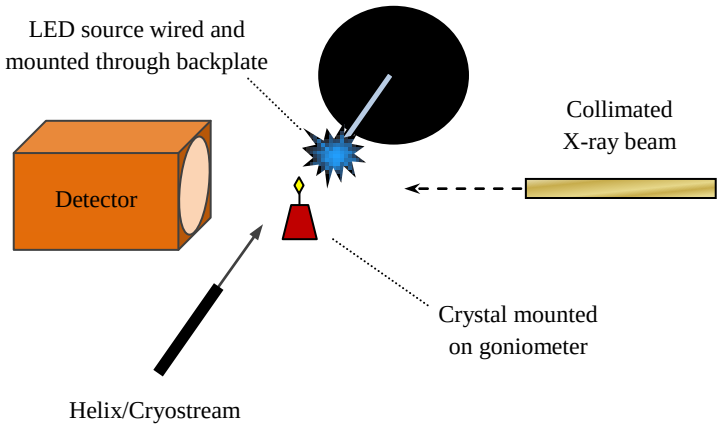

Figure 4.5 Schematic of experimental set-up

The experimental set-up can be seen in figures 4.5 and 4.6. The light source used in these experiments was a bunch of four LEDs wired through a metal tube, mounted onto the back-plate behind

the crystal as can be seen in figure 4.7. The advantages of using LEDs as a light source means specific wavelengths of irradiation can be selected for excitation. They are also cheap, and do not have the safety issues associated with a high power laser. Previous experiments involved the use of a broadband white light-source, however no change in structure was observed. Both the light source and the helix/cryostream were attached to electronic circuits allowing them to be operated from outside the hutch if necessary to avoid disturbing the experimental area.

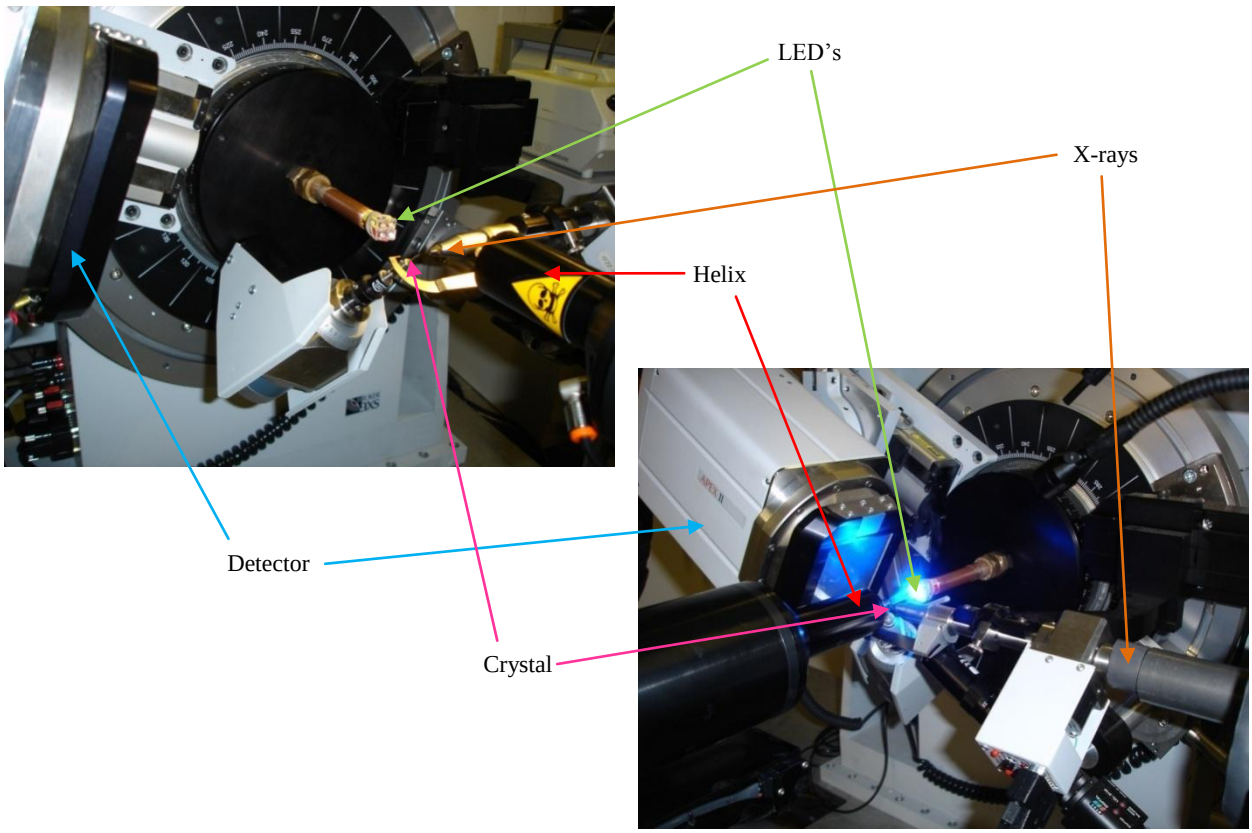

Figure 4.6 Experimental set-up on Station 9.8 with LEDs off (top) and on (bottom)

Figure 4.7 LED's wired through metal tube mounted onto back-plate

4.3.1.4 Analysis of Results

A couple of points need to be considered before a closer analysis of the experimental results is undertaken. The first is that the percentage excitation achieved for these experiments was determined solely via crystallography and has not been confirmed using any other analytical technique. This allows the results to be comparable between experiments, however any values may not be absolute due to the correlation between atomic occupancies and their displacement parameters. The second point for consideration is that an accurate comparison of bond lengths is not possible. This is due mainly to the large amounts of disorder within the nitro group fragments in the excited state, as well as the relatively low levels of excitation for some of the metastable isomers obtained in some of the experiments.

4.4 Results

4.4.1 $[Ni(aep)_2(NO_2)_2]$

4.4.1.1 Collection Strategy and Excitation Results

As mentioned in the introduction to this chapter both nitro and nitrito isomers of $[Ni(aep)_2(NO_2)_2]$ can be chemically synthesised.[9] Both isomers crash out of a methanolic solution, the major product being the purple nitro form. A solution of $[Ni(aep)_2(NO_2)_2]$ was irradiated in the dark using a UV lamp over two days and the majority of crystals which deposited from the solution were blue in colour. These crystals were found to be the nitrito isomer. It was postulated therefore that this isomerisation could possibly occur in the solid state and the sample was suitable for a photocrystallographic experiment.

Initial photocrystallographic experiments proved unsuccessful. The sample was irradiated at 30K with a broad-band white light source, a methodology that had proved successful for SO_2 complexes,[16] and no change in structure was observed. The light source was then switched for two UV LEDs that emit just above 400nm - one mounted behind the sample and the other aligned along the helix using a fibre optic to focus on the sample. Again at 30K no change in structure was observed. A final attempt with the UV LEDs at 100K resulted in two new Q-peaks in the electron density map in the plane around the nitro group after two hours irradiation. These peaks were assigned as a new endo-*O*-bound isomer, with Ni-O and O-N bond distances comparable with the chemically synthesised exo-nitrito species. The metastable isomer accounted for approximately 10% of the solid state structure.

Further experiments were carried out on the $[Ni(aep)_2(NO_2)_2]$ sample, however the UV LEDs were substituted for blue LEDs which emit at 467nm with a far greater intensity. The experimental set-up illustrated in figures 4.5 and 4.6 was employed for all further experimentation. A summary of the data collected can be seen in tables 4.1, 4.2 and 4.3. When the excitation appeared to have maximised, the

temperature was lowered to 30K to try and trap more of the metastable species. However, any excitation that had previously been observed disappeared. When the sample was subsequently warmed back to 100K it appeared that in fact the metastable species had been quenched and needed repopulating. Initial experimentation with temperature variation is summarised in Table 4.1.

Sample Number	Irradiation Time (min)	Temperature (K)	Type of Excitation	Total % Excitation
Bath 412	0 – ground state	100	-	0
Bath 417	420	100	Endo-nitrito	8
Bath 418	480	100	Endo-nitrito	9
Bath 419	540	30	No visible excitation	0
Bath 420	0	100	-	0
Bath 421	60	100	Peaks observed but too small to model	0
Bath 422	120	100	Endo-nitrito	8.5
Bath 423	180	120	No visible excitation	0
Bath 424	60	100	Peaks observed but too small to model	0
Bath 425	180	100	Peaks observed but too small to model	0
Bath 426	300	100	Endo-nitrito	7
Bath 427	360	90	Endo-nitrito	7
Bath 428	420	80	Endo-nitrito	7.5

Table 4.1 Excitation of $[Ni(aep)_2(NO_2)_2]$

After excitation had achieved a similar level as had been observed previously at 100K the decision was taken to perform a full temperature variation study to identify the temperature limitations of the metastable isomeric state. Initially the temperature was dropped to 90K and then 80K to see if any change in the percentage excitation was observed (Table 4.1). After it was shown to affect the percentage excitation, the temperature was ramped back to 100K and a complete study was performed from 100K to 30K with a rate of cooling of 10K/hour. The results are shown below in table 4.2. The excitation appeared to reach a maximum between 80 and 90K.

Sample Number	Irradiation Time (min)	Temperature (K)	Type of Excitation	Total % Excitation
Bath 429a	480	100-90	Endo-nitrito	9
Bath 429b	540	90-80	Endo-nitrito	10
Bath 429c	600	80-70	Endo-nitrito	9
Bath 429d	660	70-60	Endo-nitrito	8.5
Bath 429e	720	60-50	Endo-nitrito	8
Bath 429f	780	50-40	No visible excitation	0
Bath 429g	840	40-30	No visible excitation	0
Bath 429h	900	30	No visible excitation	0

Table 4.2 Temperature studies on $[Ni(aep)_2(NO_2)_2]$ from 100K to 30K

A similar temperature variation study was next undertaken to find the upper limits of the new isomeric state. The temperature was ramped at a rate of 5K/hour starting at 85K when the percentage excitation appeared to have reached a maximum (Table 4.3).

Sample Number	Irradiation Time (min)	Temperature (K)	Type of Excitation	Total % Excitation
Bath 432	180	85	Endo-nitrito	7.5
Bath 433a	240	85-91	Endo-nitrito	8
Bath 433b	300	91-97	Endo-nitrito	8.5
Bath 433c	360	97-102	Endo-nitrito	9
Bath 433d	420	102-108	Endo-nitrito	10
Bath 433e	480	108-113	Endo-nitrito	10
Bath 433f	540	113-119	No visible excitation	0

Table 4.3 Temperature studies on $[Ni(aep)_2(NO_2)_2]$ from 85K to 120K

Finally it was decided to try and excite a crystal of $[Ni(aep)_2(NO_2)_2]$ at 90K to see what the maximum percentage excitation that could be observed was under these conditions. Once the excitation appeared to have peaked, the lights were then removed from the sample and further data collections were undertaken to test for metastability of the endo-nitrito isomer.

Sample Number	Irradiation Time (min)	Temperature (K)	Type of Excitation	Total % Excitation
Bath 434a	60	90	-	0
Bath 434b	120	90	Peaks observed but too small to model	0
Bath 434c	180	90	Endo-nitrito	5
Bath 434d	240	90	Endo-nitrito	6.5
Bath 434e	300	90	Endo-nitrito	6.5
Bath 434f	360	90	Endo-nitrito	7
Bath 434g	420	90	Endo-nitrito	7
Bath 434h	480	90	Endo-nitrito	8.5
Bath 435	600	90	Endo-nitrito	11
Bath 436	Lights off	90	Endo-nitrito	9
Bath 437	Lights off	90	Endo-nitrito	9
Bath 438	Lights off	90	Endo-nitrito	9
Bath 439	Lights off	90	Endo-nitrito	9

Table 4.4 $[Ni(aep)_2(NO_2)_2]$ experiments at 90K to try and achieve a maximum excitation and test for metastability

Two further experiments were performed in order to try and excite the sample at 30K and 120K however both were unsuccessful and no excitation was observed after irradiation for more than 5h. However, it is clear from these experiments that a new endo-nitrito isomer which is metastable, can be formed from excitation using blue LEDs and exists between 50K and 120K. The solid state molecular structure of both the ground state and metastable state is described below.

4.4.1.2 Ground State Structure

The crystal was kept in the dark at room temperature and cooled to 100K to obtain a clean unpolluted ground state structure. Any excitation achieved during the experiment was shown to be fully reversible, and ground state structures obtained at various points during the experiment appeared comparable to the initial structure refinements. The crystal quality appeared to remain good throughout the duration of the excitation and temperature variation studies.

$[Ni(aep)_2(NO_2)_2]$ crystallised in the space group $P2_1/c$, with an 18.5% disorder present around the ethyl chain. The solid state molecular structure (without disorder shown) can be seen in figure 4.8. The asu contains half the complete molecule, with the nickel atom sitting on a crystallographic centre of symmetry. The coordination geometry around the nickel metal centre is octahedral with the two nitrite ligands *trans* to each other and N(1) is related to N(1') by the symmetry operation *-x*+1, *-y*, *-z*. The nitrite has a O_1-N_1-O_2 bond angle of 117.24(18)° and adopts an η^1 coordination geometry to the metal centre through the nitrogen atom.

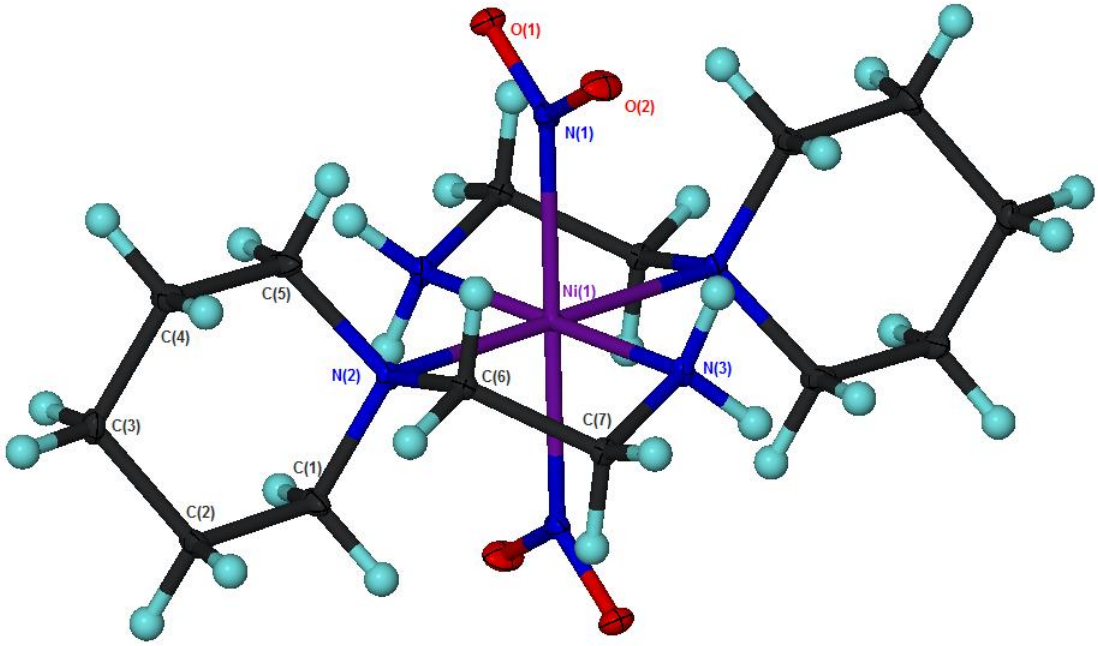

Figure 4.8 Complete ground state structure of $[Ni(aep)_2(NO_2)_2]$ at 100K with 30% probability ellipsoids shown (Bath 412)

An analysis of the packing revealed no hydrogen bonding between adjacent molecules of $[Ni(aep)_2(NO_2)_2]$, however there are some intramolecular short contacts present in the structure with donor...acceptor (D…A) distances of 3.185(3)Å (N_3-H_{15}…O_1) and 2.909(3)Å (N_3-H_{16}…O_2) and bond

angles of 149.1° and 122.0°, respectively. The short contacts can be seen in figure 4.9 below with the disorder in the ethyl chain removed for clarity.

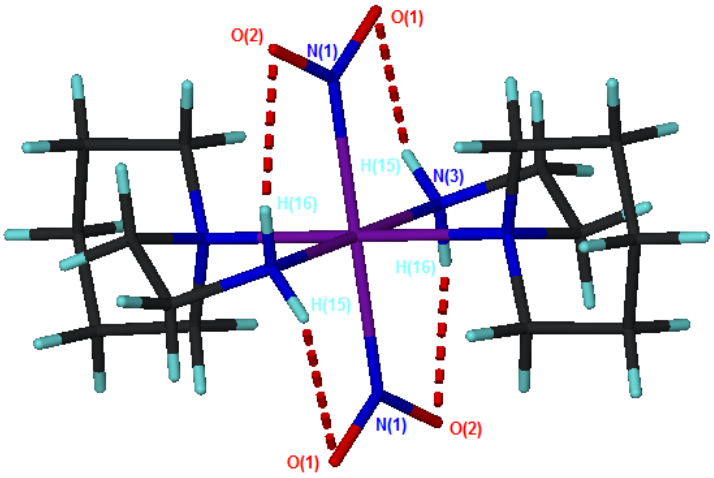

Figure 4.9 Intramolecular short contacts in $[Ni(aep)_2(NO_2)_2]$

4.4.1.3 Excited State Structure

The crystal structure obtained after 10h irradiation with blue LEDs at 90K, (Bath 435), is illustrated in figure 4.10 (again, the disorder around the ethyl chain has been removed for clarity). The overall structure contained approximately 11% of the endo-nitrito isomer, and maintained the same $P2_1/c$ crystal symmetry as the ground state.

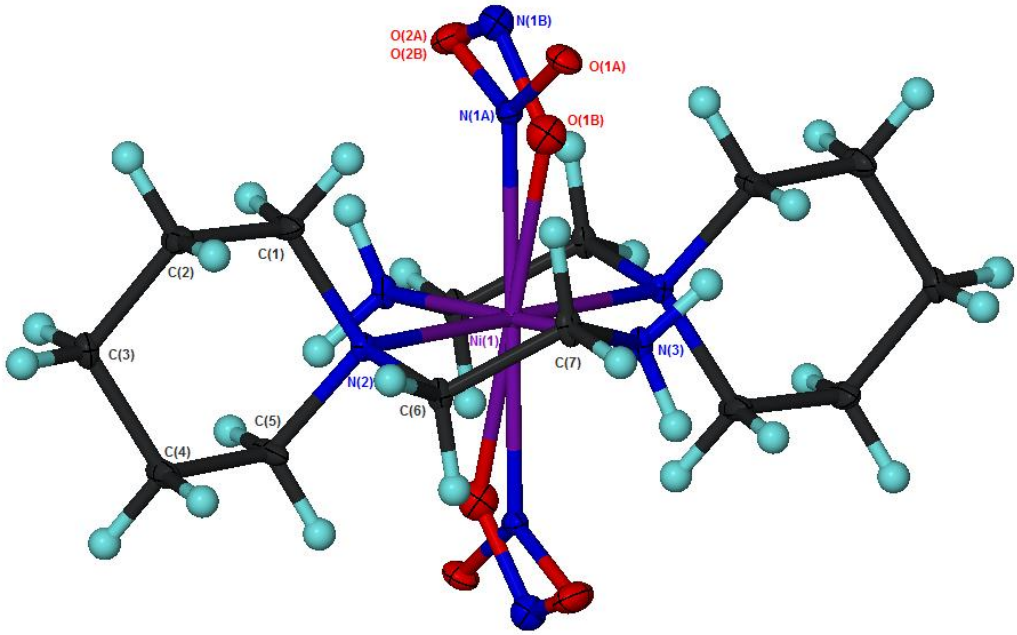

Figure 4.10 Complete excited state structure of $[Ni(aep)_2(NO_2)_2]$ at 90K with 30% probability ellipsoids shown (Bath 435)

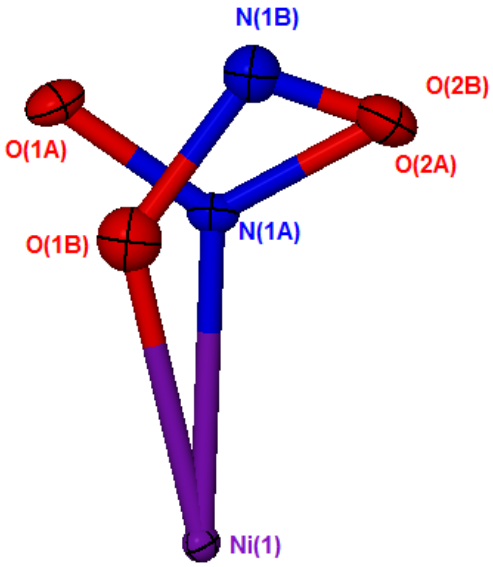

Figure 4.11 Close up of the endo-nitrito conformation in $[Ni(aep)_2(NO_2)_2]$

The nitrito ligand takes the endo conformation ((iii) in figure 4.1), not the exo form which is more common and a product of the synthesis of the ground state. The endo species however is consistent with less movement in the crystal, and can be seen more closely in figure 4.11.

The excitation in $[Ni(aep)_2(NO_2)_2]$ was modelled as a disordered fragment and the occupancies of the nitrite species were calculated using free variables. The residual peaks associated with O_{1B} and N_{1B} were easily identified in the electron density map, however the peak pertaining to O_{2B} was considerably smaller due to the proximity of atom O_{2A}. The command EXYZ was therefore used to place the atom O_{2B} at the same coordinates as O_{2A} and EADP to give the atoms the same displacement parameters. As a result the bond distance between N_{1B} and O_{2B} is rather shorter than would be expected. The endo-nitrito isomer maintains a six coordinate octahedral geometry as in the ground state species, however it is distorted and the isomer has an O_{1B}-N_{1B}-O_{2B} angle of 107.82(8)°.

An analysis of the bonding in the metastable state structure shows the same short contacts present as in the ground state, as well as the presence of a further short contact (N_3-H_{15}…O_{1B}) with a D…A distance of 2.531(4)Å. There is also an intermolecular hydrogen bond between N_3-H_{15}…N_{1B} which is moderate/weak in strength with a distance (N_3…N_{1B}) of 2.839(1)Å and a bond angle of 138.01°. The overall bonding within the structure can be seen in figure 4.12. Although the additional bonding interactions are generally weak it is possible that their presence may help in stabilising the metastable linkage isomer.

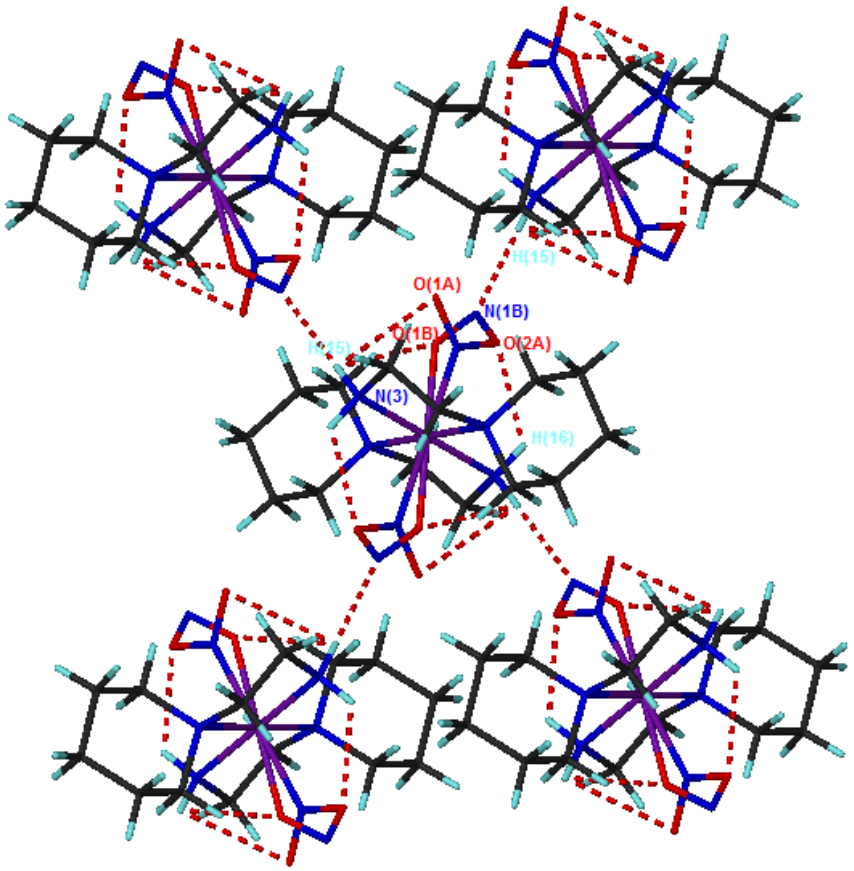

Figure 4.12 Hydrogen bonding and short contacts observed in the excited state of $[Ni(aep)_2(NO_2)_2]$

Small changes were observed in the unit cell parameters between the ground and most excited state structure, shown in table 4.5 below. Upon excitation a small increase was observed in both the *b* and *c* axes, whereas the *a* axis remained constant within experimental error. There was also a slight increase in the β angle. Overall this resulted in a general increase in cell volume of approximately 6Å^3.

	***a* (Å)**	***b* (Å)**	***c* (Å)**	**α (°)**	**β (°)**	**γ (°)**	**V (Å^3)**
Ground State Bath 412	9.6309 (14)	8.2557 (12)	11.8340 (17)	90	109.065 (1)	90	889.3 (2)
Metastable State Bath 435	9.6301 (6)	8.2875 (5)	11.8754 (8)	90	109.103 (1)	90	895.58 (10)

Table 4.5 Comparison of unit cell data for $[Ni(aep)_2(NO_2)_2]$

4.4.1.4 Slant Plane Fourier Maps

Slant plane Fourier maps were generated using WinGX. For the analysis, fragments pertaining to the metastable endo-nitrito isomer were removed from the crystal structure and the structure refined using the ground state coordinates only. Any residual electron density observed in the maps would therefore be due to the linkage isomer. Figure 4.13 shows maps pertaining to both the ground state (Bath 412) and the highest excited state (Bath 435). It is clear that in the ground state all the electron density within the solid state molecular structure has been accounted for, however in the excited state there are three relatively large peaks around the nitro group.

Maps were also generated for the temperature variation studies and can be used to identify the limitations of the metastable state. Figure 4.14 shows Fourier maps for experiments between 100-30K and figure 4.15 shows Fourier maps for experiments between 85-120K. It is clear from these diagrams that the excitation disappears between 40 and 50K and 114-118K.

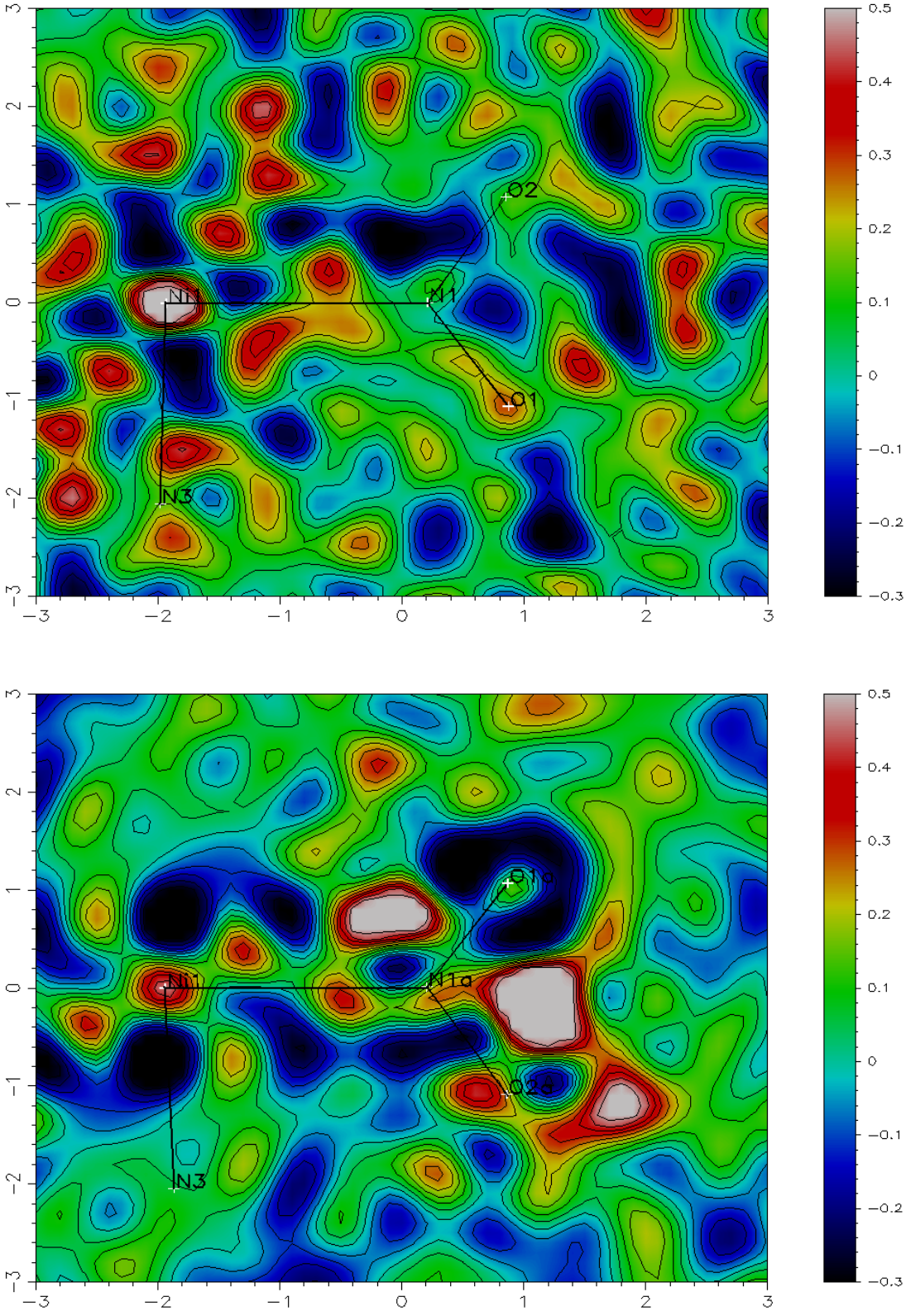

Figure 4.13 Slant plane Fourier maps for the ground state Bath 412 (top) and highest excited state Bath 435 (bottom)

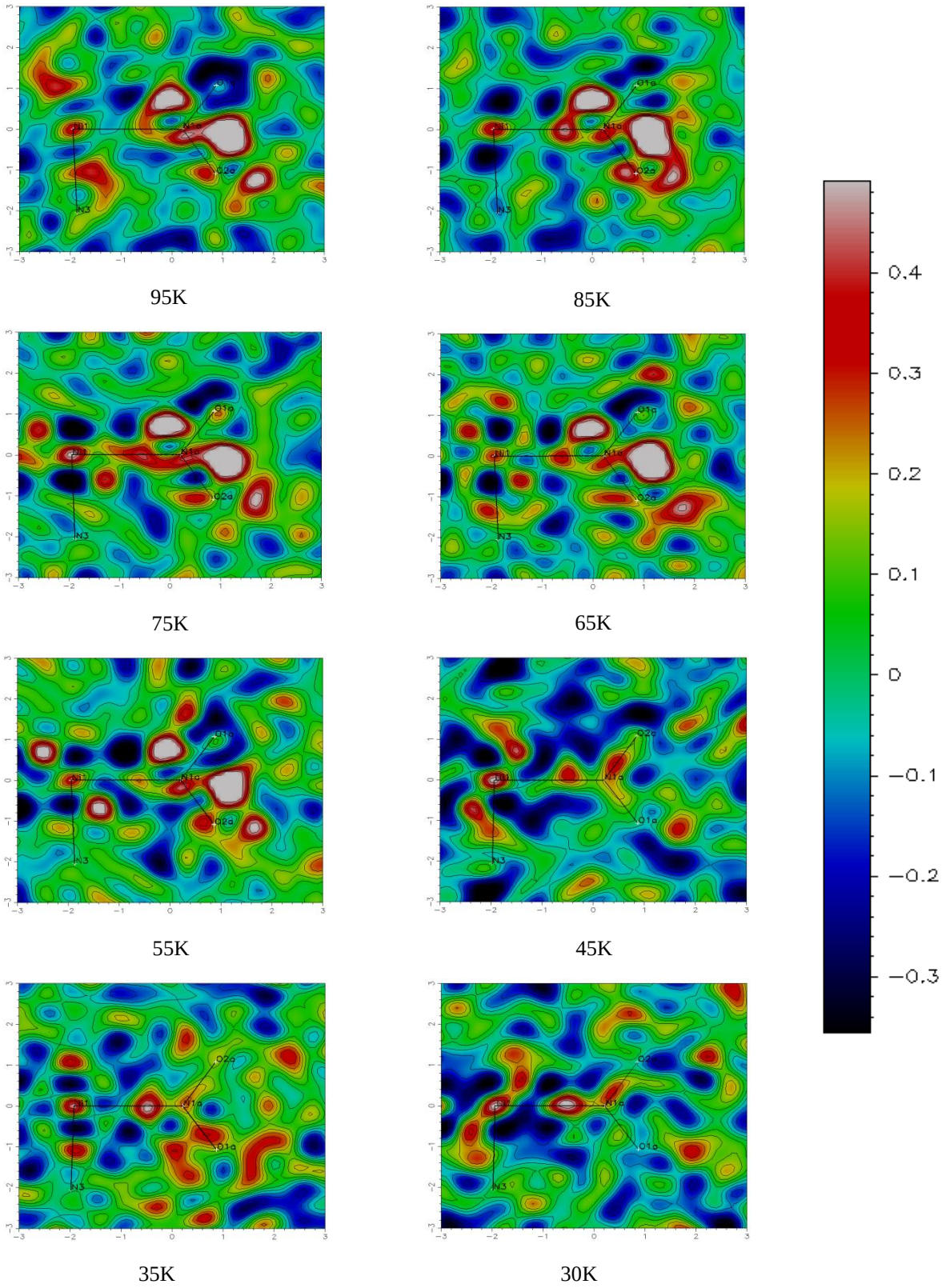

Figure 4.14 Slant plane Fourier maps for temperature variation study of $[Ni(aep)_2(NO_2)_2]$ from 100K to 30K

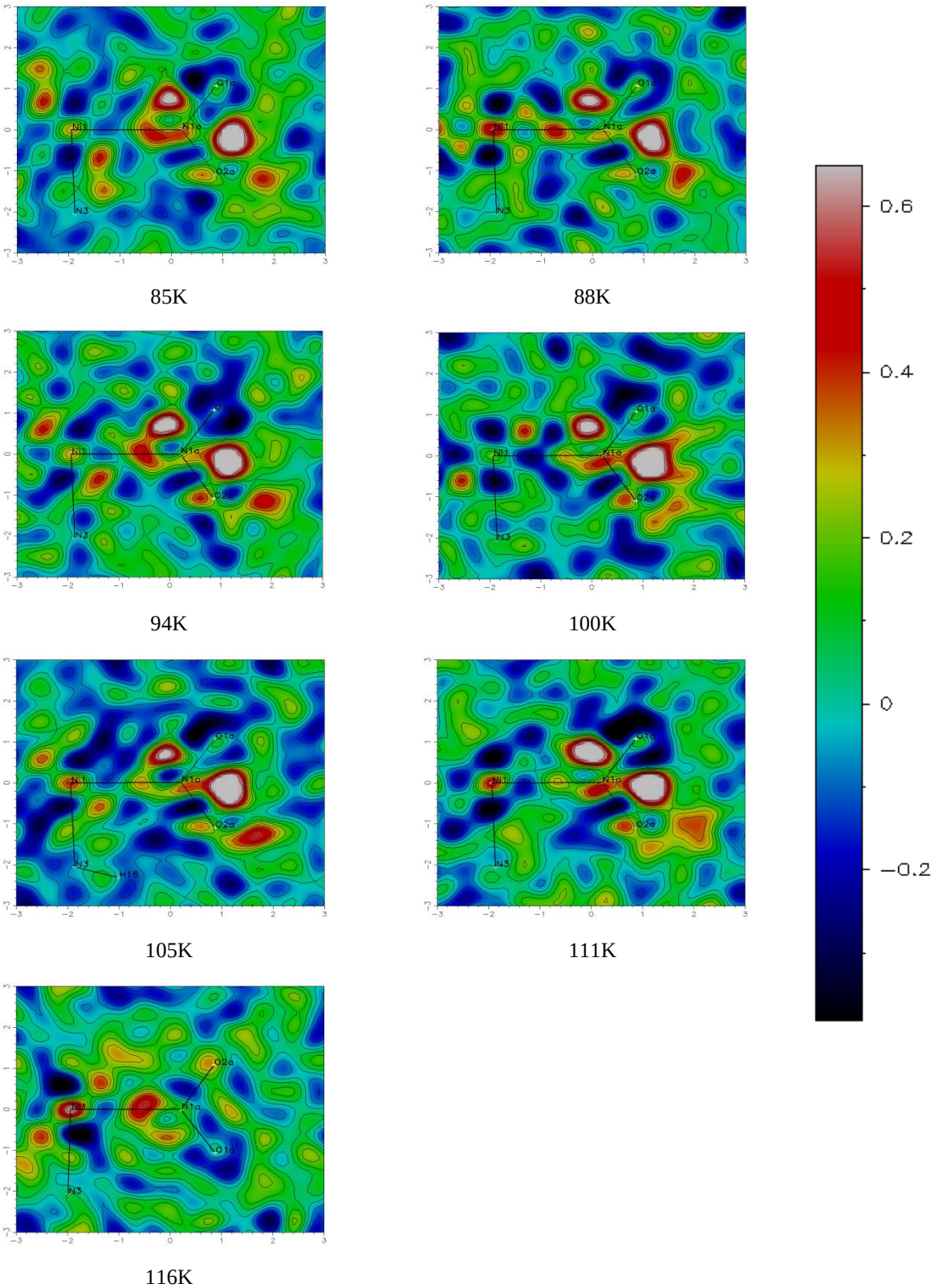

Figure 4.15 Slant plane Fourier maps for temperature variation study of $[Ni(aep)_2(NO_2)_2]$ from 80K to 120K

4.4.2 $[Ni(aem)_2(NO_2)_2]$

4.4.2.1 Collection Strategy and Excitation Results

Unlike $[Ni(aep)_2(NO_2)_2]$ only the nitro isomer is formed upon crystallisation of $[Ni(aem)_2(NO_2)_2]$. Initial experimentation using UV LEDs as the stimulus resulted in a very small amount of excitation (approximately 5%). A second experiment using four blue LEDs was far more successful. The results presented here were all performed on the same crystal which was glued to the fibre. A summary of the initial data collected on this sample can be seen below in table 4.6. No data was collected under Bath 544.

Sample Number	Irradiation Time (min)	Temperature (K)	Type of Excitation	Total % Excitation
Bath 541	0 – ground state	100	-	0
Bath 542	30	100	Endo-nitrito	8.5
Bath 543	90	100	2x Endo-nitrito	25
Bath 545	150	100	2x Endo-nitrito	26.5

Table 4.6 Excitation of $[Ni(aem)_2(NO2)_2]$

After excitation had appeared to stabilise a temperature variation study was performed to identify the limits of the metastable state that had been identified. The first study went down in temperature from 100K to 30K at a rate of 10K/hour for each data set and the results are highlighted below in table 4.7.

Sample Number	Irradiation Time (min)	Temperature (K)	Type of Excitation	Total % Excitation
Bath 545	150	100	2x Endo-nitrito	26.5
Bath 546	210	100-90	2x Endo-nitrito	28.5
Bath 547	270	90-80	2x Endo-nitrito	29
Bath 548	330	80-70	2x Endo-nitrito	30
Bath 549	390	70-60	2x Endo-nitrito	30.5
Bath 550	450	60-50	2x Endo-nitrito	31
Bath 551	510	50-40	2x Endo-nitrito	32
Bath 551b	570	40-30	2x Endo-nitrito	32
Bath 552	630	30	2x Endo-nitrito	31

Table 4.7 Temperature studies on $[Ni(aem)_2(NO_2)_2]$ from 100K to 30K

The temperature was ramped back to 100K to test the quality of the crystal. A second temperature variation study was undertaken to identify the temperature at which the sample was quenched (table 4.8). Again the temperature was ramped at a rate of 10K/hour for each data collection. At this point during the experiment only two blue LEDs remained working, however there appeared to be no significant reduction in the percentage excitation so no attempt was made to add additional LEDs.

Sample Number	Irradiation Time (min)	Temperature (K)	Type of Excitation	Total % Excitation
Bath 554	800	100	2x Endo-nitrito	29.5
Bath 555	860	100-110	Endo-nitrito	11
Bath 556	920	110-120	Endo-nitrito	10.5
Bath 557	980	120-130	Endo-nitrito	9
Bath 558	1040	130-140	-	0

Table 4.8 Temperature studies on $[Ni(aem)_2(NO_2)_2]$ from 100K to 140K

4.4.2.2 Ground State Structure

The crystal was kept in the dark at room temperature and then cooled to 100K in order to obtain a clean unpolluted ground state structure. As with the analogous aep system, any excitation achieved during the experiment was fully reversible. The crystal quality appeared to deteriorate during the excitation process resulting in the spot shape changing to an hour glass formation. However, when the same sample was relaxed back to the ground state and further data collected, these spots returned to normal and the data was comparable to initial ground state data refinements.

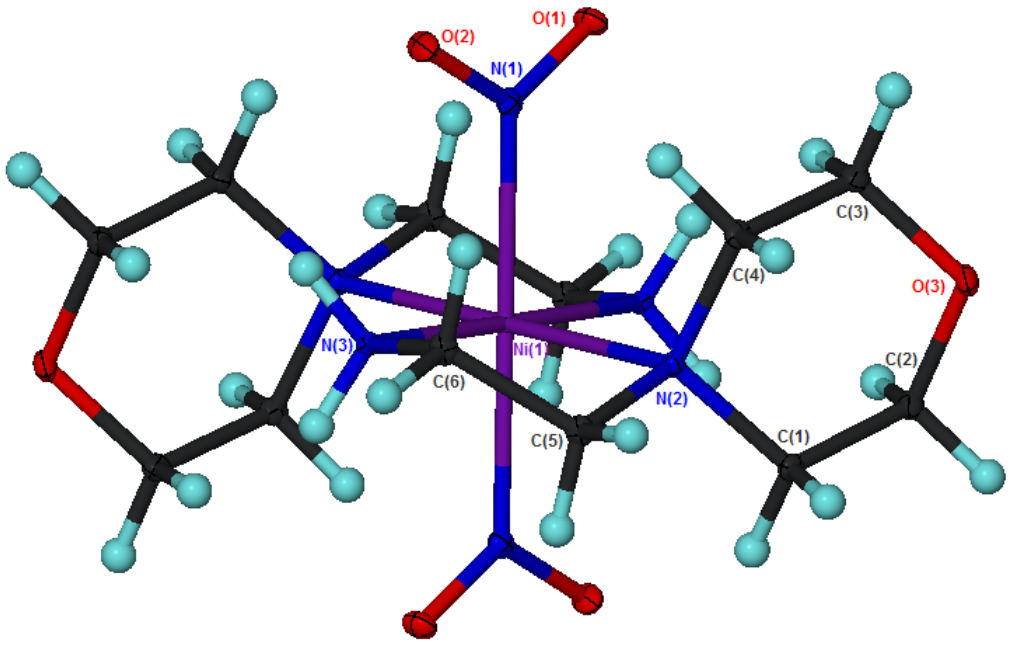

Figure 4.16 Complete ground state structure of $[Ni(aem)_2(NO_2)_2]$ at 100K with 30% probability ellipsoids shown (Bath 541)

Figure 4.16 shows the solid state molecular structure of $[Ni(aem)_2(NO_2)_2]$ (Bath 541), which crystallised in the space group *P*-1 not *P*1 as reported in the initial paper.[12] The asu contains half the complete molecule, with the nickel atom sitting on a crystallographic centre of symmetry. The

coordination geometry around the nickel centre is octahedral and both nitrite ligands are *trans* to each other, with N(1) related to N(1') by the symmetry operation -*x*+1, -*y*, -*z*+1. The nitrite ligand has an O_1-N_1-O_2 angle of 117.24(18)° and adopts an η^1 coordination geometry through the nitrogen atom, which is identical to that in the analogous aep system.

The overall bonding interactions observed in the ground state of the morpholine system is relatively complex and can be considered in three stages. There are intramolecular short contacts between the oxygen atoms of the nitro group and the hydrogen atoms on N_3 analogous to those observed in the equivalent piperidine structure. The N_3-H_{13}…O_1, D…A distance is 2.986(3)Å with an angle of 119.4° and the N_3-H_{14}…O_2 bond distance (D…A) is 2.892(3)Å with an angle of 112.1°. These intramolecular contacts can be seen in figure 4.17.

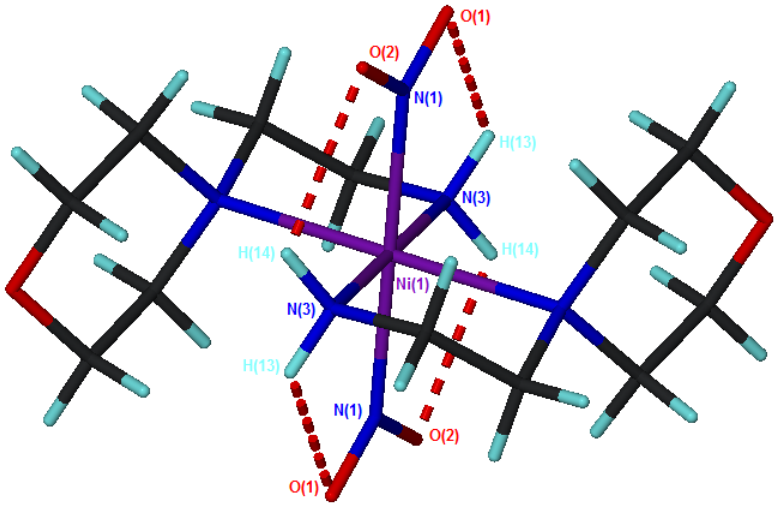

Figure 4.17 Intramolecular short contacts in $[Ni(aem)_2(NO_2)_2]$

Two types of intermolecular hydrogen bond are also present, the first is between N_3-H_{14}…O_2 and there are four of these per molecule linking adjacent molecules in a ribbon type nature (figure 4.18). The N_3-H_{14}…O_2 has a D…A distance of 3.019(3) with a bond angle of 131.5°. The second type of intermolecular hydrogen bonds, involve the oxygen atom on the morpholine rings. Again there are four of these bonds per molecule, linking together adjacent molecules to form ribbons (figure 4.19). The N_3-H_{13}…O_3 has a D…A distance of 3.134(3) with a bond angle of 147.2°.

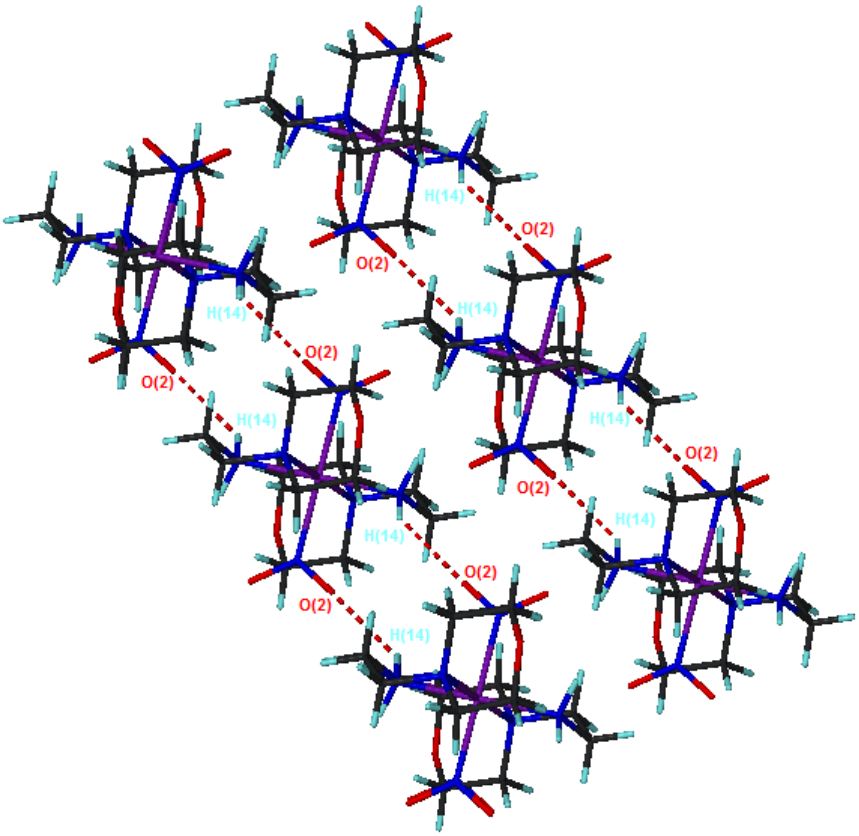

Figure 4.18 Intermolecular hydrogen bonding involving an oxygen atom in the nitro group, forming ribbon type layers in $[Ni(aem)_2(NO_2)_2]$

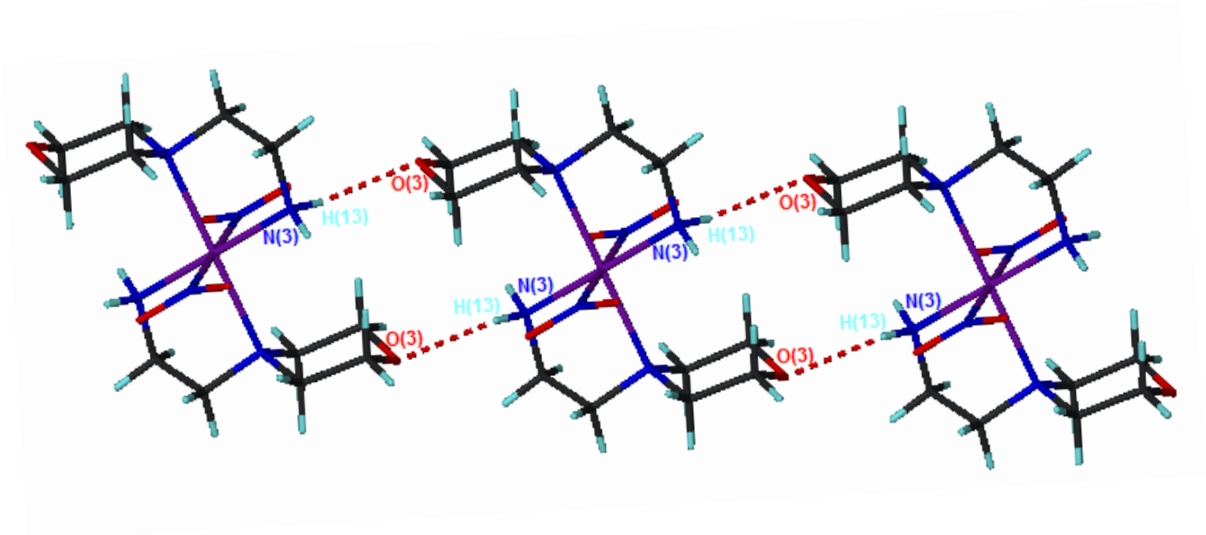

Figure 4.19 Intermolecular hydrogen bonding involving the oxygen atom in the morpholine ring, forming ribbon type layers in $[Ni(aem)_2(NO_2)_2]$

The combination of the two types of intermolecular bond results in a sheet type structure illustrated in figures 4.20 and 4.21. The intramolecular hydrogen bonds have been removed for clarity.

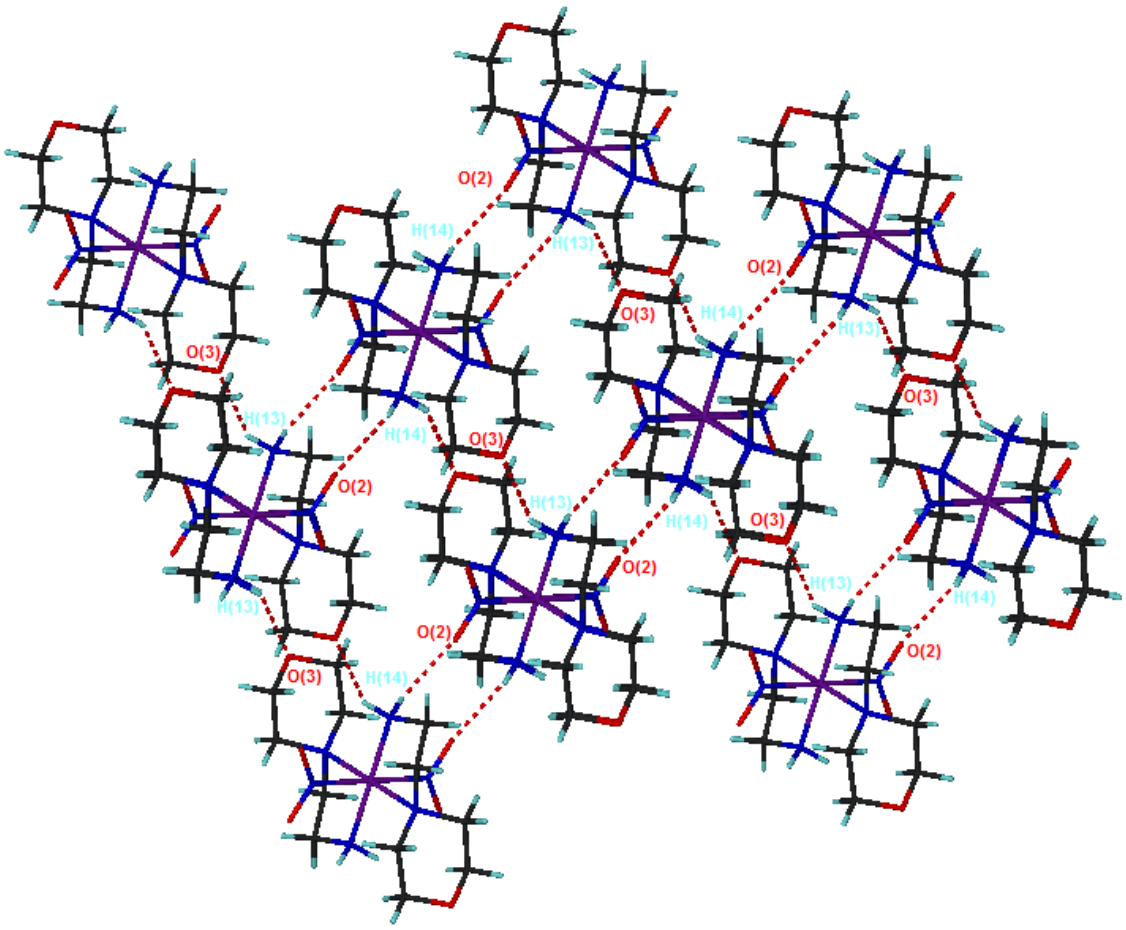

Figure 4.20 Sheet structure formed from combination of the two types of intermolecular hydrogen bond in $[Ni(aem)_2(NO_2)_2]$

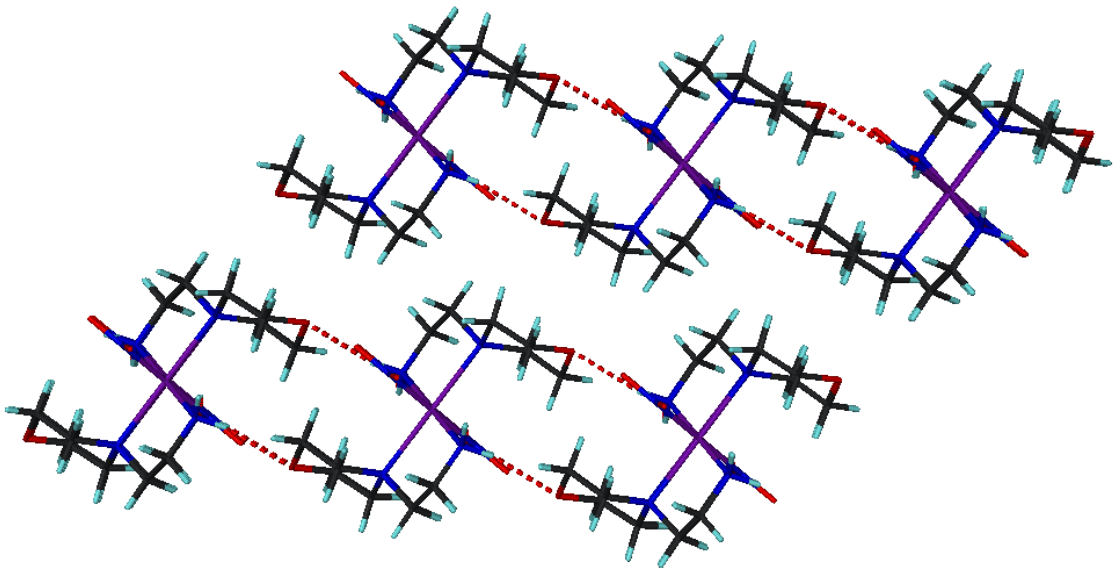

Figure 4.21 Side on view of two sheets in $[Ni(aem)_2(NO_2)_2]$

4.4.2.3 Excited State Structure

The solid state molecular structure obtained after 8.5h irradiation with blue LEDs at 45K, (Bath 551), is illustrated in figure 4.22. The overall structure contained approximately 32% of two endo-nitrito isomers, the major isomer (O_{1B}-N_{1B}-O_{2B}) accounting for around 21%. The overall crystal structure maintained the same *P*-1 crystal symmetry as observed for the ground state.

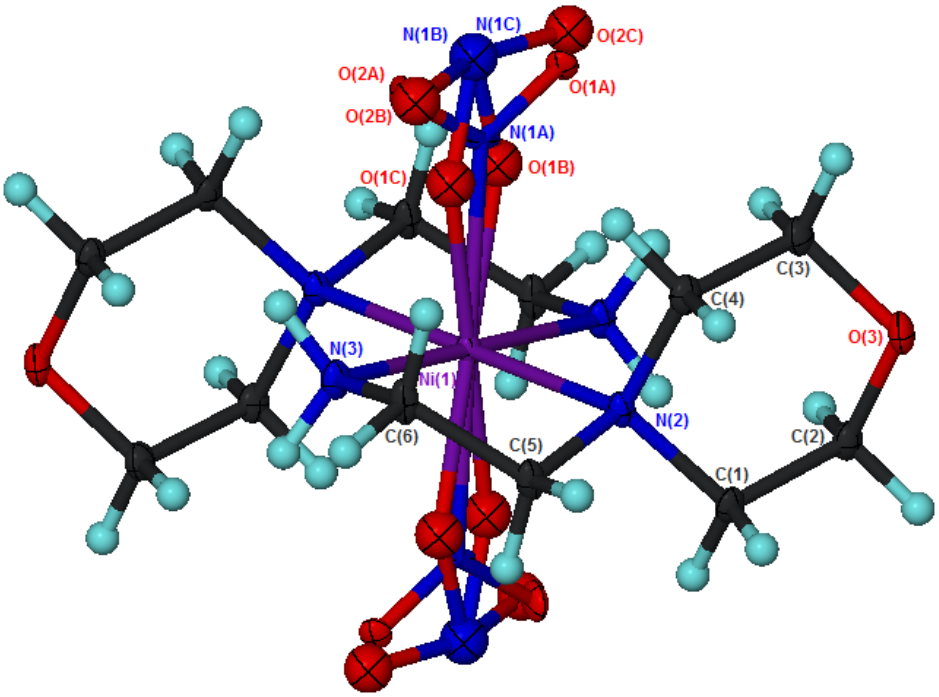

Figure 4.22 Complete excited state structure of [Ni(aem)$_2$(NO$_2$)$_2$] at 45K with 30% probability ellipsoids shown (Bath 551)

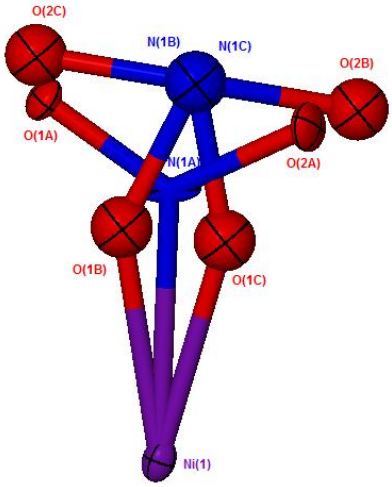

Figure 4.23 Close up of the two endo-nitrito conformations in [Ni(aem)$_2$(NO$_2$)$_2$]

The endo-nitrito conformations ((iii) in figure 4.1) adopted upon excitation can be seen more closely in figure 4.23. The excitation in [Ni(aem$_2$)(NO$_2$)$_2$] was modelled as two disordered fragments and the occupancies of the nitrite species were calculated using free variables. In this instance due to the

presence of three different nitrite fragments, the sum of the free variables were set to equal one using the SUMP command. The command EXYZ was used to place the atom N_{1B} at the same coordinates as N_{1C} and SADI was used to restrain the N-O distances to be the same in the excited state fragments. Both endo-nitrito isomers exhibit a distorted octahedral geometry with η^1 coordination to the metal centre. The major isomer O_{1B}-N_{1B}-O_{2B}* has a bond angle of 105.48°, and the minor isomer which accounts for around 11% of the overall structure has an O_{1C}-N_{1C}-O_{2C}* angle of 107.63°.

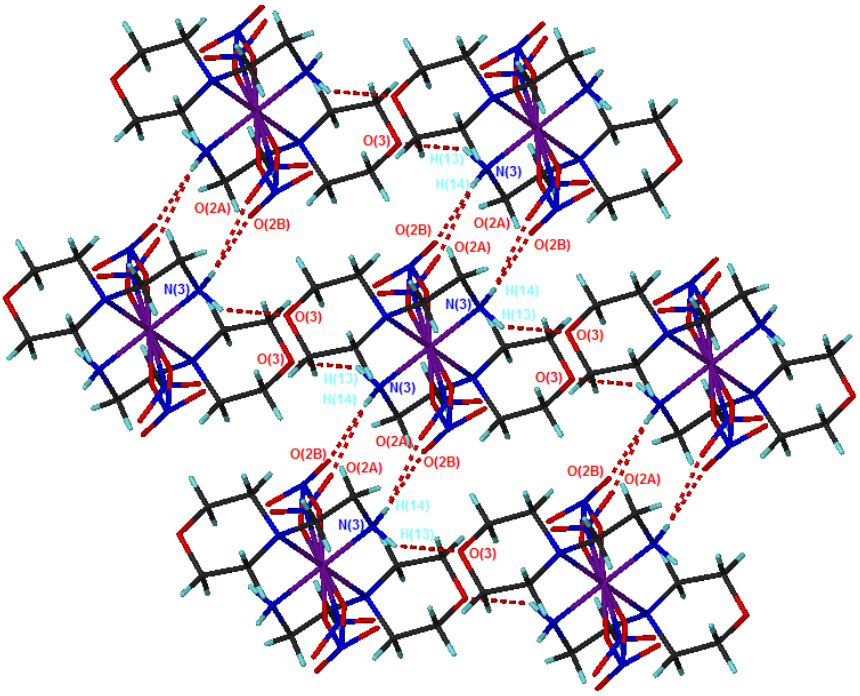

Figure 4.24 Sheet structure formed in the metastable state of $[Ni(aem)_2(NO_2)_2]$

As with the ground state a number of bonding interactions are observed. The intramolecular short contacts are comparable in length and with similar bond angles. The N_3-H_{13}…O_{1A} has a D…A distance of 2.986(5)Å with an angle of 119.7° and the N_3-H_{14}…O_{2A} bond distance (D…A) of 2.920(4)Å with an angle of 112.2°. There are possibly further short contacts between the oxygen atoms of the nitrito groups and the hydrogen attached to nitrogen on the amino groups however the distance between the oxygen atoms and the nitrogen donor atom are approximately 3.30Å and an angle of around 125° which would make it a very weak interaction. The same two intermolecular hydrogen bonds are also observed. N_3-H_{14}…O_{2A} again has four contacts per molecule with a D…A distance of 3.037(5) with an angle of 135.2 and N_3-H_{13}…O_3 also has four contacts per molecule with a D…A distance of 3.145(3) with a bond angle of 147.2°. A further intermolecular hydrogen bond is present - N_3-H_{14}…O_{2B} which is similar in nature to N_3-H_{14}…O_{2A}. This hydrogen bond has an N_3- O_{2B} distance of 2.856(17) and a bond angle of 147.4°. The overall hydrogen bonded sheet network can be seen in figure 4.24.

* Constrained atoms

Small changes were again observed in the unit cell parameters between ground and excited states and are shown in table 4.9. Upon excitation a small increase was observed in both the *a* and *b* axes, but a decrease in the *c* axis. There was also approximately a 2° decrease in β and a 1° increase in α, resulting in an overall increase in cell volume of approximately 4Å^3.

	***a* (Å)**	***b* (Å)**	***c* (Å)**	**α (°)**	**β (°)**	**γ (°)**	**V (Å^3)**
Ground State Bath 541	7.172 (5)	7.988 (5)	8.330 (5)	94.306 (5)	112.642 (5)	100.496 (5)	427.5 (5)
Metastable State Bath 551	7.2011 (17)	8.0007 (18)	8.2916 (19)	94.620 (3)	110.884 (3)	101.434 (3)	431.46 (17)

Table 4.9 Comparison of unit cell data for $[Ni(aem)_2(NO_2)_2]$

4.4.2.4 Slant Plane Fourier Maps

For analysis, fragments pertaining to either both or just one metastable endo-nitrito isomer were removed from the crystal structure and the structure refined using the ground state coordinates only. Any residual electron density observed in the maps would again be as a result of the presence of linkage isomers. Figure 4.25 shows maps pertaining to both the ground state (Bath 541) and the highest excited state (Bath 551). All electron density within the solid state molecular structure has been accounted for in the ground state seen from the Fourier map, however in the excited state large smears of unaccounted electron density mainly focused around the nitro group, particularly in the position where both atoms N_{1B} and N_{1C} would reside.

Fourier maps were also generated for the temperature variation studies and can be used to identify the limitations of the metastable states. Figure 4.26 shows Fourier maps for experiments between 100-30K. It is clear from these diagrams that both endo-nitrito isomers are present all the way down to 30K and the percentage excitation gradually increases as the temperature is reduced. Figure 4.27 illustrates Fourier maps for experiments between 100-140K. Both isomers appear to be present at 100K, however between 105-125K only one of the endo-nitrito isomers truly appears to be present which is due to O_{1B}-N_{1B}-O_{2B}. This isomer gradually diminishes and finally disappears around 135K.

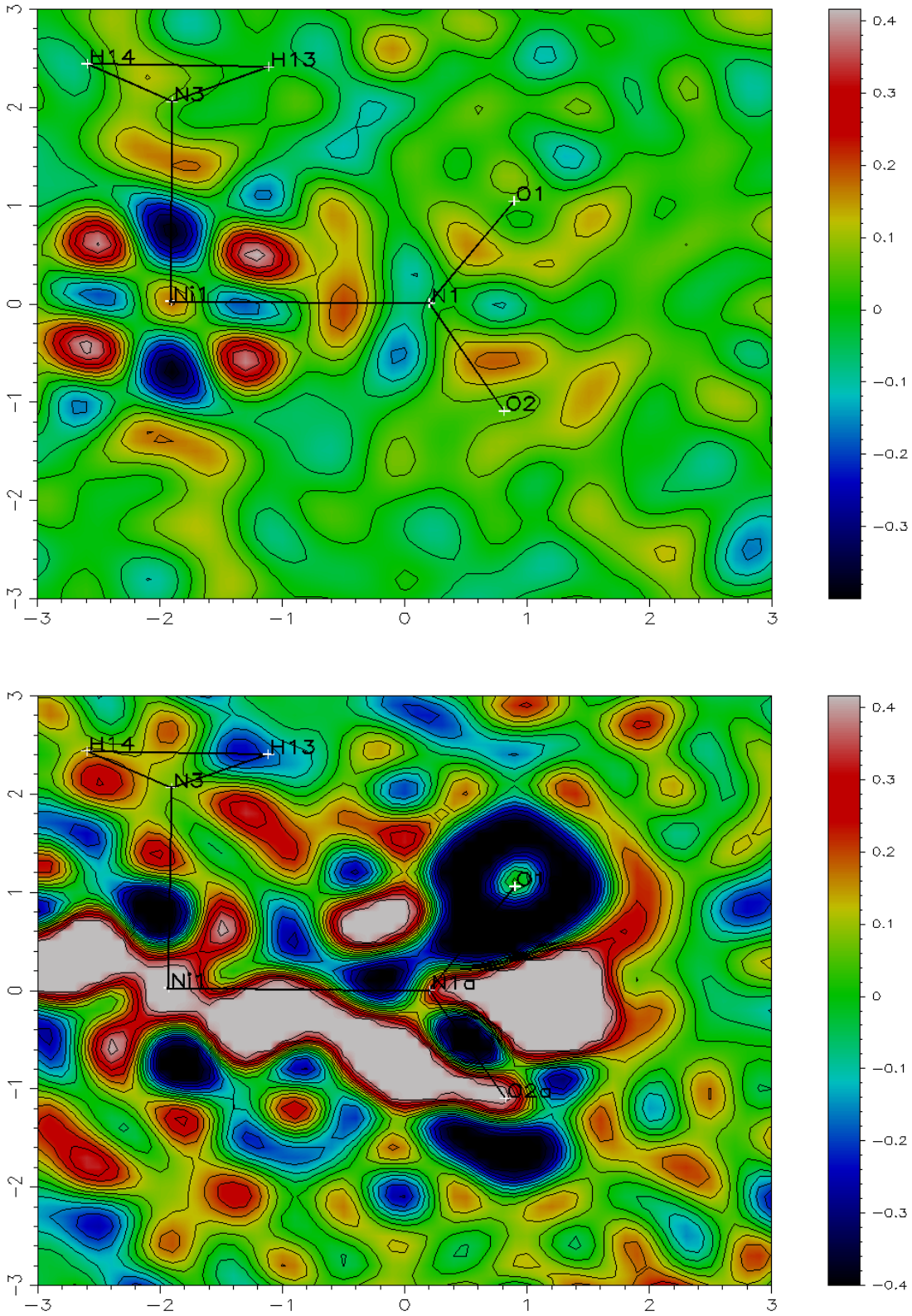

Figure 4.25 Slant plane Fourier maps for the ground state Bath 541 (top) and highest excited state Bath 551 (bottom)

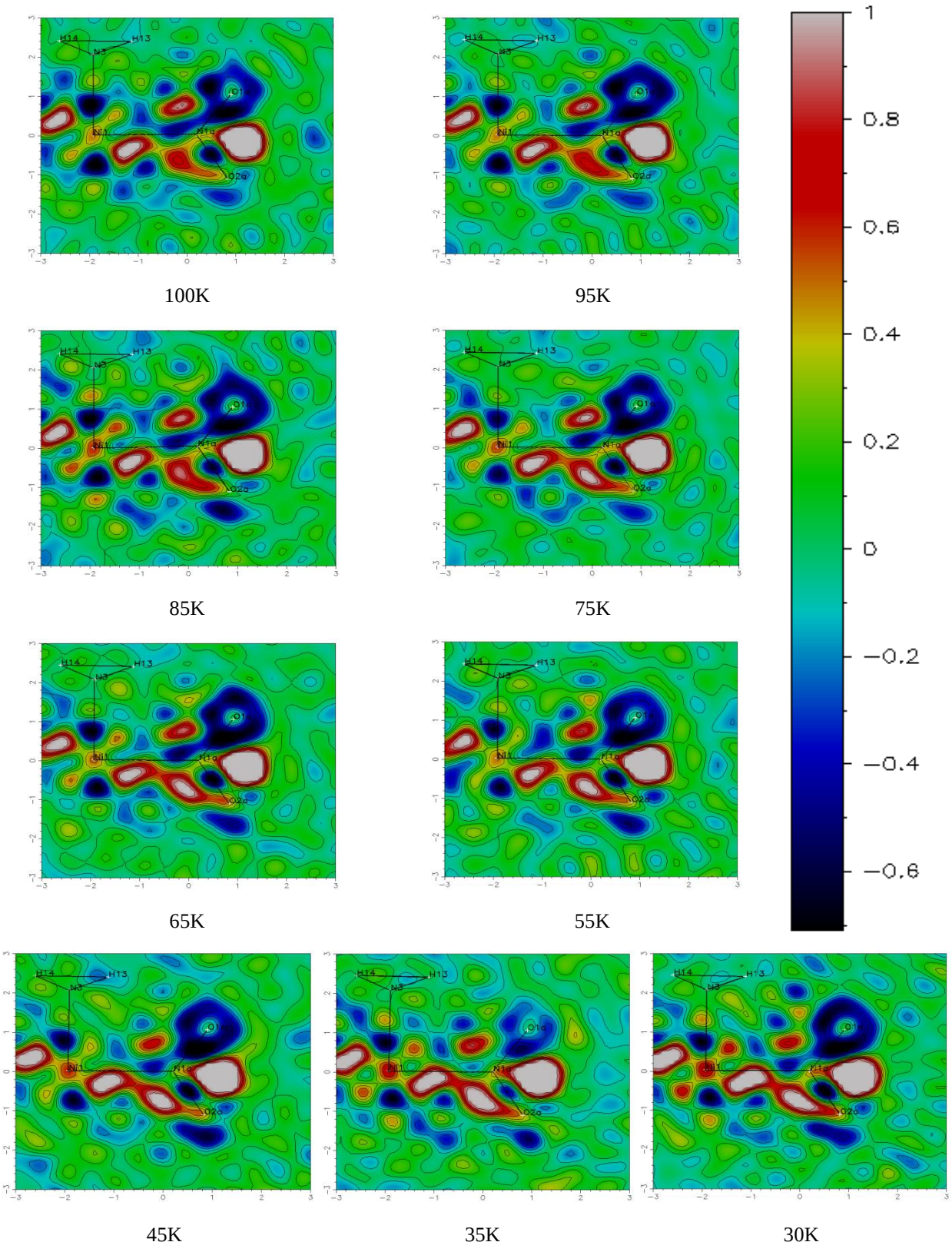

Figure 4.26 Slant plane Fourier maps for temperature variation study of $[Ni(aem)_2(NO_2)_2]$ from 100K to 30K

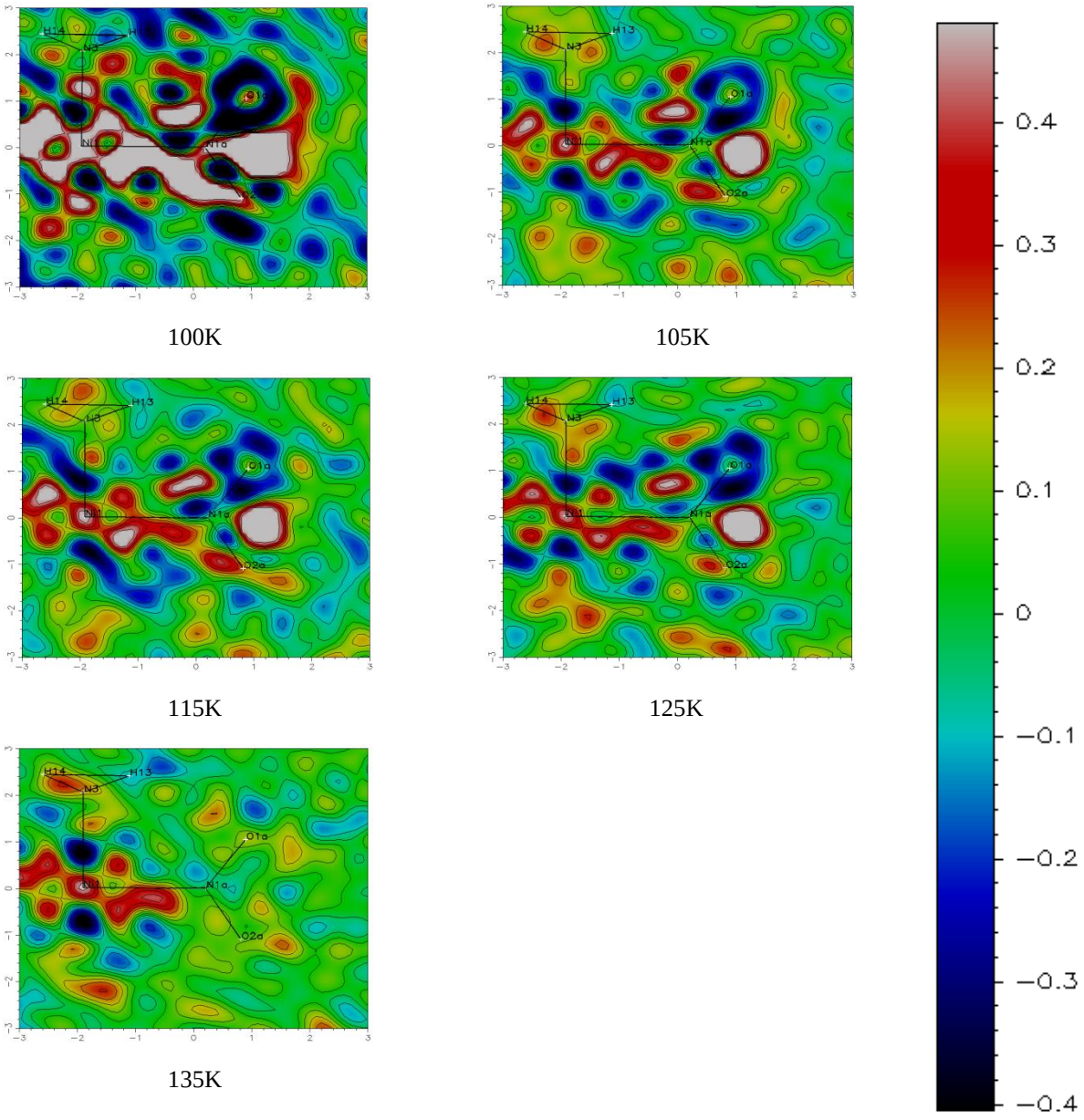

Figure 4.27 Slant plane Fourier maps for temperature variation study of $[Ni(aem)_2(NO_2)_2]$ from 100K to 140K

4.4.3 $[Ni(aepy)_2(NO)_2]$

4.4.3.1 Collection Strategy and Excitation Results

As with $[Ni(aem)_2(NO_2)_2]$ only the nitro form can be isolated from crystallisation of $[Ni(aepy)_2(NO_2)_2]$. Like both previous systems discussed in this chapter, initial experimentation using UV LEDs as the stimulus resulted in a very small amount of excitation and further investigation blue LEDs was more successful. The work presented in this section was performed using a few different crystals. The excitation results on the first crystal are shown in table 4.10 below. After approximately 5h irradiation the lights were turned off and after waiting a further half an hour a data collection was undertaken to confirm if the sample was metastable (Bath 519).

Sample Number	Irradiation Time (min)	Temperature (K)	Type of Excitation	% Excitation	Total % Excitation
Bath 515	0	100	-	0	0
Bath 516	100	100	Endo-nitrito Exo-nitrito	11.5 10	21.5
Bath 517	160	100	Endo-nitrito Exo-nitrito	15 13	28
Bath 518	240	100	Endo-nitrito Exo-nitrito	18 13	31
Bath 519	-	100	Endo-nitrito Exo-nitrito	17.5 15	32.5

Table 4.10 Excitation of $[Ni(aepy)_2(NO2)_2]$

Sample Number	Irradiation Time (min)	Temperature (K)	Type of Excitation	% Excitation	Total % Excitation
Bath 520	0	100	-	0	0
Bath 521	60	100	Peaks observed but too small to model	0	0
Bath 522	140	100	Endo-nitrito Exo-nitrito	5 5	10
Bath 523	240	100	Endo-nitrito Exo-nitrito	6 7.5	13.5
Bath 524a	300	100-105	Endo-nitrito Exo-nitrito	6.50 9.5	16
Bath 524b	360	105-110	Endo-nitrito Exo-nitrito	11.5 9	20.5
Bath 524c	420	110-115	Endo-nitrito Exo-nitrito	11 9	20

Table 4.11 Temperature studies on $[Ni(aepy)_2(NO_2)_2]$ from 100K to 115K

The crystal used for the initial excitation studies was lost during de-icing of the sample so a new crystal was used for the temperature variation studies. Only two LEDs were still working at this stage of

the investigation but as the sample still appeared to excite the decision was made to carry on with the experiment. The temperature was ramped at a rate of 5K/hour. Unfortunately during the study there was further ice build up during the data collection of Bath 524d and the sample was again lost. The temperature variation study was therefore resumed at the very end of the experiment on a different crystal and due to time restraints the temperature was ramped from 100K to 120K and then at a rate of 10K/hour. The data is summarised in tables 4.11 and 4.12 for both crystals used.

Sample Number	Irradiation Time (min)	Temperature (K)	Type of Excitation	% Excitation	Total % Excitation
Bath 562	0	100	-	0	0
Bath 566	240	100	Endo-nitrito Exo-nitrito	5.5 6	11.5
Bath 567	300	120	Exo-nitrito	7	7
Bath 568	360	120-130	-	0	0

Table 4.12 Temperature studies on $[Ni(aepy)_2(NO_2)_2]$ from 100K to 130K

To investigate whether the metastable states observed were also stable at low temperature, a temperature variation study was undertaken from 100K to 30K (table 4.13).

Sample Number	Irradiation Time (min)	Temperature (K)	Type of Excitation	% Excitation	Total % Excitation
Bath 525	0	100	-	0	0
Bath 530	80	100	Endo-nitrito Exo-nitrito	8 9	17
Bath 531	140	100	Endo-nitrito Exo-nitrito	13 9	22
Bath 532	200	100-90	Endo-nitrito Exo-nitrito	13.5 12.5	26
Bath 533	260	90-80	Endo-nitrito Exo-nitrito	15.5 13	28
Bath 534	320	80-70	Endo-nitrito Exo-nitrito	16 14	30
Bath 536	-	60	Endo-nitrito Exo-nitrito	18.5 15.5	34
Bath 537	60	60-50	Endo-nitrito Exo-nitrito	15 17	32
Bath 538	120	50-40	Endo-nitrito Exo-nitrito	15.5 16.5	32
Bath 539	180	40-30	Endo-nitrito Exo-nitrito	16 17.5	33.5
Bath 540	240	30	Endo-nitrito Exo-nitrito	13 16	29

Table 4.13 Temperature studies on $[Ni(aepy)_2(NO_2)_2]$ from 100K to 30K

Data was collected for Bath 526-529 however there was only one LED working and very little excitation was observed, so they were all replaced. No data was collected for Bath 535 as the synchrotron beam was lost during data collection. The beam returned after 10 hours but the lights had remained off during this period. The sample had been maintained at 60K for the duration, so the decision was made to undertake a further data collection to see whether any metastable states were still present. As the sample was still shown to be excited the lights were switched back on and the study continued from 60K to 30K.

4.4.3.2 Ground State Structure

As with both previously discussed samples, the crystal was kept in the dark at room temperature and then cooled to 100K in order to obtain a clean unpolluted ground state structure. Any excitation achieved during the investigation was shown to be fully reversible and ground state structures obtained at various points during experiments were comparable to initial data refinements. The crystal quality appeared to remain good throughout the excitation process.

$[Ni(aepy)_2(NO_2)_2]$ crystallised in the space group $P2_1/c$. The complete solid state molecular structure can be seen in figure 4.28. The asu contains half the complete molecule, with the nickel atom sitting on a crystallographic centre of symmetry. The coordination geometry around the nickel metal centre is octahedral and as with both $[Ni(aep)_2(NO_2)_2]$ and $[Ni(aem)_2(NO_2)_2]$ both nitrite ligands are *trans* to each other. N(1) is related to N(1') by the symmetry operation *-x, -y, -z*+1. The nitrite has an O_1-N_1-O_2 angle of 116.91(19)° and adopts an η^1 coordination geometry through the nitrogen atom.

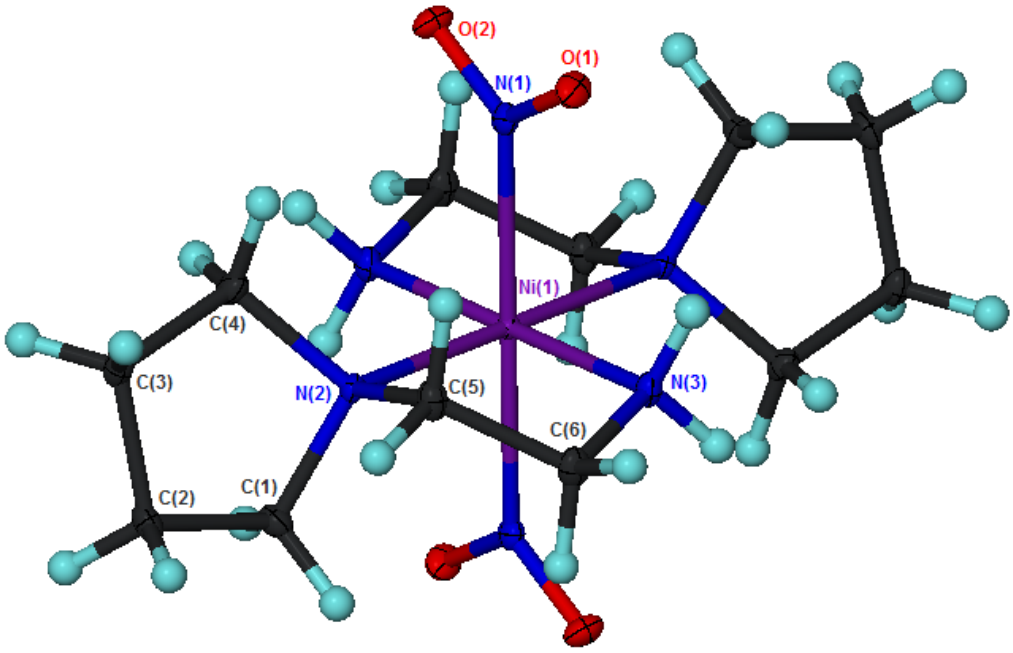

Figure 4.28 Complete ground state structure of $[Ni(aepy)_2(NO_2)_2]$ at 100K with 30% probability ellipsoids shown (Bath 515)

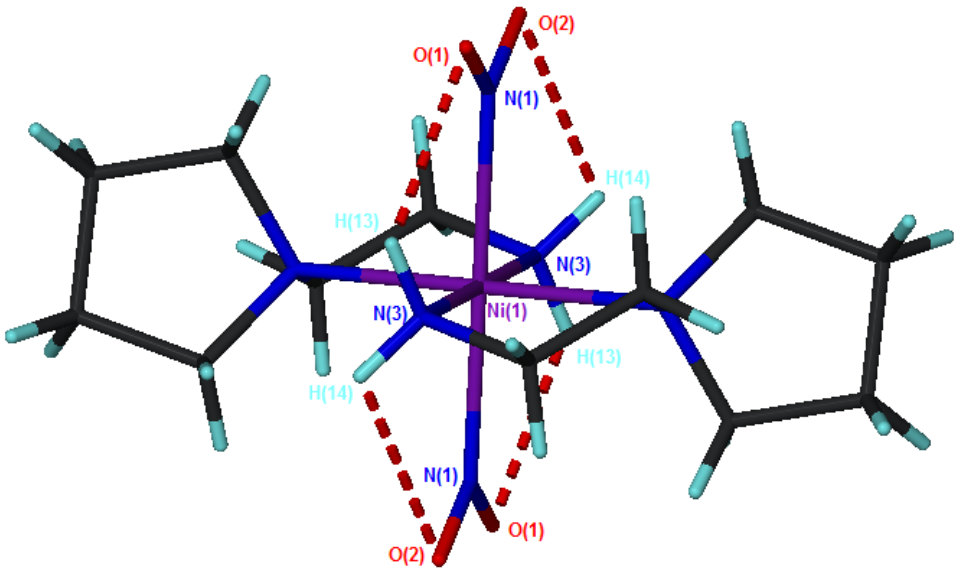

Figure 4.29 Intramolecular short contacts observed in $[Ni(aepy)_2(NO_2)_2]$

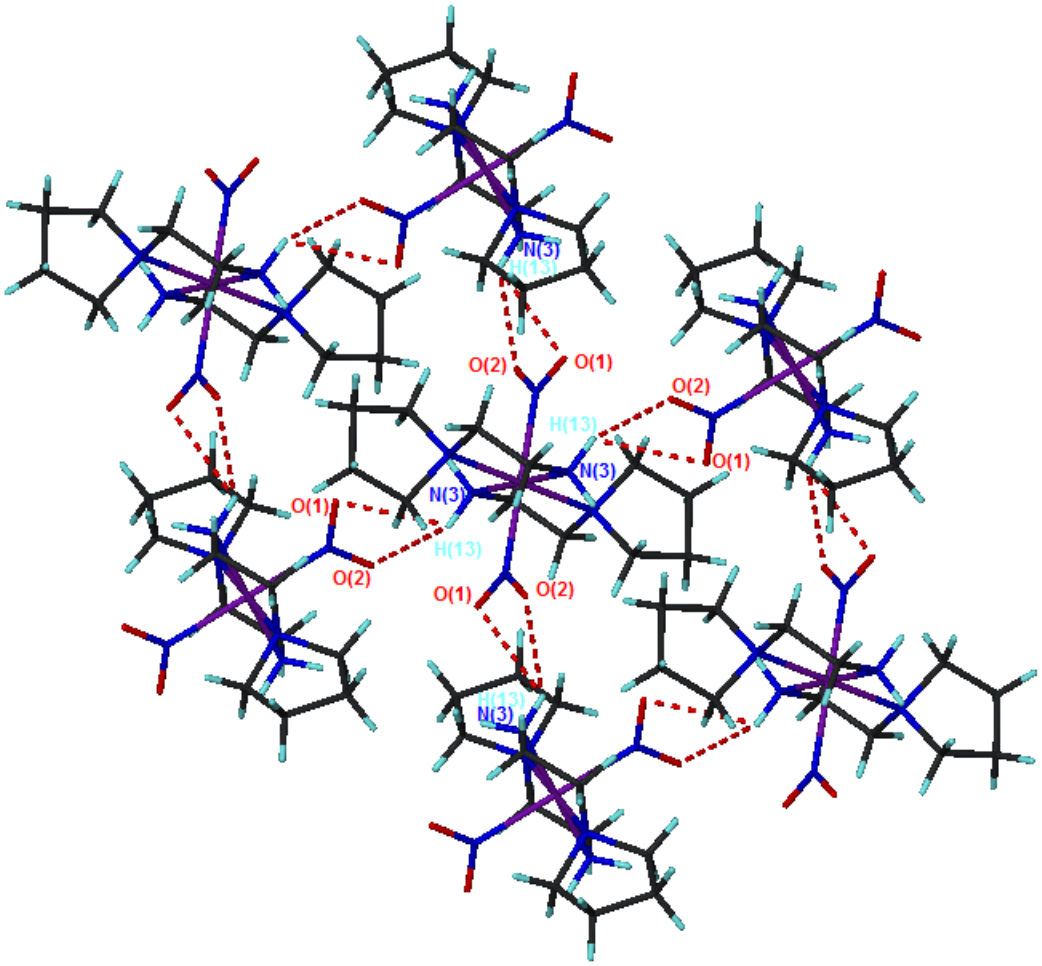

Figure 4.30 Intermolecular hydrogen bonds between oxygen atoms on the nitro group and the hydrogen atom (H_{13}) on the ammine group in $[Ni(aepy)_2(NO_2)_2]$

The bonding observed in the ground state of $[Ni(aepy)_2(NO_2)_2]$ is similar to that found in the analogous morpholine system, with two intramolecular short contacts between the oxygen atoms of the nitro group and the hydrogen atoms on N_3 (figure 4.29). The N_3 - O_1 distance is 2.961(2)Å with a bond angle of 120.5° and the N_3-H_{14}…O_2 bond distance (D…A) is 2.999Å with an angle of 105°.

There are two weak intermolecular hydrogen bonds present, from both oxygen atoms of the nitro group to the same hydrogen atom attached to N_3. In total there are eight intermolecular hydrogen bonds per molecule linking adjacent molecules in a sheet type structure. The N_3-H_{13}…O_1 has a N_3 - O_1 distance of 3.136(3)Å with a bond angle of 113.2° and the N_3-H_{13}…O_2 has a N_3 - O_2 distance of 3.229(2)Å with a bond angle of 130.1°. The intermolecular hydrogen bonding can be seen in figures 4.30 and 4.31.

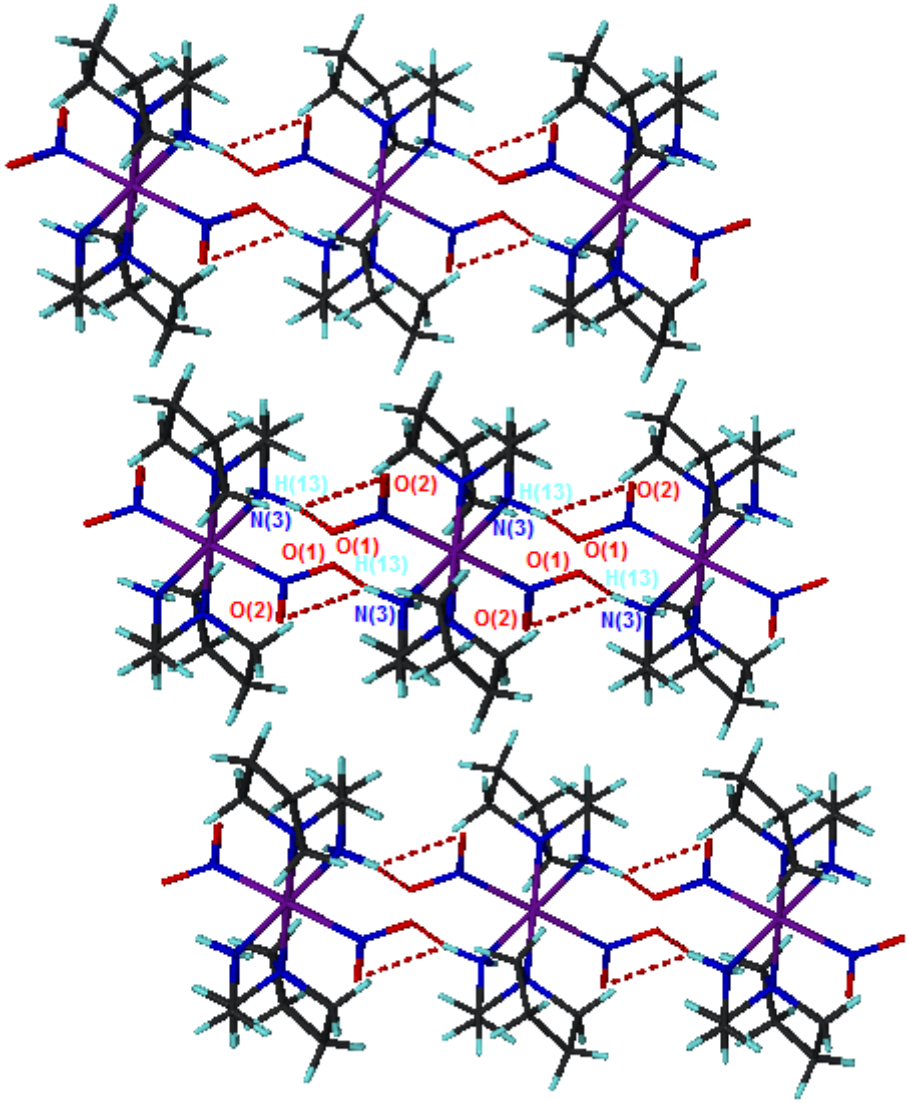

Figure 4.31 Side on view of three sheets in $[Ni(aepy)_2(NO_2)_2]$ exhibiting intermolecular hydrogen bonding

4.4.3.3 Excited State Structure

The crystal structure obtained after 6h irradiation with four blue LEDs at 60K, (Bath 536), is shown in figure 4.32. The structure maintained the same $P2_1/c$ crystal symmetry as the ground state and has approximately 23% disorder observed around the ethyl chain (the percentage appears to increase as the overall excitation is also increased) which has been removed for clarity.

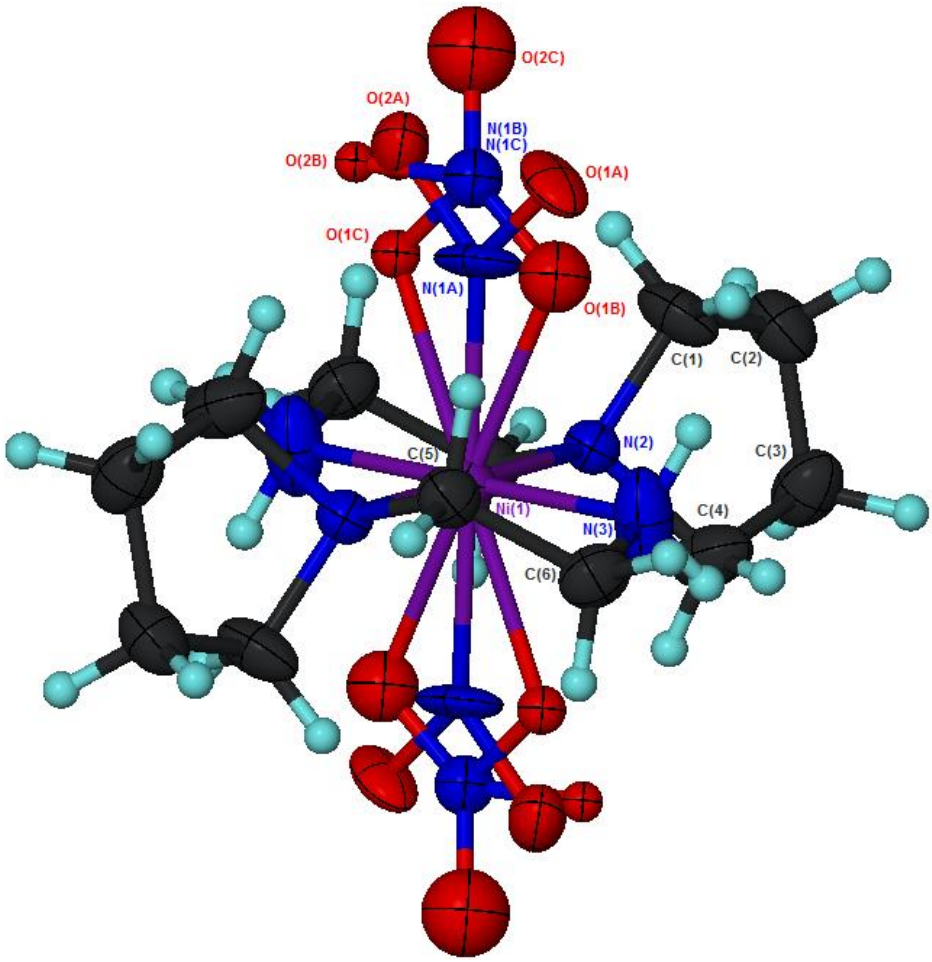

Figure 4.32 Complete excited state structure (Bath with both endo-nitrito and exo-nitrito metastable isomers in $[Ni(aepy)_2(NO_2)_2]$ at 60K with 30% probability ellipsoids shown (Bath 536)

Two different metastable isomers can be seen in the solid state molecular structure which account for almost 34% of the total structure. The major isomer (O_{1B}-N_{1B}-O_{2B} - figure 4.33) which is endo-nitrito η^1 coordinated ((iii) in figure 4.1) to the nickel centre accounts for just under 19% of the total excitation. The second isomer (O_{1C}-N_{1C}-O_{2C} - figure 4.34) is also η^1 coordinated to the metal but adopts an exo-nitrito conformation ((ii) in figure 4.1) and has a slightly lower occupancy at 15% of the overall structure. A close up of the different conformations adopted upon excitation can be seen in figure 4.35.

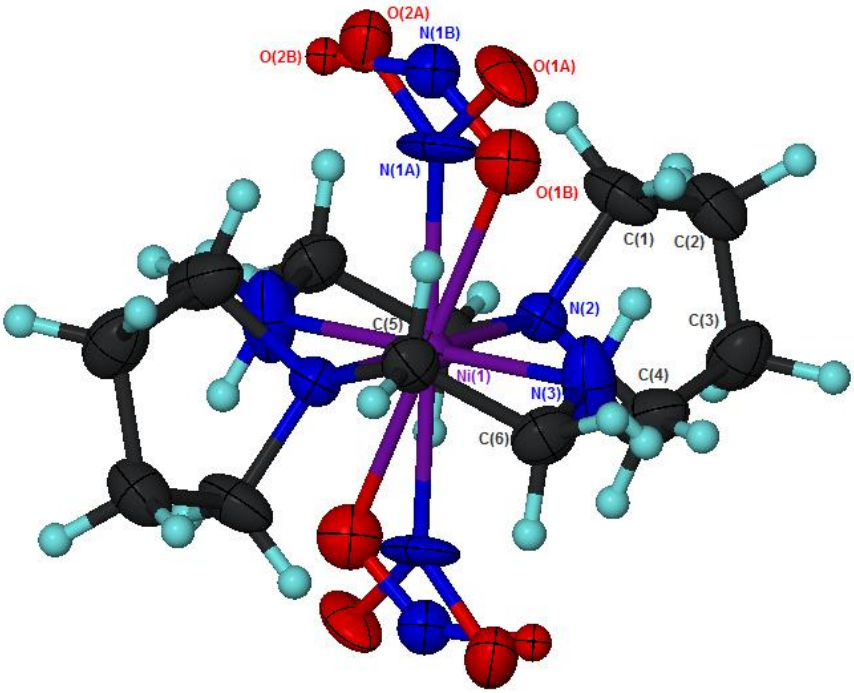

Figure 4.33 Endo-nitrito isomer O_{1B}-N_{1B}-O_{2B} in $[Ni(aepy)_2(NO_2)_2]$

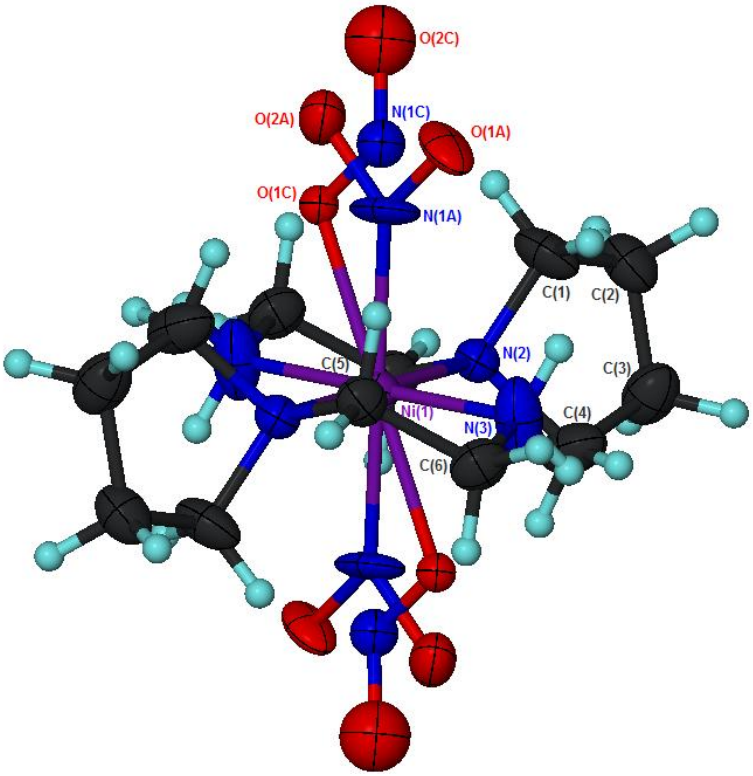

Figure 4.34 Exo-nitrito isomer O_{1C}-N_{1C}-O_{2C} in $[Ni(aepy)_2(NO_2)_2]$

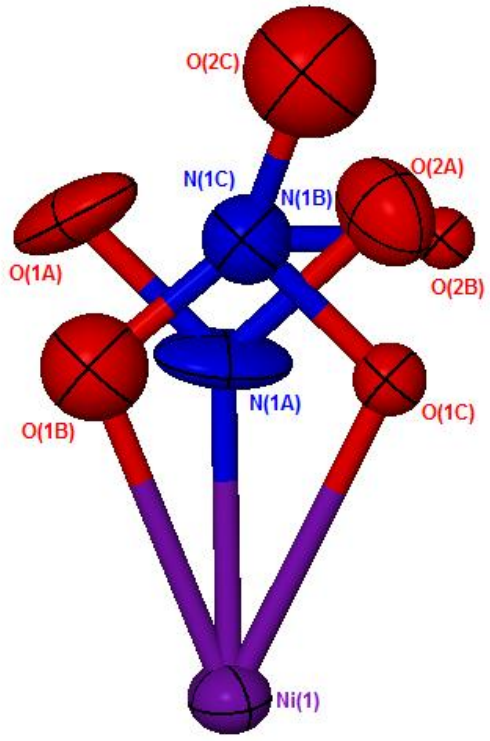

Figure 4.35 Close up of the endo-nitrito and exo-nitrito conformations in $[Ni(aepy)_2(NO_2)_2]$

The excitation in $[Ni(aepy)_2(NO_2)_2]$ was modelled as two disordered fragments and as in previous examples discussed in this chapter, the occupancies of the nitrite metastable isomers were calculated using free variables. SUMP was used to set the sum of the free variables pertaining to the three separate nitrite fragments equal to one. The command EXYZ was used to place atom N_{1B} at the same coordinates as N_{1C} and EADP to give the atoms the same displacement parameters. The command SADI was used to restrain the N-O distances to be the same in both excited state fragments.

Both isomers adopt a distorted octahedral geometry. The endo-nitrito isomer has a bond angle (O_{1B}-N_{1B}-O_{2B}) of 139.21(3)° which is slightly larger than the other endo-nitrito isomers discussed previously. This may be due to the distance of O_{1B} to the nickel metal centre being fixed using the command SADI to match that of O_{1C} to the metal centre. The exo-nitrito isomer has an O_{1C}-N_{1C}-O_{2C}* bond angle of 112.16°.

An analysis of the bonding in the metastable state structure reveals that the bonding is the same as in the ground state. As with $[Ni(aem)_2(NO_2)_2]$ it is possible that a further intramolecular hydrogen bond is present between the nitrito group involving O_{2B} and the hydrogen on N_3 which has a D…A distance of 2.921Å and a bond angle of 112.78° but it would be very weak.

* Constrained atoms

Changes were observed between the unit cell parameters of the ground and excited state and are shown in table 4.14. There was a significant decrease in the *a* axis and a small increase in the *b* axis, however the largest change was an increase in the *c* axis upon excitation of approximately 0.4Å. Overall there was an increase in cell volume of 13Å^3.

	***a* (Å)**	***b* (Å)**	***c* (Å)**	**α (°)**	**β (°)**	**γ (°)**	**V (Å^3)**
Ground State Bath 515	8.6169 (5)	8.5490 (5)	11.5680 (7)	90	104.008 (1)	90	826.83 (8)
Metastable State Bath 536	8.3535 (13)	8.6657 (13)	11.9144 (18)	90	103.127 (2)	90	839.9 (2)

Table 4.14 Comparison of unit cell data for $[Ni(aepy)_2(NO_2)_2]$

4.4.3.4 Slant Plane Fourier Maps

For analysis, fragments pertaining to metastable isomers were removed from the solid state structure and was refined using the ground state coordinates only. Any residual electron density observed in the maps that arise are as a result of the presence of linkage isomers. Figure 4.36 shows maps pertaining to both the ground state (Bath 515) and the highest excited state (Bath 536). The Fourier map shows that all electron density within the solid state molecular structure of the ground state has been accounted for. However, in the excited state structure using the same scale, large smears of unaccounted electron density (mainly focused around the nitro group), reside.

Fourier maps were also generated for the temperature variation studies and can be used to identify the limitations of the metastable states. Figure 4.37 shows Fourier maps relating to the temperature variation study between 100K and 30K. The maps illustrate that both the endo-nitrito and exo-nitrito isomers are stable down to 30K. Figures 4.38 and 4.39 show Fourier maps pertaining to temperature variation studies between 100K to 115K and 100K to 130K respectively. Two separate diagrams were created as the studies were performed on two different crystals and the relative levels of excitation were significantly different. Figure 4.31 shows that at 120K, the exo-nitrito isomer is slightly more dominant however by 125K both isomers had been quenched.

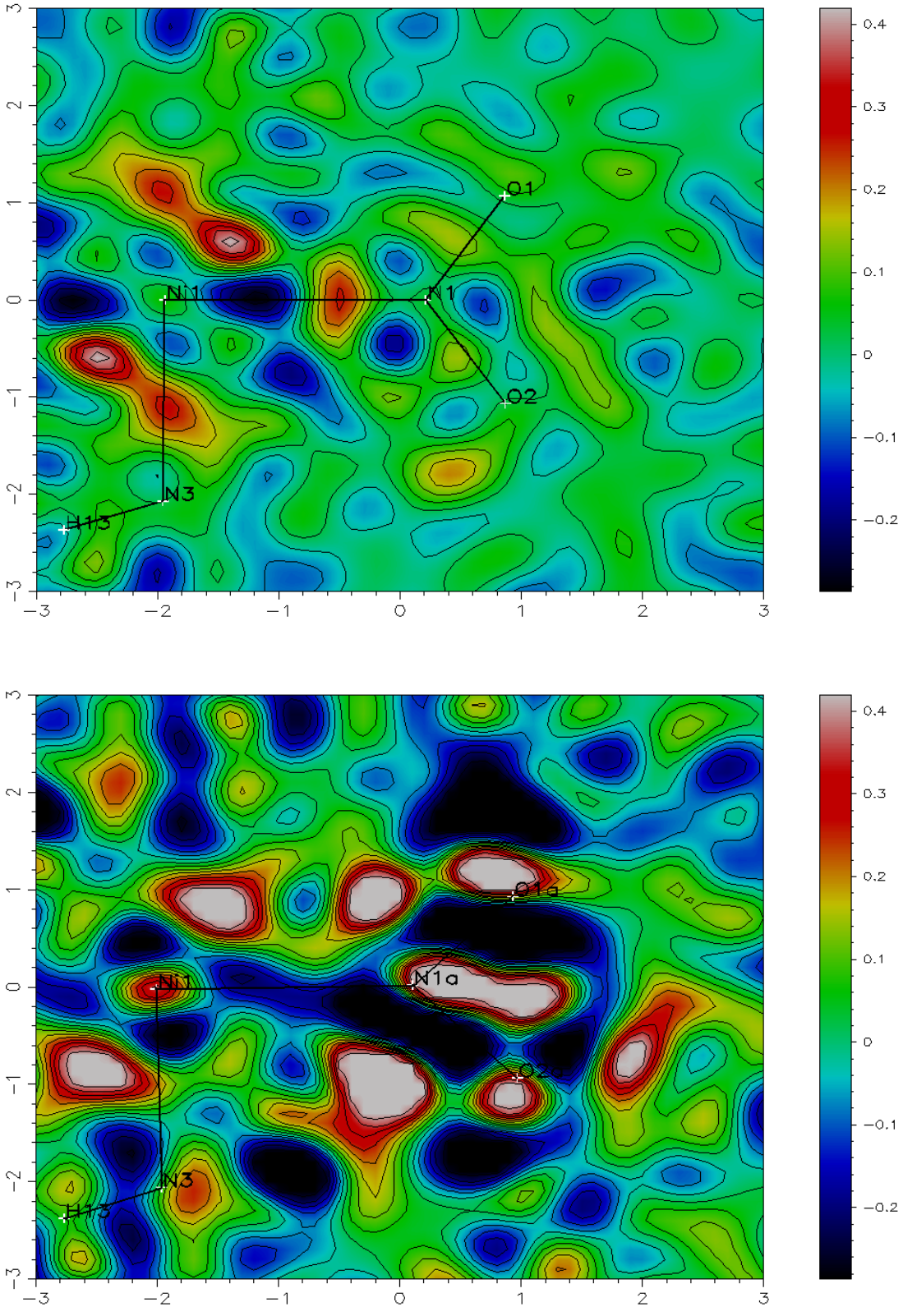

Figure 4.36 Slant plane Fourier maps for the ground state Bath 515 (top) and highest excited state Bath 536 (bottom)

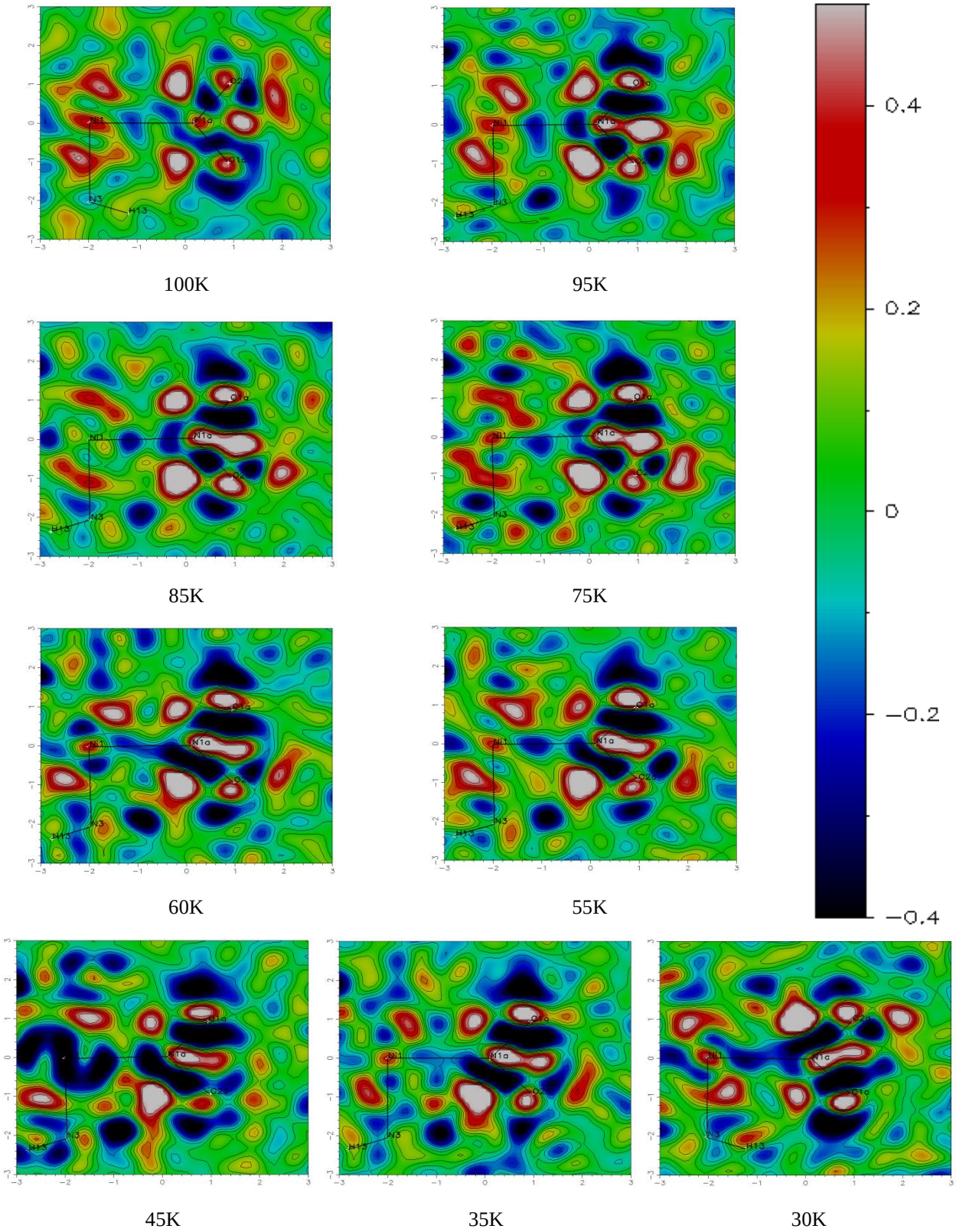

Figure 4.37 Slant plane Fourier maps for temperature variation study of $[Ni(aepy)_2(NO_2)_2]$ from 100K to 30K

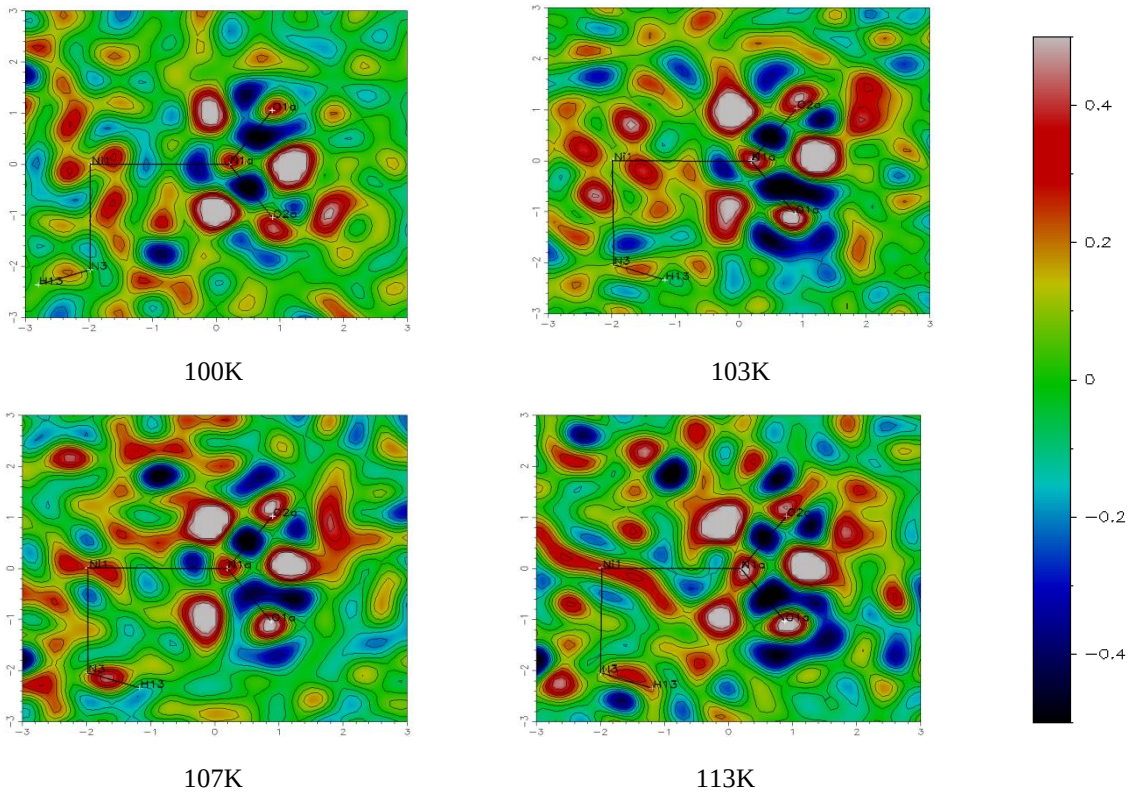

Figure 4.38 Slant plane Fourier maps for temperature variation study of $[Ni(aepy)_2(NO_2)_2]$ from 100K to 115K

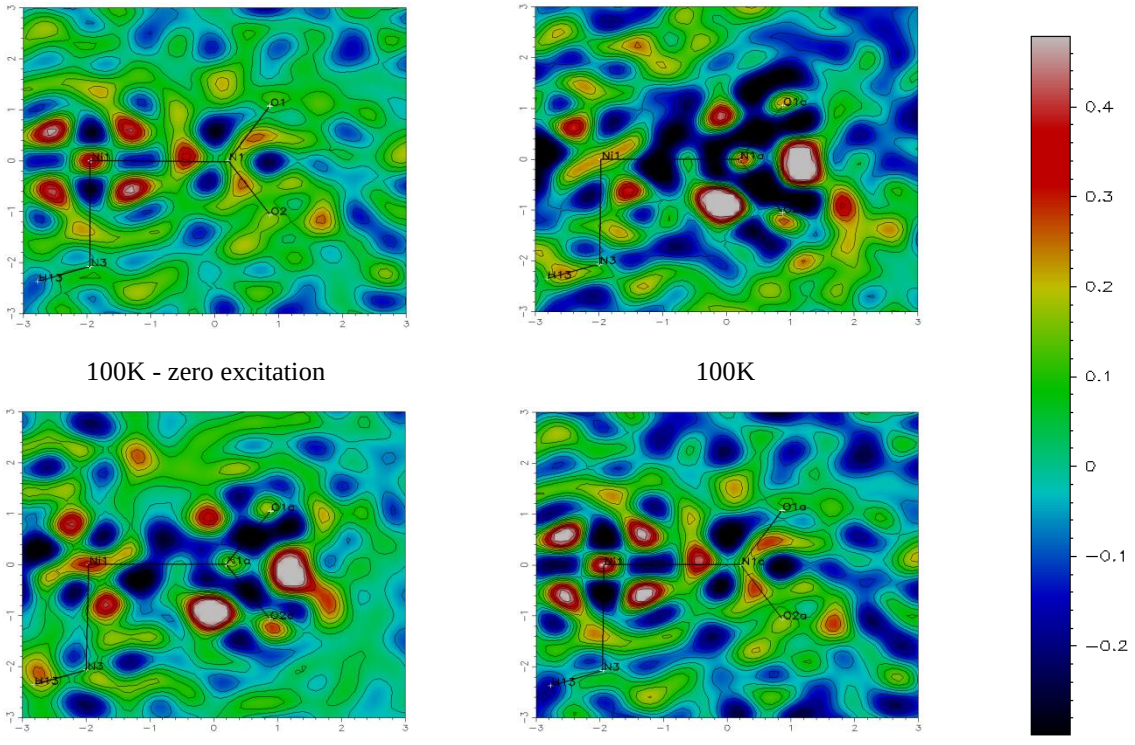

Figure 4.39 Slant plane Fourier maps for temperature variation study of $[Ni(aepy)_2(NO_2)_2]$ from 100K to 130K

4.5 Discussion and Conclusion

The results presented in this section are the first reported evidence for NO_2 linkage isomerism in a neutral species using photocrystallography. Initial experimentation for all three nickel systems using a broadband white light source yielded no results. Due to the multiple wavelengths being generated from the light source, it is possible that at the same time as the metastable state was being populated, there was also a destructive process occurring simultaneously at an alternate wavelength, resulting in no overall change in the crystal structure.

As mentioned earlier in the chapter a solution of $[Ni(aep)_2(NO_2)_2]$ yields both nitro and exo-nitrito crystals with the former as the major isomer. It was discovered that when this solution was irradiated with UV light in a dark room, the majority of crystals that deposited from solution were in fact the nitrito isomer. Photocrystallographic experiments were then attempted using two UV LEDs on a crystal of $[Ni(aep)_2(NO_2)_2]$ to see if the isomerisation process would occur in the solid state. Initial tests at 30K showed no excitation however, when the temperature was raised to 100K experimentation highlighted the presence of two new peaks in the electron density map, focused around the position of the nitro group. Further experiments were then conducted on both $[Ni(aem)_2(NO_2)_2]$ and $[Ni(aepy)_2(NO_2)_2]$ and also resulted in a small amount of excitation. In the case of $[Ni(aem)_2(NO_2)_2]$ however, the excitation was too small to model despite the presence of some small Q-peaks pertaining to a possible endo-nitrito isomer being observed as residual electron density in the electron density map.

For the following experiment at Daresbury on Station 9.8 the decision was made to swap the LEDs which emitted at 400nm for some blue LEDs which emit at 467nm but with far greater intensity than possible for UV LEDs available for purchase. The decision was made to mount four LEDs directly behind the sample through the back plate on the diffractometer and the experimental set-up can be seen in figure 4.6. The experiments undertaken using blue LEDs resulted in far greater levels of excitation and are those which are presented here in this thesis.

The advantages of using LEDs for this type of experiment have proved invaluable. Not only do they provide the option to be selective as to which wavelength is used during the experiment, a wide variety of intensities at each wavelength are also readily available. This means that if the LEDs appear to be causing crystals to fracture at the wavelength needed for excitation, a different LED which emits at the same wavelength but with a lower intensity can be used to try and overcome this problem. There is also the advantage that they are extremely cost effective and significantly cheaper than a laser.

Each of the complexes $[Ni(aep)_2(NO_2)_2]$, $[Ni(aem)_2(NO_2)_2]$ and $[Ni(aepy)_2(NO_2)_2]$ behave slightly differently upon excitation. All three compounds exhibit endo-nitrito linkage isomerism upon excitation

with both $[Ni(aep)_2(NO_2)_2]$ and $[Ni(aepy)_2(NO_2)_2]$ forming one unique endo-nitrito metastable species upon irradiation per molecule and $[Ni(aem)_2(NO_2)_2]$ with two. $[Ni(aepy)_2(NO_2)_2]$ however also forms a exo-nitrito species during the excitation process.

It is unclear why the aep complex only forms one conformation of nitrito isomer upon excitation, yet the other two complexes adopt two nitrito conformations (albeit in the case of the aem species it is the same endo-nitrito form in two different orientations). These differences do not appear to correlate with differences in crystal packing as determined by the analyses of the hydrogen bonding networks. It is possible that due to the lower levels of excitation that only one metastable linkage isomer is formed when a crystal of $[Ni(aep)_2(NO_2)_2]$ is irradiated, and if further excitation could be achieved the presence of a second metastable form may appear. It could also be the case that an LED with a different wavelength and intensity may excite the sample better than the blue LEDs that were used for these experiments. When initial tests were carried out using UV LEDs it was actually the aep system that showed the greatest amount of excitation. In the future it may be worth trying to excite the $[Ni(aep)_2(NO_2)_2]$ system again with UV LEDs which emit with a greater intensity. The other interesting point is that the isomer formed upon excitation when $[Ni(aep)_2(NO_2)_2]$ is irradiated is endo-nitrito and not exo-nitrito like the crystals obtained when the complex is initially synthesised (figure 4.40). This may be a result of there being less movement in the crystal when forming the endo-nitrito species as opposed to the exo form.

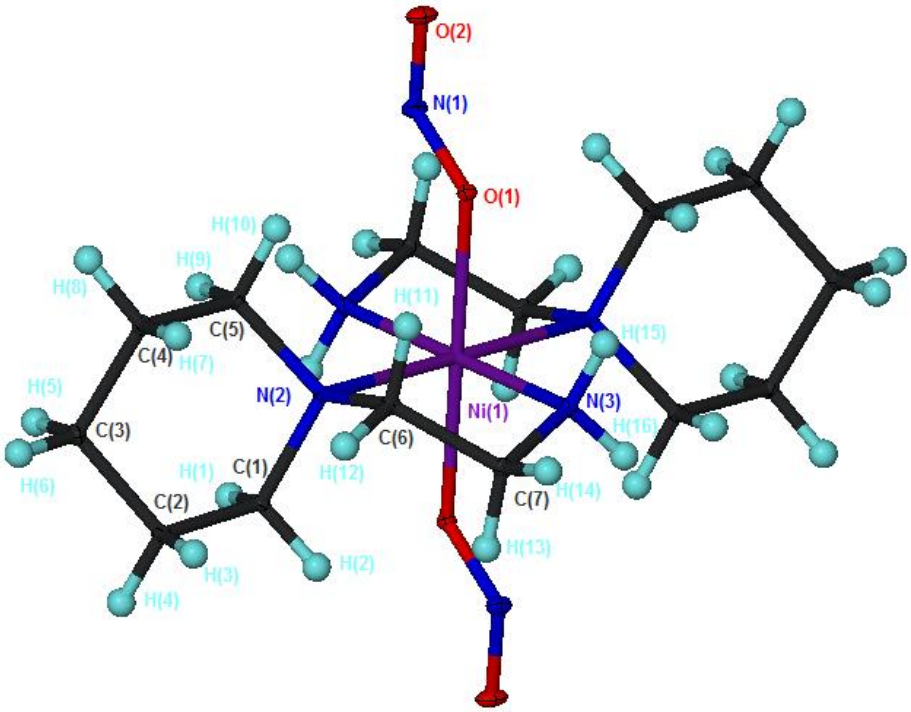

Figure 4.40 Crystal structure of exo-nitrito isomer of $[Ni(aep)_2(NO_2)_2]$ (Bath 486)

The exo-nitrito isomer obtained during the initial synthesis (Bath 486) has a O_1-N_1-O_2 bond angle of 114.54(1)° with an O_1-N_1 bond length of 1.2921(13)Å and an O_2-N_1 bond length of 1.2349(14)Å. The Ni_1-O_1 bond distance is 2.1047(8)Å. The exo-nitito isomer obtained from excitation in the $[Ni(aepy)_2(NO_2)_2]$ is fairly similar to this with a O_{1C}-N_{1C}-O_{1C} bond angle of 112.16°, O-N bond distances of around 1.22Å and a Ni_1-O_{1C} distance of 2.20(2)Å.

Analyses of the bonding interactions within the solid state molecular structures were undertaken in order to determine whether the species formed upon excitation was governed by a stabilising bonding interaction. This however does not appear to be the case and the majority of interactions identified are generally too weak to influence the conformations adopted by the metastable states.

A closer inspection of van de Waals space filling diagrams of excited state structures reveals that there is only a small amount of space available above the nitro ligand for both $[Ni(aep)_2(NO_2)_2]$ (figure 4.41) and $[Ni(aem)_2(NO_2)_2]$ (figure 4.42) for isomerisation. This may account for the formation of the endo-nitrito conformation over the exo species as it requires a smaller amount of movement within the crystalline lattice. The space filling diagram for the excited state of $[Ni(aepy)_2(NO_2)_2]$ is shown in figure 4.43. From the diagram, it appears there is slightly more space available above the nitro ligand to accommodate the exo-nitrito conformation than in the aep and aem excited state structures and it may be solely for this reason that the metastable exo form only occurs in this sturcture.

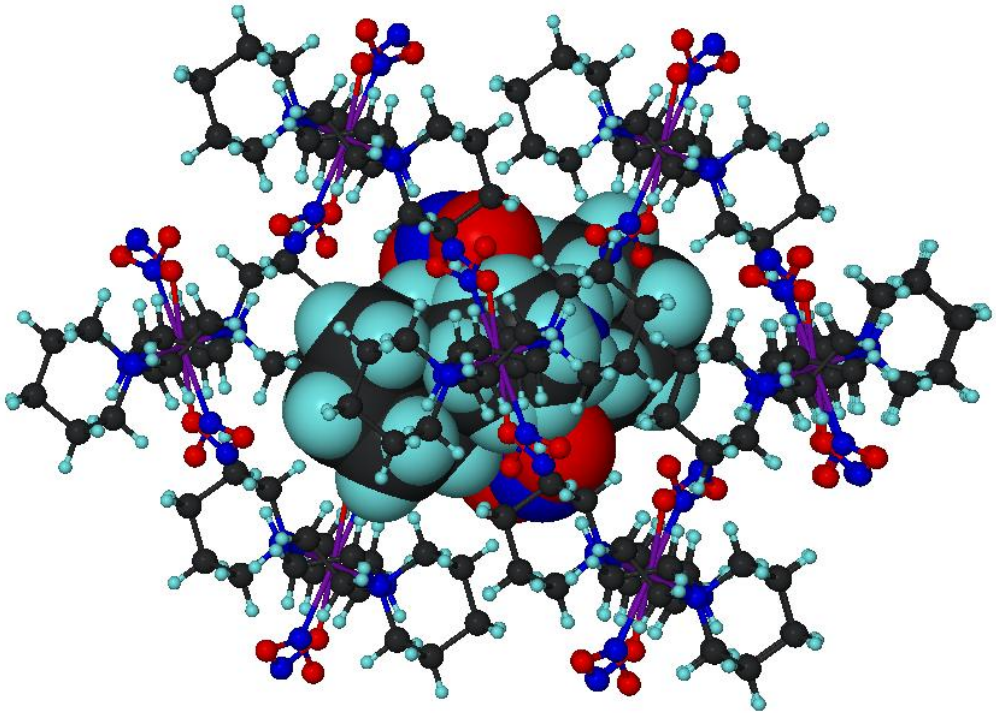

Figure 4.41 Space filling diagram for the excited state structure of $[Ni(aep)_2(NO_2)_2]$

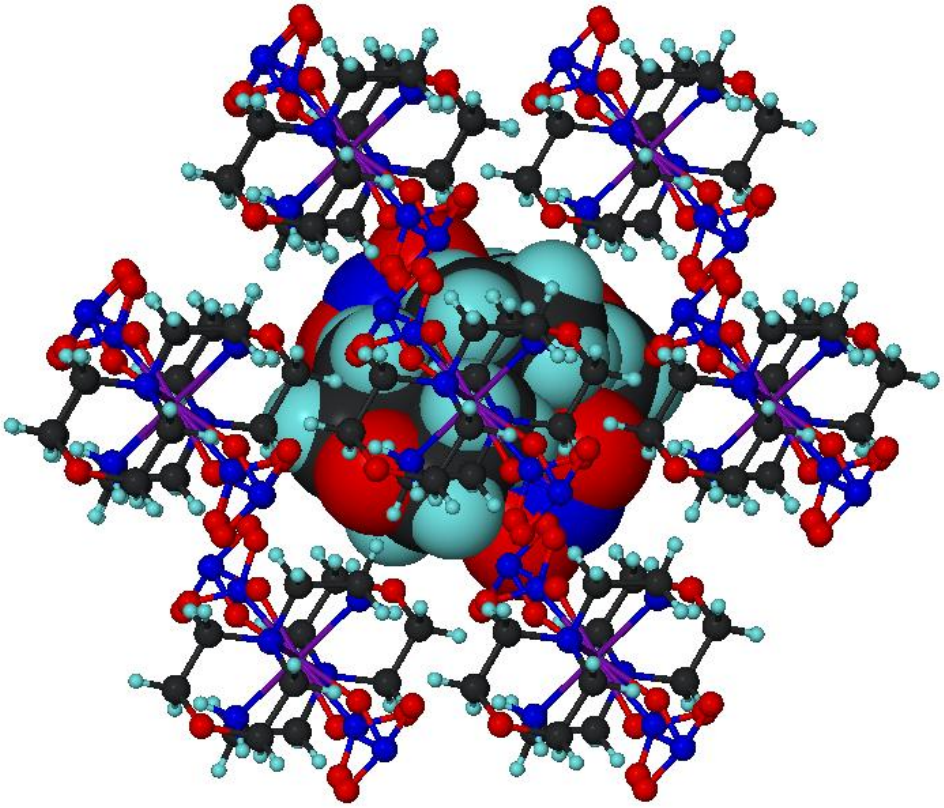

Figure 4.42 Space filling diagram for the excited state structure of $[Ni(aem)_2(NO_2)_2]$

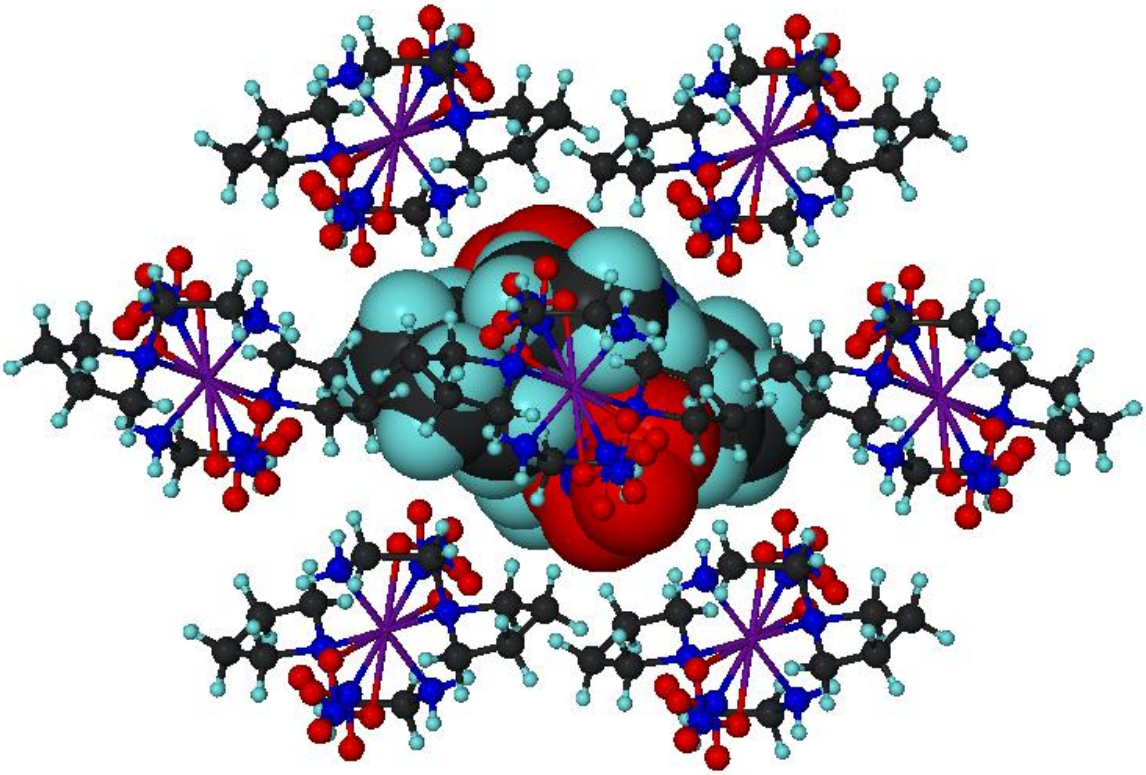

Figure 4.43 Space filling diagram for the excited state structure of $[Ni(aepy)_2(NO_2)_2]$

Future work on these systems would involve trying to maximise the percentage conversion from the ground state to metastable state species. Ideally one hundred percent conversion is the ultimate goal in photoisomerisation reactions, but may not be possible in these systems perhaps because of strain on the crystalline lattice causing the crystal to shatter if it is over exposed to irradiation from a light source.

Investigations were also undertaken to identify whether the exo-nitrito isomer of $[Ni(aep)_2(NO_2)_2]$ would isomerise back to the nitro species upon irradiation. Yellow LEDs were utilised, however experiments performed on this species proved unsuccessful. It could be possible that light of a different wavelength may cause this structure to photoisomerise, but due to time restrictions we were unable to test this further.

Ideally DFT calculations which model the excitation processes would be carried out to identify the differences in energy between various states. This would help in the selection of suitable light sources with the appropriate wavelength for excitation, however initial calculations used to try and excite the molecules refused to converge despite several attempts.

Similar structures with NCS ligands in place of the NO_2 groups can also be synthesised and are reported in the literature.[17] This is another ligand capable of isomerisation and it may be worth investigating to see if thiocyanate to isothiocyanate rearrangements are possible in the solid state with the use of light as the stimulus.

In order for these molecules to be used as molecular switches, it is important to identify molecules which can isomerise at room temperature. At present the structures presented here can only isomerise at low temperature and would not be suitable for use in electronic devices.

4.6 Summary of Crystallographic Data

Compound	Bath 412	Bath 435
Empirical Formula	C14 H32 N6 Ni O4	C14 H32 N6 Ni O4
M_r	407.17	407.17
Temperature (K)	100(2)	90(2)
Crystal System	Monoclinic	Monoclinic
Space Group	$P2_1/c$	$P2_1/c$
Wavelength (Å)	0.6703	0.6703
***a* (Å)**	9.6309(14)	9.6301(6)
***b* (Å)**	8.2557(12)	8.2875(5)
***c* (Å)**	11.8340(17)	11.8754(8)
α (°)	90	90
β (°)	109.0650(10)	109.1030(10)
γ (°)	90	90
V (Å^3)	889.3(2)	895.58(10)
Z	2	2
Absorption coefficient (mm^{-1})	1.124	1.116
Reflections collected	10846	10094
Independent reflections	3195	2715
R_{int}	0.0648	0.0626
R_1, w$R2$	0.0522, 0.1235	0.0465, 0.1273
***R* indices (all data)**	0.0634, 0.1349	0.0500, 0.1314

Table 4.15 Comparison of crystal data for ground and excited structures of $[Ni(aep)_2(NO_2)_2]$

Compound	Bath 541	Bath 551
Empirical Formula	$C_{12}H_{28}N_6Ni_1O_6$	$C_{12}H_{28}N_6Ni_1O_6$
M_r	411.11	411.11
Temperature (K)	100(2)	45(2)
Crystal System	Triclinic	Triclinic
Space Group	*P*-1	*P*-1
Wavelength (Å)	0.68960	0.68960
***a* (Å)**	7.172(5)	7.2011(17)
***b* (Å)**	7.988(5)	8.0007(18)
***c* (Å)**	8.330(5)	8.2916(19)
α (°)	94.306(5)	94.620(3)
β (°)	112.642(5)	110.884(3)
γ (°)	100.496(5)	101.434(3)
V ($Å^3$)	427.5(5)	431.46(17)
Z	1	1
Absorption coefficient (mm^{-1})	1.179	1.168
Reflections collected	2143	2181
Independent reflections	869	888
R_{int}	0.0159	0.0134
R_1, w*R*2	0.0215, 0.0543	0.0280, 0.0735
***R* indices (all data)**	0.0216, 0.0543	0.0286, 0.0740

Table 4.16 Comparison of crystal data for ground and excited structures of $[Ni(aem)_2(NO_2)_2]$

Compound	Bath 515	Bath 536
Empirical Formula	C12 H28 N6 Ni O4	C12 H28 N6 Ni O4
M_r	379.11	379.11
Temperature (K)	100(2)	60(2)
Crystal System	Monoclinic	Monoclinic
Space Group	$P2_1/c$	$P2_1/c$
Wavelength (Å)	0.6896	0.6896
***a* (Å)**	8.6169(5)	8.3535(13)
***b* (Å)**	8.5490(5)	8.6657(13)
***c* (Å)**	11.5680(7)	11.9144(18)
α (°)	90	90
β (°)	104.008(1)	103.127(2)
γ (°)	90	90
V (Å^3)	826.83(8)	839.9(2)
Z	2	2
Absorption coefficient (mm^{-1})	1.203	1.184
Reflections collected	4023	4129
Independent reflections	846	869
R_{int}	0.0243	0.0296
R_1, w$R2$	0.0212, 0.0520	0.0473, 0.1222
***R* indices (all data)**	0.0226, 0.0530	0.0513, 0.1257

Table 4.17 Comparison of crystal data for ground and excited structures of $[Ni(aepy)_2(NO_2)_2]$

4.7 References

[1] C. M. Gordon, R. D. Feltham, J. J. Turner, *J. Phys. Chem.* **1991**, *95*, 2889.
[2] S. M. Jørgenson, *Z. Anorg. Chem.* **1894**, *5*, 147.
[3] B. Adell, *Z. Anorg. Allg. Chem.* **1955**, 219.
[4] P. Coppens, I. Novozhilova, A. Kovalevsky, *Chem. Rev.* **2002**, *102*, 861.
[5] I. Grenthe, E. Nordin, *Inorg. Chem.* **1979**, *18*, 1869.
[6] S. Ahrland, J. Chatt, N. R. Davies, *Q. Rev., Chem. Soc.* **1958**, *12*, 265.
[7] M. Kubota, S. Ohba, *Acta Crystallogr. Sect. B* **1992**, *48*, 627.
[8] V. Balzani, R. Ballardini, N. Sabbatini, L. Moggi, *Inorg. Chem.* **1968**, *7*, 1398.
[9] D. Das, I. R. Laskar, A. Ghosh, A. Mondal, K. Okamoto, N. R. Chaudhuri, *J. Chem. Soc. Dalton Trans.* **1998**, 3987.
[10] A. J. Finney, M. A. Hitchman, C. L. Raston, G. L. Rowbottom, A. H. White, *Aust. J. Chem.* **1981**, *34*, 2061.
[11] M. J. Goldberg, R. E. Marsh, *Acta Crystallogr. Sect. B* **1979**, *35*, 960.
[12] T. Chattopadhyay, M. Ghosh, A. Majee, M. Nethaji, D. Das, *Polyhedron* **2005**, *24*, 1677.
[13] T. Chattopadhyay, M. Ghosh, A. Banerjee, K. S. Banu, D. Das, M. Nethaji, *Transition Met. Chem.* **2007**, *32*, 531.
[14] T. Chattopadhyay, N. Podder, K. S. Banu, A. Banerjee, M. Ghosh, E. Suresh, M. Nethaji, D. Das, *J. Mol. Struct.* **2007**, *839*, 69.
[15] I. R. Laskar, D. Das, G. Mostafa, T. H. Lu, T. C. Keng, J. C. Wang, A. Ghosh, N. R. Chaudhuri, *N. J. Chem.* **2001**, *25*, 764.
[16] K. F. Bowes, J. M. Cole, S. L. G. Husheer, P. R. Raithby, T. L. Savarese, H. A. Sparkes, S. J. Teat, J. E. Warren, *Chem. Commun.* **2006**, 2448.
[17] I. R. Laskar, T. K. Maji, D. Das, T. H. Lu, W. T. Wong, K. Okamoto, N. R. Chaudhuri, *Polyhedron* **2001**, *20*, 2073.

Chapter 5

Crystal Engineering

5.1 Introduction

Crystal formation is a non-equilibrium phenomenon in which both the thermodynamic and kinetic aspects of the reaction conditions contribute to a final structure. The structure obtained is often a result of the crystallisation conditions used and it is hard to predict the outcome as the crystallisation process is controlled by a vast number of long and short range interactions.[1]

Crystal engineering was initially identified by Arthur von Hippel who described its fundamental characteristics in detail under the term 'molecular engineering'.[2] Modern crystal engineering, however, was developed as a technique to facilitate understanding in the regioselectivity and product distribution of solid state molecular reactions in the early 1960s. Investigations were originally performed on species such as α,β-unsaturated acids in a field termed topochemistry developed by Schmidt.[3] The area has developed rapidly over the past few decades especially with the development of modern crystallographic techniques and now encompasses many aspects of solid state chemistry. It is readily used in structure prediction and control as well as an aid in the synthesis of novel molecular building blocks and crystalline materials.[1]

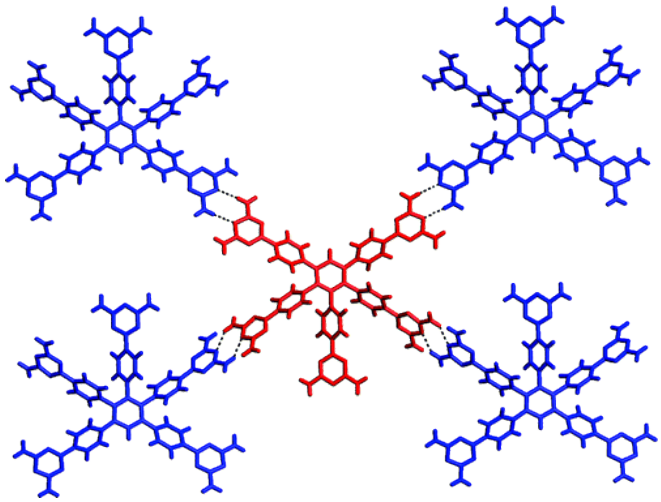

Figure 5.1 Example of crystal engineering where the overall network is held together by hydrogen bonds

Crystal engineering can be described as the design and preparation of a crystalline solid based on the knowledge and exploitation of the steric, topological and intermolecular bonding capabilities of the constituent molecules (figure 5.1).[4] The crystalline material is comprised of molecular 'building blocks' held together by supramolecular interactions such as hydrogen bonds. An understanding of the kinetics and thermodynamics of crystal nucleation the requirements of crystal close packing and the relative importance of the multiplicity of interactions that go together to assemble the crystalline entity are also of importance.[1]

One of the particular attractions to crystal engineering is the ability to tune the chemical and physical properties of a solid. Due to the structural damage sustained by the rearrangement of an ambidentate ligand in a single crystal upon excitation in photocrystallographic experiments, it is hoped that crystal engineering can help overcome the risk of crystal shattering by extending the size of the crystalline lattice. As a result, it is hoped that greater excitation would be observed as the percentage of the total crystal structure isomerising would be small, reducing the strain on the overall lattice.[5] Several crystal engineering methods could be employed to provide a solution.

One solution involves the use of host-guest chemistry. Commonly the host is a large molecule or aggregate possessing a sizeable hole or cavity with the guest being a considerably smaller molecule which has the potential to bind and reside in the space.[1] Examples of common hosts include porphyrins, crown ethers, cyclodextrins and calixarenes.

The example in figure 5.2 shows an inclusion compound where a molecule of β-cyclodextrin acts as a host to coumarin.[6] The coumarin molecule can undergo a photodimerisation reaction with 64% yield while residing within the cyclodextrin. The cyclodextrin molecules form a reaction nanotube rather than serving merely as reaction vessel in the solid state due to significant interactions between adjacent β-cyclodextrin units which result in the molecules lining up in rows.[7] This example demonstrates the ability for large guest molecules to encapsulate and facilitate photo-excitation reactions of smaller guest species.

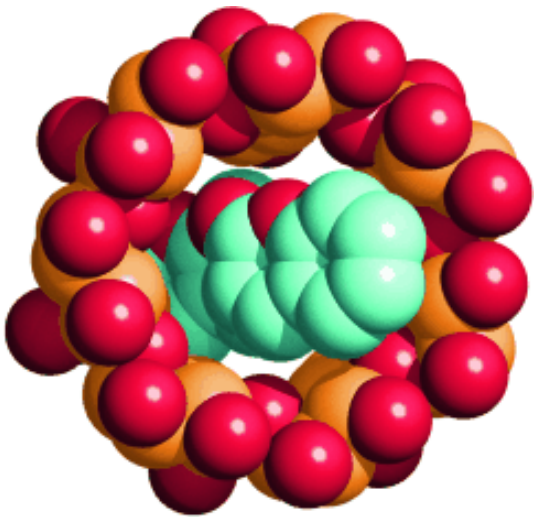

Figure 5.2 Space filling diagram of β-cyclodextrin acting as a host (red and orange), with a guest molecule of coumarin (predominantly turquoise)

Another example of crystal engineering host-guest chemistry where π-stacking interactions are exploited, is when $[Ni(phen)_3]^{2+}$ is reacted with *p*-sulfonatocalix[4]arene anions (where phen is 1,10-phenanthroline). An infinite π-stacked chain is formed when the compound is recrystallised from a mixture of acetone and water with half of the cations sitting within the cavity as shown in figure 5.3.[8] If a photo-active molecule with a ligand capable of π-stacking was crystallised within the calixarene cavities there may be ample space for the ambidentate ligand to isomerise without placing too much strain on the overall lattice.

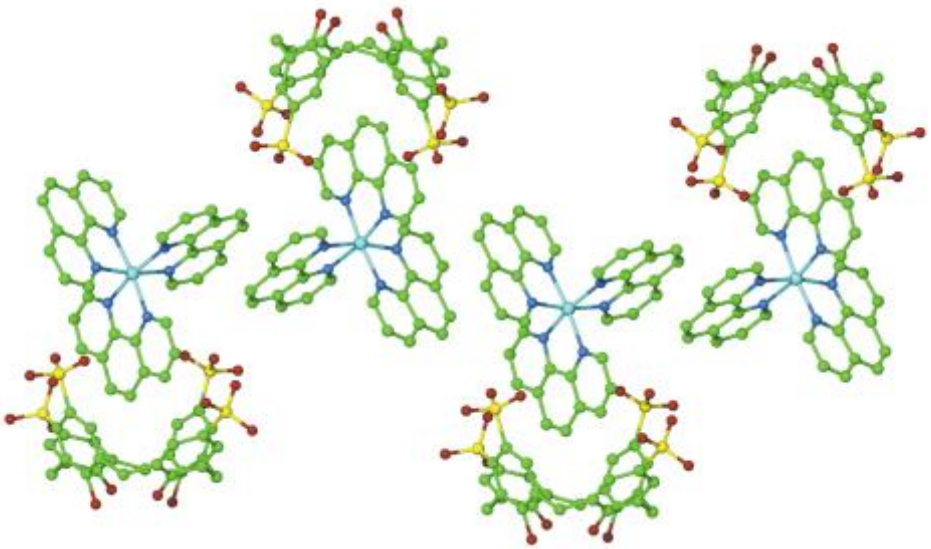

Figure 5.3 π-stacked chain showing the inclusion of one $[Ni(phen)_3]^{2+}$ cations within the cavity of *p*-sulfonatocalix[4]arene anions. Other $[Ni(phen)_3]^{2+}$ cations sit between chain layers to balance the charges

Zheng and co-workers demonstrated by embedding photoactive molecules of tiglic acid in an inert host lattice consisting of C-ethylcalix[4]resorcinarene, that three-dimensional periodicity can be retained as the acid moiety undergoes an *E* to *Z* isomerisation. Approximately 30% isomerisation is achieved from the *E* to the Z configuration of tiglic acid using 325nm light from a 48mW He/Cd laser over a period of several hours (figure 5.4).[9]

Desipite the percentage conversion of molecules undergoing isomerisation being relatively high, and with both the shape of the guest and its general position reorienting in the solid state, the unit cell changes observed are minor (ca. 1%). This evidence confirms that the host molecules form a stable molecular scaffold that preserves the overall structural integrity of the crystal.[9]

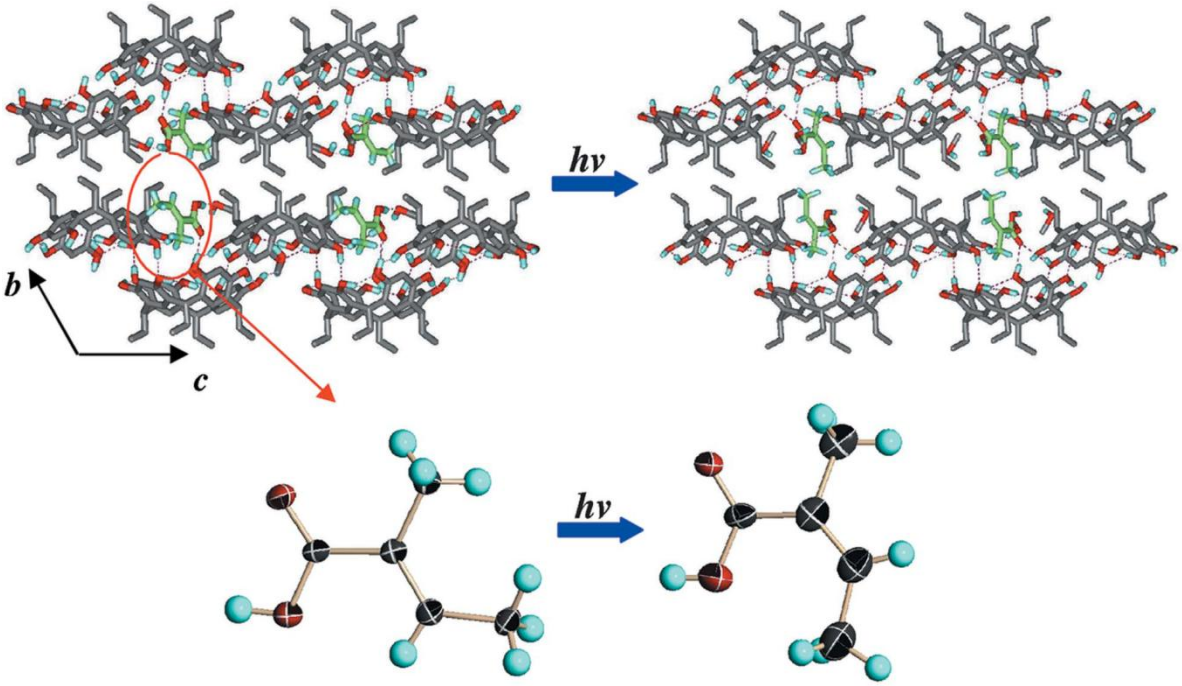

Figure 5.4 Three dimensional supramolecular architecture showing *E* (left) to *Z* (right) isomerisation of the tiglic acid molecule after 3hrs irradiation

A step on the way to fully encapsulating molecules for photocrystallographic studies is to co-crystallise cationic species that can undergo photo-excitation with large anions that dominate the lattice spacing and do not change upon excitation. The smaller cations can reside in the cavities between the anions which provide room for them to isomerise. In the majority of crystallographic studies carried out previously, only small counterions have been included in the lattice. In this chapter we now report the results of some crystal engineering studies targeted at producing crystals with larger counterions, the presence of which may help to reduce crystal strain in photocrystallographic experiments.

5.2 Experimental Aims

The experiments within this chapter looks at the crystal engineering of two complexes - $[Co(NH_3)_5NO_2]Cl_2$ and $[Ru(NH_3)_4(SO_2)Cl]Cl$.

The main objective is as follows:

- *To investigate the possibility of expanding the overall size of the crystal lattice using crystal engineering.* Attempts are made at counter-ion exchange to increase the overall size of the crystalline lattice. This may help facilitate the photoisomerisation process by reducing the potential strain on the crystal, as the overall percentage of the solid state molecular structure that is involved in the isomerisation process is reduced.

5.3 Experimental

5.3.1 Data Collection

X-ray single crystal diffraction data were collected at the University of Bath or on Station 9.8 at the STFC Daresbury Laboratory. Powder diffraction data was collected at room temperature at the University of Bath. The details of hardware, software and equipment used are discussed in Chapter 6.

5.4 Results

5.4.1 $[Co(NH_3)_5(NO_2)]Cl_2$

As discussed in Chapters 1 and 4, linkage isomerism was first identified by Alfred Werner in his studies on this complex.[10] The nitro to nitrito isomerisation process was shown to proceed photochemically by Adell with exposure to sunlight.[11] Single crystal photocrystallographic experiments on this compound have proved to show a small percentage of isomerisation.[12] The small amounts of excitation achieved for the dication - $[Co(NH_3)_5(NO)_2]^{2+}$ may have only been restricted due to lattice strain, particularly when the counterion here is very small. This complex was therefore deemed a suitable candidate for crystal engineering experiments.

5.4.1.1 Single Crystal Data

Single crystal X-ray diffraction measurements were made on a red block shaped crystal of $[Co(NH_3)_5(NO)_2]Cl_2$ (structure number k06prr06) with dimensions 0.15 x 0.15 x 0.01mm at 150(2)K on a Kappa CCD diffractometer. A summary of the crystal data can be seen in table 5.1 and the complete solid state molecular structure can be seen in figure 5.5. The structure is consistent with that reported previously.[12]

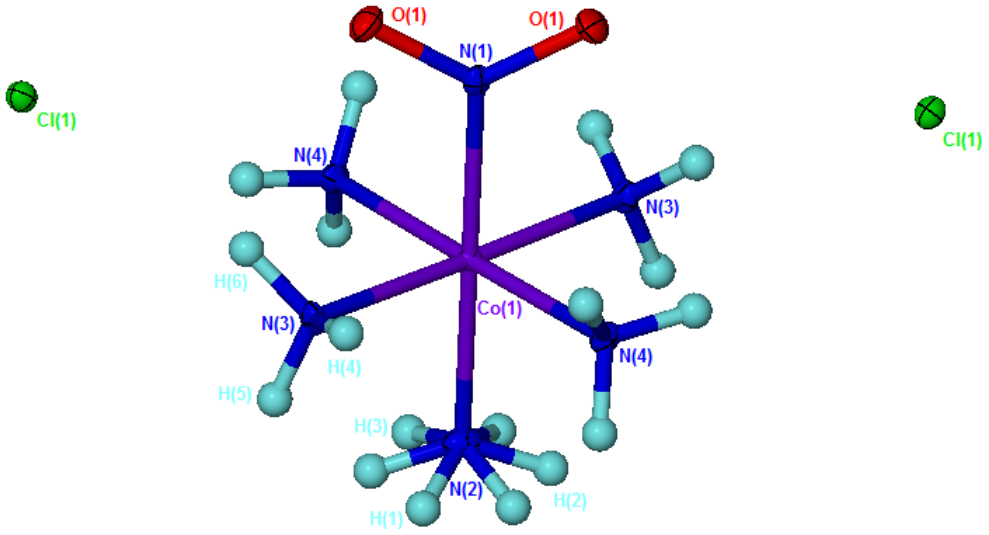

Figure 5.5 Solid state molecular structure of $[Co(NH_3)_5(NO_2)]Cl_2$ with 30% probability ellipsoids shown

The solid state molecular structure consists of a metal cation with two chloride counter-ions, which are the target for replacement in this complex. The two orientations of the methyl hydrogen atoms on N_2 are shown, consistent with the molecule sitting on a 2-fold rotational axis. This ammine group also exhibits the longest Co-N bond at 1.980(3)Å. The O_1-N_1-O_1 bond angle is 121.3(3)° with a N_1-O_1bond length of 1.229(2)Å.

Empirical Formula	H_{15} Co N_6 O_2 Cl_2
M_r	261.01
Temperature (K)	150(2)
Crystal System	Monoclinic
Space Group	*C*2/*c*
Wavelength (Å)	0.71073
***a* (Å)**	10.1910(3)
***b* (Å)**	8.6830(3)
***c* (Å)**	10.7260(3)
α (°)	90
β (°)	95.307(10)
γ (°)	90
V (Å^3)	945.06(5)
Z	4
Absorption coefficient (mm^{-1})	2.352
Reflections collected	7837
Independent reflections	1420
R_{int}	0.0450
R_1, w*R*2	0.0343, 0.0802
***R* indices (all data)**	0.0431, 0.0838

Table 5.1 Summary of crystal data for $[Co(NH_3)_5(NO_2)]Cl_2$

5.4.1.2 Powder Diffraction Data

The powder diffraction pattern for $[Co(NH_3)_5(NO_2)]Cl_2$ can be seen in figure 5.6. The experimentally obtained powder pattern is in black while the powder pattern in red is a simulated pattern generated from single crystal data for comparison. Correlation between the experimentally obtained and

calculated powder patterns suggest that the solid state molecular structure obtained matches that of the bulk sample.

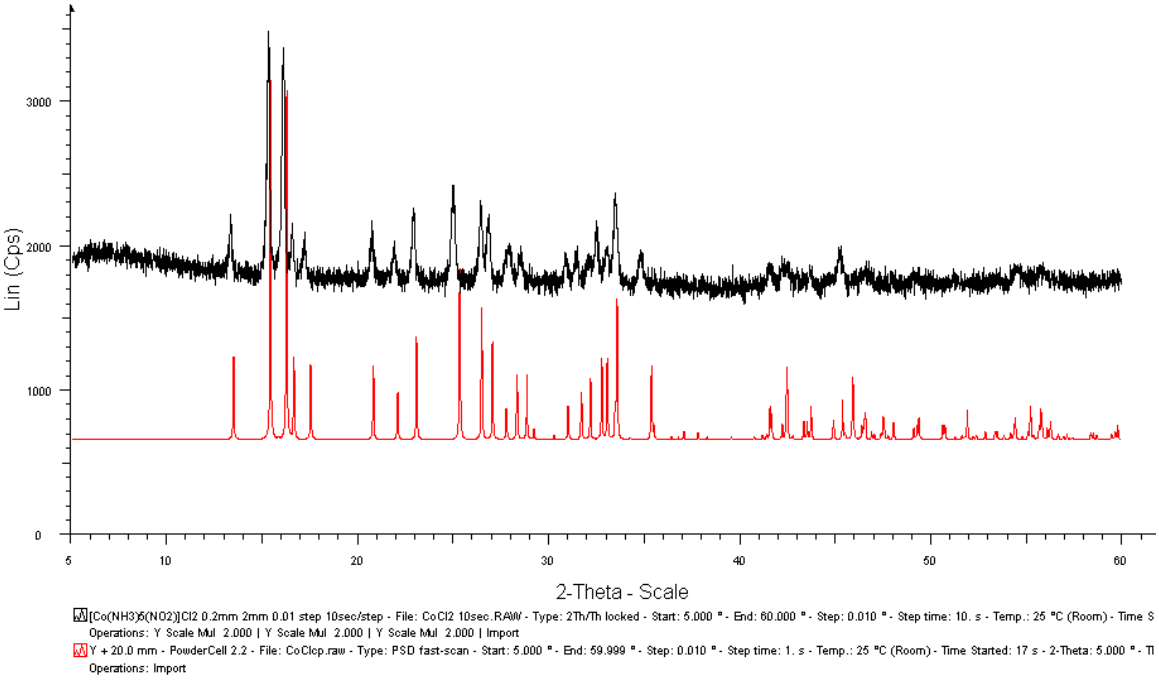

Figure 5.6 Predicted (red) and experimentally obtained (black) powder pattern of $[Co(NH_3)_5(NO_2)]Cl_2$

5.4.2. $[Co(NH_3)_5(NO_2)]PF_6$

5.4.2.1 Single Crystal Data

Single crystal X-ray diffraction measurements were made on a orange needle shaped crystal of $[Co(NH_3)_5(NO_2)]PF_6$ (structure number Bath 185) with dimensions 0.08 x 0.045 x 0.045mm at 150(2)K on a AXS SMART diffractometer. A summary of the crystal data can be seen in table 5.2 and the solid state molecular structure which is twice the asu can be seen in figure 5.7. Both the cation and anion are sat on a crystallographic mirror plane.

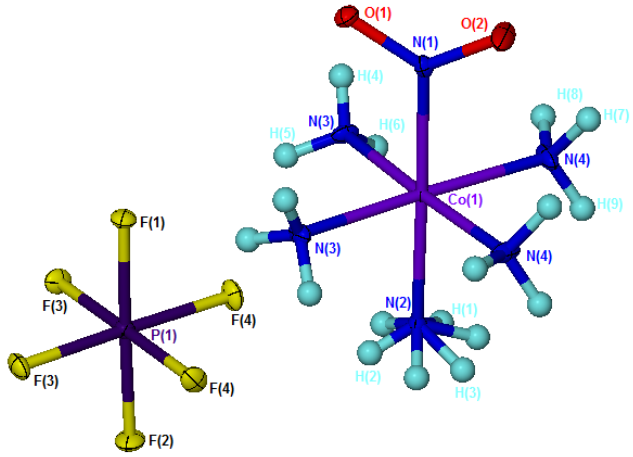

Figure 5.7 Solid state molecular structure of $[Co(NH_3)_5(NO_2)]PF_6$ with 30% probability ellipsoids shown

The metal cation again has an octahedral geometry and as with the $[Co(NH_3)_5(NO_2)]Cl_2$ structure, there is a 50% disorder of the hydrogens on the ammine group *trans* to the nitro ligand, arising as a result of the crystal symmetry. The O_1-N_1-O_2 bond angle is 120.8(2)° with a N_1-O_1bond length of 1.222(3)Å and a N_1-O_2 bond length of 1.221(3)Å.

The solid state molecular structure surprisingly consists of a metal cation with a single PF_6^- counter-ion, suggesting that the cobalt metal centre has been reduced from Co^{III} to Co^{II}. This can be confirmed by looking at the crystal packing (figure 5.8) and also by examination of the elemental analysis results (Chapter 6).

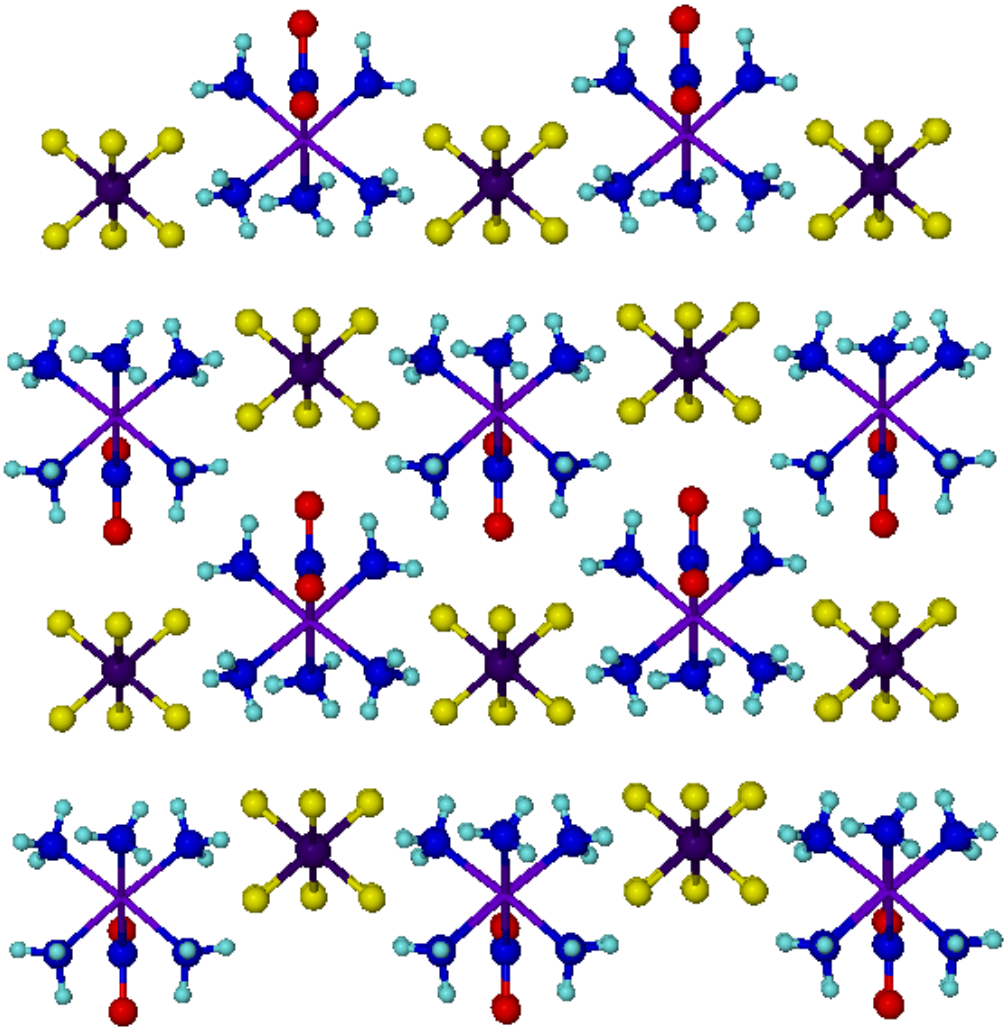

Figure 5.8 Crystal packing in $[Co(NH_3)_5(NO_2)]PF_6$

Empirical Formula	H_{15} Co F_6 N_6 O_2 P
M_r	335.08
Temperature (K)	150(2)
Crystal System	Monoclinic
Space Group	$P2_1/m$
Wavelength (Å)	0.6727
***a* (Å)**	6.4632(10)
***b* (Å)**	7.9053(12)
***c* (Å)**	10.1371(15)
α (°)	90
β (°)	100.916(10)
γ (°)	90
V (Å^3)	508.57(13)
Z	2
Absorption coefficient (mm^{-1})	1.935
Reflections collected	6563
Independent reflections	1912
R_{int}	0.0378
R_1, w$R2$	0.0334, 0.0810
***R* indices (all data)**	0.0421, 0.0856

Table 5.2 Summary of crystal data for $[Co(NH_3)_5(NO_2)]PF_6$

5.4.2.2 Powder Diffraction Data

The powder diffraction pattern for $[Co(NH_3)_5(NO_2)]PF_6$ can be seen in figure 5.9. The experimentally obtained powder pattern is in black while the powder pattern in red is a simulated pattern generated from single crystal data for comparison. Some additional peaks were present in the experimentally determined powder pattern so the sample was taken and washed with cold water and thoroughly dried before a second powder pattern was recorded (shown in blue). Although this improved the correlation between the observed and the calculated pattern, a contaminant still appears to be present, which may have caused the reduction of the cobalt from Co^{III} to Co^{II}.

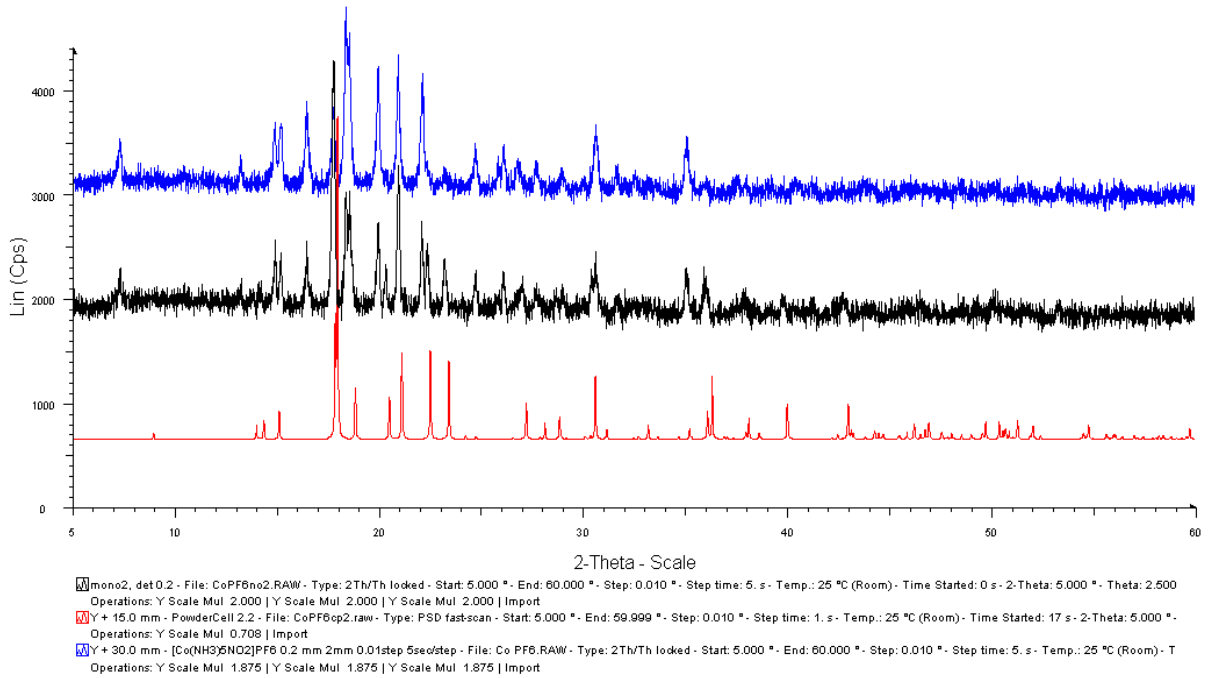

Figure 5.9 Predicted (red), initial powder pattern (black) and purified powder pattern (blue) of $[Co(NH_3)_5(NO_2)]PF_6$

5.4.3 $[Co(NH_3)_5(NO_2)][Fe(CN)_5(NO)].1½H_2O$

As mentioned in Chapter 1, the nitroprusside anion is capable of linkage isomerism and photocrystallographic experiments have successfully been performed on $Na_2[Fe(CN)_5(NO)].2H_2O$.[13] It was decided to try and exchange the chloride anions in $[Co(NH_3)_5(NO_2)]Cl_2$ with a single $[Fe(CN)_5(NO)]^{2-}$ anion to increase the overall size of the lattice. The complex $[Co(NH_3)_5(NO_2)][Fe(CN)_5(NO)].1½H_2O$ has been previously synthesised and reported in the literature.[14] With two photoactive species present, the nitro and nitrosyl ligands could potentially isomerise together when irradiated or isomerise individually when irradiated with light of different wavelengths (cf. the complex discussed in Chapter 1 investigated by Kovalevsky et al.).[15]

5.4.3.1 Single Crystal Data

Single crystal X-ray diffraction measurements were performed on a red block shaped crystal of $[Co(NH_3)_5(NO_2)][Fe(CN)_5(NO)].1½H_2O$ (structure number h05prr44) with dimensions 0.38 x 0.38 x 0.22mm at 150(2)K on a Kappa CCD diffractometer. A summary of the crystallographic data is summarised in table 5.3.

Empirical Formula	$C_5 H_{18} Co Fe N_{12} O_{4.5}$
M_r	433.07
Temperature (K)	150(2)
Crystal System	Monoclinic
Space Group	*C*2/*c*
Wavelength (Å)	0.71073
***a* (Å)**	28.4040(3)
***b* (Å)**	6.39700(10)
***c* (Å)**	22.3480(4)
α (°)	90
β (°)	123.9820(10)
γ (°)	90
V (Å^3)	3367.13(9)
Z	8
Absorption coefficient (mm^{-1})	1.888
Reflections collected	33581
Independent reflections	5127
R_{int}	0.0609
R_1, w*R*2	0.0370, 0.0863
***R* indices (all data)**	0.0633, 0.0956

Table 5.3 Summary of crystal data for $[Co(NH_3)_5(NO_2)][Fe(CN)_5(NO)].1½H_2O$

The solid state molecular structure consists of a dication with a cobalt metal centre that has octahedral geometry and a dianion with an iron metal centre that has a distorted octahedral geometry (illustrated in figure 5.10). The average Co-N bond distance for the ammine groups is 1.96Å, the longest belonging to the ammine group *trans* to the nitro group. The Co_1-N_1 bond distance is 1.9077(16)Å and the O_1-N_1-O_2 bond angle of the nitro ligand is 120.41(16)° with N_1-O_1 and N_1-O_2 bond distances of 1.236(2)Å and 1.239(2)Å respectively.

The nitroprusside anion has an average Fe-C bond length of 1.935Å. The distorted octahedral geometry arises from the fact that the cyano ligands in equatorial positions are pointing away from the nitrosyl group. The solid state molecular structure is in good general agreement with that previously reported.[14]

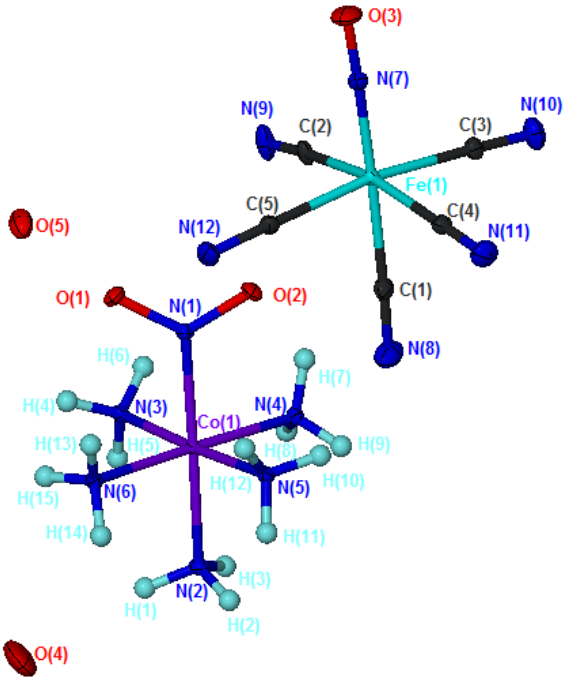

Figure 5.10 Solid state molecular structure of $[Co(NH_3)_5(NO_2)][Fe(CN)_5(NO)].1½H_2O$ with 30% probability ellipsoids shown

There is a significant amount of hydrogen bonding present within the structure and a list of bond lengths and angles are shown in table 5.4. There are hydrogen bonds which are occur between the protons on the ammine groups of the cation and the nitrogen atoms on the cyano groups of the nitroprusside anions (figure 5.11).

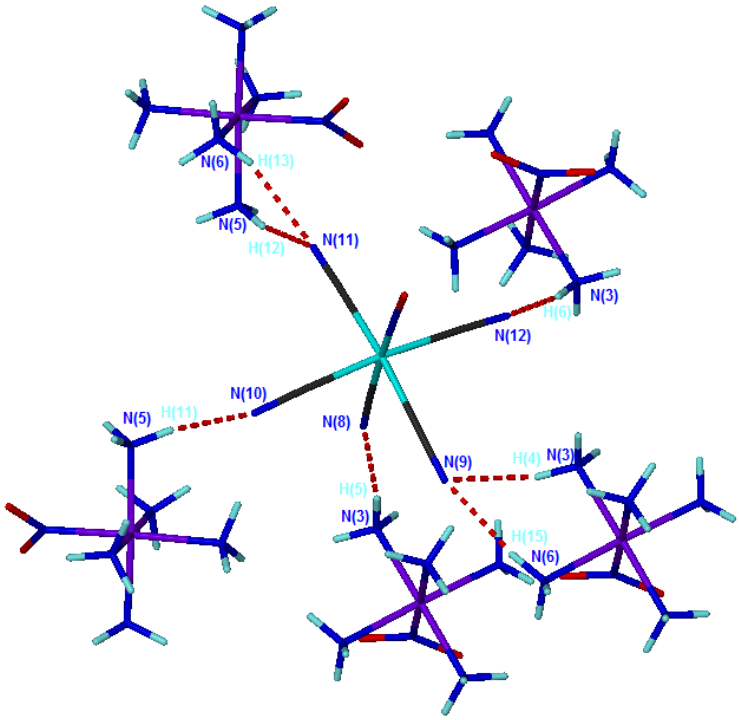

Figure 5.11 Hydrogen bonds between nitroprusside anion and cobalt cation in $[Co(NH_3)_5(NO_2)][Fe(CN)_5(NO)].1½H_2O$

There are also hydrogen bonds between the cations from the oxygen atoms on the nitro groups and again the protons on the ammine groups (figure 5.12). The N_4-H_9...O_1 bond is weaker than the N_5-H_{10}...O_2 as a result of the acute bond angle of 135.4°. Hydrogen bonding involving the oxygen atoms on water molecules contained within the crystal lattice, and the hydrogen atoms on ammine groups are present, with donor…acceptor distances N_2…O_4 of 3.159(2)Å and N_4…O_5 of 2.913(2)Å. The overall 3D network can be seen in figure 5.13.

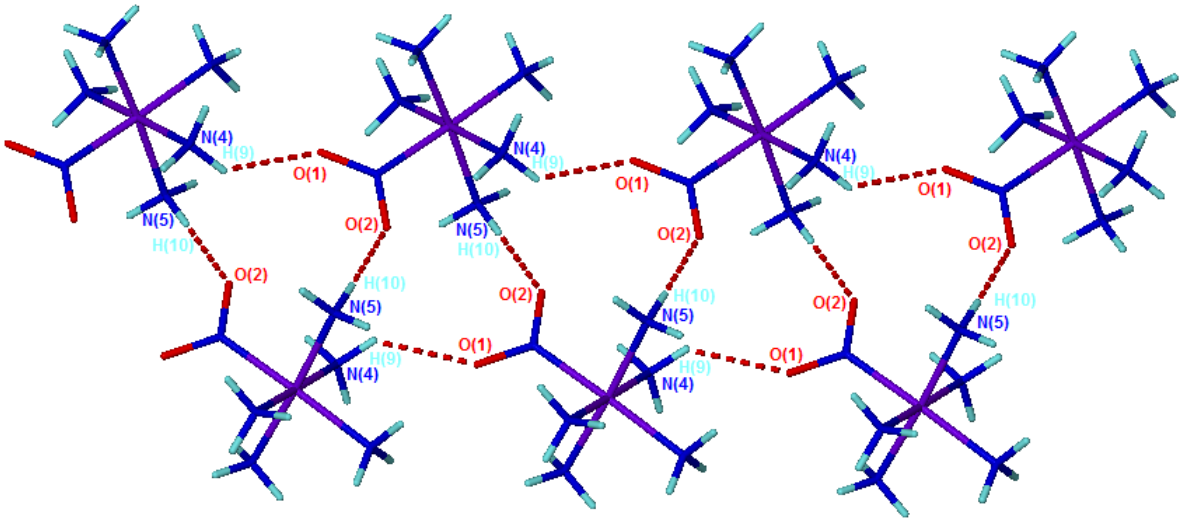

Figure 5.12 Hydrogen bonds between cations in $[Co(NH_3)_5(NO_2)][Fe(CN)_5(NO)].1½H_2O$

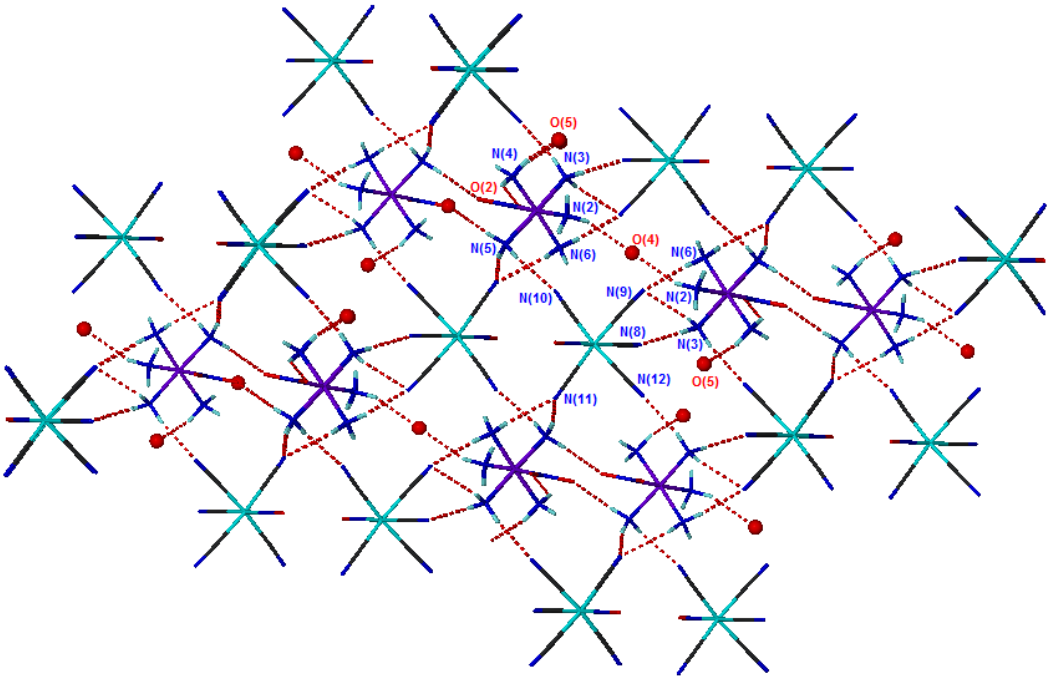

Figure 5.13 Hydrogen bonding network in $[Co(NH_3)_5(NO_2)][Fe(CN)_5(NO)].1½H_2O$

D-H...A	d(H...A) (Å)	d(D...A) (Å)	<(DHA) (°)
N_3-H_5...N_8	2.08	2.983(3)	170.4
N_3-H_4...N_9	2.28	3.016(3)	137.7
N_3-H_6...N_{12}	2.13	3.032(3)	170.8
N_4-H_9...O_1	2.33	3.049(2)	135.4
N_5-H_{10}...O_2	2.09	2.997(2)	175.3
N_5-H_{11}...N_{10}	2.18	2.999(3)	148.6
N_5-H_{12}...N_{11}	2.20	3.078(3)	160.9
N_6-H_{15}...N_9	2.17	3.070(3)	171.2
N_6-H_{13}...N_{11}	2.29	3.102(3)	148.9

Table 5.4 Hydrogen bond lengths (Å) and angles (°) in $[Co(NH_3)_5(NO_2)][Fe(CN)_5(NO)].1½H_2O$

5.4.3.2 Powder Diffraction Data

Powder diffraction data was collected for $[Co(NH_3)_5(NO_2)][Fe(CN)_5(NO)].1½H_2O$ and is shown in figure 5.14. The experimentally obtained powder pattern is depicted in black while the predicted pattern generated from single crystal data is shown in red. There is good general agreement between the observed and predicted powder patterns suggesting that the solid state molecular structure is the same as for that in the bulk sample.

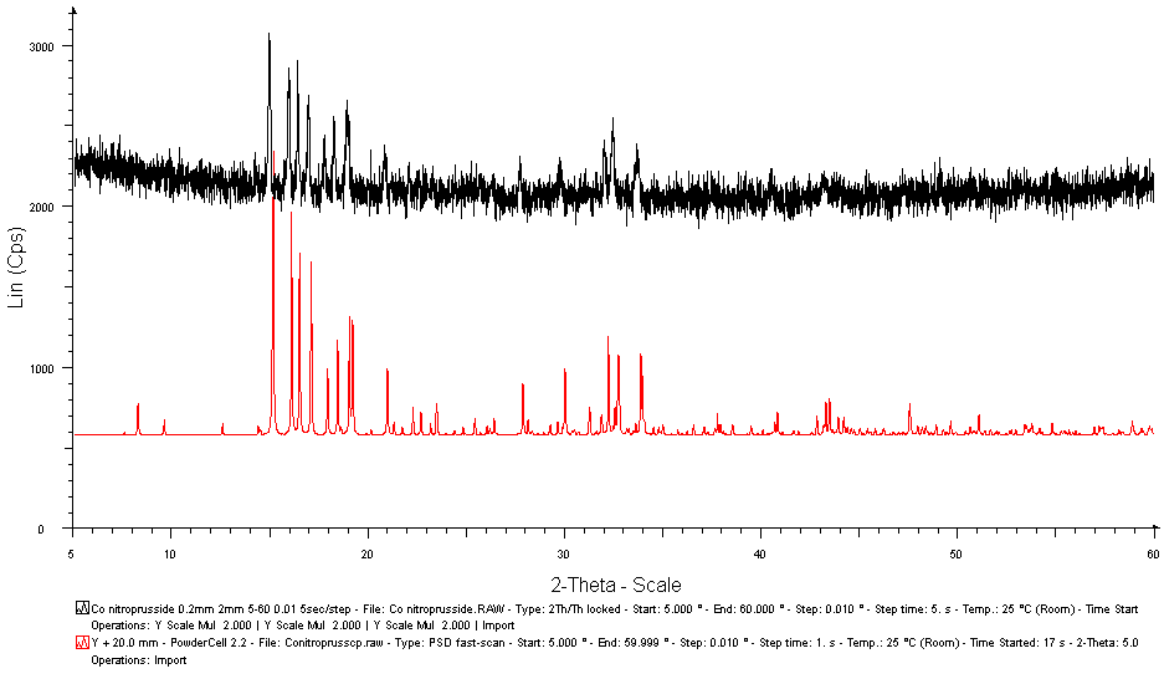

Figure 5.14 Predicted (red) and experimentally obtained (black) powder pattern of $[Co(NH_3)_5(NO_2)][Fe(CN)_5(NO)].1½H_2O$

5.4.4 $[Co(NH_3)_5(NO_2)](Hbs)_2.2H_2O$

5.4.4.1 Single Crystal Data

Single crystal X-ray diffraction measurements were performed on an orange block shaped crystal of $[Co(NH_3)_5(NO_2)](Hbs)_2.2H_2O$ (where Hbs is 4-hydroxybenzene sulphonate, structure number k06prr07) with dimensions 0.33 x 0.25 x 0.20mm at 150(2)K on a Kappa CCD diffractometer. A summary of the crystallographic data can be found in table 5.5.

Empirical Formula	$C_{12}\ H_{29}\ Co\ N_6\ O_{12}\ S_2$
M_r	572.46
Temperature (K)	150(2)
Crystal System	Orthorhombic
Space Group	$P2_12_12_1$
Wavelength (Å)	0.71073
***a* (Å)**	7.0220(1)
***b* (Å)**	11.9940(1)
***c* (Å)**	26.7510(2)
α (°)	90
β (°)	90
γ (°)	90
V (Å^3)	2253.02(4)
Z	4
Absorption coefficient (mm^{-1})	1.019
Reflections collected	40610
Independent reflections	6109
R_{int}	0.0546
R_1, w$R2$	0.0272, 0.0575
***R* indices (all data)**	0.0350, 0.0634
Flack parameter	-0.008(8)

Table 5.5 Summary of crystal data for $[Co(NH_3)_5(NO_2)](Hbs)_2.2H_2O$

The solid state molecular structure has two Hbs anions to each cation and can be seen in figure 5.15. The average Co-N bond distance for the ammine groups is 1.97Å and comparable with the other structures presented in this chapter. The nitro group is η^1 coordinated through the nitrogen atom with a

O_1-N_1-O_2 bond angle of 119.85(16)° with N_1-O_1 and N_1-O_2 bond distances of 1.246(2)Å and 1.236(2)Å respectively.

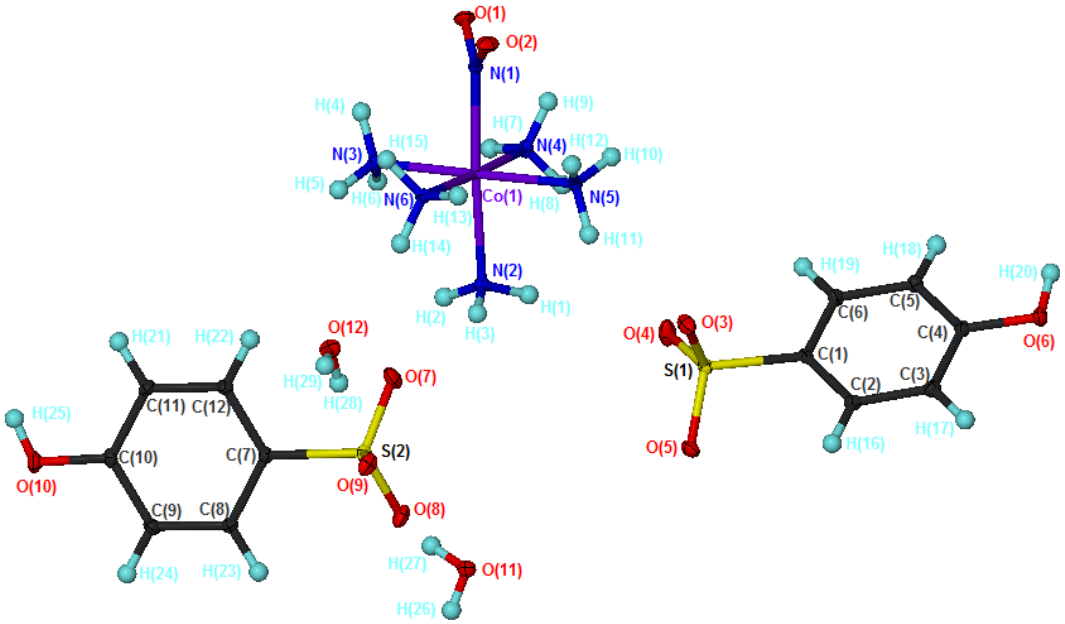

Figure 5.15 Solid state molecular structure of $[Co(NH_3)_5(NO_2)](Hbs)_2.2H_2O$ with 30% probability ellipsoids shown

There are a series of weak to moderate strength hydrogen bonds forming a 3D network (figure 5.16). A list of hydrogen bond lengths and angles can be found in table 5.6.

D-H...A	d(H...A) (Å)	d(D...A) (Å)	<(DHA) (°)
N_2-H_2...O_7	2.07	2.889(2)	148.7
N_2-H_3...O_2	2.20	3.049(2)	154.2
N_3-H_5...O_6	2.08	2.980(2)	168.7
N_3-H_6...O_5	2.13	3.020(2)	165.7
N_4-H_7...O_5	2.27	3.123(2)	156.1
N_4-H_8...O_{11}	2.04	2.942(2)	168.4
N_5-H_{10}...O_8	2.02	2.923(2)	173.6
N_5-H_{12}...O_{11}	2.15	3.051(2)	169.5
N_6-H_{14}...O_{12}	2.22	3.119(2)	170.3
N_6-H_{15}...O_5	2.08	2.965(2)	163.7
O_6-H_{20}...O_{12}	1.83	2.608(2)	154.0
O_{10}-H_{25}...O_3	1.96	2.786(2)	169.8

Table 5.6 Hydrogen bond lengths (Å) and angles (°) in $[Co(NH_3)_5(NO_2)](Hbs)_2.2H_2O$

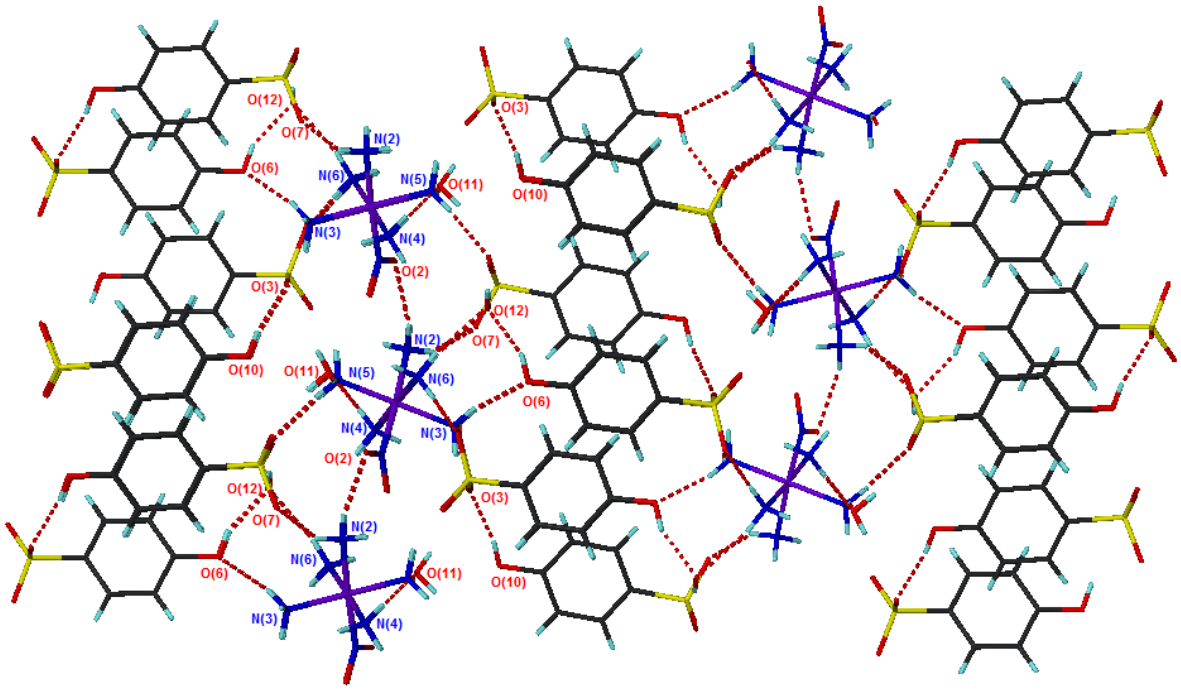

Figure 5.16 Hydrogen bonding network in $[Co(NH_3)_5(NO_2)](Hbs)_2.2H_2O$

Hydrogen bonds are present between adjacent Hbs anions from the hydrogen atom of the hydroxyl group to an oxygen atom from the sulphonate group (O_{10}-H_{25}...O_3). There is also a single hydrogen bond present between the dications (N_2-H_3...O_2). The remainder of the hydrogen bonds are located between the hydrogens on the ammine groups and the hydroxyl oxygen or oxygen atoms on the sulphonate groups. The packing shown in the hydrogen bonded network also demonstrates that the cations and anions form alternate layers.

5.4.4.2 Powder Diffraction Data

Powder diffraction data was collected for $[Co(NH_3)_5(NO_2)](Hbs)_2.2H_2O$ and is shown in figure 5.17. The experimentally obtained powder pattern is shown in black while the predicted pattern generated from single crystal data is shown in red for comparison. There is good general agreement between the experimentally obtained and calculated powder patterns, which suggests that the solid state molecular structure is a good representation of the bulk sample synthesised.

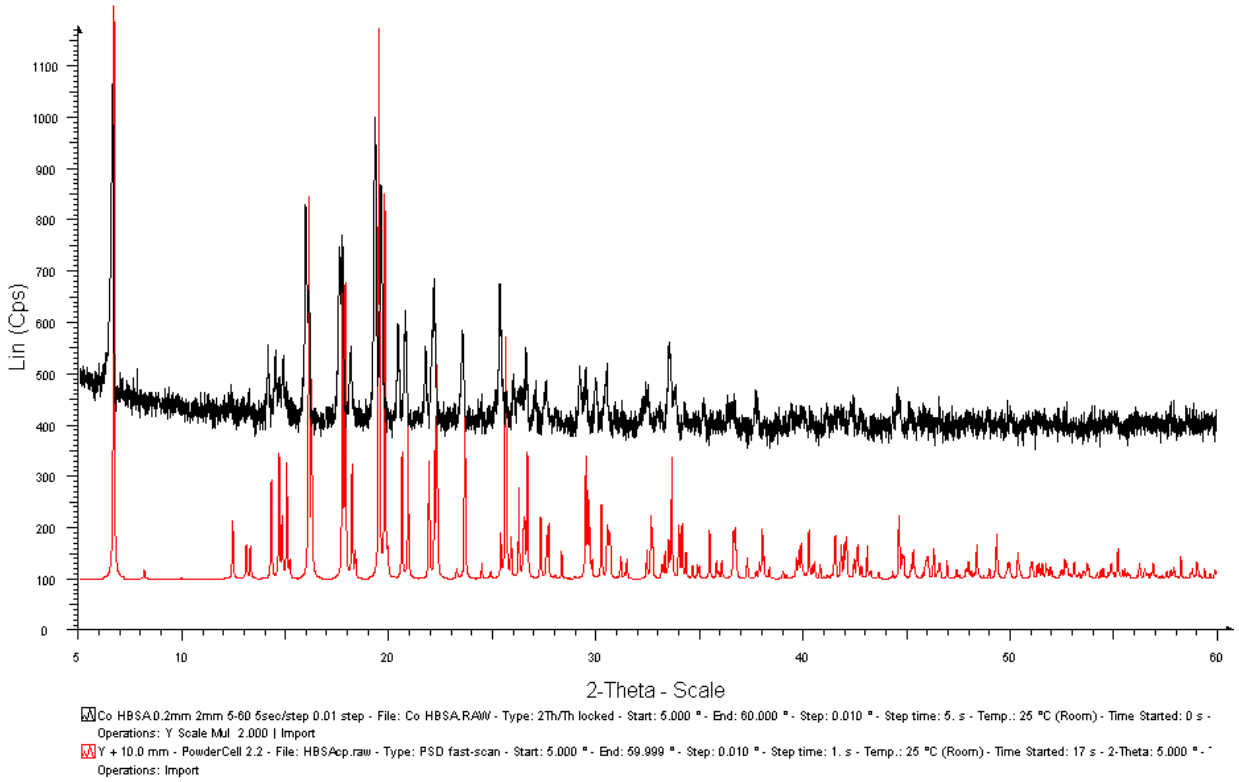

Figure 5.17 Predicted (red) and experimentally obtained (black) powder pattern of $[Co(NH_3)_5(NO_2)](Hbs)_2.2H_2O$

5.4.5 $[Co(NH_3)_5(NO_2)](BPh_4)_2.2H_2O$

5.4.5.1 Single Crystal Data

Single crystal X-ray diffraction measurements were performed on an orange triangular prismatic shaped crystal of $[Co(NH_3)_5(NO_2)](BPh_4)_2.2H_2O$ (structure number k05prr55) with dimensions 0.275 x 0.25 x 0.075mm at 150(2)K on a Kappa CCD diffractometer. A summary of the crystallographic data is summarised in table 5.7.

The solid state molecular structure of $[Co(NH_3)_5(NO_2)](BPh_4)_2.2H_2O$ is shown in figure 5.18. The two chloride ions have been successfully replaced by two tetraphenyl borate anions, with each anion possessing tetrahedral geometry (all four C-B-C bond angles are close to 109°). There are also two water molecules present. The average Co-N bond distance for the ammine groups is 1.97Å with the Co-N ligand *trans* to the nitro group being the longest. The nitro group is η^1 coordinated through the nitrogen atom with a O_1-N_1-O_2 bond angle of 121.1(2)° with N_1-O_1 and N_1-O_2 bond distances of 1.229(3)Å and 1.236(3)Å respectively. These values are consistent with those reported earlier in this chapter.

No hydrogen bonding is present between the ions in the solid state molecular structure. However, there are hydrogen bonds arising between one of the water molecules and ammine groups on the cobalt ion in the crystal lattice, with $O_3 \ldots N_4$ and $O_3 \ldots N_5$ distances of 2.971Å and 2.890Å respectively. The crystal structure packing is shown in figure 5.19.

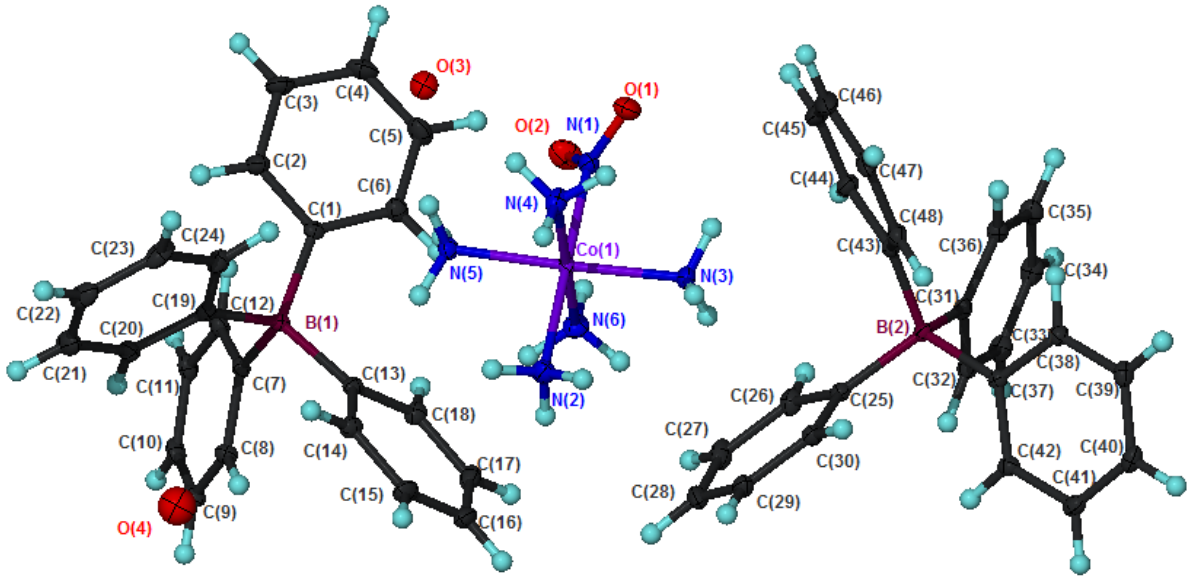

Figure 5.18 Solid state molecular structure of $[Co(NH_3)_5(NO_2)](BPh_4)_2.2H_2O$ with 30% probability ellipsoids shown

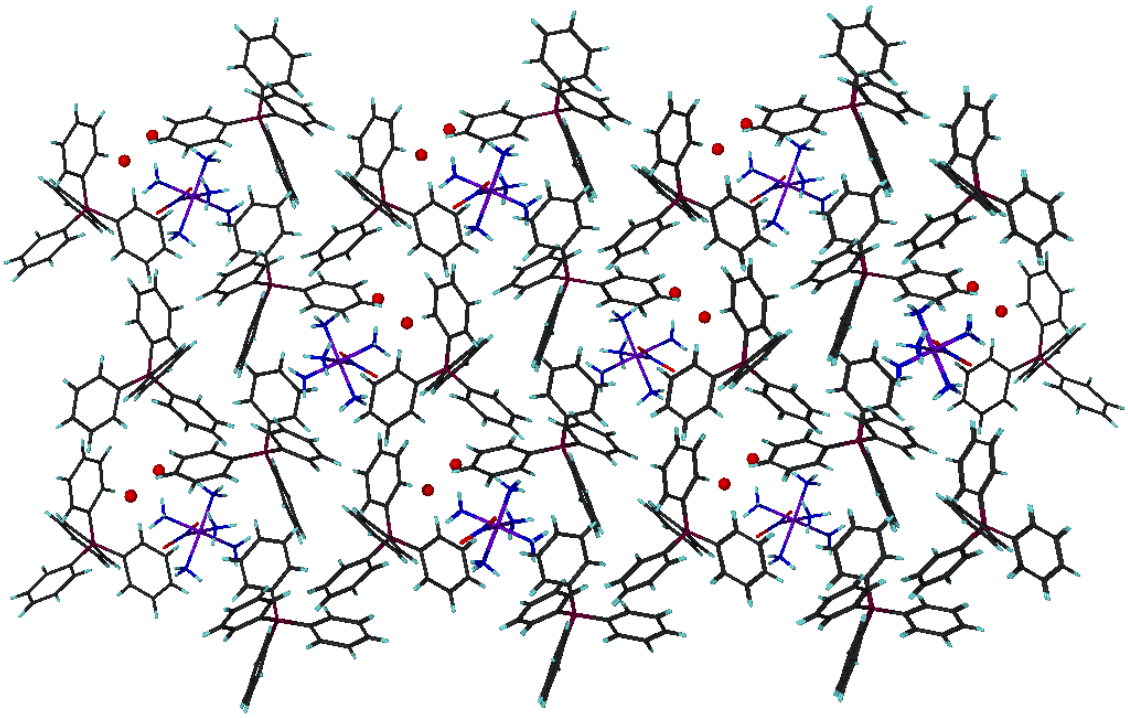

Figure 5.19 Crystal packing in $[Co(NH_3)_5(NO_2)](BPh_4)_2.2H_2O$

Empirical Formula	$C_{48}\ H_{59}\ B_2\ Co\ N_6\ O_4$
M_r	860.53
Temperature (K)	150(2)
Crystal System	Orthorhombic
Space Group	*Pc*2$_1$*n* (non standard form of *Pna*2$_1$)
Wavelength (Å)	0.71073
***a* (Å)**	9.6900(1)
***b* (Å)**	16.1610(1)
***c* (Å)**	28.6570(3)
α (°)	90
β (°)	90
γ (°)	90
V (Å^3)	4487.69(7)
Z	4
Absorption coefficient (mm^{-1})	0.433
Reflections collected	69123
Independent reflections	13236
R_{int}	0.0616
R_1, w*R*2	0.0474, 0.1177
***R* indices (all data)**	0.0629, 0.1296
Flack parameter	-0.001(1)

Table 5.7 Summary of crystal data for $[Co(NH_3)_5(NO_2)](BPh_4)_2.2H_2O$

5.4.5.2 Powder Diffraction Data

Powder diffraction data was collected for $[Co(NH_3)_5(NO_2)](BPh_4)_2.2H_2O$ and is shown in figure 5.20. The experimentally obtained powder pattern is shown in black while the predicted pattern generated from single crystal data is shown in red for comparison. There is good general agreement between the experimentally obtained and calculated powder patterns suggesting that the solid state molecular structure is a good representation of the bulk material obtained from synthesis.

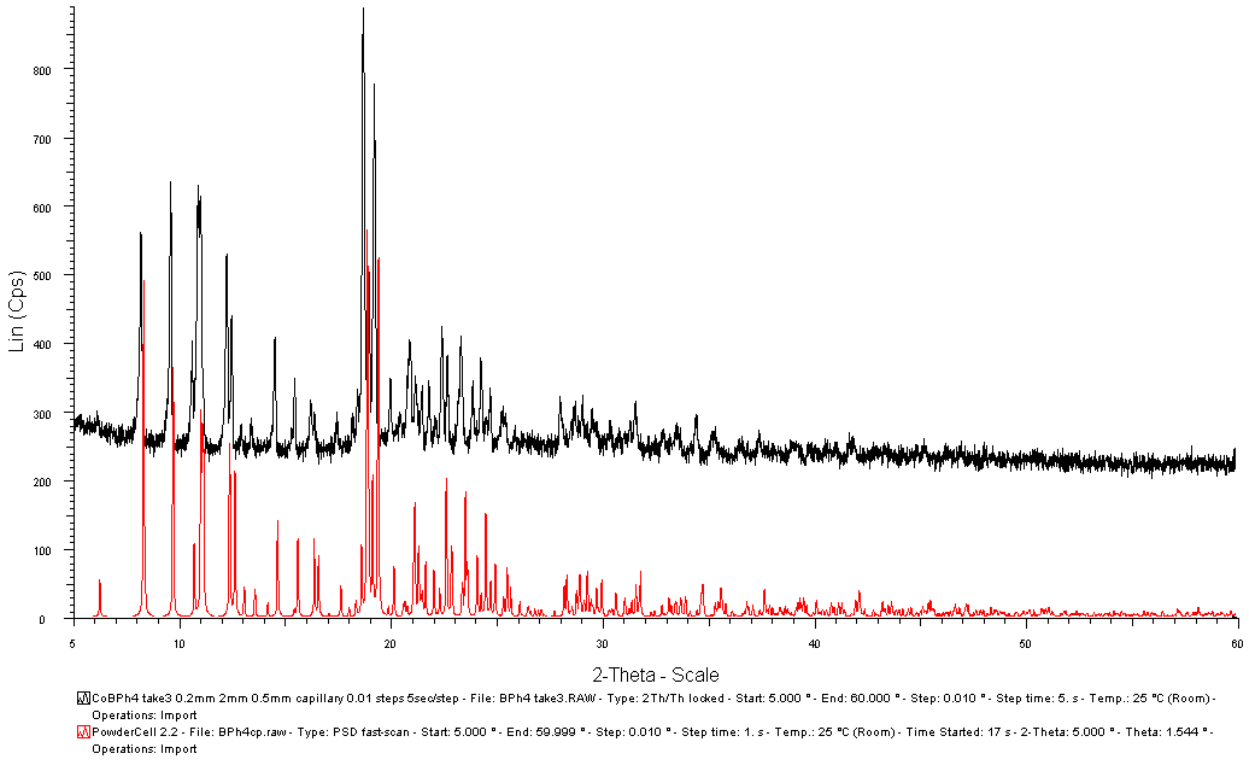

Figure 5.20 Predicted (red) and experimentally obtained (black) powder pattern of $[Co(NH_3)_5(NO_2)](BPh_4)_2.2H_2O$

5.4.6 $[Ru(NH_3)_4(SO_2)(H_2O)]_2[(OC_7H_4SO_3)_4].C_2H_5OH.3H_2O$

Photocrystallographic experiments on $[Ru(NH_3)_4(SO_2)(H_2O)](Tos)_2$ have shown that the sulphur dioxide group isomerises upon irradiation.[16, 17] As mentioned earlier in this chapter calixarenes are often used in crystal engineering as host molecules due to their large cavities. If a $[Ru(NH_3)_4(SO_2)(H_2O)]^{2+}$ cation could reside in the cavity, it is possible that higher levels of excitation could be achieved.

5.4.6.1 Single Crystal Data

Single crystal X-ray diffraction measurements were made on a colourless needle of $[Ru(NH_3)_4(SO_2)(H_2O)]_2[(OC_7H_4SO_3)_4].C_2H_5OH.3H_2O$ (structure number Bath 241) with dimensions 0.3 x 0.05 x 0.05mm at 150(2)K on a AXS SMART diffractometer. A summary of the crystal data is shown in table 5.8 and the solid state molecular structure is illustrated in figure 5.21.

The solid state molecular structure shows that two ruthenium cations are present with the calixarene anion, however there is an ethanol molecule residing in the host cavity that would have been ideal to sit one of the ruthenium molecules in. There are also three water molecules present. The sulphur dioxide ligands are η^1 coordinated through the sulphur atoms with an O_1-S_1-O_2 bond angle of 115.8(3)° and O_4-S_2-O_5 bond angle of 114.4(4)°.

Empirical Formula	$C_{30}\ H_{56}\ N_8\ O_{26}\ Ru_2\ S_6$
M_r	1335.30
Temperature (K)	150(2)
Crystal System	Tetragonal
Space Group	I-4
Wavelength (Å)	0.71073
***a* (Å)**	28.029
***b* (Å)**	28.029
***c* (Å)**	13.663
α (°)	90
β (°)	90
γ (°)	90
V ($Å^3$)	10734.0
Z	8
Absorption coefficient (mm^{-1})	0.883
Reflections collected	62808
Independent reflections	17372
R_{int}	0.0848
R_1, w*R*2	0.0607, 0.1670
***R* indices (all data)**	0.0729, 0.1762
Flack parameter	0.04(3)

Table 5.8 Summary of crystal data for $[Ru(NH_3)_4(SO_2)(H_2O)]_2[(OC_7H_4SO_3)_4].C_2H_5OH.3H_2O$

There are a series of weak to moderate strength hydrogen bonds within the crystal structure, with bond lengths and angles summarised in table 5.9. All the hydrogen bonds identified are between proton atoms on ammine groups and either oxygen atoms on the sulphate groups or oxygen atoms in water molecules. The hydrogen bonding for $[Ru(NH_3)_4(SO_2)(H_2O)]_2[(OC_7H_4SO_3)_4].C_2H_5OH.3H_2O$ can be seen in figure 5.22.

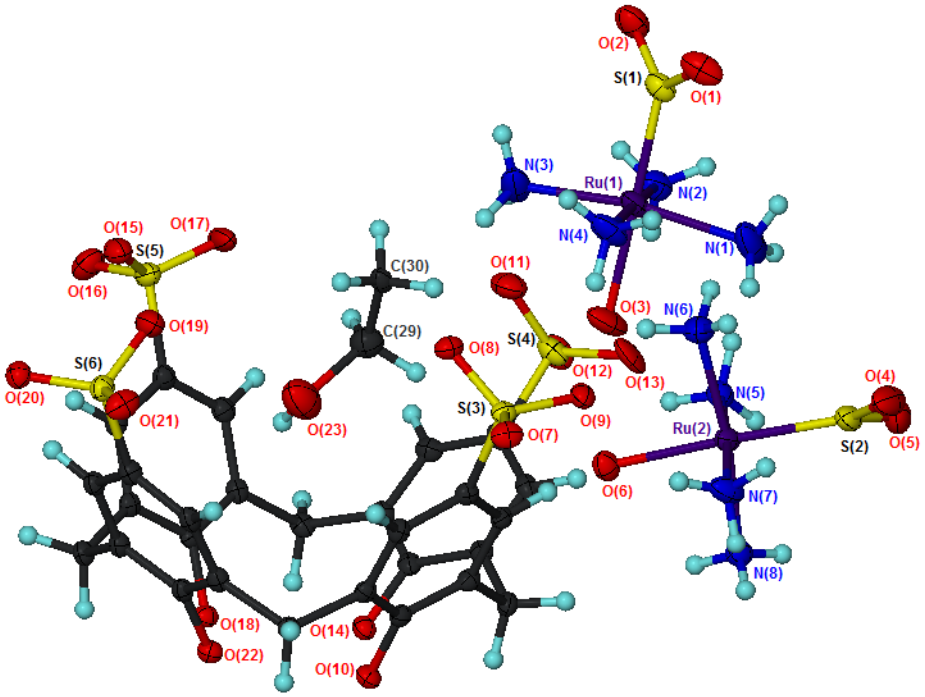

Figure 5.21 Solid state molecular structure of $[Ru(NH_3)_4(SO_2)(H_2O)]_2[(OC_7H_4SO_3)_4].C_2H_5OH.3H_2O$ with 30% probability ellipsoids shown. Water molecules have been removed for clarity

D-H...A	d(H...A) (Å)	d(D...A) (Å)	<(DHA) (°)
N_1-H_3...O_{24}	2.37	3.178(1)	147.1
N_2-H_4...O_8	2.15	3.030(6)	162.1
N_2-H_5...O_{13}	2.28	3.182(1)	170.5
N_2-H_6...O_{19}	2.08	2.986(7)	171.5
N_4-H_{10}...O_9	2.00	2.898(7)	168.3
N_4-H_{11}...O_{17}	2.36	3.244(8)	162.9
N_4-H_{12}...O_{11}	2.34	3.190(12)	155.8
N_5-H_{13}...O_{17}	2.12	3.024(7)	170.2
N_5-H_{14}...O_9	2.24	3.063(6)	150.9
N_7-H_{19}...O_{15}	2.16	3.053(7)	165.6
N_7-H_{21}...O_{26}	2.34	3.040(12)	133.7
N_8-H_{22}...O_{20}	2.30	3.019(6)	135.9
N_8-H_{23}...O_{15}	2.23	3.114(7)	164.0

Table 5.9 Hydrogen bond lengths (Å) and angles (°) in $[Ru(NH_3)_4(SO_2)(H_2O)]_2[(OC_7H_4SO_3)_4].C_2H_5OH.3H_2O$

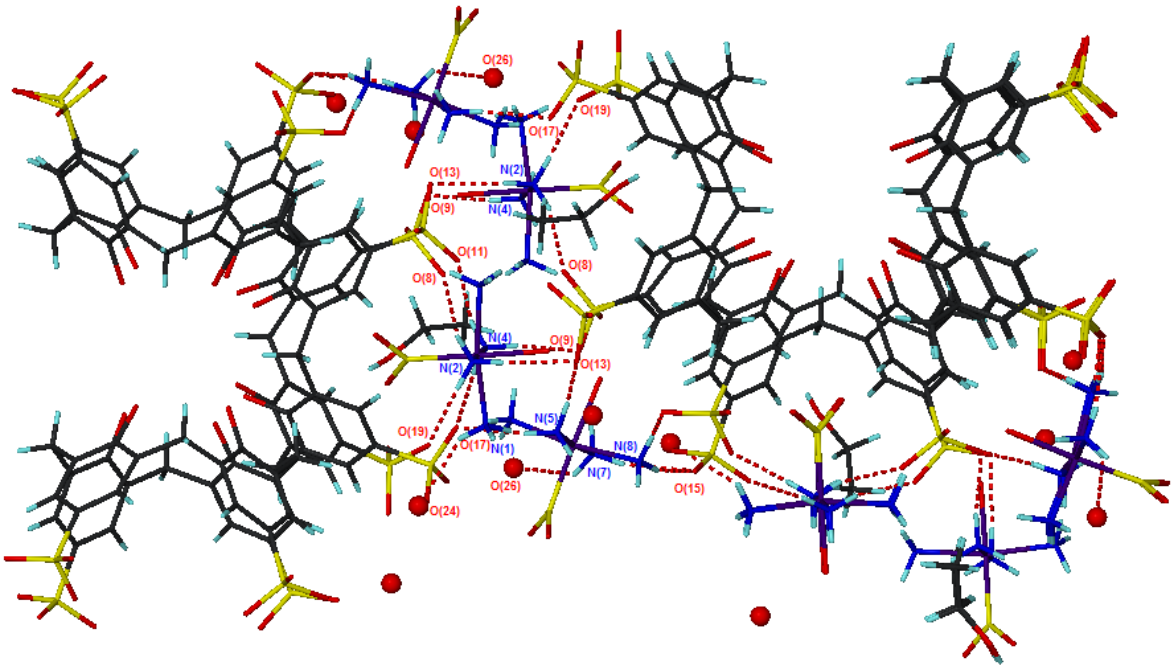

Figure 5.22 Hydrogen bonding observed in $[Ru(NH_3)_4(SO_2)(H_2O)]_2[(OC_7H_4SO_3)_4].C_2H_5OH.3H_2O$

An analysis of the packing reveals that there are cavities where sulphur dioxide ligands point toward. These cavities could be big enough for isomerisation to occur without causing too much strain on the crystal lattice (figures 5.23 and 5.24).

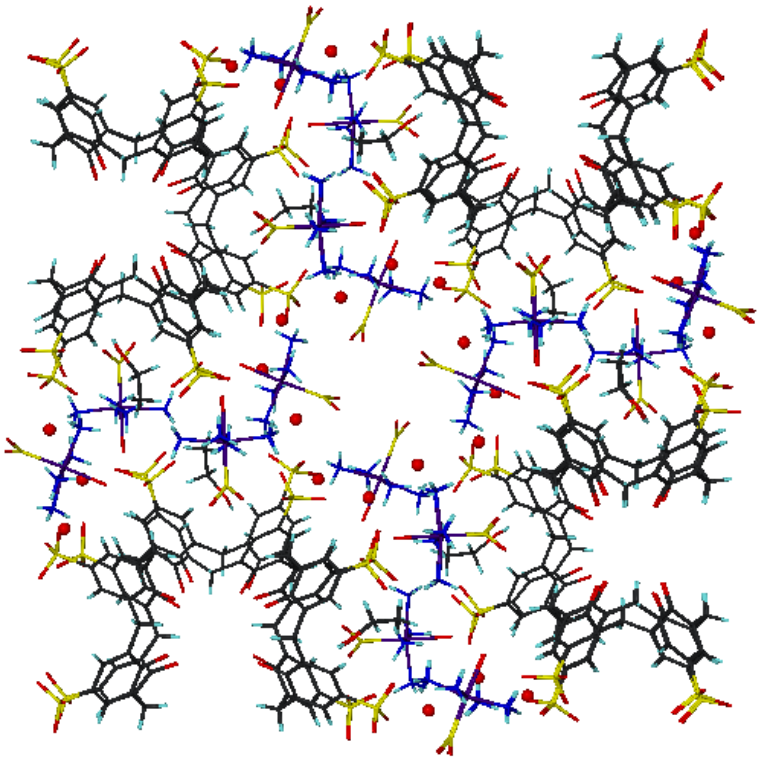

Figure 5.23 Packing diagram for $[Ru(NH_3)_4(SO_2)(H_2O)]_2[(OC_7H_4SO_3)_4].C_2H_5OH.3H_2O$

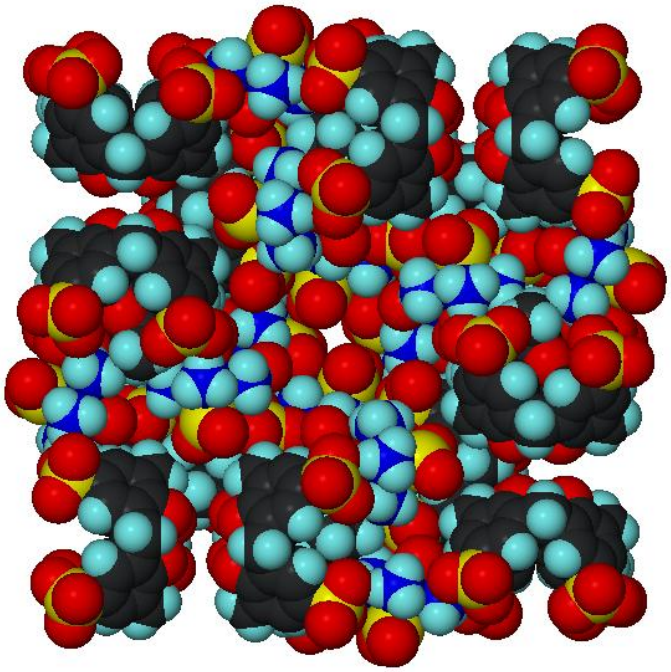

Figure 5.24 Space filling diagram showing cavity where isomerisation could occur

5.5 Discussion and Conclusion

The results in this chapter have shown the successful crystal engineering in extending the crystal lattice for both $[Co(NH_3)_5NO_2]Cl_2$ and $[Ru(NH_3)_4(SO_2)Cl]Cl$. For the cobalt complexes a comparison of the unit cell volume is shown in table 5.10 below.

Complex	Unit Cell Volume $(Å)^3$	Z
$[Co(NH_3)_5(NO_2)]PF_6$	508.6	2
$[Co(NH_3)_5(NO_2)]Cl_2$	945.0	4
$[Co(NH_3)_5(NO_2)](Hbs)_2.2H_2O$	2253.0	4
$[Co(NH_3)_5(NO_2)][Fe(CN)_5(NO)].1½H_2O$	3367.1	8
$[Co(NH_3)_5(NO_2)](BPh_4)_2.2H_2O$	4487.7	4

Table 5.10 Comparison of unit cell volumes for cobalt complexes

As can be seen from the table when the counter-ion was exchanged for nitroprusside, Hbs^- and BPh_4^-, there was a successful increase in the overall size of the crystal lattice, consistent with the increase in the number and size of the ions in the cell. This will hopefully make these samples suitable candidates for photocrystallographic experiments.

Several attempts were made to crystallise different calixarenes and crown ethers with both $[Co(NH_3)_5NO_2]Cl_2$ and $[Ru(NH_3)_4(SO_2)Cl]Cl$, however the only successful crystallisation was between 4-sulfonic calix[4]arene and the ruthenium complex. Although the ruthenium cations did not sit in the cavity of the calixarene, channels were created where there is significant space for the sulphur dioxide groups to isomerise in, making this a suitable candidate for photocrystallography experiments. The only disadvantage is that only one or two crystals were obtained from the synthesis and these were all small, so single crystal X-ray diffraction photocrystallography would most likely have to be performed at a synchrotron source.

Crystal engineering has proved successful in synthesising a range of different complexes by ion exchange or by incorporation of photoactive ions into arrays and extended networks which have the potential to be photo-excited. The size of the crystalline lattice was shown to have increased in the majority of complexes synthesised in this chapter. Unfortunately time did not allow for photocrystallographic experiments on these samples to be carried out, so their potential is currently unknown. Future work would therefore involve performing a range of experiments on these samples to see whether linkage isomerism is possible. If successful, it would be interesting to see whether higher levels of excitation are achieved than in previous experiments for analogous systems.

5.6 References

[1] J. W. Steed, J. L. Atwood, *Supramolecular Chemistry*, John Wiley & Sons, **2000**.
[2] A. R. von Hippel, *Science* **1962**, *138*, 91.
[3] G. M. J. Schmidt, *J. Chem. Soc.* **1964**, 2014.
[4] K. E. Maly, E. Gagnon, T. Maris, J. D. Wuest, *J. Am. Chem. Soc.* **2007**, *129*, 4306.
[5] P. Coppens, S. L. Zheng, M. Gembicky, M. Messerschmidt, P. M. Dominiak, *Cryst. Eng. Comm.* **2006**, *8*, 735.
[6] D. Braga, F. Grepioni, *Angew. Chem. Int. Ed.* **2004**, *43*, 4002.
[7] T. J. Brett, J. M. Alexander, J. L. Clark, C. R. Ross, G. S. Harbison, J. J. Stezowski, *Chem. Commun.* **1999**, 1275.
[8] P. J. Nichols, C. L. Raston, J. W. Steed, *Chem. Commun.* **2001**, 1062.
[9] S. L. Zheng, M. Messerschmidt, P. Coppens, *Acta Crystallogr. Sect. B* **2007**, *63*, 644.
[10] A. Werner, *Brt.* **1907**, *40*, 765.
[11] B. Adell, *Z. Anorg. Allg. Chem.* **1955**, 219.
[12] M. Kubota, S. Ohba, *Acta Crystallogr. Sect. B* **1992**, *48*, 627.
[13] M. D. Carducci, M. R. Pressprich, P. Coppens, *J. Am. Chem. Soc.* **1997**, *119*, 2669.
[14] D. B. Soria, M. E. C. Villalba, O. E. Piro, P. J. Aymonino, *Polyhedron* **2002**, *21*, 1767.
[15] A. Y. Kovalevsky, G. King, K. A. Bagley, P. Coppens, *Chem. Eur. J.* **2005**, *11*, 7254.
[16] K. F. Bowes, J. M. Cole, S. L. G. Husheer, P. R. Raithby, T. L. Savarese, H. A. Sparkes, S. J. Teat, J. E. Warren, *Chem. Commun.* **2006**, 2448.
[17] A. Y. Kovalevsky, K. A. Bagley, J. M. Cole, P. Coppens, *Inorg. Chem.* **2003**, *42*, 140.

Chapter 6

General Experimental

6.1 Reagents, Materials and Solvents

All manipulations involving air sensitive reagents were performed under an atmosphere of purified nitrogen using standard Schlenk techniques. All solvents used in air sensitive reactions were dried prior to use using an automatic solvent purification system. Unless otherwise stated, all chemicals were purchased from commercial sources and used without further purification.

LEDs were purchased from rswww.com: 5mm UV LEDs, peak wavelength 400nm, luminous intensity 350mcd, 3.7V, 20mA. PCB mount SuperFlux Blue LEDs: peak wavelength 467nm, luminous intensity 6000mcd, 4.4V, 30mA. The broadband light source used for excitation in powder diffraction experiments was 'white' microscope lights.

6.2 Spectroscopy and Elemental Analysis

Infrared spectra were recorded using a Nicolet Nexus FT-IR spectrometer with samples as Nujol mulls mounted between NaCl disks. UV/Vis spectra were obtained using a PerkinElmer 650 UV/Vis spectrophotometer. Emmision spectra were obtained using a PerkinElmer LS55 Luminescence Spectrometer. Carbon, hydrogen and nitrogen elemental analysis was obtained using Exeter Analytical, CE-440 Elemental Analyzer.

6.3 X-ray Crystallography

Single crystal X-ray diffraction data were collected on a Nonius Kappa CCD diffractometer at the University of Bath or on a Bruker AXS SMART diffractometer on Station 9.8 at the STFC Daresbury Laboratory synchrotron source. Both diffractometers were equipped with Oxford Cryostream cooling apparatus or a helijet.

Absorption corrections on data sets were carried out using SORTAV[1] or SADABS[2] programs. Structure solution was achieved using either direct methods or Patterson techniques. Non-hydrogen atoms in solid state molecular structures were assigned anisotropic displacement parameters where possible, with hydrogen atoms occupying idealized positions. Refinement was carried out using a full-matrix least squares method on F^2 with SHELXL.[3]

Powder diffraction data was collected using a Bruker AXS diffractometer at the University of Bath with 2θ values between 5° and 60°. Photocrystallographic powder experiments were performed on Station 2.3 at the STFC Daresbury Laboratory synchrotron using a hybrid diffractometer built on site using Huber circles. The diffractometer was operated in Debye-Scherrer mode and data was collected between 2θ values of 5° and 60°.

6.4 Computational Methods

Geometry optimisation, orbital calculations and transition state calculations were performed using the B3LYP functional,[4] as implemented within the Gaussian 03 software package,[5] with a 3-21G* basis set for ruthenium atoms and a 6-31G** basis set for all other atoms. Default criteria within the software were employed for geometry optimisation, which places uncertainty of less then ±0.005Å on bond lengths. The results of the orbital calculations were displayed graphically using the Molekel software package.[6]

6.5 Synthesis for Chapter 3

6.5.1 Synthesis of $[Ru^{III}(NH_3)_5Cl]Cl_2$[7]

5g (0.016mol) of $[Ru^{III}(NH_3)_6]Cl_3$ was dissolved in 54ml of water by gently warming. To this solution 54ml of conc. HCl was added and the solution was refluxed for 3.5h. During this period a yellow crystalline precipitate formed. The precipitate was filtered off, washed first with 1:1 water:HCl followed by methanol, before being air dried under vacuum at room temperature.

Yield: 87% (4.13g, 0.014mol). IR (nujol): $\nu(NH_3)$ 3207cm^{-1}, 1605cm^{-1} and 782cm^{-1}.

6.5.2 Synthesis of $[Ru^{II}(NH_3)_4(HSO_3)_2]$[7]

4g (0.014mol) of $[Ru^{III}(NH_3)_5Cl]Cl_2$ was dissolved in 160ml of water at 80°C. To this solution 5.66g (0.054mol) of solid $NaHSO_3$ was added. The solution which was maintained at 75°C using an oil bath and sulphur dioxide gas was slowly bubbled through the solution for 1h. The solution was cooled to room temperature with continued saturation of sulphur dioxide. Yellow crystals were formed during the reaction and were filtered off, washed first with water followed by methanol, before being air dried under vacuum at room temperature.

Yield: 75% (3.42g, 0.010mol). IR (nujol): $\nu(NH_3)$ 3263cm^{-1}, 1637cm^{-1} and 780cm^{-1}.

6.5.3 Synthesis of $[Ru^{II}(NH_3)_4(SO_2)Cl]Cl$[7]

2.77g (8mmol) of $[Ru^{II}(NH_3)_4(HSO_3)_2]$ was dissolved in 325ml of 1:1 water;HCl by heating to boiling for ca. 15mins. The deep red coloured solution was filtered hot and the filtrate was subsequently reheated to redissolve any crystals that had formed. The solution was left to cool slowly and red needle shaped crystals of $[Ru^{II}(NH_3)_4(SO_2)Cl]Cl$ deposited overnight. The crystals were washed with 1:1 water:HCl followed by methanol, before being air dried under vacuum at room temperature.

Yield: 89% (2.19g, 7mmol). IR (nujol): $\nu(NH_3)$ 3225cm^{-1}, 1631cm^{-1} and 778cm^{-1}, ν(SO) 1303cm^{-1} and 1281cm^{-1}.

6.5.4 Synthesis of $[Ru^{II}(NH_3)_4(H_2O)(SO_2)](Tos)_2$[8, 9]

p-toluene sulphonic acid monohydrate 1.6g (8mmol) was dissolved in 20ml of water. 0.4g (0.013mol) of $[Ru^{II}(NH_3)_4(SO_2)Cl]Cl$ was added and the mixture heated to 90°C with vigorous stirring. The resulting solution was left to cool slowly and orange block crystals of $[Ru^{II}(NH_3)_4(H_2O)(SO_2)](Tos)_2$ deposited overnight. The crystals were washed with diethyl-ether before being air dried.

Yield: 82% (0.64g, 0.011mol). IR (nujol): $\nu(NH_3)$ 3209cm^{-1}, 1621cm^{-1} and 781cm^{-1}, ν(SO) 1283 cm^{-1} and 1113cm^{-1}, $\nu(SO_3)$ 1165cm^{-1} and 570cm^{-1} ν(CH) 3100cm^{-1}, $\nu(CH_3)$ 2965cm^{-1}, 2885cm^{-1} and 1382cm^{-1}. Analysis for $Ru^{II}(NH_3)_4(H_2O)(SO_2)](Tos)_2$ Calculated: C 28.33%, H 4.75%, N 9.43%. Found: C 29.01%, H 4.94%, N 9.22%.

6.6 Synthesis for Chapter 4

6.6.1 Synthesis of $K_4[Ni^{II}(NO_2)_6].H_2O$[10]

An excess of potassium nitrate (80g, 0.791mol) was dissolved in 25ml of water. This solution was added to a separate solution of nickel^{II}chloride 20g (0.084mol) dissolved in 20ml of water. An orange precipitate formed which was filtered washed with cold methanol and subsequently air dried at room temperature.

Yield: 89% (2.19g, 7mmol).

6.6.2 Synthesis of $[Ni(aep)_2(NO_2)_2]$ and $[Ni(aep)_2(ONO)_2]$[11]

The complexes $[Ni(aep)_2(NO_2)_2]$ (purple) and $[Ni(aep)_2(ONO)_2]$ (blue) were synthesised by adding a methanolic solution (5ml) of 1-(2-aminoethyl)piperidine (0.26g, 2mmol) to a methanolic suspension (10ml) of $K_4[Ni^{II}(NO_2)_6].H_2O$ (0.5g, 1mmol). The resulting dark green solution was kept in a $CaCl_2$ dessicator. After a few days a mixture of purple and blue crystals was obtained.

Yield: 83% (0.34g, 0.8mmol). For $[Ni(aep)_2(NO_2)_2]$: IR (nujol): $\nu(NO_2)$ 1362cm^{-1}, 1284cm^{-1} and 819cm^{-1}. Analysis for $NiC_{14}H_{32}N_6O_4$ - Calculated: C 41.30%, H 7.92%, N 20.64% Found: C 42.01%, H 8.33%, N19.90%. For $[Ni(aep)_2(ONO)_2]$: IR (nujol): $\nu(ONO)$ 1373cm^{-1}, 1150cm^{-1} and 819cm^{-1}. Found C 41.92%, H 8.14%, N 20.01%.

6.6.3 Synthesis of $[Ni(aem)_2(NO_2)_2]$[12]

$[Ni(aem)_2(NO_2)_2]$ was synthesised by adding 4-(2-aminoethyl)morpholine (0.26g, 2mmol) in methanol (5ml) dropwise to a methanolic suspension (10ml) of $K_4[Ni^{II}(NO_2)_6].H_2O$ (0.5g, 1mmol) with vigorous stirring. Initially a clear green solution was formed, but within a few minutes a violet-blue precipitate appeared. After 1h of stirring the mixture was filtered and the green coloured filtrate was kept in a $CaCl_2$ dessicator. After a few days large purple crystals were obtained.

Yield: 61% (0.25g, 0.6mmol). IR (nujol): $\nu(NO_2)$ 1352cm^{-1}, 1300 cm^{-1} and 810cm^{-1}. Analysis for $[Ni(aem)_2(NO_2)_2]$ Calculated: C 35.06%, H 6.87%, N 20.44%. Found: C 35.33%, H 7.01%, N 19.76%.

6.6.4 Synthesis of $[Ni(aepy)_2(NO_2)_2]$[13]

$[Ni(aepy)_2(NO_2)_2]$ was synthesised by adding a methanolic solution (5ml) of 1-(2-aminoethyl)pyrrolidine (0.23g, 2mmol) to a methanolic suspension of (10ml) of $K_4[Ni^{II}(NO_2)_6].H_2O$ (0.5g, 1mmol) with vigorous stirring. The resulting green solution was kept in a $CaCl_2$ dessicator and after a few days purple/brown crystals were obtained.

Yield: 58% (0.22g, 0.5mmol). IR (nujol): $\nu(NO_2)$ 1361cm^{-1}, 1296cm^{-1} and 817cm^{-1}. Analysis for $[Ni(aepy)_2(NO_2)_2]$ Calculated: C 38.02%, H 7.44%, N 22.17%. Found: C 38.17%, H 7.36%, N 21.88%.

6.7 Synthesis for Chapter 5

6.7.1 Synthesis of $[Co^{III}(NH_3)_5Cl]Cl_2$[14]

Ammonium chloride (2g, 0.038mol) was dissolved in 9ml conc. ammonia. The solution was continuously stirred while $CoCl_2.6H_2O$ (4g, 0.017mol) was added in equal aliquots. 2ml of 30% hydrogen peroxide was added to the warm solution with stirring. Once effervescence ceased 6ml conc. HCl was added to the solution with vigorous stirring. The solution is heated to boiling and maintained at this temperature for 15mins during which time a purple precipitate forms. The mixture is cooled to room temperature and filtered. The product is washed with 4ml 1:1 water:HCl which was cooled below 10°C. The product was then placed in an oven for 1h to dry.

Yield: 91% (3.88g, 0.015mol).

6.7.2 Synthesis of $[Co(NH_3)_5(ONO)]Cl_2$[14]

2g (7.6mmol) of $[Co^{III}(NH_3)_5Cl]Cl_2$ was dissolved (with stirring) into a solution of 3ml conc. ammonia in 40ml of water. The precipitate was filtered off and the filtrate was cooled to 10°C in an ice bath. Once cooled ca. 4ml of HCl was added dropwise to neutralise the solution. Sodium nitrite (2g, 0.029mol) was added to the solution followed by 1ml of conc. HCl. The solution was left on an ice bath for 1h during which time salmon pink microcrystals formed. The crystals were filtered then washed with 5ml ice-cold water followed by 5ml of ethanol before being left to air dry.

Yield: 89% (1.85g, 7mmol).

6.7.3 Synthesis of $[Co(NH_3)_5(NO_2)]Cl_2$[14]

To a hot solution of water (4ml) containing a few drops of conc. ammonia, 0.5g (1.9mmol) of $[Co(NH_3)_5(ONO)]Cl_2$ was added. Upon cooling 4ml of conc. HCl was added. The mixture was further cooled on an ice-bath. After a short period of time a precipitate formed. The precipitate was filtered and washed with ethanol and left to air dry. The product was recrystallised in water and red/brown block crystals formed in 2-3 days.

Yield: 82% (0.41g, 1.6mmol) IR (nujol): $\nu(NO_2)$ 1323cm^{-1}, 1290cm^{-1} and 825cm^{-1}, $\nu(NH_3)$ 3300cm^{-1}, 3151cm^{-1}, 1562cm^{-1} and 779cm^{-1}.

6.7.4 Synthesis of $[Co(NH_3)_5(NO_2)]PF_6$

To a solution of $NaPF_6$ (0.336g, 2mmol) in 10ml of water, a solution of $[Co(NH_3)_5(NO_2)]Cl_2$ (0.26g, 1mmol) in 10ml of water was added slowly. No precipitate was observed upon mixing and small orange crystals formed within a week.

IR (nujol): $\nu(NO_2)$ 1407cm^{-1}, 1320cm^{-1} and 835cm^{-1}, $\nu(NH_3)$ 3320cm^{-1}, 3222cm^{-1}, 1621cm^{-1} and 765cm^{-1}. Analysis for $[Co(NH_3)_5(NO_2)]PF_6$ Calculated: C 0.00%, H 4.51%, N 25.08%. Found: C 0.21%, H 4.32%, N 24.8%.

6.7.4 Synthesis of $[Co(NH_3)_5(NO_2)][Fe(CN)_5(NO)].1½H_2O$[15]

To a solution of $Na_2[Fe(CN)_5(NO)].2H_2O$ (0.30g, 1mmol) in 10ml of water, a solution of $[Co(NH_3)_5(NO_2)]Cl_2$ (0.26g, 1mmol) in 10ml of water was added slowly. No precipitate formed on mixing, however after a few days dark red block crystals had deposited from the solution.

IR (nujol): $\nu(CN)$ 2140cm^{-1}, $\nu(NO)$ 1931cm^{-1}, $\nu(NO_2)$ 1414cm^{-1}, 1330cm^{-1} C, $\nu(NH_3)$ 3300cm^{-1}, 3150cm^{-1}, 1620cm^{-1} and 773cm^{-1}. Analysis for $[Co(NH_3)_5(NO_2)][Fe(CN)_5(NO)].1½H_2O$ Calculated: C 13.62%, H 3.43%, N 38.27%. Found: C 13.80%, H 4.33%, N 38.4%.

6.7.5 Synthesis of $[Co(NH_3)_5(NO_2)](Hbs)_2.2H_2O$

To a solution of $NaHOC_6H_4SO_3$ (0.46g, 2mmol) in 10ml of water, a solution of $[Co(NH_3)_5(NO_2)]Cl_2$ (0.26g, 1mmol) in 10ml of water was added slowly. No precipitate formed on mixing however orange block crystals formed after a period of two weeks.

IR (nujol): ν(SO) 1030cm^{-1}, ν(OH) 3531cm^{-1}, ν(NO_2) 1429cm^{-1}, 1345cm^{-1} and 833 cm^{-1}, ν(NH_3) 3300cm^{-1}, 3192cm^{-1}, 1600cm^{-1} and 750cm^{-1}. Analysis for $[Co(NH_3)_5(NO_2)](Hbs)_2.2H_2O$ Calculated: C 25.17%, H 5.11%, N 14.68%. Found: C 23.89%, H 4.67%, N 15.11%.

6.7.5 Synthesis of $[Co(NH_3)_5(NO_2)](BPh_4)_2.2H_2O$

To a solution of $NaBPh_4$ (0.7g, 2mmol) in 10ml of water, a solution of $[Co(NH_3)_5(NO_2)]Cl_2$ (0.26g, 1mmol) in 10ml of water was added slowly. Upon mixing a white precipitate formed which was filtered off. The filtrate was left to crystallise and after a few days orange triangular crystals appeared.

IR (nujol): ν(C-H) 3060cm^{-1} and 744cm^{-1}, ν(NO_2) 1430cm^{-1} ,1305cm^{-1} and 825cm^{-1}, ν(NH_3) 3280cm^{-1}, 3230cm^{-1}, 1600cm^{-1} and 768cm^{-1}.

6.7.6 Synthesis of $[Ru(NH_3)_4(SO_2)(OH)]_2[(OC_7H_4SO_3)_4].C_2H_5OH.3H_2O$

To a solution of 4-sulfonic calix[4]arene (0.36g, 0.5mmol) in 5ml water with a couple of drops of ethanol, a solution of $[Ru(NH_3)_4(SO_2)Cl]Cl$ (1.6g, 0.5mmol) in 5ml of water was added. A precipitate formed upon mixing which was redissolved in boiling solvent, the solution was filtered and left to crystallise. A few needle crystals were obtained after several days.

6.8 References

[1] R. H. Blessing, *Acta Crystallogr. Sect. A* **1995**, *51*, 33.
[2] S. P. Sinha, *Z. Naturforsch* **1965**, *20*, 1661.
[3] G. M. Sheldrick, *SHELXL A program for crystal stucture refinement*, **1986**.
[4] A. D. Becke, *J. Chem. Phys.* **1993**, *98*, 5648.
[5] M. J. Frisch, G. W. Trucks, H. B. Schlegel, G. E. Scuseria, M. A. Robb, J. R. Cheeseman, J. A. Montgomery, Jr., T. Vreven, K. N. Kudin, J. C. Burant, J. M. Millam, S. S. Iyengar, J. Tomasi, V. Barone, B. Mennucci, M. Cossi, G. Scalmani, N. Rega, G. A. Petersson, H. Nakatsuji, M. Hada, M. Ehara, K. Toyota, R. Fukuda, J. Hasegawa, M. Ishida, T. Nakajima, Y. Honda, O. Kitao, H. Nakai, M. Klene, X. Li, J. E. Knox, H. P. Hratchian, J. B. Cross, V. Bakken, C. Adamo, J. Jaramillo, R. Gomperts, R. E. Stratmann, O. Yazyev, A. J. Austin, R. Cammi, C. Pomelli, J. W. Ochterski, P. Y. Ayala, K. Morokuma, G. A. Voth, P. Salvador, J. J. Dannenberg, V. G. Zakrzewski, S. Dapprich, A. D. Daniels, M. C. Strain, O. Farkas, D. K. Malick, A. D. Rabuck, K. Raghavachari, J. B. Foresman, J. V. Ortiz, Q. Cui, A. G. Baboul, S. Clifford, J. Cioslowski, B. B. Stefanov, G. Liu, A. Liashenko, P. Piskorz, I. Komaromi, R. L. Martin, D. J. Fox, T. Keith, M. A. Al-Laham, C. Y. Peng, A. Nanayakkara, M. Challacombe, P. M. W. Gill, B. Johnson, W. Chen, M. W. Wong, C. Gonzalez, J. A. Pople, *Gaussian 03, Revision B.04*, Gaussian, Inc., Pittsburgh PA, **2003**.
[6] H. P. Luthi, J. Weber, *Molekel, Revision 4.0, Flükiger*, Swiss Center for Scientific Computing, Manno Switzerland, **2000**.
[7] L. H. Vogt, Jr., J. L. Katz, Wiberley, *Inorg. Chem.* **1965**, *4*, 1157.
[8] A. Y. Kovalevsky, K. A. Bagley, J. M. Cole, P. Coppens, *Inorg. Chem.* **2003**, *42*, 140.
[9] H. A. Sparkes, *Solid State X-Ray Structural Studies*, University of Bath, Dept. of Chem., **2005**.
[10] R. W. Green, B. Bell, *Aust. J. Chem.* **1973**, *26*, 1663.
[11] D. Das, I. R. Laskar, A. Ghosh, A. Mondal, K. Okamoto, N. R. Chaudhuri, *J. Chem. Soc. Dalton Trans.* **1998**, 3987.
[12] T. Chattopadhyay, M. Ghosh, A. Majee, M. Nethaji, D. Das, *Polyhedron* **2005**, *24*, 1677.
[13] I. R. Laskar, T. K. Maji, D. Das, T. H. Lu, W. T. Wong, K. Okamoto, N. R. Chaudhuri, *Polyhedron* **2001**, *20*, 2073.
[14] G. Schlessinger, *Inorganic Laboratory Preparations*, Chemical Publishing Company, New York, **1962**.
[15] D. B. Soria, M. E. C. Villalba, O. E. Piro, P. J. Aymonino, *Polyhedron* **2002**, *21*, 1767.

Appendix

7.1 Crystal Data for Chapter 3

7.1.1 Crystal data for h04prr27 - *trans*-[$Ru(NH_3)_4(SO_2)Cl]Cl$

Table 1. Crystal data and structure refinement for h04prr27 - *trans*-[$Ru(NH_3)_4(SO_2)Cl]Cl$.

Identification code	*trans*-[$Ru(NH_3)_4(SO_2)Cl]Cl$
Empirical formula	$H_{12}\ Cl_2\ N_4\ O_2\ Ru\ S$
Formula weight	304.17
Temperature	150(2)K
Wavelength	0.71073Å
Crystal system, space group	Orthorhombic, *Pmcn*
Unit cell dimensions	a = 7.2430(4)Å alpha = 90°
	b = 9.2710(5)Å beta = 90°
	c = 13.9710(8)Å gamma = 90°
Volume	938.15(9)$Å^3$
Z, Calculated density	4, 2.154 Mg/m^3
Absorption coefficient	2.421 mm^{-1}
F(000)	600
Crystal size	0.22 x 0.08 x 0.03 mm
Theta range for data collection	4.05 to 27.50 deg.
Limiting indices	-9<=h<=9, -12<=k<=12, -18<=l<=18
Reflections collected / unique	14661 / 1164 [R(int) = 0.1637]
Completeness to theta = 27.50	99.5 %
Absorption correction	Sortav
Max. and min. transmission	0.9419 and 0.6119
Refinement method	Full-matrix least-squares on F^2
Data / restraints / parameters	1164 / 0 / 58
Goodness-of-fit on F^2	1.003
Final R indices [I>2sigma(I)]	R1 = 0.0597, wR2 = 0.1400
R indices (all data)	R1 = 0.1209, wR2 = 0.1656
Largest diff. peak and hole	4.320 and -1.375 $e.Å^{-3}$

Table 2. Atomic coordinates (x 10^4) and equivalent isotropic displacement parameters (A^2 x 10^3) for *trans*-[$Ru(NH_3)_4(SO_2)Cl]Cl$.
U(eq) is defined as one third of the trace of the orthogonalized Uij tensor.

	x	y	z	U(eq)
Ru(1)	2500	7222(1)	863(1)	18(1)
Cl(1)	2500	4927(4)	30(3)	37(1)
S(1)	2500	9123(4)	1651(2)	28(1)
N(1)	456(9)	7931(7)	-114(5)	23(2)
Cl(2)	2500	4357(3)	3482(2)	29(1)
N(2)	419(9)	6345(8)	1753(5)	30(2)
O(1)	2500	10477(11)	1315(8)	41(2)
O(2)	2500	9003(11)	2682(7)	53(3)

Table 3. Bond lengths [Å] and angles [°] for *trans*-[$Ru(NH_3)_4(SO_2)Cl]Cl$.

Ru(1)-S(1)	2.078(3)
Ru(1)-N(2)#1	2.117(6)
Ru(1)-N(2)	2.117(6)
Ru(1)-N(1)#1	2.118(6)
Ru(1)-N(1)	2.118(6)
Ru(1)-Cl(1)	2.425(4)
S(1)-O(1)	1.340(11)
S(1)-O(2)	1.445(11)
S(1)-Ru(1)-N(2)#1	90.8(2)
S(1)-Ru(1)-N(2)	90.8(2)
N(2)#1-Ru(1)-N(2)	90.8(4)
S(1)-Ru(1)-N(1)#1	94.5(2)
N(2)#1-Ru(1)-N(1)#1	90.0(3)
N(2)-Ru(1)-N(1)#1	174.6(3)
S(1)-Ru(1)-N(1)	94.5(2)
N(2)#1-Ru(1)-N(1)	174.6(3)
N(2)-Ru(1)-N(1)	90.0(3)
N(1)#1-Ru(1)-N(1)	88.7(4)
S(1)-Ru(1)-Cl(1)	176.68(13)
N(2)#1-Ru(1)-Cl(1)	86.8(2)
N(2)-Ru(1)-Cl(1)	86.8(2)
N(1)#1-Ru(1)-Cl(1)	87.90(19)
N(1)-Ru(1)-Cl(1)	87.90(19)
O(1)-S(1)-O(2)	114.9(6)
O(1)-S(1)-Ru(1)	127.5(5)
O(2)-S(1)-Ru(1)	117.6(4)

Symmetry transformations used to generate equivalent atoms:
#1 -x+1/2,y,z

Table 4. Anisotropic displacement parameters (A^2 x 10^3) for *trans*-[$Ru(NH_3)_4(SO_2)Cl]Cl$.
The anisotropic displacement factor exponent takes the form: -2 pi^2 [h^2 a*^2 U11 + ... + 2 h k a* b* U12]

	U11	U22	U33	U23	U13	U12
Ru(1)	14(1)	19(1)	21(1)	3(1)	0	0
Cl(1)	26(2)	31(2)	54(2)	5(2)	0	0
S(1)	19(2)	37(2)	28(2)	-5(2)	0	0
N(1)	21(3)	18(4)	29(4)	2(3)	-5(3)	-1(3)
Cl(2)	35(2)	22(2)	31(2)	4(1)	0	0
N(2)	16(4)	35(5)	38(4)	11(3)	3(3)	-4(3)
O(1)	20(5)	33(6)	70(7)	-19(5)	0	0
O(2)	58(7)	46(7)	54(7)	-15(5)	0	0

7.1.2 Crystal Data for h07prr14 - *trans*-$[Ru(NH_3)_4(SO_2)(H_2O)](Tos)_2$

Table 1. Crystal data and structure refinement for *trans*-$[Ru(NH_3)_4(SO_2)(H_2O)](Tos)_2$.

Identification code	*trans*-$[Ru(NH_3)_4(SO_2)(H_2O)](Tos)_2$	
Empirical formula	$C_{14}\ H_{28}\ N_4\ O_9\ Ru\ S_3$	
Formula weight	593.65	
Temperature	150(2)K	
Wavelength	0.71073Å	
Crystal system, space group	Triclinic, *P*-1	
Unit cell dimensions	a = 6.6950(2)Å	alpha = 94.531(2)°
	b = 13.1000(5)Å	beta = 92.848(2)°
	c = 13.6240(5)Å	gamma = 103.542(2)°
Volume	1155.17(7)Å^3	
Z, Calculated density	2, 1.707 Mg/m^3	
Absorption coefficient	1.002 mm^{-1}	
F(000)	608	
Crystal size	0.09 x 0.05 x 0.03mm	
Theta range for data collection	3.27 to 30.49°	
Limiting indices	-9<=h<=9, -17<=k<=18, -16<=l<=19	
Reflections collected / unique	14721 / 6021 [R(int) = 0.0681]	
Completeness to theta = 30.49	85.3 %	
Absorption correction	Sortav	
Max. and min. transmission	0.9706 and 0.9153	
Refinement method	Full-matrix least-squares on F^2	
Data / restraints / parameters	6021 / 2 / 292	
Goodness-of-fit on F^2	0.990	
Final R indices [I>2sigma(I)]	R1 = 0.0460, wR2 = 0.0881	
R indices (all data)	R1 = 0.0909, wR2 = 0.1008	
Largest diff. peak and hole	1.172 and -1.445 e.Å^{-3}	

Table 2. Atomic coordinates (x 10^4) and equivalent isotropic displacement parameters (A^2 x 10^3) for *trans*-$[Ru(NH_3)_4(SO_2)(H_2O)](Tos)_2$.
U(eq) is defined as one third of the trace of the orthogonalized Uij tensor.

	x	y	z	U(eq)
Ru(1)	3126(1)	9944(1)	2446(1)	14(1)
S(1)	4015(1)	8574(1)	1962(1)	18(1)
O(1)	5646(4)	8588(2)	1309(2)	24(1)
O(2)	2985(4)	7555(2)	2239(2)	28(1)
O(3)	2290(4)	11365(2)	2905(2)	17(1)
N(1)	6019(4)	10712(2)	3195(2)	16(1)
N(2)	2115(4)	9335(2)	3773(2)	19(1)
N(3)	92(4)	9365(2)	1784(2)	20(1)
N(4)	4032(4)	10633(2)	1135(2)	19(1)
S(2)	-422(1)	12056(1)	818(1)	17(1)
O(4)	-1728(4)	11423(2)	-2(2)	26(1)
O(5)	1766(4)	12236(2)	689(2)	24(1)
O(6)	-949(4)	11591(2)	1753(2)	20(1)
C(1)	-1025(5)	13302(3)	920(2)	15(1)
C(2)	-3003(5)	13391(3)	655(2)	19(1)
C(3)	-3482(6)	14359(3)	829(3)	21(1)
C(4)	-2013(6)	15253(3)	1237(3)	23(1)
C(5)	-22(6)	15142(3)	1473(3)	25(1)
C(6)	464(6)	14172(3)	1320(3)	22(1)
C(7)	-2542(7)	16303(3)	1422(3)	31(1)
S(3)	-3081(1)	8204(1)	4461(1)	18(1)
O(7)	-2657(4)	8695(2)	3546(2)	20(1)
O(8)	-1363(4)	8603(2)	5212(2)	21(1)

O(9)	-5053(4)	8298(2)	4820(2)	23(1)
C(8)	-3199(6)	6845(3)	4205(2)	20(1)
C(9)	-1403(6)	6498(3)	4272(3)	25(1)
C(10)	-1463(6)	5448(3)	4011(3)	26(1)
C(11)	-3298(7)	4727(3)	3695(3)	27(1)
C(12)	-5089(7)	5086(3)	3635(3)	30(1)
C(13)	-5039(6)	6151(3)	3882(3)	23(1)
C(14)	-3334(7)	3585(3)	3426(3)	38(1)

Table 3. Bond lengths [Å] and angles [°] for *trans*-[$Ru(NH_3)_4(SO_2)(H_2O)$]$(Tos)_2$.

Ru(1)-S(1)	2.0877(9)
Ru(1)-N(2)	2.112(3)
Ru(1)-N(4)	2.117(3)
Ru(1)-N(3)	2.122(3)
Ru(1)-O(3)	2.123(2)
Ru(1)-N(1)	2.129(3)
S(1)-O(1)	1.440(2)
S(1)-O(2)	1.441(2)
O(3)-H(1)	0.841(10)
O(3)-H(2)	0.839(10)
N(1)-H(3)	0.9100
N(1)-H(4)	0.9100
N(1)-H(5)	0.9100
N(2)-H(6)	0.9100
N(2)-H(7)	0.9100
N(2)-H(8)	0.9100
N(3)-H(9)	0.9100
N(3)-H(10)	0.9100
N(3)-H(11)	0.9100
N(4)-H(12)	0.9100
N(4)-H(13)	0.9100
N(4)-H(14)	0.9100
S(2)-O(5)	1.450(2)
S(2)-O(4)	1.455(3)
S(2)-O(6)	1.478(2)
S(2)-C(1)	1.768(3)
C(1)-C(6)	1.381(5)
C(1)-C(2)	1.389(5)
C(2)-C(3)	1.385(5)
C(2)-H(15)	0.9500
C(3)-C(4)	1.397(5)
C(3)-H(16)	0.9500
C(4)-C(5)	1.399(5)
C(4)-C(7)	1.504(5)
C(5)-C(6)	1.386(5)
C(5)-H(17)	0.9500
C(6)-H(18)	0.9500
C(7)-H(19)	0.9800
C(7)-H(20)	0.9800
C(7)-H(21)	0.9800
S(3)-O(7)	1.458(2)
S(3)-O(9)	1.459(2)
S(3)-O(8)	1.469(2)
S(3)-C(8)	1.769(3)
C(8)-C(13)	1.377(5)
C(8)-C(9)	1.383(5)
C(9)-C(10)	1.384(5)
C(9)-H(22)	0.9500
C(10)-C(11)	1.388(6)

C(10)-H(23)	0.9500
C(11)-C(12)	1.387(6)
C(11)-C(14)	1.506(5)
C(12)-C(13)	1.401(5)
C(12)-H(24)	0.9500
C(13)-H(25)	0.9500
C(14)-H(26)	0.9800
C(14)-H(27)	0.9800
C(14)-H(28)	0.9800

S(1)-Ru(1)-N(2)	92.60(8)
S(1)-Ru(1)-N(4)	91.10(8)
N(2)-Ru(1)-N(4)	176.17(10)
S(1)-Ru(1)-N(3)	92.72(8)
N(2)-Ru(1)-N(3)	89.32(11)
N(4)-Ru(1)-N(3)	89.53(11)
S(1)-Ru(1)-O(3)	178.05(7)
N(2)-Ru(1)-O(3)	89.22(10)
N(4)-Ru(1)-O(3)	87.09(10)
N(3)-Ru(1)-O(3)	87.99(10)
S(1)-Ru(1)-N(1)	95.43(8)
N(2)-Ru(1)-N(1)	89.58(11)
N(4)-Ru(1)-N(1)	91.04(11)
N(3)-Ru(1)-N(1)	171.82(10)
O(3)-Ru(1)-N(1)	83.88(10)
O(1)-S(1)-O(2)	116.08(15)
O(1)-S(1)-Ru(1)	122.13(11)
O(2)-S(1)-Ru(1)	121.77(11)
Ru(1)-O(3)-H(1)	123(3)
Ru(1)-O(3)-H(2)	122(3)
H(1)-O(3)-H(2)	90(3)
Ru(1)-N(1)-H(3)	109.5
Ru(1)-N(1)-H(4)	109.5
H(3)-N(1)-H(4)	109.5
Ru(1)-N(1)-H(5)	109.5
H(3)-N(1)-H(5)	109.5
H(4)-N(1)-H(5)	109.5
Ru(1)-N(2)-H(6)	109.5
Ru(1)-N(2)-H(7)	109.5
H(6)-N(2)-H(7)	109.5
Ru(1)-N(2)-H(8)	109.5
H(6)-N(2)-H(8)	109.5
H(7)-N(2)-H(8)	109.5
Ru(1)-N(3)-H(9)	109.5
Ru(1)-N(3)-H(10)	109.5
H(9)-N(3)-H(10)	109.5
Ru(1)-N(3)-H(11)	109.5
H(9)-N(3)-H(11)	109.5
H(10)-N(3)-H(11)	109.5
Ru(1)-N(4)-H(12)	109.5
Ru(1)-N(4)-H(13)	109.5
H(12)-N(4)-H(13)	109.5
Ru(1)-N(4)-H(14)	109.5
H(12)-N(4)-H(14)	109.5
H(13)-N(4)-H(14)	109.5
O(5)-S(2)-O(4)	114.16(15)
O(5)-S(2)-O(6)	111.45(15)
O(4)-S(2)-O(6)	110.03(14)
O(5)-S(2)-C(1)	107.31(15)
O(4)-S(2)-C(1)	107.28(15)
O(6)-S(2)-C(1)	106.17(14)
C(6)-C(1)-C(2)	120.7(3)

C(6)-C(1)-S(2)	118.9(3)
C(2)-C(1)-S(2)	120.3(3)
C(3)-C(2)-C(1)	119.0(3)
C(3)-C(2)-H(15)	120.5
C(1)-C(2)-H(15)	120.5
C(2)-C(3)-C(4)	121.8(3)
C(2)-C(3)-H(16)	119.1
C(4)-C(3)-H(16)	119.1
C(3)-C(4)-C(5)	117.8(3)
C(3)-C(4)-C(7)	121.5(4)
C(5)-C(4)-C(7)	120.7(3)
C(6)-C(5)-C(4)	121.0(3)
C(6)-C(5)-H(17)	119.5
C(4)-C(5)-H(17)	119.5
C(1)-C(6)-C(5)	119.8(3)
C(1)-C(6)-H(18)	120.1
C(5)-C(6)-H(18)	120.1
C(4)-C(7)-H(19)	109.5
C(4)-C(7)-H(20)	109.5
H(19)-C(7)-H(20)	109.5
C(4)-C(7)-H(21)	109.5
H(19)-C(7)-H(21)	109.5
H(20)-C(7)-H(21)	109.5
O(7)-S(3)-O(9)	112.58(14)
O(7)-S(3)-O(8)	110.87(14)
O(9)-S(3)-O(8)	112.38(14)
O(7)-S(3)-C(8)	107.12(15)
O(9)-S(3)-C(8)	107.66(16)
O(8)-S(3)-C(8)	105.80(16)
C(13)-C(8)-C(9)	120.2(3)
C(13)-C(8)-S(3)	120.3(3)
C(9)-C(8)-S(3)	119.3(3)
C(8)-C(9)-C(10)	119.6(4)
C(8)-C(9)-H(22)	120.2
C(10)-C(9)-H(22)	120.2
C(9)-C(10)-C(11)	121.4(4)
C(9)-C(10)-H(23)	119.3
C(11)-C(10)-H(23)	119.3
C(12)-C(11)-C(10)	118.3(4)
C(12)-C(11)-C(14)	121.1(4)
C(10)-C(11)-C(14)	120.6(4)
C(11)-C(12)-C(13)	120.7(4)
C(11)-C(12)-H(24)	119.6
C(13)-C(12)-H(24)	119.6
C(8)-C(13)-C(12)	119.7(4)
C(8)-C(13)-H(25)	120.2
C(12)-C(13)-H(25)	120.2
C(11)-C(14)-H(26)	109.5
C(11)-C(14)-H(27)	109.5
H(26)-C(14)-H(27)	109.5
C(11)-C(14)-H(28)	109.5
H(26)-C(14)-H(28)	109.5
H(27)-C(14)-H(28)	109.5

Symmetry transformations used to generate equivalent atoms:

Table 4. Anisotropic displacement parameters (A^2 x 10^3) for *trans*-[$Ru(NH_3)_4(SO_2)(H_2O)](Tos)_2$.
The anisotropic displacement factor exponent takes the form: -2 pi^2 [h^2 a*^2 U11 + ... + 2 h k a* b* U12]

	U11	U22	U33	U23	U13	U12
Ru(1)	14(1)	15(1)	15(1)	1(1)	0(1)	4(1)
S(1)	16(1)	18(1)	21(1)	-3(1)	-2(1)	6(1)
O(1)	21(1)	28(1)	23(1)	-3(1)	2(1)	11(1)
O(2)	25(1)	17(1)	40(2)	-2(1)	1(1)	4(1)
O(3)	20(1)	19(1)	15(1)	-1(1)	0(1)	9(1)
N(1)	15(2)	19(2)	14(1)	-1(1)	1(1)	5(1)
N(2)	18(2)	21(2)	20(2)	1(1)	1(1)	8(1)
N(3)	20(2)	18(2)	21(2)	-1(1)	-1(1)	6(1)
N(4)	19(2)	21(2)	19(2)	0(1)	0(1)	7(1)
S(2)	18(1)	18(1)	16(1)	2(1)	1(1)	7(1)
O(4)	35(2)	21(1)	21(1)	-5(1)	-8(1)	11(1)
O(5)	19(1)	28(1)	29(1)	9(1)	7(1)	10(1)
O(6)	21(1)	21(1)	20(1)	8(1)	7(1)	7(1)
C(1)	17(2)	16(2)	13(2)	2(1)	2(1)	6(1)
C(2)	22(2)	17(2)	18(2)	5(2)	1(2)	2(2)
C(3)	20(2)	27(2)	21(2)	8(2)	3(2)	8(2)
C(4)	36(2)	19(2)	17(2)	6(2)	9(2)	11(2)
C(5)	29(2)	20(2)	24(2)	-4(2)	4(2)	2(2)
C(6)	19(2)	22(2)	23(2)	-1(2)	2(2)	5(2)
C(7)	46(3)	22(2)	29(2)	4(2)	9(2)	14(2)
S(3)	21(1)	19(1)	15(1)	2(1)	3(1)	7(1)
O(7)	23(1)	22(1)	15(1)	3(1)	2(1)	7(1)
O(8)	21(1)	25(1)	17(1)	-2(1)	0(1)	7(1)
O(9)	22(1)	29(1)	23(1)	4(1)	7(1)	14(1)
C(8)	27(2)	17(2)	16(2)	2(2)	1(2)	6(2)
C(9)	28(2)	24(2)	24(2)	4(2)	-1(2)	7(2)
C(10)	32(2)	22(2)	31(2)	5(2)	9(2)	14(2)
C(11)	43(3)	21(2)	18(2)	8(2)	10(2)	8(2)
C(12)	36(2)	26(2)	23(2)	0(2)	4(2)	0(2)
C(13)	23(2)	28(2)	19(2)	4(2)	2(2)	8(2)
C(14)	65(3)	15(2)	32(2)	1(2)	15(2)	4(2)

Table 5. Hydrogen bonds for h07prr14 [Å and °].

D-H...A	d(D-H)	d(H...A)	d(D...A)	<(DHA)
N(1)-H(3)...O(7)#1	0.91	2.17	3.042(4)	159.7
N(1)-H(4)...O(9)#2	0.91	2.19	3.071(3)	162.8
N(1)-H(5)...O(6)#1	0.91	2.12	2.994(3)	161.6
N(2)-H(6)...O(7)	0.91	2.34	3.100(4)	140.7
N(2)-H(6)...S(3)	0.91	2.91	3.648(3)	139.5
N(2)-H(7)...O(8)#2	0.91	2.22	3.094(4)	161.2
N(2)-H(7)...S(3)#2	0.91	2.92	3.774(3)	157.3
N(2)-H(8)...O(9)#1	0.91	2.05	2.954(4)	171.4
N(3)-H(9)...O(4)#3	0.91	2.09	2.925(4)	152.3
N(3)-H(9)...S(2)#3	0.91	3.00	3.913(3)	178.0
N(3)-H(10)...O(6)	0.91	2.28	3.156(4)	160.9
N(3)-H(11)...O(7)	0.91	2.35	3.152(4)	147.7
N(4)-H(12)...O(6)#1	0.91	2.47	3.340(4)	160.0
N(4)-H(12)...O(4)#1	0.91	2.55	3.293(4)	139.7
N(4)-H(12)...S(2)#1	0.91	2.94	3.807(3)	158.9
N(4)-H(13)...O(5)	0.91	2.07	2.947(4)	162.9

N(4)-H(14)...O(4)#3	0.91	2.21	3.029(4)	149.4
O(3)-H(1)...O(8)#2	0.841(10)	1.879(18)	2.670(3)	156(4)
O(3)-H(1)...S(3)#2	0.841(10)	2.93(3)	3.582(2)	136(3)
O(3)-H(2)...O(6)	0.839(10)	1.888(15)	2.700(3)	162(4)
O(3)-H(2)...S(2)	0.839(10)	2.83(2)	3.587(2)	151(3)

Symmetry transformations used to generate equivalent atoms:
#1 x+1,y,z #2 -x,-y+2,-z+1 #3 -x,-y+2,-z

7.2 Crystal Data for Chapter 4

7.2.1 Crystal Data for Bath 412 - $[Ni(aep)_2(NO_2)_2]$ ground state

Table 1. Crystal data and structure refinement for Bath 412.

Identification code	Bath 412
Empirical formula	$C_{14}\ H_{32}\ N_6\ Ni\ O_4$
Formula weight	407.17
Temperature	100(2)K
Wavelength	0.67030Å
Crystal system, space group	Monoclinic, $P2_1/c$
Unit cell dimensions	a = 9.6309(14)Å alpha = 90°
	b = 8.2557(12)Å beta = 109.0650(10)°
	c = 11.8340(17)Å gamma = 90°
Volume	889.3(2)$Å^3$
Z, Calculated density	2, 1.521 Mg/m^3
Absorption coefficient	1.124 mm^{-1}
F(000)	436
Crystal size	0.15 x 0.12 x 0.08 mm
Theta range for data collection	3.14 to 31.05°
Limiting indices	-14<=h<=14, -12<=k<=12, -17<=l<=17
Reflections collected / unique	10846 / 3195 [R(int) = 0.0648]
Completeness to theta = 31.05	94.1 %
Absorption correction	SADABS
Max. and min. transmission	0.9154 and 0.8495
Refinement method	Full-matrix least-squares on F^2
Data / restraints / parameters	3195 / 0 / 114
Goodness-of-fit on F^2	1.183
Final R indices [I>2sigma(I)]	R1 = 0.0522, wR2 = 0.1235
R indices (all data)	R1 = 0.0634, wR2 = 0.1349
Largest diff. peak and hole	1.095 and -0.611 e.$Å^{-3}$

Table 2. Atomic coordinates (x 10^4) and equivalent isotropic displacement parameters (A^2 x 10^3) for Bath 412. U(eq) is defined as one third of the trace of the orthogonalized Uij tensor.

	x	y	z	U(eq)
Ni(1)	5000	0	0	11(1)
N(1)	4239(2)	978(2)	-1771(2)	16(1)
O(1)	4753(2)	529(2)	-2562(2)	22(1)
O(2)	3234(2)	2017(2)	-2061(2)	27(1)
N(2)	2959(2)	-1507(2)	-473(2)	14(1)
C(1)	3139(3)	-2915(3)	336(2)	22(1)
C(2)	1838(3)	-4078(3)	37(2)	23(1)
C(3)	1397(3)	-4649(3)	-1251(2)	21(1)
C(4)	1165(3)	-3210(3)	-2080(2)	23(1)

C(5)	2532(3)	-2135(3)	-1724(2)	23(1)
N(3)	3710(2)	1681(2)	485(2)	15(1)
C(6)	1805(3)	-339(3)	-424(2)	15(1)
C(7)	2400(3)	829(3)	603(3)	16(1)
C(6')	2107(12)	-603(14)	237(11)	13(3)
C(7')	2196(12)	1199(13)	71(11)	12(2)

Table 3. Bond lengths [Å] and angles [°] for Bath 412.

Ni(1)-N(3)	2.0651(17)
Ni(1)-N(3)#1	2.0651(17)
Ni(1)-N(1)#1	2.1401(18)
Ni(1)-N(1)	2.1401(18)
Ni(1)-N(2)	2.2378(17)
Ni(1)-N(2)#1	2.2378(17)
N(1)-O(1)	1.249(2)
N(1)-O(2)	1.254(2)
N(2)-C(1)	1.480(3)
N(2)-C(6)	1.487(3)
N(2)-C(5)	1.494(3)
N(2)-C(6')	1.545(11)
C(1)-C(2)	1.525(3)
C(2)-C(3)	1.517(3)
C(3)-C(4)	1.511(3)
C(4)-C(5)	1.529(3)
N(3)-C(7')	1.434(11)
N(3)-C(7)	1.490(3)
C(6)-C(7)	1.510(4)
C(6')-C(7')	1.507(16)
N(3)-Ni(1)-N(3)#1	180.00(7)
N(3)-Ni(1)-N(1)#1	91.50(7)
N(3)#1-Ni(1)-N(1)#1	88.50(7)
N(3)-Ni(1)-N(1)	88.50(7)
N(3)#1-Ni(1)-N(1)	91.50(7)
N(1)#1-Ni(1)-N(1)	180.00(10)
N(3)-Ni(1)-N(2)	83.34(7)
N(3)#1-Ni(1)-N(2)	96.66(7)
N(1)#1-Ni(1)-N(2)	91.56(7)
N(1)-Ni(1)-N(2)	88.44(7)
N(3)-Ni(1)-N(2)#1	96.66(7)
N(3)#1-Ni(1)-N(2)#1	83.34(7)
N(1)#1-Ni(1)-N(2)#1	88.44(7)
N(1)-Ni(1)-N(2)#1	91.56(7)
N(2)-Ni(1)-N(2)#1	180.00(6)
O(1)-N(1)-O(2)	117.24(18)
O(1)-N(1)-Ni(1)	121.92(14)
O(2)-N(1)-Ni(1)	120.84(14)
C(1)-N(2)-C(6)	114.51(19)
C(1)-N(2)-C(5)	107.77(17)
C(6)-N(2)-C(5)	107.28(18)
C(1)-N(2)-C(6')	89.9(5)
C(6)-N(2)-C(6')	29.4(4)
C(5)-N(2)-C(6')	133.1(5)
C(1)-N(2)-Ni(1)	111.54(13)
C(6)-N(2)-Ni(1)	103.66(13)
C(5)-N(2)-Ni(1)	112.06(13)
C(6')-N(2)-Ni(1)	100.0(4)
N(2)-C(1)-C(2)	115.51(18)
C(3)-C(2)-C(1)	111.6(2)

C(4)-C(3)-C(2)	109.99(19)
C(3)-C(4)-C(5)	110.24(19)
N(2)-C(5)-C(4)	114.07(19)
C(7')-N(3)-C(7)	26.3(5)
C(7')-N(3)-Ni(1)	110.8(4)
C(7)-N(3)-Ni(1)	108.27(14)
N(2)-C(6)-C(7)	110.7(2)
N(3)-C(7)-C(6)	109.7(2)
C(7')-C(6')-N(2)	110.1(8)
C(6')-C(7')-N(3)	108.9(8)

Symmetry transformations used to generate equivalent atoms:
#1 -x+1,-y,-z

Table 4. Anisotropic displacement parameters (A^2 x 10^3) for Bath 412.The anisotropic displacement factor exponent takes the form: -2 pi^2 [h^2 a*^2 U11 + ... + 2 h k a* b* U12]

	U11	U22	U33	U23	U13	U12
Ni(1)	11(1)	11(1)	11(1)	0(1)	4(1)	0(1)
N(1)	17(1)	15(1)	15(1)	1(1)	5(1)	-4(1)
O(1)	25(1)	26(1)	15(1)	0(1)	8(1)	1(1)
O(2)	31(1)	26(1)	22(1)	11(1)	8(1)	13(1)
N(2)	13(1)	13(1)	17(1)	-1(1)	7(1)	0(1)
C(1)	24(1)	22(1)	16(1)	4(1)	0(1)	-10(1)
C(2)	25(1)	21(1)	21(1)	4(1)	4(1)	-10(1)
C(3)	22(1)	17(1)	24(1)	-7(1)	7(1)	-6(1)
C(4)	21(1)	28(1)	16(1)	1(1)	1(1)	-10(1)
C(5)	22(1)	32(1)	14(1)	2(1)	3(1)	-11(1)
N(3)	13(1)	13(1)	18(1)	-3(1)	5(1)	-1(1)

Table 5. Hydrogen bonds for Bath 412 [Å and °].

D-H...A	d(D-H)	d(H...A)	d(D...A)	<(DHA)
N(3)-H(15)...O(1)#2	0.92	2.36	3.185(3)	149.1
N(3)-H(16)...O(2)	0.92	2.31	2.909(3)	122.0

Symmetry transformations used to generate equivalent atoms:
#1 -x+1,-y,-z #2 x,-y+1/2,z+1/2

7.2.2 Crystal Data for Bath 435 - $[Ni(aep)_2(NO_2)_2]$ excited state

Table 1. Crystal data and structure refinement for Bath 435.

Identification code	Bath 435
Empirical formula	$C_{14}\ H_{32}\ N_6\ Ni\ O_4$
Formula weight	407.17
Temperature	90(2)K
Wavelength	0.67030Å
Crystal system, space group	Monoclinic, $P2_1/c$
Unit cell dimensions	a = 9.6301(6)Å alpha = 90°
	b = 8.2875(5)Å beta = 109.1030(10)°
	c = 11.8754(8)Å gamma 90°

Volume	895.58(10)Å^3
Z, Calculated density	2, 1.510 Mg/m^3
Absorption coefficient	1.116 mm^{-1}
F(000)	436
Crystal size	0.15 x 0.12 x 0.08 mm
Theta range for data collection	3.14 to 28.59°
Limiting indices	-13<=h<=13, -11<=k<=11, -16<=l<=16
Reflections collected / unique	10094 / 2715 [R(int) = 0.0626]
Completeness to theta = 28.59	99.6 %
Absorption correction	SADABS
Max. and min. transmission	0.9160 and 0.8504
Refinement method	Full-matrix least-squares on F^2
Data / restraints / parameters	2715 / 0 / 133
Goodness-of-fit on F^2	1.069
Final R indices [I>2sigma(I)]	R1 = 0.0465, wR2 = 0.1273
R indices (all data)	R1 = 0.0500, wR2 = 0.1314
Largest diff. peak and hole	0.666 and -0.614 e. Å^{-3}

Table 2. Atomic coordinates (x 10^4) and equivalent isotropic displacement parameters (A^2 x 10^3) for Bath 435. U(eq) is defined as one third of the trace of the orthogonalized Uij tensor.

	x	y	z	U(eq)
Ni(1)	10000	0	10000	13(1)
O(2A)	11769(2)	2021(2)	2072(2)	35(1)
N(1A)	10743(2)	964(3)	11772(2)	18(1)
O(1A)	10223(2)	523(2)	12558(1)	26(1)
N(1B)	11210(20)	1530(30)	12477(19)	29(5)
O(1B)	10380(30)	410(40)	11770(20)	37(6)
O(2B)	11769(2)	2021(2)	12072(2)	35(1)
N(2)	12040(2)	-1505(2)	10469(1)	16(1)
C(1)	11854(2)	-2916(3)	9668(2)	28(1)
C(2)	13161(2)	-4073(2)	9967(2)	26(1)
C(3)	13605(2)	-4634(3)	11255(2)	23(1)
C(4)	13839(2)	-3196(3)	12074(2)	26(1)
C(5)	12470(2)	-2113(3)	11717(2)	26(1)
N(3)	11301(2)	1684(2)	9541(2)	19(1)
C(6)	13198(3)	-337(3)	10430(3)	19(1)
C(7)	12610(3)	842(3)	9415(3)	23(1)
C(7')	12814(11)	1196(12)	10059(11)	22(2)
C(6')	12885(10)	-619(11)	9797(10)	17(2)

Table 3. Bond lengths [Å] and angles [°] for Bath 435.

Ni(1)-O(1B)#1	2.04(3)
Ni(1)-O(1B)	2.04(3)
Ni(1)-N(3)#1	2.0644(15)
Ni(1)-N(3)	2.0644(15)
Ni(1)-N(1A)	2.1432(18)
Ni(1)-N(1A)#1	2.1432(18)
Ni(1)-N(2)	2.2383(14)
Ni(1)-N(2)#1	2.2383(14)
O(2A)-N(1A)	1.280(3)
N(1A)-O(1A)	1.250(3)
N(1B)-O(1B)	1.33(3)
N(2)-C(1)	1.481(2)
N(2)-C(5)	1.490(2)

N(2)-C(6)	1.490(3)
N(2)-C(6')	1.505(9)
C(1)-C(2)	1.529(3)
C(2)-C(3)	1.520(3)
C(3)-C(4)	1.508(3)
C(4)-C(5)	1.536(3)
N(3)-C(7')	1.442(10)
N(3)-C(7)	1.490(3)
C(6)-C(7)	1.510(4)
C(7')-C(6')	1.542(15)

O(1B)#1-Ni(1)-O(1B)	180.000(9)
O(1B)#1-Ni(1)-N(3)#1	103.8(8)
O(1B)-Ni(1)-N(3)#1	76.2(8)
O(1B)#1-Ni(1)-N(3)	76.2(8)
O(1B)-Ni(1)-N(3)	103.8(8)
N(3)#1-Ni(1)-N(3)	180.0
O(1B)#1-Ni(1)-N(1A)	164.5(8)
O(1B)-Ni(1)-N(1A)	15.5(8)
N(3)#1-Ni(1)-N(1A)	91.67(8)
N(3)-Ni(1)-N(1A)	88.33(8)
O(1B)#1-Ni(1)-N(1A)#1	15.5(8)
O(1B)-Ni(1)-N(1A)#1	164.5(8)
N(3)#1-Ni(1)-N(1A)#1	88.33(8)
N(3)-Ni(1)-N(1A)#1	91.67(8)
N(1A)-Ni(1)-N(1A)#1	180.0
O(1B)#1-Ni(1)-N(2)	90.6(7)
O(1B)-Ni(1)-N(2)	89.4(7)
N(3)#1-Ni(1)-N(2)	96.68(5)
N(3)-Ni(1)-N(2)	83.32(5)
N(1A)-Ni(1)-N(2)	88.82(6)
N(1A)#1-Ni(1)-N(2)	91.18(6)
O(1B)#1-Ni(1)-N(2)#1	89.4(7)
O(1B)-Ni(1)-N(2)#1	90.6(7)
N(3)#1-Ni(1)-N(2)#1	83.32(5)
N(3)-Ni(1)-N(2)#1	96.68(5)
N(1A)-Ni(1)-N(2)#1	91.18(6)
N(1A)#1-Ni(1)-N(2)#1	88.82(6)
N(2)-Ni(1)-N(2)#1	180.00(8)
O(1A)-N(1A)-O(2A)	116.96(18)
O(1A)-N(1A)-Ni(1)	122.51(17)
O(2A)-N(1A)-Ni(1)	120.52(15)
N(1B)-O(1B)-Ni(1)	130(2)
C(1)-N(2)-C(5)	107.93(15)
C(1)-N(2)-C(6)	115.31(17)
C(5)-N(2)-C(6)	106.51(17)
C(1)-N(2)-C(6')	91.0(4)
C(5)-N(2)-C(6')	132.1(5)
C(6)-N(2)-C(6')	29.0(4)
C(1)-N(2)-Ni(1)	111.61(11)
C(5)-N(2)-Ni(1)	111.81(11)
C(6)-N(2)-Ni(1)	103.59(12)
C(6')-N(2)-Ni(1)	100.3(4)
N(2)-C(1)-C(2)	115.38(16)
C(3)-C(2)-C(1)	111.37(17)
C(4)-C(3)-C(2)	109.90(16)
C(3)-C(4)-C(5)	110.54(16)
N(2)-C(5)-C(4)	113.94(15)
C(7')-N(3)-C(7)	30.9(5)
C(7')-N(3)-Ni(1)	108.3(4)
C(7)-N(3)-Ni(1)	108.44(12)
N(2)-C(6)-C(7)	110.9(2)

N(3)-C(7)-C(6)	109.40(19)
N(3)-C(7')-C(6')	107.0(8)
N(2)-C(6')-C(7')	107.6(8)

Symmetry transformations used to generate equivalent atoms:
#1 -x+2,-y,-z+2

Table 4. Anisotropic displacement parameters (A^2 x 10^3) for Bath 435. The anisotropic displacement factor exponent takes the form: -2 pi^2 [h^2 a*^2 U11 + ... + 2 h k a* b* U12]

	U11	U22	U33	U23	U13	U12
Ni(1)	12(1)	14(1)	13(1)	0(1)	4(1)	0(1)
O(2A)	43(1)	31(1)	30(1)	-9(1)	9(1)	-9(1)
N(1A)	19(1)	17(1)	15(1)	-1(1)	3(1)	4(1)
O(1A)	30(1)	34(1)	16(1)	1(1)	8(1)	3(1)
O(2B)	43(1)	31(1)	30(1)	-9(1)	9(1)	-9(1)
N(2)	15(1)	15(1)	19(1)	2(1)	7(1)	0(1)
C(1)	30(1)	27(1)	19(1)	-7(1)	-1(1)	12(1)
C(2)	30(1)	25(1)	21(1)	-6(1)	4(1)	11(1)
C(3)	23(1)	19(1)	27(1)	7(1)	8(1)	5(1)
C(4)	24(1)	32(1)	18(1)	-1(1)	2(1)	12(1)
C(5)	24(1)	36(1)	13(1)	-2(1)	2(1)	13(1)
N(3)	15(1)	17(1)	26(1)	5(1)	7(1)	1(1)
C(6)	13(1)	18(1)	26(2)	6(1)	7(1)	1(1)
C(7)	19(1)	23(1)	32(2)	11(1)	15(1)	4(1)

7.2.3 Crystal Data for Bath 541 - $[Ni(aem)_2(NO_2)_2]$ ground state

Table 1. Crystal data and structure refinement for Bath 541.

Identification code	Bath 541
Empirical formula	$C_{12}\ H_{28}\ N_6\ Ni\ O_6$
Formula weight	411.11
Temperature	100(2)K
Wavelength	0.68960Å
Crystal system, space group	Triclinic, *P*-1
Unit cell dimensions	a = 7.172(5) Å alpha = 94.306(5)°
	b = 7.988(5) Å beta = 112.642(5)°
	c = 8.330(5) Å gamma = 100.496(5)°
Volume	427.5(5) $Å^3$
Z, Calculated density	1, 1.597 Mg/m^3
Absorption coefficient	1.179 mm^{-1}
F(000)	218
Crystal size	0.15 x 0.14 x 0.08 mm
Theta range for data collection	3.84 to 20.16°
Limiting indices	-7<=h<=7, -7<=k<=7, -8<=l<=8
Reflections collected / unique	143 / 869 [R(int) = 0.0159]
Completeness to theta = 20.16	97.2 %
Absorption correction	SADABS
Max. and min. transmission	0.9116 and 0.8430
Refinement method	Full-matrix least-squares on F^2
Data / restraints / parameters	869 / 0 / 115
Goodness-of-fit on F^2	1.068
Final R indices [I>2sigma(I)]	R1 = 0.0215, wR2 = 0.0543
R indices (all data)	R1 = 0.0216, wR2 = 0.0543

Largest diff. peak and hole 0.217 and -0.191 e.Å^{-3}

Table 2. Atomic coordinates (x 10^4) and equivalent isotropic displacement parameters (A^2 x 10^3) for Bath 541. U(eq) is defined as one third of the trace of the orthogonalized Uij tensor.

	x	y	z	U(eq)
Ni(1)	5000	0	5000	11(1)
N(1)	7377(3)	-1145(2)	6536(3)	14(1)
O(1)	7250(2)	-1991(2)	7702(2)	20(1)
O(2)	8984(2)	-1035(2)	6244(2)	22(1)
N(2)	3647(3)	-2580(2)	015(2)	13(1)
C(1)	5077(4)	-3448(3)	2530(3)	15(1)
C(2)	5664(4)	-2692(3)	1136(3)	16(1)
O(3)	3884(2)	-2681(2)	-411(2)	18(1)
C(3)	2613(4)	-1720(3)	54(3)	18(1)
C(4)	1888(4)	-2525(3)	1349(3)	15(1)
N(3)	3064(3)	-1214(2)	6055(2)	13(1)
C(5)	2866(4)	-3692(3)	4080(3)	16(1)
C(6)	1680(4)	-2826(3)	4905(3)	17(1)

Table 3. Bond lengths [Å] and angles [°] for Bath 541.

Ni(1)-N(3)#1	2.054(2)
Ni(1)-N(3)	2.054(2)
Ni(1)-N(1)	2.108(2)
Ni(1)-N(1)#1	2.108(2)
Ni(1)-N(2)#1	2.334(2)
Ni(1)-N(2)	2.334(2)
N(1)-O(1)	1.245(2)
N(1)-O(2)	1.256(3)
N(2)-C(4)	1.483(3)
N(2)-C(5)	1.487(3)
N(2)-C(1)	1.493(3)
C(1)-C(2)	1.510(3)
C(2)-O(3)	1.425(3)
O(3)-C(3)	1.433(3)
C(3)-C(4)	1.504(3)
N(3)-C(6)	1.476(3)
C(5)-C(6)	1.506(3)
N(3)#1-Ni(1)-N(3)	180.0
N(3)#1-Ni(1)-N(1)	89.67(9)
N(3)-Ni(1)-N(1)	90.33(9)
N(3)#1-Ni(1)-N(1)#1	90.33(9)
N(3)-Ni(1)-N(1)#1	89.67(9)
N(1)-Ni(1)-N(1)#1	180.0
N(3)#1-Ni(1)-N(2)#1	82.10(8)
N(3)-Ni(1)-N(2)#1	97.90(8)
N(1)-Ni(1)-N(2)#1	92.80(7)
N(1)#1-Ni(1)-N(2)#1	87.20(7)
N(3)#1-Ni(1)-N(2)	97.90(8)
N(3)-Ni(1)-N(2)	82.10(8)
N(1)-Ni(1)-N(2)	87.20(7)
N(1)#1-Ni(1)-N(2)	92.80(8)
N(2)#1-Ni(1)-N(2)	180.00(6)
O(1)-N(1)-O(2)	117.24(18)
O(1)-N(1)-Ni(1)	123.22(15)

O(2)-N(1)-Ni(1)	119.50(15)
C(4)-N(2)-C(5)	109.25(18)
C(4)-N(2)-C(1)	107.07(18)
C(5)-N(2)-C(1)	106.74(17)
C(4)-N(2)-Ni(1)	114.44(14)
C(5)-N(2)-Ni(1)	98.96(13)
C(1)-N(2)-Ni(1)	119.52(14)
N(2)-C(1)-C(2)	113.65(19)
O(3)-C(2)-C(1)	111.86(19)
C(2)-O(3)-C(3)	108.96(17)
O(3)-C(3)-C(4)	111.12(19)
N(2)-C(4)-C(3)	112.03(19)
C(6)-N(3)-Ni(1)	111.71(14)
N(2)-C(5)-C(6)	112.11(19)
N(3)-C(6)-C(5)	108.76(19)

Symmetry transformations used to generate equivalent atoms:
#1 -x+1,-y,-z+1

Table 4. Anisotropic displacement parameters (A^2 x 10^3) for Bath 541. The anisotropic displacement factor exponent takes the form: -2 pi^2 [h^2 a*^2 U11 + ... + 2 h k a* b* U12]

	U11	U22	U33	U23	U13	U12
Ni(1)	9(1)	12(1)	12(1)	3(1)	4(1)	2(1)
N(1)	15(1)	13(1)	13(1)	0(1)	5(1)	1(1)
O(1)	20(1)	22(1)	20(1)	11(1)	9(1)	7(1)
O(2)	15(1)	38(1)	22(1)	11(1)	12(1)	12(1)
N(2)	14(1)	12(1)	13(1)	2(1)	6(1)	3(1)
C(1)	16(1)	13(1)	14(1)	1(1)	5(1)	3(1)
C(2)	16(1)	17(1)	14(1)	1(1)	7(1)	4(1)
O(3)	19(1)	25(1)	12(1)	2(1)	7(1)	6(1)
C(3)	16(1)	21(1)	15(1)	2(1)	4(1)	6(1)
C(4)	13(1)	15(1)	14(1)	-1(1)	2(1)	1(1)
N(3)	13(1)	13(1)	13(1)	2(1)	5(1)	4(1)
C(5)	17(1)	12(1)	17(1)	2(1)	8(1)	0(1)
C(6)	18(1)	15(1)	17(1)	2(1)	8(1)	0(1)

Table 5. Hydrogen bonds for Bath 541 [Å and °].

D-H...A	d(D-H)	d(H...A)	d(D...A)	<(DHA)
N(3)-H(13)...O(3)#2	0.92	2.32	3.134(3)	147.2
N(3)-H(13)...O(1)	0.92	2.42	2.986(3)	119.4
N(3)-H(14)...O(2)#3	0.92	2.33	3.019(3)	131.5
N(3)-H(14)...O(2)#1	0.92	2.42	2.892(3)	112.1

Symmetry transformations used to generate equivalent atoms:
#1 -x+1,-y,-z+1 #2 x,y,z+1 #3 x-1,y,z

7.2.4 Crystal Data for Bath 551 - $[Ni(aem)_2(NO_2)_2]$ excited state

Table 1. Crystal data and structure refinement for Bath 551.

Identification code	Bath 551
Empirical formula	C_{12} H_{28} N_6 Ni O_6
Formula weight	411.11
Temperature	45(2)K
Wavelength	0.68960Å
Crystal system, space group	Triclinic, *P*-1
Unit cell dimensions	a = 7.2011(17)Å alpha = 94.620(3)°
	b = 8.0007(18)Å beta = 110.884(3)°
	c = 8.2916(19)Å gamma = 101.434(3)°
Volume	431.46(17)Å^3
Z, Calculated density	1, 1.582 Mg/m^3
Absorption coefficient	1.168 mm^{-1}
F(000)	218
Crystal size	0.15 x 0.13 x 0.08 mm
Theta range for data collection	3.85 to 20.15°
Limiting indices	-7<=h<=7, -7<=k<=7, -8<=l<=8
Reflections collected / unique	2181 / 888 [R(int) = 0.0134]
Completeness to theta = 20.15	98.6 %
Absorption correction	SADABS
Max. and min. transmission	0.9124 and 0.8443
Refinement method	Full-matrix least-squares on F^2
Data / restraints / parameters	888 / 10 / 133
Goodness-of-fit on F^2	1.097
Final R indices [I>2sigma(I)]	R1 = 0.0280, wR2 = 0.0735
R indices (all data)	R1 = 0.0286, wR2 = 0.0740
Largest diff. peak and hole	0.388 and -0.231 e.A^{-3}

Table 2. Atomic coordinates (x 10^4) and equivalent isotropic displacement parameters (A^2 x 10^3) for Bath 551. U(eq) is defined as one third of the trace of the orthogonalized Uij tensor.

	x	y	z	U(eq)
Ni(1)	5000	0	5000	19(1)
N(1A)	7401(7)	-1121(7)	6565(8)	23(2)
O(1A)	7207(7)	-1942(7)	7721(7)	21(1)
O(2A)	9010(7)	-920(6)	6267(5)	28(1)
O(1B)	6690(20)	-1240(30)	6480(30)	50
N(1B)	8530(20)	-1489(15)	7093(18)	50
O(2B)	9660(20)	-300(20)	6590(30)	50
O(1C)	7410(40)	-650(40)	6060(40)	50
N(1C)	8530(20)	-1489(15)	7093(18)	50
O(2C)	7530(70)	-2170(70)	8020(60)	50
N(2)	3695(4)	-2598(3)	3073(3)	21(1)
C(1)	5133(5)	-3420(4)	2558(4)	23(1)
C(2)	5668(5)	-2687(4)	1113(4)	26(1)
O(3)	3899(3)	-2740(3)	-389(2)	28(1)
C(3)	2629(5)	-1808(4)	99(4)	28(1)
C(4)	1932(5)	-2603(4)	1428(4)	25(1)
N(3)	3084(4)	-1217(3)	6111(3)	25(1)
C(5)	2951(5)	-3709(4)	4170(4)	26(1)
C(6)	1753(5)	-2869(4)	5015(4)	28(1)

Table 3. Bond lengths [Å] and angles [°] for Bath 551.

Ni(1)-O(1C)	1.84(2)
Ni(1)-O(1C)#1	1.84(2)
Ni(1)-O(1B)	1.89(2)
Ni(1)-O(1B)#1	1.89(2)
Ni(1)-N(3)#1	2.054(2)
Ni(1)-N(3)	2.054(2)
Ni(1)-N(1A)	2.164(5)
Ni(1)-N(1A)#1	2.164(5)
Ni(1)-N(2)	2.319(2)
Ni(1)-N(2)#1	2.319(2)
N(1A)-O(1A)	1.237(8)
N(1A)-O(2A)	1.251(8)
O(1B)-N(1B)	1.302(15)
N(1B)-O(2B)	1.319(14)
N(2)-C(5)	1.481(4)
N(2)-C(1)	1.492(4)
N(2)-C(4)	1.495(4)
C(1)-C(2)	1.509(4)
C(2)-O(3)	1.420(4)
O(3)-C(3)	1.429(4)
C(3)-C(4)	1.500(4)
N(3)-C(6)	1.475(4)
C(5)-C(6)	1.508(4)

O(1C)-Ni(1)-O(1C)#1	180.000(4)
O(1C)-Ni(1)-O(1B)	25.4(10)
O(1C)#1-Ni(1)-O(1B)	154.6(10)
O(1C)-Ni(1)-O(1B)#1	154.6(10)
O(1C)#1-Ni(1)-O(1B)#1	25.4(10)
O(1B)-Ni(1)-O(1B)#1	180.000(2)
O(1C)-Ni(1)-N(3)#1	75.9(9)
O(1C)#1-Ni(1)-N(3)#1	104.1(9)
O(1B)-Ni(1)-N(3)#1	101.2(5)
O(1B)#1-Ni(1)-N(3)#1	78.8(5)
O(1C)-Ni(1)-N(3)	104.1(9)
O(1C)#1-Ni(1)-N(3)	75.9(9)
O(1B)-Ni(1)-N(3)	78.8(5)
O(1B)#1-Ni(1)-N(3)	101.2(5)
N(3)#1-Ni(1)-N(3)	180.00(10)
O(1C)-Ni(1)-N(1A)	14.2(9)
O(1C)#1-Ni(1)-N(1A)	165.8(9)
O(1B)-Ni(1)-N(1A)	11.2(6)
O(1B)#1-Ni(1)-N(1A)	168.8(6)
N(3)#1-Ni(1)-N(1A)	90.12(17)
N(3)-Ni(1)-N(1A)	89.88(17)
O(1C)-Ni(1)-N(1A)#1	165.8(9)
O(1C)#1-Ni(1)-N(1A)#1	14.2(9)
O(1B)-Ni(1)-N(1A)#1	168.8(6)
O(1B)#1-Ni(1)-N(1A)#1	11.2(6)
N(3)#1-Ni(1)-N(1A)#1	89.88(17)
N(3)-Ni(1)-N(1A)#1	90.12(17)
N(1A)-Ni(1)-N(1A)#1	180.0(3)
O(1C)-Ni(1)-N(2)	89.7(10)
O(1C)#1-Ni(1)-N(2)	90.3(10)
O(1B)-Ni(1)-N(2)	84.1(8)
O(1B)#1-Ni(1)-N(2)	95.9(8)
N(3)#1-Ni(1)-N(2)	97.84(9)
N(3)-Ni(1)-N(2)	82.16(9)
N(1A)-Ni(1)-N(2)	87.35(15)

N(1A)#1-Ni(1)-N(2)	92.65(15)
O(1C)-Ni(1)-N(2)#1	90.3(10)
O(1C)#1-Ni(1)-N(2)#1	89.7(10)
O(1B)-Ni(1)-N(2)#1	95.9(8)
O(1B)#1-Ni(1)-N(2)#1	84.1(8)
N(3)#1-Ni(1)-N(2)#1	82.16(9)
N(3)-Ni(1)-N(2)#1	97.84(9)
N(1A)-Ni(1)-N(2)#1	92.65(15)
N(1A)#1-Ni(1)-N(2)#1	87.35(15)
N(2)-Ni(1)-N(2)#1	180.0
O(1A)-N(1A)-O(2A)	120.4(5)
O(1A)-N(1A)-Ni(1)	121.6(4)
O(2A)-N(1A)-Ni(1)	118.0(4)
N(1B)-O(1B)-Ni(1)	144.4(15)
O(1B)-N(1B)-O(2B)	105.5(13)
C(5)-N(2)-C(1)	107.0(2)
C(5)-N(2)-C(4)	109.2(2)
C(1)-N(2)-C(4)	107.1(2)
C(5)-N(2)-Ni(1)	99.19(16)
C(1)-N(2)-Ni(1)	118.87(17)
C(4)-N(2)-Ni(1)	114.69(18)
N(2)-C(1)-C(2)	113.9(2)
O(3)-C(2)-C(1)	112.2(2)
C(2)-O(3)-C(3)	109.1(2)
O(3)-C(3)-C(4)	111.2(2)
N(2)-C(4)-C(3)	112.0(2)
C(6)-N(3)-Ni(1)	111.72(18)
N(2)-C(5)-C(6)	112.0(2)
N(3)-C(6)-C(5)	108.7(2)

Symmetry transformations used to generate equivalent atoms:
#1 -x+1,-y,-z+1

Table 4. Anisotropic displacement parameters (A^2 x 10^3) for Bath 551. The anisotropic displacement factor exponent takes the form: -2 pi^2 [h^2 a*^2 U11 + ... + 2 h k a* b* U12]

	U11	U22	U33	U23	U13	U12
Ni(1)	24(1)	14(1)	17(1)	1(1)	10(1)	1(1)
N(1A)	28(4)	10(3)	15(3)	-7(2)	-10(4)	10(3)
O(1A)	26(3)	13(2)	23(3)	7(2)	10(2)	3(2)
O(2A)	27(3)	42(3)	23(2)	9(2)	18(2)	8(2)
N(2)	28(2)	16(1)	19(1)	1(1)	11(1)	0(1)
C(1)	32(2)	14(2)	24(2)	-1(1)	14(2)	4(1)
C(2)	33(2)	19(2)	26(2)	-1(1)	15(2)	2(1)
O(3)	37(1)	26(1)	19(1)	-1(1)	15(1)	2(1)
C(3)	33(2)	26(2)	21(2)	0(1)	11(2)	4(2)
C(4)	27(2)	19(2)	24(2)	-4(1)	10(2)	-2(1)
N(3)	33(2)	17(1)	23(1)	-2(1)	13(1)	0(1)
C(5)	38(2)	15(2)	23(2)	-1(1)	16(2)	-1(1)
C(6)	37(2)	19(2)	25(2)	-2(1)	18(2)	-6(1)

Table 5. Hydrogen bonds for Bath 551 [Å and °].

D-H...A	d(D-H)	d(H...A)	d(D...A)	<(DHA)
N(3)-H(13)...O(3)#2	0.92	2.33	3.145(3)	147.2
N(3)-H(13)...O(1A)	0.92	2.42	2.986(5)	119.7
N(3)-H(13)...O(2C)	0.92	2.69	3.30(4)	124.5
N(3)-H(14)...O(2B)#3	0.92	2.04	2.856(17)	147.4
N(3)-H(14)...O(2A)#3	0.92	2.31	3.037(5)	135.2
N(3)-H(14)...O(2A)#1	0.92	2.45	2.920(4)	112.2

Symmetry transformations used to generate equivalent atoms:
#1 -x+1,-y,-z+1 #2 x,y,z+1 #3 x-1,y,z

7.2.5 Crystal Data for Bath 515 - $[Ni(aepy)_2(NO_2)_2]$ ground state

Table 1. Crystal data and structure refinement for Bath 515.

Identification code	Bath 515
Empirical formula	$C_{12}\ H_{28}\ N_6\ Ni\ O_4$
Formula weight	379.11
Temperature	100(2)K
Wavelength	0.68960Å
Crystal system, space group	Monoclinic, $P2_1/c$
Unit cell dimensions	a = 8.6169(5)Å alpha = 90°
	b = 8.5490(5)Å beta = 104.0080(10)°
	c = 11.5680(7)Å gamma = 90°
Volume	826.83(8)$Å^3$
Z, Calculated density	2, 1.523 Mg/m^3
Absorption coefficient	1.203 mm^{-1}
F(000)	404
Crystal size	0.11 x 0.11 x 0.07 mm
Theta range for data collection	4.21 to 20.17°
Limiting indices	-8<=h<=8, -8<=k<=8, -11<=l<=11
Reflections collected / unique	4023 / 846 [R(int) = 0.0243]
Completeness to theta = 20.17	97.7 %
Absorption correction	SADABS
Max. and min. transmission	0.9205 and 0.8791
Refinement method	Full-matrix least-squares on F^2
Data / restraints / parameters	846 / 0 / 106
Goodness-of-fit on F^2	1.080
Final R indices [I>2sigma(I)]	R1 = 0.0212, wR2 = 0.0520
R indices (all data)	R1 = 0.0226, wR2 = 0.0530
Largest diff. peak and hole	0.186 and -0.163 $e.A^{-3}$

Table 2. Atomic coordinates (x 10^4) and equivalent isotropic displacement parameters (A^2 x 10^3) for Bath 515. U(eq) is defined as one third of the trace of the orthogonalized Uij tensor.

	x	y	z	U(eq)
Ni(1)	0	0	5000	13(1)
N(1)	986(2)	-1064(2)	3651(2)	19(1)
O(1)	469(2)	-729(2)	2569(1)	26(1)
O(2)	2065(2)	-2074(2)	3902(2)	27(1)
N(2)	1951(2)	1663(2)	5445(2)	15(1)
C(1)	2914(3)	1840(3)	4549(2)	22(1)

C(2)	3902(3)	3340(3)	4881(2)	23(1)
C(3)	2923(3)	4329(3)	5556(2)	24(1)
C(4)	1463(3)	3319(3)	5568(2)	23(1)
N(3)	1490(2)	-1341(2)	6298(2)	20(1)
C(5)	2964(3)	1098(3)	6595(2)	24(1)
C(6)	3095(3)	-655(3)	6598(2)	24(1)

Table 3. Bond lengths [Å] and angles [°] for Bath 515.

Ni(1)-N(3)#1	2.0699(18)
Ni(1)-N(3)	2.0699(18)
Ni(1)-N(1)	2.151(2)
Ni(1)-N(1)#1	2.151(2)
Ni(1)-N(2)#1	2.1665(18)
Ni(1)-N(2)	2.1665(18)
N(1)-O(2)	1.251(2)
N(1)-O(1)	1.256(2)
N(2)-C(1)	1.484(3)
N(2)-C(5)	1.485(3)
N(2)-C(4)	1.493(3)
C(1)-C(2)	1.536(3)
C(2)-C(3)	1.534(4)
C(3)-C(4)	1.529(3)
N(3)-C(6)	1.465(3)
C(5)-C(6)	1.502(4)
N(3)#1-Ni(1)-N(3)	180.00(9)
N(3)#1-Ni(1)-N(1)	89.57(8)
N(3)-Ni(1)-N(1)	90.43(8)
N(3)#1-Ni(1)-N(1)#1	90.43(8)
N(3)-Ni(1)-N(1)#1	89.57(8)
N(1)-Ni(1)-N(1)#1	180.00(6)
N(3)#1-Ni(1)-N(2)#1	83.21(7)
N(3)-Ni(1)-N(2)#1	96.79(7)
N(1)-Ni(1)-N(2)#1	88.30(7)
N(1)#1-Ni(1)-N(2)#1	91.70(7)
N(3)#1-Ni(1)-N(2)	96.79(7)
N(3)-Ni(1)-N(2)	83.21(7)
N(1)-Ni(1)-N(2)	91.70(7)
N(1)#1-Ni(1)-N(2)	88.30(7)
N(2)#1-Ni(1)-N(2)	180.00(10)
O(2)-N(1)-O(1)	116.91(19)
O(2)-N(1)-Ni(1)	121.76(15)
O(1)-N(1)-Ni(1)	121.31(15)
C(1)-N(2)-C(5)	110.64(18)
C(1)-N(2)-C(4)	100.82(18)
C(5)-N(2)-C(4)	109.93(18)
C(1)-N(2)-Ni(1)	115.73(14)
C(5)-N(2)-Ni(1)	104.67(13)
C(4)-N(2)-Ni(1)	115.13(13)
N(2)-C(1)-C(2)	106.23(19)
C(3)-C(2)-C(1)	104.40(19)
C(4)-C(3)-C(2)	104.36(19)
N(2)-C(4)-C(3)	106.47(18)
C(6)-N(3)-Ni(1)	109.53(14)
N(2)-C(5)-C(6)	110.73(19)
N(3)-C(6)-C(5)	109.43(19)

Symmetry transformations used to generate equivalent atoms:
#1 -x,-y,-z+1

Table 4. Anisotropic displacement parameters (A^2 x 10^3) for Bath 515. The anisotropic displacement factor exponent takes the form: -2 pi^2 [h^2 a*^2 U11 + ... + 2 h k a* b* U12]

	U11	U22	U33	U23	U13	U12
Ni(1)	15(1)	11(1)	15(1)	0(1)	4(1)	0(1)
N(1)	20(1)	14(1)	23(1)	-2(1)	6(1)	-4(1)
O(1)	36(1)	26(1)	17(1)	2(1)	8(1)	4(1)
O(2)	26(1)	25(1)	29(1)	-2(1)	6(1)	9(1)
N(2)	18(1)	11(1)	16(1)	0(1)	3(1)	0(1)
C(1)	23(1)	24(1)	21(1)	-3(1)	8(1)	-5(1)
C(2)	24(1)	25(1)	21(1)	1(1)	6(1)	-9(1)
C(3)	22(1)	18(1)	32(2)	1(1)	2(1)	-2(1)
C(4)	21(1)	16(1)	31(2)	-4(1)	6(1)	-1(1)
N(3)	21(1)	15(1)	24(1)	2(1)	3(1)	-2(1)
C(5)	24(1)	21(2)	23(2)	3(1)	0(1)	-5(1)
C(6)	21(1)	23(2)	26(2)	5(1)	-1(1)	0(1)

Table 5. Hydrogen bonds for Bath 515 [Å and °].

D-H...A	d(D-H)	d(H...A)	d(D...A)	<(DHA)
N(3)-H(13)...O(1)#1	0.92	2.39	2.961(2)	120.5
N(3)-H(13)...O(2)#2	0.92	2.56	3.229(2)	130.1
N(3)-H(13)...O(1)#2	0.92	2.66	3.136(2)	113.2

Symmetry transformations used to generate equivalent atoms:
#1 -x,-y,-z+1 #2 x,-y-1/2,z+1/2

7.2.6 Crystal Data for Bath 536 - $[Ni(aepy)_2(NO_2)_2]$ excited state

Table 1. Crystal data and structure refinement for Bath 536.

Identification code	Bath 536
Empirical formula	$C_{12} H_{28} N_6 Ni O_4$
Formula weight	379.11
Temperature	60(2)K
Wavelength	0.68960Å
Crystal system, space group	Monoclinic, *P*21/*c*
Unit cell dimensions	a = 8.3535(13)Å alpha = 90°
	b = 8.6657(13)Å beta = 103.127(2)°
	c = 11.9144(18)Å gamma = 90°
Volume	839.9(2)$Å^3$
Z, Calculated density	2, 1.499 Mg/m^3
Absorption coefficient	1.184 mm^{-1}
F(000)	404
Crystal size	0.13 x 0.10 x 0.10 mm
Theta range for data collection	3.48 to 20.17°
Limiting indices	-8<=h<=8, -8<=k<=8, -11<=l<=11
Reflections collected / unique	4129 / 869 [R(int) = 0.0296]
Completeness to theta = 20.17	99.0 %
Absorption correction	SADABS
Max. and min. transmission	0.8908 and 0.8613
Refinement method	Full-matrix least-squares on F^2

Data / restraints / parameters	869 / 39 / 138
Goodness-of-fit on F^2	1.079
Final R indices [I>2sigma(I)]	R1 = 0.0473, wR2 = 0.1222
R indices (all data)	R1 = 0.0513, wR2 = 0.1257
Largest diff. peak and hole	0.486 and -0.232 e.$Å^{-3}$

Table 2. Atomic coordinates (x 10^4) and equivalent isotropic displacement parameters (A^2 x 10^3) for Bath 536. U(eq) is defined as one third of the trace of the orthogonalized Uij tensor.

	x	y	z	U(eq)
Ni(1)	0	0	5000	52(1)
N(1A)	950(13)	-952(15)	3683(9)	85(4)
O(2A)	2202(14)	-1952(13)	3710(11)	85(3)
O(1A)	621(10)	-847(8)	2591(6)	87(4)
O(1B)	450(40)	-310(40)	3260(20)	91(15)
N(1B)	1480(30)	-1320(20)	3318(18)	64(6)
O(2B)	2210(40)	-2270(30)	4010(20)	30(7)
O(1C)	1750(30)	-1470(20)	4366(16)	43(8)
N(1C)	1480(30)	-1320(20)	3318(18)	64(6)
O(2C)	2660(50)	-1700(50)	2940(40)	137(17)
N(2)	1946(5)	1685(5)	5400(3)	59(1)
C(1)	2819(8)	1992(8)	4497(5)	92(2)
C(2)	3782(8)	3416(8)	4791(5)	90(2)
C(3)	2844(8)	4338(8)	5509(7)	96(2)
C(4)	1422(8)	3317(7)	5593(7)	98(2)
N(3)	1570(7)	-1293(6)	6209(5)	108(2)
C(5)	2958(9)	1204(9)	6501(7)	69(3)
C(6)	3207(13)	-576(13)	6497(12)	79(3)
C(5')	3570(40)	630(40)	5940(30)	74(8)
C(6')	2910(40)	-330(40)	6800(30)	41(8)

Table 3. Bond lengths [Å] and angles [°] for Bath 536.

Ni(1)-N(3)	2.047(5)
Ni(1)-N(3)#1	2.047(5)
Ni(1)-N(1A)	2.083(9)
Ni(1)-N(1A)#1	2.083(9)
Ni(1)-N(2)#1	2.156(4)
Ni(1)-N(2)	2.156(4)
Ni(1)-O(1C)#1	2.20(2)
Ni(1)-O(1C)	2.20(2)
Ni(1)-O(1B)	2.21(2)
Ni(1)-O(1B)#1	2.21(2)
N(1A)-O(1A)	1.270(13)
N(1A)-O(2A)	1.352(19)
O(1B)-N(1B)	1.22(2)
N(1B)-O(2B)	1.22(2)
N(2)-C(5)	1.452(8)
N(2)-C(1)	1.455(7)
N(2)-C(4)	1.514(7)
N(2)-C(5')	1.64(3)
C(1)-C(2)	1.471(8)
C(2)-C(3)	1.512(9)
C(3)-C(4)	1.503(9)
N(3)-C(6')	1.45(3)
N(3)-C(6)	1.471(12)

C(5)-C(6)	1.556(15)
C(5')-C(6')	1.51(5)
N(3)-Ni(1)-N(3)#1	180.0(3)
N(3)-Ni(1)-N(1A)	91.2(5)
N(3)#1-Ni(1)-N(1A)	88.8(5)
N(3)-Ni(1)-N(1A)#1	88.8(5)
N(3)#1-Ni(1)-N(1A)#1	91.2(5)
N(1A)-Ni(1)-N(1A)#1	180.0(3)
N(3)-Ni(1)-N(2)#1	96.61(18)
N(3)#1-Ni(1)-N(2)#1	83.39(18)
N(1A)-Ni(1)-N(2)#1	87.9(2)
N(1A)#1-Ni(1)-N(2)#1	92.1(2)
N(3)-Ni(1)-N(2)	83.39(18)
N(3)#1-Ni(1)-N(2)	96.61(18)
N(1A)-Ni(1)-N(2)	92.1(2)
N(1A)#1-Ni(1)-N(2)	87.9(2)
N(2)#1-Ni(1)-N(2)	180.0(2)
N(3)-Ni(1)-O(1C)#1	116.5(5)
N(3)#1-Ni(1)-O(1C)#1	63.5(5)
N(1A)-Ni(1)-O(1C)#1	152.3(6)
N(1A)#1-Ni(1)-O(1C)#1	27.7(6)
N(2)#1-Ni(1)-O(1C)#1	86.7(6)
N(2)-Ni(1)-O(1C)#1	93.3(6)
N(3)-Ni(1)-O(1C)	63.5(5)
N(3)#1-Ni(1)-O(1C)	116.5(5)
N(1A)-Ni(1)-O(1C)	27.7(6)
N(1A)#1-Ni(1)-O(1C)	152.3(6)
N(2)#1-Ni(1)-O(1C)	93.3(6)
N(2)-Ni(1)-O(1C)	86.7(6)
O(1C)#1-Ni(1)-O(1C)	180.0(9)
N(3)-Ni(1)-O(1B)	112.0(7)
N(3)#1-Ni(1)-O(1B)	68.0(7)
N(1A)-Ni(1)-O(1B)	21.2(7)
N(1A)#1-Ni(1)-O(1B)	158.8(7)
N(2)#1-Ni(1)-O(1B)	89.5(10)
N(2)-Ni(1)-O(1B)	90.5(10)
O(1C)#1-Ni(1)-O(1B)	131.5(9)
O(1C)-Ni(1)-O(1B)	48.5(9)
N(3)-Ni(1)-O(1B)#1	68.0(7)
N(3)#1-Ni(1)-O(1B)#1	112.0(7)
N(1A)-Ni(1)-O(1B)#1	158.8(7)
N(1A)#1-Ni(1)-O(1B)#1	21.2(7)
N(2)#1-Ni(1)-O(1B)#1	90.5(10)
N(2)-Ni(1)-O(1B)#1	89.5(10)
O(1C)#1-Ni(1)-O(1B)#1	48.5(9)
O(1C)-Ni(1)-O(1B)#1	131.5(9)
O(1B)-Ni(1)-O(1B)#1	180.000(6)
O(1A)-N(1A)-O(2A)	93.3(10)
O(1A)-N(1A)-Ni(1)	135.4(11)
O(2A)-N(1A)-Ni(1)	131.3(10)
N(1B)-O(1B)-Ni(1)	107.8(19)
O(2B)-N(1B)-O(1B)	139(3)
C(5)-N(2)-C(1)	115.7(5)
C(5)-N(2)-C(4)	105.0(5)
C(1)-N(2)-C(4)	98.7(5)
C(5)-N(2)-C(5')	39.2(11)
C(1)-N(2)-C(5')	83.4(12)
C(4)-N(2)-C(5')	134.7(12)
C(5)-N(2)-Ni(1)	105.1(4)
C(1)-N(2)-Ni(1)	116.1(3)
C(4)-N(2)-Ni(1)	115.9(3)

C(5')-N(2)-Ni(1)	102.9(10)
N(2)-C(1)-C(2)	108.5(5)
C(1)-C(2)-C(3)	104.6(5)
C(4)-C(3)-C(2)	104.2(5)
C(3)-C(4)-N(2)	106.3(5)
C(6')-N(3)-C(6)	20.8(12)
C(6')-N(3)-Ni(1)	109.1(13)
C(6)-N(3)-Ni(1)	110.2(5)
N(2)-C(5)-C(6)	109.4(7)
N(3)-C(6)-C(5)	107.6(8)
C(6')-C(5')-N(2)	100(2)
N(3)-C(6')-C(5')	110(2)

Symmetry transformations used to generate equivalent atoms:
#1 -x,-y,-z+1

Table 4. Anisotropic displacement parameters (A^2 x 10^3) for Bath 536. The anisotropic displacement factor exponent takes the form: -2 pi^2 [h^2 a*^2 U11 + ... + 2 h k a* b* U12]

	U11	U22	U33	U23	U13	U12
Ni(1)	56(1)	56(1)	50(1)	1(1)	22(1)	4(1)
N(1A)	71(7)	108(10)	97(9)	-41(9)	64(7)	-13(7)
O(2A)	88(6)	67(6)	107(9)	20(7)	37(8)	10(5)
O(1A)	146(7)	85(5)	39(5)	-14(3)	40(4)	-30(5)
N(2)	62(3)	60(3)	57(3)	2(2)	20(2)	1(2)
C(1)	97(5)	116(5)	76(4)	-17(4)	46(4)	-40(4)
C(2)	103(5)	99(5)	71(4)	2(3)	25(4)	-24(4)
C(3)	70(4)	80(4)	134(6)	-1(4)	15(4)	4(4)
C(4)	77(4)	87(5)	137(6)	-30(4)	41(4)	-6(4)
N(3)	88(4)	95(4)	122(5)	44(3)	-16(3)	-21(3)
C(5)	60(5)	77(5)	70(5)	6(4)	13(4)	3(4)
C(6)	64(6)	82(7)	88(8)	-7(6)	11(5)	8(5)

Table 5. Hydrogen bonds for Bath 536 [Å and °].

D-H...A	d(D-H)	d(H...A)	d(D...A)	<(DHA)
N(3)-H(13)...O(1A)#1	0.92	2.60	3.165(10)	120.0
N(3)-H(13)...O(1A)#2	0.92	2.64	3.175(9)	118.0
N(3)-H(13)...O(2A)#2	0.92	2.62	3.280(13)	129.6

Symmetry transformations used to generate equivalent atoms:
#1 -x,-y,-z+1 #2 x,-y-1/2,z+1/2

7.2.7 Crystal Data for Bath 486 - $[Ni(aep)_2(ONO)_2]$

Table 1. Crystal data and structure refinement for Bath 486.

Identification code	Bath 486
Empirical formula	$C_{14}\ H_{32}\ N_6\ Ni\ O_4$
Formula weight	407.17
Temperature	100(2)K
Wavelength	0.68950Å
Crystal system, space group	Orthorhombic, *Pbca*

Unit cell dimensions	a = 9.3904(4)Å alpha = 90°
	b = 9.5733(4)Å beta = 90°
	c = 19.8660(9)Å gamma = 90°
Volume	1785.90(13)Å^3
Z, Calculated density	4, 1.514 Mg/m^3
Absorption coefficient	1.120 mm^{-1}
F(000)	872
Crystal size	0.20 x 0.10 x 0.10 mm
Theta range for data collection	2.90 to 29.49°
Limiting indices	-13<=h<=13, -13<=k<=13, -27<=l<=28
Reflections collected / unique	18950 / 2713 [R(int) = 0.0481]
Completeness to theta = 29.49	99.4 %
Absorption correction	SADABS
Max. and min. transmission	0.8963 and 0.8071
Refinement method	Full-matrix least-squares on F^2
Data / restraints / parameters	2713 / 0 / 115
Goodness-of-fit on F^2	1.090
Final R indices [I>2sigma(I)]	R1 = 0.0308, wR2 = 0.0792
R indices (all data)	R1 = 0.0347, wR2 = 0.0818
Largest diff. peak and hole	0.508 and -0.574 e.Å^{-3}

Table 2. Atomic coordinates (x 10^4) and equivalent isotropic displacement parameters (A^2 x 10^3) for bath486. U(eq) is defined as one third of the trace of the orthogonalized Uij tensor.

	x	y	z	U(eq)
Ni(1)	0	0	0	8(1)
N(1)	2(1)	2794(1)	622(1)	15(1)
O(1)	-843(1)	1919(1)	330(1)	11(1)
O(2)	-560(1)	3910(1)	784(1)	20(1)
N(2)	-53(1)	-964(1)	1023(1)	9(1)
C(1)	-908(1)	-94(1)	1495(1)	12(1)
C(2)	-1075(1)	-698(1)	2206(1)	15(1)
C(3)	-1651(1)	-2193(1)	2189(1)	15(1)
C(4)	-717(1)	-3071(1)	1724(1)	12(1)
C(5)	-651(1)	-2408(1)	1025(1)	11(1)
N(3)	2082(1)	490(1)	262(1)	11(1)
C(6)	1477(1)	-1005(1)	1213(1)	11(1)
C(7)	2245(1)	312(1)	996(1)	12(1)

Table 3. Bond lengths [Å] and angles [°] for Bath 486.

Ni(1)-N(3)#1	2.0763(10)
Ni(1)-N(3)	2.0763(10)
Ni(1)-O(1)#1	2.1047(8)
Ni(1)-O(1)	2.1047(8)
Ni(1)-N(2)	2.2317(10)
Ni(1)-N(2)#1	2.2317(10)
N(1)-O(2)	1.2349(14)
N(1)-O(1)	1.2921(13)
N(2)-C(6)	1.4861(14)
N(2)-C(1)	1.4898(15)
N(2)-C(5)	1.4919(15)
C(1)-C(2)	1.5337(17)
C(2)-C(3)	1.5299(18)
C(3)-C(4)	1.5272(17)
C(4)-C(5)	1.5265(16)

N(3)-C(7)	1.4769(15)
C(6)-C(7)	1.5152(16)
N(3)#1-Ni(1)-N(3)	180.00(5)
N(3)#1-Ni(1)-O(1)#1	94.52(4)
N(3)-Ni(1)-O(1)#1	85.48(4)
N(3)#1-Ni(1)-O(1)	85.48(4)
N(3)-Ni(1)-O(1)	94.52(4)
O(1)#1-Ni(1)-O(1)	180.00(6)
N(3)#1-Ni(1)-N(2)	96.50(4)
N(3)-Ni(1)-N(2)	83.50(4)
O(1)#1-Ni(1)-N(2)	86.04(3)
O(1)-Ni(1)-N(2)	93.96(3)
N(3)#1-Ni(1)-N(2)#1	83.50(4)
N(3)-Ni(1)-N(2)#1	96.50(4)
O(1)#1-Ni(1)-N(2)#1	93.96(3)
O(1)-Ni(1)-N(2)#1	86.04(3)
N(2)-Ni(1)-N(2)#1	180.00(5)
O(2)-N(1)-O(1)	114.54(10)
N(1)-O(1)-Ni(1)	118.34(7)
C(6)-N(2)-C(1)	112.04(9)
C(6)-N(2)-C(5)	109.76(9)
C(1)-N(2)-C(5)	108.25(9)
C(6)-N(2)-Ni(1)	102.76(7)
C(1)-N(2)-Ni(1)	110.77(7)
C(5)-N(2)-Ni(1)	113.27(7)
N(2)-C(1)-C(2)	115.12(10)
C(3)-C(2)-C(1)	111.67(10)
C(4)-C(3)-C(2)	108.95(10)
C(5)-C(4)-C(3)	110.20(10)
N(2)-C(5)-C(4)	113.83(9)
C(7)-N(3)-Ni(1)	108.60(7)
N(2)-C(6)-C(7)	111.48(9)
N(3)-C(7)-C(6)	109.12(10)

Symmetry transformations used to generate equivalent atoms:
#1 -x,-y,-z

Table 4. Anisotropic displacement parameters (A^2 x 10^3) for Bath 486. The anisotropic displacement factor exponent takes the form: -2 pi^2 [h^2 a*^2 U11 + ... + 2 h k a* b* U12]

	U11	U22	U33	U23	U13	U12
Ni(1)	7(1)	8(1)	8(1)	-1(1)	0(1)	0(1)
N(1)	15(1)	13(1)	17(1)	-4(1)	-3(1)	1(1)
O(1)	12(1)	11(1)	11(1)	-2(1)	0(1)	-1(1)
O(2)	21(1)	13(1)	25(1)	-8(1)	-4(1)	4(1)
N(2)	8(1)	9(1)	10(1)	-1(1)	0(1)	0(1)
C(1)	14(1)	12(1)	11(1)	-1(1)	3(1)	2(1)
C(2)	20(1)	14(1)	11(1)	-2(1)	4(1)	0(1)
C(3)	19(1)	14(1)	13(1)	1(1)	5(1)	-1(1)
C(4)	13(1)	11(1)	13(1)	2(1)	0(1)	-1(1)
C(5)	12(1)	10(1)	11(1)	0(1)	0(1)	-2(1)
N(3)	11(1)	13(1)	10(1)	0(1)	0(1)	-1(1)
C(6)	9(1)	12(1)	13(1)	2(1)	-2(1)	0(1)
C(7)	10(1)	14(1)	11(1)	1(1)	-2(1)	-2(1)

Table 5. Hydrogen bonds for bath486 [Å and °].

D-H...A	d(D-H)	d(H...A)	d(D...A)	<(DHA)
N(3)-H(15)...O(2)#2	0.92	2.57	3.0899(14)	116.5
N(3)-H(16)...O(1)#2	0.92	2.56	3.3660(13)	145.8

Symmetry transformations used to generate equivalent atoms:
#1 -x,-y,-z #2 x+1/2,-y+1/2,-z

7.3 Crystal Data for Chapter 5

7.3.1 Crystal Data for k06prr06 - $[Co(NH_3)_5(NO_2)]Cl_2$

Table 1. Crystal data and structure refinement for $[Co(NH_3)_5(NO_2)]Cl_2$.

Identification code	$[Co(NH_3)_5(NO_2)]Cl_2$
Empirical formula	H_{15} Co N_6 O_2 Cl_2
Formula weight	261.01
Temperature	150(2)K
Wavelength	0.71073Å
Crystal system, space group	Monoclinic, *C*2/*c*
Unit cell dimensions	a = 10.1910(3)Å alpha = 90°
	b = 8.6830(3)Å beta = 95.3070(10)°
	c = 10.7260(3)Å gamma = 90°
Volume	945.06(5)$Å^3$
Z, Calculated density	4, 1.834 Mg/m^3
Absorption coefficient	2.352 mm^{-1}
F(000)	536
Crystal size	0.15 x 0.15 x 0.10 mm
Theta range for data collection	3.73 to 30.47°
Limiting indices	-14<=h<=14, -12<=k<=12, -15<=l<=14
Reflections collected / unique	7837 / 1420 [R(int) = 0.0450]
Completeness to theta = 30.47	98.1 %
Absorption correction	Sortav
Max. and min. transmission	0.7988 and 0.7192
Refinement method	Full-matrix least-squares on F^2
Data / restraints / parameters	1420 / 0 / 55
Goodness-of-fit on F^2	1.172
Final R indices [I>2sigma(I)]	R1 = 0.0343, wR2 = 0.0802
R indices (all data)	R1 = 0.0431, wR2 = 0.0838
Largest diff. peak and hole	0.933 and -0.911 $e.Å^{-3}$

Table 2. Atomic coordinates (x 10^4) and equivalent isotropic displacement parameters (A^2 x 10^3) for $[Co(NH_3)_5(NO_2)]Cl_2$. U(eq) is defined as one third of the trace of the orthogonalized Uij tensor.

	x	y	z	U(eq)
Co(1)	0	2119(1)	7500	13(1)
Cl(1)	2929(1)	-191(1)	9851(1)	19(1)
N(1)	0	-106(3)	7500	16(1)
N(4)	234(2)	2101(2)	9333(2)	18(1)
N(3)	1916(2)	2095(2)	7441(2)	18(1)
O(1)	739(2)	-800(2)	6852(2)	26(1)
N(2)	0	4399(4)	7500	23(1)

Table 3. Bond lengths [Å] and angles [°] for $[Co(NH_3)_5(NO_2)]Cl_2$.

Co(1)-N(1)	1.932(3)
Co(1)-N(4)#1	1.9583(19)
Co(1)-N(4)	1.9583(19)
Co(1)-N(3)	1.9597(19)
Co(1)-N(3)#1	1.9597(19)
Co(1)-N(2)	1.980(3)
N(1)-O(1)	1.229(2)
N(1)-O(1)#1	1.229(2)
N(1)-Co(1)-N(4)#1	89.56(6)
N(1)-Co(1)-N(4)	89.56(6)
N(4)#1-Co(1)-N(4)	179.13(13)
N(1)-Co(1)-N(3)	89.41(6)
N(4)#1-Co(1)-N(3)	89.80(9)
N(4)-Co(1)-N(3)	90.19(9)
N(1)-Co(1)-N(3)#1	89.41(6)
N(4)#1-Co(1)-N(3)#1	90.19(9)
N(4)-Co(1)-N(3)#1	89.80(9)
N(3)-Co(1)-N(3)#1	178.82(13)
N(1)-Co(1)-N(2)	180.000(1)
N(4)#1-Co(1)-N(2)	90.44(6)
N(4)-Co(1)-N(2)	90.44(6)
N(3)-Co(1)-N(2)	90.59(6)
N(3)#1-Co(1)-N(2)	90.59(6)
O(1)-N(1)-O(1)#1	121.3(3)
O(1)-N(1)-Co(1)	119.35(15)
O(1)#1-N(1)-Co(1)	119.35(15)

Symmetry transformations used to generate equivalent atoms:
#1 -x,y,-z+3/2

Table 4. Anisotropic displacement parameters (A^2 x 10^3) for $[Co(NH_3)_5(NO_2)]Cl_2$. The anisotropic displacement factor exponent takes the form: -2 pi^2 [h^2 a*^2 U11 + ... + 2 h k a* b* U12]

	U11	U22	U33	U23	U13	U12
Co(1)	14(1)	13(1)	11(1)	0	0(1)	0
Cl(1)	21(1)	20(1)	17(1)	0(1)	2(1)	2(1)
N(1)	15(1)	22(1)	10(1)	0	-1(1)	0
N(4)	22(1)	19(1)	12(1)	0(1)	0(1)	2(1)
N(3)	12(1)	23(1)	18(1)	2(1)	2(1)	-2(1)
O(1)	32(1)	22(1)	25(1)	-4(1)	9(1)	6(1)
N(2)	32(2)	16(1)	20(1)	0	-3(1)	0

7.3.2 Crystal Data for Bath 185 - $[Co(NH_3)_5(NO_2)]PF_6$

Table 1. Crystal data and structure refinement for Bath 185 - $[Co(NH_3)_5(NO_2)]PF_6$.

Identification code	$[Co(NH_3)_5(NO_2)]PF_6$
Empirical formula	H_{15} Co F_6 N_6 O_2 P
Formula weight	335.08
Temperature	150(2)K
Wavelength	0.67270Å

Crystal system, space group	Monoclinic, $P2_1/m$
Unit cell dimensions	a = 6.4632(10)Å alpha = 90°
	b = 7.9053(12)Å beta = 100.916(10)°
	c = 10.1371(15)Å gamma = 90°
Volume	508.57(13)Å^3
Z, Calculated density	2, 2.188 Mg/m^3
Absorption coefficient	1.935 mm^{-1}
F(000)	338
Crystal size	0.08 x 0.05 x 0.05mm
Theta range for data collection	1.94 to 30.93°
Limiting indices	-9<=h<=9, -11<=k<=11, -15<=l<=15
Reflections collected / unique	6563 / 1912 [R(int) = 0.0378]
Completeness to theta = 30.93	94.7 %
Absorption correction	SADABS
Max. and min. transmission	0.9180 and 0.8606
Refinement method	Full-matrix least-squares on F^2
Data / restraints / parameters	1912 / 9 / 119
Goodness-of-fit on F^2	1.023
Final R indices [I>2sigma(I)]	R1 = 0.0334, wR2 = 0.0810
R indices (all data)	R1 = 0.0421, wR2 = 0.0856
Extinction coefficient	0.000(4)
Largest diff. peak and hole	0.886 and -0.450 e.A^{-3}

Table 2. Atomic coordinates (x 10^4) and equivalent isotropic displacement parameters (A^2 x 10^3) for $Co(NH_3)_5(NO_2)]PF_6$. U(eq) is defined as one third of the trace of the orthogonalized Uij tensor.

	x	y	z	U(eq)
Co(1)	7423(1)	2500	2125(1)	11(1)
N(1)	4696(4)	2500	951(2)	16(1)
O(1)	3087(3)	2500	1420(2)	22(1)
O(2)	4611(3)	2500	-262(2)	43(1)
N(2)	10186(3)	2500	3351(2)	15(1)
N(3)	6513(3)	711(2)	3218(2)	20(1)
N(4)	8385(3)	806(3)	977(2)	26(1)
P(1)	8275(1)	2500	6897(1)	16(1)
F(1)	5878(2)	2500	5911(2)	21(1)
F(2)	10707(3)	2500	7847(2)	31(1)
F(3)	7550(2)	985(2)	7882(1)	24(1)
F(4)	9062(2)	999(2)	5917(1)	26(1)

Table 3. Bond lengths [Å] and angles [°] for $[Co(NH_3)_5(NO_2)]PF_6$.

Co(1)-N(1)	1.931(2)
Co(1)-N(4)	1.9522(17)
Co(1)-N(4)#1	1.9522(17)
Co(1)-N(3)#1	1.9544(16)
Co(1)-N(3)	1.9544(16)
Co(1)-N(2)	1.974(2)
N(1)-O(2)	1.221(3)
N(1)-O(1)	1.222(3)
P(1)-F(1)	1.6767(16)
P(1)-F(2)	1.6804(17)
P(1)-F(3)#1	1.6815(12)
P(1)-F(3)	1.6815(12)
P(1)-F(4)	1.6870(12)
P(1)-F(4)#1	1.6870(12)

N(1)-Co(1)-N(4)	89.38(7)
N(1)-Co(1)-N(4)#1	89.38(7)
N(4)-Co(1)-N(4)#1	86.64(14)
N(1)-Co(1)-N(3)#1	90.69(7)
N(4)-Co(1)-N(3)#1	176.98(9)
N(4)#1-Co(1)-N(3)#1	90.34(9)
N(1)-Co(1)-N(3)	90.69(7)
N(4)-Co(1)-N(3)	90.34(9)
N(4)#1-Co(1)-N(3)	176.98(9)
N(3)#1-Co(1)-N(3)	92.68(12)
N(1)-Co(1)-N(2)	179.05(10)
N(4)-Co(1)-N(2)	91.32(8)
N(4)#1-Co(1)-N(2)	91.32(8)
N(3)#1-Co(1)-N(2)	88.65(7)
N(3)-Co(1)-N(2)	88.65(7)
O(2)-N(1)-O(1)	120.8(2)
O(2)-N(1)-Co(1)	118.87(18)
O(1)-N(1)-Co(1)	120.33(17)
F(1)-P(1)-F(2)	178.41(9)
F(1)-P(1)-F(3)#1	91.39(6)
F(2)-P(1)-F(3)#1	89.73(6)
F(1)-P(1)-F(3)	91.39(6)
F(2)-P(1)-F(3)	89.73(6)
F(3)#1-P(1)-F(3)	90.82(9)
F(1)-P(1)-F(4)	89.80(6)
F(2)-P(1)-F(4)	89.06(7)
F(3)#1-P(1)-F(4)	178.59(7)
F(3)-P(1)-F(4)	89.90(6)
F(1)-P(1)-F(4)#1	89.80(6)
F(2)-P(1)-F(4)#1	89.06(7)
F(3)#1-P(1)-F(4)#1	89.90(6)
F(3)-P(1)-F(4)#1	178.59(7)
F(4)-P(1)-F(4)#1	89.36(9)

Symmetry transformations used to generate equivalent atoms:
#1 x,-y+1/2,z

Table 4. Anisotropic displacement parameters (A^2 x 10^3) for $[Co(NH_3)_5(NO_2)]PF_6$.
The anisotropic displacement factor exponent takes the form: -2 pi^2 [h^2 a*^2 U11 + ... + 2 h k a* b* U12]

	U11	U22	U33	U23	U13	U12
Co(1)	10(1)	12(1)	10(1)	0	2(1)	0
N(1)	21(1)	14(1)	15(1)	0	5(1)	0
O(1)	14(1)	27(1)	25(1)	0	4(1)	0
O(2)	19(1)	93(2)	15(1)	0	0(1)	0
N(2)	13(1)	18(1)	13(1)	0	2(1)	0
N(3)	16(1)	20(1)	23(1)	7(1)	0(1)	-5(1)
N(4)	20(1)	36(1)	20(1)	-13(1)	-2(1)	10(1)
P(1)	17(1)	15(1)	15(1)	0	1(1)	0
F(1)	15(1)	26(1)	19(1)	0	-4(1)	0
F(2)	15(1)	47(1)	26(1)	0	-5(1)	0
F(3)	28(1)	25(1)	20(1)	9(1)	4(1)	-5(1)
F(4)	35(1)	20(1)	23(1)	-4(1)	8(1)	10(1)

Table 5. Hydrogen bonds for $[Co(NH_3)_5(NO_2)]PF_6$ [Å and °].

D-H...A	d(D-H)	d(H...A)	d(D...A)	<(DHA)
N(2)-H(1)...F(4)#2	0.88(6)	2.09(6)	2.8814(14)	149(5)
N(2)-H(2)...F(4)#1	0.75(5)	2.37(5)	3.068(3)	157(5)
N(2)-H(2)...F(4)	0.75(5)	2.75(5)	3.068(3)	109(4)
N(2)-H(3)...O(1)#3	0.93(5)	2.23(4)	2.956(3)	135(4)
N(2)-H(2)...F(4)#4	0.75(5)	2.40(5)	2.8814(14)	123(4)
N(3)-H(4)...F(3)#5	0.77(3)	2.21(3)	2.972(2)	177(3)
N(3)-H(5)...F(4)	0.84(3)	2.33(3)	2.923(2)	128(3)
N(3)-H(5)...F(1)	0.84(3)	2.35(4)	3.169(2)	165(3)
N(3)-H(6)...F(4)#2	0.88(3)	2.36(3)	3.135(2)	148(3)
N(4)-H(7)...F(3)#6	0.91(3)	2.22(3)	3.084(2)	158(2)
N(4)-H(7)...O(2)	0.91(3)	2.36(3)	2.857(3)	113.9(19)
N(4)-H(8)...F(2)#2	0.85(3)	2.20(3)	2.886(2)	138(3)
N(4)-H(8)...O(2)#7	0.85(3)	2.50(3)	3.251(3)	147(3)
N(4)-H(9)...F(3)#2	0.87(4)	2.35(4)	3.015(2)	133(3)
N(4)-H(9)...O(1)#3	0.87(4)	2.52(4)	3.273(3)	146(3)

Symmetry transformations used to generate equivalent atoms:
#1 x,-y+1/2,z #2 -x+2,-y,-z+1 #3 x+1,y,z
#4 -x+2,y+1/2,-z+1 #5 -x+1,-y,-z+1 #6 x,y,z-1
#7 -x+1,-y,-z

7.3.3 Crystal Data for h05prr44 - $[Co(NH_3)_5(NO_2)][Fe(CN)_5(NO)].1½H_2O$

Table 1. Crystal data and structure refinement for h05prr44 - $[Co(NH_3)_5(NO_2)][Fe(CN)_5(NO)].1½H_2O$.

Identification code	$[Co(NH_3)_5NO_2][Fe(CN)_5(NO)].1½H_2O$	
Empirical formula	$C_5 H_{18} Co Fe N_{12} O_{4.5}$	
Formula weight	433.07	
Temperature	150(2)K	
Wavelength	0.71073Å	
Crystal system, space group	Monoclinic, *C*2/*c*	
Unit cell dimensions	a = 28.4040(3)Å	alpha = 90°
	b = 6.39700(10)Å	beta = 123.9820(10)°
	c = 22.3480(4)Å	gamma = 90°
Volume	3367.13(9)Å^3	
Z, Calculated density	8, 1.697 Mg/m^3	
Absorption coefficient	1.888 mm^{-1}	
F(000)	1744	
Crystal size	0.38 x 0.38 x 0.22mm	
Theta range for data collection	3.63 to 30.52°	
Limiting indices	-40<=h<=40, -8<=k<=9, -31<=l<=31	
Reflections collected / unique	33581 / 5127 [R(int) = 0.0609]	
Completeness to theta = 30.52	99.7 %	
Absorption correction	Sortav	
Max. and min. transmission	0.6760 and 0.5378	
Refinement method	Full-matrix least-squares on F^2	
Data / restraints / parameters	5127 / 0 / 219	
Goodness-of-fit on F^2	1.049	
Final R indices [I>2sigma(I)]	R1 = 0.0370, wR2 = 0.0863	
R indices (all data)	R1 = 0.0633, wR2 = 0.0956	
Extinction coefficient	0.00154(17)	
Largest diff. peak and hole	1.140 and -1.039 e.Å^{-3}	

Table 2. Atomic coordinates (x 10^4) and equivalent isotropic displacement parameters (A^2 x 10^3) for $[Co(NH_3)_5NO_2][Fe(CN)_5(NO)].1½H_2O$.
U(eq) is defined as one third of the trace of the orthogonalized Uij tensor.

	x	y	z	U(eq)
Co(1)	3404(1)	55(1)	2221(1)	13(1)
N(1)	3015(1)	-2298(2)	2272(1)	17(1)
O(1)	3158(1)	-4097(2)	2233(1)	26(1)
O(2)	2612(1)	-2006(2)	2329(1)	26(1)
N(2)	3804(1)	2462(3)	2138(1)	20(1)
N(3)	3281(1)	-1145(3)	1341(1)	18(1)
N(4)	2682(1)	1558(2)	1644(1)	19(1)
N(5)	3505(1)	1133(2)	3107(1)	18(1)
N(6)	4136(1)	-1378(2)	2838(1)	18(1)
Fe(1)	803(1)	-313(1)	-340(1)	15(1)
N(7)	535(1)	-2446(3)	-216(1)	23(1)
O(3)	364(1)	-3931(3)	-129(1)	46(1)
C(1)	1122(1)	2114(3)	-498(1)	25(1)
N(8)	1312(1)	3522(3)	-613(1)	45(1)
C(2)	679(1)	-1224(3)	-1243(1)	24(1)
N(9)	627(1)	-1707(3)	-1772(1)	39(1)
C(3)	96(1)	1214(3)	-876(1)	23(1)
N(10)	-318(1)	2154(3)	-1210(1)	37(1)
C(4)	988(1)	1119(3)	533(1)	21(1)
N(11)	1094(1)	2009(3)	1039(1)	36(1)
C(5)	1566(1)	-1440(3)	156(1)	21(1)
N(12)	2020(1)	-2091(3)	436(1)	34(1)
O(4)	5000	1014(6)	2500	116(2)
O(5)	2722(1)	-5852(3)	601(1)	40(1)

Table 3. Bond lengths [Å] and angles [°] for $[Co(NH_3)_5NO_2][Fe(CN)_5(NO)].1½H_2O$.

Co(1)-N(1)	1.9077(16)
Co(1)-N(3)	1.9520(16)
Co(1)-N(4)	1.9593(16)
Co(1)-N(5)	1.9598(16)
Co(1)-N(6)	1.9642(16)
Co(1)-N(2)	1.9827(16)
N(1)-O(2)	1.236(2)
N(1)-O(1)	1.239(2)
N(2)-H(1)	0.9100
N(2)-H(2)	0.9100
N(2)-H(3)	0.9100
N(3)-H(5)	0.9100
N(3)-H(6)	0.9100
N(4)-H(7)	0.9100
N(4)-H(8)	0.9100
N(4)-H(9)	0.9100
N(5)-H(10)	0.9100
N(5)-H(11)	0.9100
N(5)-H(12)	0.9100
N(6)-H(13)	0.9100
N(6)-H(14)	0.9100
N(6)-H(15)	0.9100
Fe(1)-N(7)	1.6595(17)
Fe(1)-C(1)	1.928(2)

Fe(1)-C(3)	1.930(2)
Fe(1)-C(2)	1.936(2)
Fe(1)-C(5)	1.940(2)
Fe(1)-C(4)	1.941(2)
N(7)-O(3)	1.131(2)
C(1)-N(8)	1.151(3)
C(2)-N(9)	1.148(3)
C(3)-N(10)	1.150(3)
C(4)-N(11)	1.146(3)
C(5)-N(12)	1.151(3)

N(1)-Co(1)-N(3)	88.06(7)
N(1)-Co(1)-N(4)	89.91(7)
N(3)-Co(1)-N(4)	89.85(7)
N(1)-Co(1)-N(5)	88.88(7)
N(3)-Co(1)-N(5)	176.93(7)
N(4)-Co(1)-N(5)	90.04(7)
N(1)-Co(1)-N(6)	90.62(7)
N(3)-Co(1)-N(6)	92.73(7)
N(4)-Co(1)-N(6)	177.39(7)
N(5)-Co(1)-N(6)	87.42(7)
N(1)-Co(1)-N(2)	178.08(7)
N(3)-Co(1)-N(2)	90.03(7)
N(4)-Co(1)-N(2)	90.03(7)
N(5)-Co(1)-N(2)	93.04(7)
N(6)-Co(1)-N(2)	89.53(7)
O(2)-N(1)-O(1)	120.41(16)
O(2)-N(1)-Co(1)	119.20(12)
O(1)-N(1)-Co(1)	120.38(13)
Co(1)-N(2)-H(1)	109.5
Co(1)-N(2)-H(2)	109.5
H(1)-N(2)-H(2)	109.5
Co(1)-N(2)-H(3)	109.5
H(1)-N(2)-H(3)	109.5
H(2)-N(2)-H(3)	109.5
Co(1)-N(3)-H(4)	109.5
Co(1)-N(3)-H(5)	109.5
H(4)-N(3)-H(5)	109.5
Co(1)-N(3)-H(6)	109.5
H(4)-N(3)-H(6)	109.5
H(5)-N(3)-H(6)	109.5
Co(1)-N(4)-H(7)	109.5
Co(1)-N(4)-H(8)	109.5
H(7)-N(4)-H(8)	109.5
Co(1)-N(4)-H(9)	109.5
H(7)-N(4)-H(9)	109.5
H(8)-N(4)-H(9)	109.5
Co(1)-N(5)-H(10)	109.5
Co(1)-N(5)-H(11)	109.5
H(10)-N(5)-H(11)	109.5
Co(1)-N(5)-H(12)	109.5
H(10)-N(5)-H(12)	109.5
H(11)-N(5)-H(12)	109.5
Co(1)-N(6)-H(13)	109.5
Co(1)-N(6)-H(14)	109.5
H(13)-N(6)-H(14)	109.5
Co(1)-N(6)-H(15)	109.5
H(13)-N(6)-H(15)	109.5
H(14)-N(6)-H(15)	109.5
N(7)-Fe(1)-C(1)	178.20(9)
N(7)-Fe(1)-C(3)	96.06(9)
C(1)-Fe(1)-C(3)	84.89(9)

N(7)-Fe(1)-C(2)	95.36(9)
C(1)-Fe(1)-C(2)	83.11(9)
C(3)-Fe(1)-C(2)	89.14(9)
N(7)-Fe(1)-C(5)	93.98(9)
C(1)-Fe(1)-C(5)	85.04(9)
C(3)-Fe(1)-C(5)	169.88(9)
C(2)-Fe(1)-C(5)	88.67(9)
N(7)-Fe(1)-C(4)	96.51(9)
C(1)-Fe(1)-C(4)	85.02(9)
C(3)-Fe(1)-C(4)	89.41(9)
C(2)-Fe(1)-C(4)	168.13(9)
C(5)-Fe(1)-C(4)	90.70(9)
O(3)-N(7)-Fe(1)	178.14(18)
N(8)-C(1)-Fe(1)	177.5(2)
N(9)-C(2)-Fe(1)	176.8(2)
N(10)-C(3)-Fe(1)	177.6(2)
N(11)-C(4)-Fe(1)	178.37(19)
N(12)-C(5)-Fe(1)	178.2(2)

Symmetry transformations used to generate equivalent atoms:

Table 4. Anisotropic displacement parameters (A^2 x 10^3) for $Co(NH_3)_5NO_2][Fe(CN)_5(NO)].1½H_2O$.
The anisotropic displacement factor exponent takes the form: -2 pi^2 [h^2 a*^2 U11 + ... + 2 h k a* b* U12]

	U11	U22	U33	U23	U13	U12
Co(1)	11(1)	13(1)	15(1)	0(1)	8(1)	-1(1)
N(1)	18(1)	17(1)	17(1)	-1(1)	10(1)	-2(1)
O(1)	33(1)	14(1)	36(1)	-2(1)	22(1)	-2(1)
O(2)	22(1)	27(1)	37(1)	0(1)	22(1)	-4(1)
N(2)	19(1)	18(1)	24(1)	2(1)	12(1)	-2(1)
N(3)	14(1)	21(1)	17(1)	0(1)	8(1)	0(1)
N(4)	15(1)	19(1)	20(1)	1(1)	8(1)	2(1)
N(5)	16(1)	18(1)	21(1)	-3(1)	10(1)	-2(1)
N(6)	14(1)	20(1)	18(1)	1(1)	8(1)	2(1)
Fe(1)	13(1)	17(1)	15(1)	0(1)	7(1)	0(1)
N(7)	22(1)	21(1)	26(1)	-4(1)	14(1)	-3(1)
O(3)	57(1)	28(1)	70(1)	-4(1)	45(1)	-16(1)
C(1)	30(1)	24(1)	30(1)	1(1)	22(1)	2(1)
N(8)	68(2)	32(1)	60(2)	0(1)	51(2)	-7(1)
C(2)	15(1)	35(1)	20(1)	-1(1)	8(1)	7(1)
N(9)	26(1)	62(2)	23(1)	-4(1)	9(1)	19(1)
C(3)	22(1)	27(1)	20(1)	1(1)	13(1)	3(1)
N(10)	30(1)	49(1)	30(1)	8(1)	15(1)	16(1)
C(4)	21(1)	22(1)	21(1)	-1(1)	13(1)	-2(1)
N(11)	41(1)	38(1)	29(1)	-10(1)	19(1)	-5(1)
C(5)	18(1)	22(1)	20(1)	-4(1)	8(1)	-1(1)
N(12)	17(1)	36(1)	37(1)	-6(1)	8(1)	2(1)
O(4)	77(3)	86(3)	234(6)	0	117(4)	0
O(5)	45(1)	33(1)	53(1)	15(1)	34(1)	11(1)

Table 5. Hydrogen bonds for $[Co(NH_3)_5NO_2][Fe(CN)_5(NO)].1½H_2O$ [Å and °].

D-H...A	d(D-H)	d(H...A)	d(D...A)	<(DHA)
N(2)-H(1)...O(4)	0.91	2.29	3.159(2)	160.6
N(2)-H(2)...N(10)#1	0.91	2.43	3.102(3)	131.3
N(2)-H(3)...O(5)#2	0.91	2.38	3.256(3)	161.3
N(3)-H(4)...N(9)#3	0.91	2.28	3.016(3)	137.7
N(3)-H(5)...N(8)#4	0.91	2.08	2.983(3)	170.4
N(3)-H(6)...N(12)	0.91	2.13	3.032(3)	170.8
N(4)-H(7)...O(2)	0.91	2.28	2.815(2)	116.9
N(4)-H(8)...O(5)#2	0.91	2.08	2.913(2)	152.0
N(4)-H(9)...O(2)#5	0.91	2.33	2.993(2)	129.4
N(4)-H(9)...O(1)#2	0.91	2.33	3.049(2)	135.4
N(5)-H(10)...O(2)#5	0.91	2.09	2.997(2)	175.3
N(5)-H(11)...N(10)#1	0.91	2.18	2.999(3)	148.6
N(5)-H(12)...N(11)#6	0.91	2.20	3.078(3)	160.9
N(6)-H(13)...N(11)#6	0.91	2.29	3.102(3)	148.9
N(6)-H(14)...N(10)#1	0.91	2.43	3.247(3)	148.8
N(6)-H(15)...N(9)#3	0.91	2.17	3.070(3)	171.2

Symmetry transformations used to generate equivalent atoms:
#1 x+1/2,-y+1/2,z+1/2 #2 x,y+1,z #3 -x+1/2,-y-1/2,-z
#4 -x+1/2,-y+1/2,-z #5 -x+1/2,y+1/2,-z+1/2
#6 -x+1/2,y-1/2,-z+1/2

7.3.4 Crystal Data for k06prr07 - $[Co(NH_3)_5(NO_2)](Hbs)_2.2H_2O$

Table 1. Crystal data and structure refinement for k06prr07 - $[Co(NH_3)_5(NO_2)](Hbs)_2.2H_2O$.

Identification code	$[Co(NH_3)_5(NO_2)](Hbs)_2.2H_2O$
Empirical formula	$C_{12}\ H_{29}\ Co\ N_6\ O_{12}\ S_2$
Formula weight	572.46
Temperature	150(2)K
Wavelength	0.71073Å
Crystal system, space group	Orthorhombic, $P2_12_12_1$
Unit cell dimensions	a = 7.02200(10)Å alpha = 90°
	b = 11.99400(10)Å beta = 90°
	c = 26.7510(2)Å gamma = 90°
Volume	2253.02(4)Å^3
Z, Calculated density	4, 1.688 Mg/m^3
Absorption coefficient	1.019 mm^{-1}
F(000)	1192
Crystal size	0.33 x 0.25 x 0.20mm
Theta range for data collection	3.40 to 30.30°
Limiting indices	-9<=h<=9, -17<=k<=15, -36<=l<=37
Reflections collected / unique	40610 / 6109 [R(int) = 0.0546]
Completeness to theta = 30.30	93.2 %
Absorption correction	Sortav
Max. and min. transmission	0.8222 and 0.7331
Refinement method	Full-matrix least-squares on F^2
Data / restraints / parameters	6109 / 0 / 322
Goodness-of-fit on F^2	1.134
Final R indices [I>2sigma(I)]	R1 = 0.0272, wR2 = 0.0575
R indices (all data)	R1 = 0.0350, wR2 = 0.0634
Absolute structure parameter	-0.008(8)
Largest diff. peak and hole	0.559 and -0.931 e.A^{-3}

Table 2. Atomic coordinates (x 10^4) and equivalent isotropic displacement parameters (A^2 x 10^3) for $[Co(NH_3)_5(NO_2)](Hbs)_2.2H_2O$.
U(eq) is defined as one third of the trace of the orthogonalized Uij tensor.

	x	y	z	U(eq)
Co(1)	1670(1)	3220(1)	2709(1)	11(1)
N(1)	317(2)	1864(1)	2580(1)	17(1)
O(1)	1103(2)	953(1)	2668(1)	25(1)
O(2)	-1313(2)	1884(1)	2406(1)	25(1)
N(2)	3125(2)	4620(1)	2800(1)	17(1)
N(3)	2199(2)	2718(1)	3395(1)	17(1)
N(4)	4020(2)	2478(1)	2485(1)	18(1)
N(5)	1087(2)	3710(1)	2028(1)	16(1)
N(6)	-689(2)	3915(1)	2946(1)	15(1)
C(1)	3898(3)	6264(2)	749(1)	16(1)
S(1)	3164(1)	6342(1)	1380(1)	16(1)
O(3)	1128(2)	6077(1)	1377(1)	26(1)
O(4)	4259(2)	5534(1)	1665(1)	31(1)
O(5)	3525(2)	7483(1)	1542(1)	22(1)
C(2)	3452(3)	7158(2)	439(1)	18(1)
C(3)	3734(3)	7067(2)	-73(1)	20(1)
C(4)	4464(3)	6084(2)	-271(1)	17(1)
O(6)	4680(2)	6035(1)	-777(1)	23(1)
C(5)	4973(3)	5204(2)	41(1)	18(1)
C(6)	4670(3)	5292(2)	554(1)	18(1)
C(7)	5678(3)	6213(2)	4453(1)	14(1)
S(2)	5587(1)	6409(1)	3800(1)	17(1)
O(7)	5732(2)	5311(1)	3576(1)	27(1)
O(8)	7193(2)	7133(1)	3672(1)	25(1)
O(9)	3773(2)	6960(1)	3688(1)	24(1)
C(8)	6344(3)	7061(2)	4764(1)	17(1)
C(9)	6325(3)	6907(2)	5279(1)	20(1)
C(10)	5635(3)	5914(2)	5480(1)	18(1)
O(10)	5653(2)	5808(1)	5987(1)	27(1)
C(11)	4994(3)	5070(2)	5167(1)	19(1)
C(12)	5009(3)	5218(2)	4653(1)	18(1)
O(11)	3235(2)	8866(1)	3066(1)	22(1)
O(12)	400(2)	5797(1)	3699(1)	24(1)

Table 3. Bond lengths [Å] and angles [°] for $[Co(NH_3)_5(NO_2)](Hbs)_2.2H_2O$.

Co(1)-N(1)	1.9140(16)
Co(1)-N(5)	1.9556(14)
Co(1)-N(6)	1.9609(16)
Co(1)-N(4)	1.9682(16)
Co(1)-N(3)	1.9681(15)
Co(1)-N(2)	1.9815(15)
N(1)-O(2)	1.236(2)
N(1)-O(1)	1.246(2)
N(2)-H(1)	0.9100
N(2)-H(2)	0.9100
N(2)-H(3)	0.9100
N(3)-H(4)	0.9100
N(3)-H(5)	0.9100
N(3)-H(6)	0.9100
N(4)-H(7)	0.9100

N(4)-H(8)	0.9100
N(4)-H(9)	0.9100
N(5)-H(10)	0.9100
N(5)-H(11)	0.9100
N(5)-H(12)	0.9100
N(6)-H(13)	0.9100
N(6)-H(14)	0.9100
N(6)-H(15)	0.9100
C(1)-C(6)	1.388(2)
C(1)-C(2)	1.391(3)
C(1)-S(1)	1.7678(18)
S(1)-O(4)	1.4524(15)
S(1)-O(5)	1.4571(14)
S(1)-O(3)	1.4649(15)
C(2)-C(3)	1.388(3)
C(2)-H(16)	0.9500
C(3)-C(4)	1.391(3)
C(3)-H(17)	0.9500
C(4)-O(6)	1.364(2)
C(4)-C(5)	1.392(3)
O(6)-H(20)	0.8400
C(5)-C(6)	1.392(3)
C(5)-H(18)	0.9500
C(6)-H(19)	0.9500
C(7)-C(12)	1.388(2)
C(7)-C(8)	1.394(2)
C(7)-S(2)	1.7646(17)
S(2)-O(7)	1.4502(15)
S(2)-O(8)	1.4640(15)
S(2)-O(9)	1.4658(14)
C(8)-C(9)	1.391(2)
C(8)-H(23)	0.9500
C(9)-C(10)	1.392(3)
C(9)-H(24)	0.9500
C(10)-O(10)	1.363(2)
C(10)-C(11)	1.388(3)
O(10)-H(25)	0.8400
C(11)-C(12)	1.388(3)
C(11)-H(21)	0.9500
C(12)-H(22)	0.9500
O(11)-H(26)	0.77(3)
O(11)-H(27)	0.81(3)
O(12)-H(28)	0.78(3)
O(12)-H(29)	0.77(4)

N(1)-Co(1)-N(5)	89.12(6)
N(1)-Co(1)-N(6)	90.00(7)
N(5)-Co(1)-N(6)	89.85(6)
N(1)-Co(1)-N(4)	88.74(7)
N(5)-Co(1)-N(4)	91.60(7)
N(6)-Co(1)-N(4)	178.06(7)
N(1)-Co(1)-N(3)	90.08(6)
N(5)-Co(1)-N(3)	178.78(7)
N(6)-Co(1)-N(3)	89.23(6)
N(4)-Co(1)-N(3)	89.30(7)
N(1)-Co(1)-N(2)	176.64(6)
N(5)-Co(1)-N(2)	88.18(6)
N(6)-Co(1)-N(2)	91.99(7)
N(4)-Co(1)-N(2)	89.34(7)
N(3)-Co(1)-N(2)	92.65(7)
O(2)-N(1)-O(1)	119.85(16)
O(2)-N(1)-Co(1)	120.72(13)

O(1)-N(1)-Co(1)	119.42(12)
Co(1)-N(2)-H(1)	109.5
Co(1)-N(2)-H(2)	109.5
H(1)-N(2)-H(2)	109.5
Co(1)-N(2)-H(3)	109.5
H(1)-N(2)-H(3)	109.5
H(2)-N(2)-H(3)	109.5
Co(1)-N(3)-H(4)	109.5
Co(1)-N(3)-H(5)	109.5
H(4)-N(3)-H(5)	109.5
Co(1)-N(3)-H(6)	109.5
H(4)-N(3)-H(6)	109.5
H(5)-N(3)-H(6)	109.5
Co(1)-N(4)-H(7)	109.5
Co(1)-N(4)-H(8)	109.5
H(7)-N(4)-H(8)	109.5
Co(1)-N(4)-H(9)	109.5
H(7)-N(4)-H(9)	109.5
H(8)-N(4)-H(9)	109.5
Co(1)-N(5)-H(10)	109.5
Co(1)-N(5)-H(11)	109.5
H(10)-N(5)-H(11)	109.5
Co(1)-N(5)-H(12)	109.5
H(10)-N(5)-H(12)	109.5
H(11)-N(5)-H(12)	109.5
Co(1)-N(6)-H(13)	109.5
Co(1)-N(6)-H(14)	109.5
H(13)-N(6)-H(14)	109.5
Co(1)-N(6)-H(15)	109.5
H(13)-N(6)-H(15)	109.5
H(14)-N(6)-H(15)	109.5
C(6)-C(1)-C(2)	120.82(16)
C(6)-C(1)-S(1)	121.13(14)
C(2)-C(1)-S(1)	117.55(14)
O(4)-S(1)-O(5)	112.25(9)
O(4)-S(1)-O(3)	112.02(10)
O(5)-S(1)-O(3)	112.04(9)
O(4)-S(1)-C(1)	108.13(9)
O(5)-S(1)-C(1)	106.45(9)
O(3)-S(1)-C(1)	105.48(8)
C(3)-C(2)-C(1)	119.68(17)
C(3)-C(2)-H(16)	120.2
C(1)-C(2)-H(16)	120.2
C(2)-C(3)-C(4)	119.64(17)
C(2)-C(3)-H(17)	120.2
C(4)-C(3)-H(17)	120.2
O(6)-C(4)-C(3)	117.06(16)
O(6)-C(4)-C(5)	122.30(17)
C(3)-C(4)-C(5)	120.64(17)
C(4)-O(6)-H(20)	109.5
C(4)-C(5)-C(6)	119.61(18)
C(4)-C(5)-H(18)	120.2
C(6)-C(5)-H(18)	120.2
C(1)-C(6)-C(5)	119.55(17)
C(1)-C(6)-H(19)	120.2
C(5)-C(6)-H(19)	120.2
C(12)-C(7)-C(8)	120.78(16)
C(12)-C(7)-S(2)	118.82(14)
C(8)-C(7)-S(2)	120.36(13)
O(7)-S(2)-O(8)	112.78(10)
O(7)-S(2)-O(9)	112.70(9)
O(8)-S(2)-O(9)	110.73(8)

O(7)-S(2)-C(7)	106.66(9)
O(8)-S(2)-C(7)	106.44(8)
O(9)-S(2)-C(7)	107.08(8)
C(9)-C(8)-C(7)	119.37(16)
C(9)-C(8)-H(23)	120.3
C(7)-C(8)-H(23)	120.3
C(8)-C(9)-C(10)	119.86(17)
C(8)-C(9)-H(24)	120.1
C(10)-C(9)-H(24)	120.1
O(10)-C(10)-C(11)	122.26(18)
O(10)-C(10)-C(9)	117.38(17)
C(11)-C(10)-C(9)	120.35(17)
C(10)-O(10)-H(25)	109.5
C(12)-C(11)-C(10)	120.08(17)
C(12)-C(11)-H(21)	120.0
C(10)-C(11)-H(21)	120.0
C(11)-C(12)-C(7)	119.55(17)
C(11)-C(12)-H(22)	120.2
C(7)-C(12)-H(22)	120.2
H(26)-O(11)-H(27)	98(3)
H(28)-O(12)-H(29)	108(3)

Symmetry transformations used to generate equivalent atoms:

Table 4. Anisotropic displacement parameters (A^2 x 10^3) for $[Co(NH_3)_5(NO_2)](Hbs)_2.2H_2O$.
The anisotropic displacement factor exponent takes the form: -2 pi^2 [h^2 a*^2 U11 + ... + 2 h k a* b* U12]

	U11	U22	U33	U23	U13	U12
Co(1)	12(1)	11(1)	11(1)	0(1)	0(1)	0(1)
N(1)	21(1)	16(1)	14(1)	0(1)	2(1)	-1(1)
O(1)	33(1)	11(1)	32(1)	0(1)	4(1)	1(1)
O(2)	24(1)	22(1)	30(1)	0(1)	-9(1)	-8(1)
N(2)	15(1)	16(1)	20(1)	-1(1)	-2(1)	-2(1)
N(3)	20(1)	19(1)	13(1)	1(1)	0(1)	3(1)
N(4)	17(1)	20(1)	16(1)	1(1)	1(1)	4(1)
N(5)	19(1)	16(1)	13(1)	1(1)	-2(1)	0(1)
N(6)	14(1)	15(1)	18(1)	0(1)	2(1)	0(1)
C(1)	14(1)	17(1)	16(1)	-2(1)	0(1)	0(1)
S(1)	16(1)	19(1)	15(1)	-2(1)	1(1)	2(1)
O(3)	19(1)	36(1)	25(1)	-10(1)	7(1)	-8(1)
O(4)	40(1)	35(1)	20(1)	5(1)	4(1)	17(1)
O(5)	23(1)	22(1)	23(1)	-7(1)	2(1)	-1(1)
C(2)	15(1)	15(1)	23(1)	-1(1)	0(1)	1(1)
C(3)	20(1)	19(1)	20(1)	3(1)	-2(1)	-1(1)
C(4)	14(1)	21(1)	16(1)	0(1)	0(1)	-3(1)
O(6)	32(1)	22(1)	15(1)	1(1)	1(1)	2(1)
C(5)	17(1)	19(1)	19(1)	-2(1)	1(1)	4(1)
C(6)	18(1)	18(1)	17(1)	0(1)	-1(1)	4(1)
C(7)	12(1)	18(1)	13(1)	1(1)	-2(1)	0(1)
S(2)	14(1)	23(1)	14(1)	3(1)	-2(1)	-1(1)
O(7)	34(1)	29(1)	19(1)	-7(1)	-5(1)	2(1)
O(8)	18(1)	36(1)	22(1)	10(1)	2(1)	-4(1)
O(9)	16(1)	31(1)	25(1)	10(1)	-4(1)	1(1)
C(8)	17(1)	16(1)	19(1)	1(1)	1(1)	-1(1)
C(9)	21(1)	21(1)	19(1)	-5(1)	-1(1)	-2(1)
C(10)	15(1)	26(1)	14(1)	0(1)	2(1)	3(1)

O(10)	33(1)	35(1)	14(1)	2(1)	2(1)	-7(1)
C(11)	18(1)	18(1)	20(1)	3(1)	3(1)	-3(1)
C(12)	18(1)	18(1)	18(1)	-1(1)	-1(1)	-4(1)
O(11)	24(1)	19(1)	23(1)	0(1)	0(1)	-1(1)
O(12)	17(1)	24(1)	29(1)	1(1)	-1(1)	-1(1)

Table 5. Hydrogen bonds for $[Co(NH_3)_5(NO_2)](Hbs)_2.2H_2O$ [Å and °].

D-H...A	d(D-H)	d(H...A)	d(D...A)	<(DHA)
N(2)-H(2)...O(7)	0.91	2.07	2.889(2)	148.7
N(2)-H(3)...O(2)#1	0.91	2.20	3.049(2)	154.2
N(3)-H(5)...O(6)#2	0.91	2.08	2.980(2)	168.7
N(3)-H(6)...O(5)#3	0.91	2.13	3.020(2)	165.7
N(4)-H(7)...O(5)#3	0.91	2.27	3.123(2)	156.1
N(4)-H(8)...O(11)#3	0.91	2.04	2.942(2)	168.4
N(5)-H(10)...O(8)#3	0.91	2.02	2.923(2)	173.6
N(5)-H(12)...O(11)#4	0.91	2.15	3.051(2)	169.5
N(6)-H(14)...O(12)	0.91	2.22	3.119(2)	170.3
N(6)-H(15)...O(5)#4	0.91	2.08	2.965(2)	163.7
O(6)-H(20)...O(12)#5	0.84	1.83	2.608(2)	154.0
O(10)-H(25)...O(3)#2	0.84	1.96	2.786(2)	169.8
O(11)-H(26)...O(4)#6	0.77(3)	2.07(3)	2.760(2)	150(3)
O(11)-H(27)...O(9)	0.81(3)	2.07(3)	2.853(2)	163(3)
O(12)-H(28)...O(9)	0.78(3)	1.97(3)	2.749(2)	176(3)
O(12)-H(29)...O(8)#7	0.77(4)	1.99(4)	2.765(2)	174(4)

Symmetry transformations used to generate equivalent atoms:
#1 -x,y+1/2,-z+1/2 #2 -x+1/2,-y+1,z+1/2 #3 -x+1,y-1/2,-z+1/2
#4 -x,y-1/2,-z+1/2 #5 -x+1/2,-y+1,z-1/2 #6 -x+1,y+1/2,-z+1/2
#7 x-1,y,z

7.3.5 Crystal Data for k05prr55 - $[Co(NH_3)_5(NO_2)](BPh_4)_2.2H_2O$

Table 1. Crystal data and structure refinement for k05prr55 - $[Co(NH_3)_5(NO_2)](BPh_4)_2.2H_2O$.

Identification code	$[Co(NH_3)_5(NO_2)](BPh_4)_2.2H_2O$
Empirical formula	$C_{48}\ H_{59}\ B_2\ Co\ N_6\ O_4$
Formula weight	860.53
Temperature	150(2)K
Wavelength	0.71073Å
Crystal system, space group	Orthorhombic, $Pc2_1n$
Unit cell dimensions	a = 9.69000(10)Å alpha = 90°
	b = 16.16100(10)Å beta = 90°
	c = 28.6570(3)Å gamma = 90°
Volume	4487.69(7)$Å^3$
Z, Calculated density	4, 1.274 Mg/m^3
Absorption coefficient	0.433 mm^{-1}
F(000)	1816
Crystal size	0.28 x 0.25 x 0.08mm
Theta range for data collection	2.89 to 30.50°
Limiting indices	-13<=h<=13, -22<=k<=22, -40<=l<=40
Reflections collected / unique	69123 / 13236 [R(int) = 0.0616]
Completeness to theta = 30.50	99.6 %
Absorption correction	None
Max. and min. transmission	0.9683 and 0.8902
Refinement method	Full-matrix least-squares on F^2
Data / restraints / parameters	13236 / 1 / 539

Goodness-of-fit on F^2	1.043
Final R indices [I>2sigma(I)]	R1 = 0.0474, wR2 = 0.1177
R indices (all data)	R1 = 0.0629, wR2 = 0.1296
Absolute structure parameter	-0.001(1)
Largest diff. peak and hole	0.883 and -0.456 e.$Å^{-3}$

Table 2. Atomic coordinates (x 10^4) and equivalent isotropic displacement parameters (A^2 x 10^3) for $Co(NH_3)_5(NO_2)](BPh_4)_2.2H_2O$.
U(eq) is defined as one third of the trace of the orthogonalized Uij tensor.

	x	y	z	U(eq)
Co(1)	5860(1)	2499(1)	1302(1)	20(1)
N(1)	7685(2)	2417(1)	1050(1)	30(1)
O(1)	8646(2)	2742(1)	1262(1)	46(1)
O(2)	7884(2)	2028(2)	685(1)	53(1)
N(2)	3949(2)	2602(2)	1572(1)	34(1)
N(3)	6534(2)	2015(1)	886(1)	30(1)
N(4)	6342(2)	3599(1)	1536(1)	33(1)
N(5)	5270(2)	2976(1)	705(1)	27(1)
N(6)	5425(2)	1406(1)	1053(1)	33(1)
B(1)	3495(2)	2215(2)	-493(1)	20(1)
C(1)	5166(2)	2271(1)	-565(1)	22(1)
C(2)	5699(2)	2771(2)	-925(1)	34(1)
C(3)	7095(3)	2814(2)	-1034(1)	41(1)
C(4)	8033(3)	2339(2)	-784(1)	44(1)
C(5)	7562(3)	1841(2)	-429(1)	42(1)
C(6)	6162(2)	1813(2)	-321(1)	31(1)
C(7)	2831(2)	1585(1)	-886(1)	22(1)
C(8)	1479(2)	1274(1)	-829(1)	26(1)
C(9)	863(2)	740(2)	-1146(1)	32(1)
C(10)	1597(3)	485(2)	-1538(1)	32(1)
C(11)	2907(2)	791(2)	-1611(1)	29(1)
C(12)	3506(2)	1330(2)	-1291(1)	26(1)
C(13)	3038(2)	1806(1)	11(1)	22(1)
C(14)	2175(2)	2205(2)	332(1)	28(1)
C(15)	1610(3)	1799(2)	719(1)	37(1)
C(16)	1893(3)	977(2)	800(1)	37(1)
C(17)	2762(3)	554(2)	494(1)	34(1)
C(18)	3320(2)	965(1)	112(1)	29(1)
C(19)	2838(2)	3155(1)	-557(1)	23(1)
C(20)	1689(2)	3330(2)	-838(1)	29(1)
C(21)	1126(3)	4122(2)	-876(1)	40(1)
C(22)	1688(3)	4777(2)	-630(1)	41(1)
C(23)	2841(3)	4629(2)	-355(1)	40(1)
C(24)	3404(3)	3842(2)	-325(1)	31(1)
B(2)	7950(2)	-171(2)	2572(1)	21(1)
C(25)	6479(2)	-86(1)	2287(1)	23(1)
C(26)	6195(3)	-419(2)	1845(1)	31(1)
C(27)	4915(3)	-317(2)	1625(1)	39(1)
C(28)	3874(3)	136(2)	1836(1)	37(1)
C(29)	4135(2)	499(2)	2263(1)	32(1)
C(30)	5398(2)	393(1)	2482(1)	26(1)
C(31)	8908(2)	-944(1)	2383(1)	23(1)
C(32)	8324(3)	-1713(1)	2256(1)	28(1)
C(33)	9122(3)	-2370(1)	2094(1)	32(1)
C(34)	10539(3)	-2296(2)	2061(1)	35(1)
C(35)	11157(3)	-1561(2)	2201(1)	33(1)
C(36)	10345(2)	903(1)	2359(1)	26(1)

C(37)	7672(2)	-360(1)	3127(1)	20(1)
C(38)	8619(2)	-131(1)	3474(1)	25(1)
C(39)	8419(3)	-301(1)	3947(1)	30(1)
C(40)	7270(3)	-736(2)	4091(1)	32(1)
C(41)	6323(3)	-996(2)	3761(1)	29(1)
C(42)	6524(2)	-810(1)	3287(1)	24(1)
C(43)	8742(2)	715(1)	2489(1)	23(1)
C(44)	9454(3)	870(2)	2067(1)	32(1)
C(45)	10101(3)	1611(2)	1975(1)	44(1)
C(46)	10037(3)	2252(2)	2301(1)	48(1)
C(47)	9332(3)	2134(2)	2710(1)	38(1)
C(48)	8676(1)	1376(1)	2797(1)	27(1)
O(3)	7172(1)	4348(1)	632(1)	44(1)
O(4)	-702(1)	3609(1)	149(1)	79(1)

Table 3. Bond lengths [Å] and angles [°] for $[Co(NH_3)_5(NO_2)](BPh_4)_2.2H_2O$.

Co(1)-N(1)	1.9146(18)
Co(1)-N(6)	1.951(2)
Co(1)-N(4)	1.956(2)
Co(1)-N(3)	1.9608(18)
Co(1)-N(5)	1.9607(19)
Co(1)-N(2)	2.0135(19)
N(1)-O(1)	1.229(3)
N(1)-O(2)	1.236(3)
N(2)-H(1)	0.9100
N(2)-H(2)	0.9100
N(2)-H(3)	0.9100
N(3)-H(4)	0.9100
N(3)-H(5)	0.9100
N(3)-H(6)	0.9100
N(4)-H(7)	0.9100
N(4)-H(8)	0.9100
N(4)-H(9)	0.9100
N(5)-H(10)	0.9100
N(5)-H(11)	0.9100
N(5)-H(12)	0.9100
N(6)-H(13)	0.9100
N(6)-H(14)	0.9100
N(6)-H(15)	0.9100
B(1)-C(1)	1.636(3)
B(1)-C(13)	1.647(3)
B(1)-C(7)	1.649(3)
B(1)-C(19)	1.657(3)
C(1)-C(6)	1.402(3)
C(1)-C(2)	1.408(3)
C(2)-C(3)	1.390(3)
C(2)-H(16)	0.9500
C(3)-C(4)	1.389(4)
C(3)-H(17)	0.9500
C(4)-C(5)	1.374(4)
C(4)-H(18)	0.9500
C(5)-C(6)	1.392(3)
C(5)-H(19)	0.9500
C(6)-H(20)	0.9500
C(7)-C(12)	1.394(3)
C(7)-C(8)	1.413(3)
C(8)-C(9)	1.388(3)
C(8)-H(21)	0.9500
C(9)-C(10)	1.393(4)

C(9)-H(22)	0.9500
C(10)-C(11)	1.378(4)
C(10)-H(23)	0.9500
C(11)-C(12)	1.392(3)
C(11)-H(24)	0.9500
C(12)-H(25)	0.9500
C(13)-C(14)	1.401(3)
C(13)-C(18)	1.415(3)
C(14)-C(15)	1.400(3)
C(14)-H(26)	0.9500
C(15)-C(16)	1.376(4)
C(15)-H(27)	0.9500
C(16)-C(17)	1.397(4)
C(16)-H(28)	0.9500
C(17)-C(18)	1.390(3)
C(17)-H(29)	0.9500
C(18)-H(30)	0.9500
C(19)-C(20)	1.402(3)
C(19)-C(24)	1.405(3)
C(20)-C(21)	1.395(4)
C(20)-H(31)	0.9500
C(21)-C(22)	1.383(4)
C(21)-H(32)	0.9500
C(22)-C(23)	1.389(4)
C(22)-H(33)	0.9500
C(23)-C(24)	1.387(4)
C(23)-H(34)	0.9500
C(24)-H(35)	0.9500
B(2)-C(43)	1.642(3)
B(2)-C(31)	1.646(3)
B(2)-C(37)	1.644(3)
B(2)-C(25)	1.648(3)
C(25)-C(26)	1.404(3)
C(25)-C(30)	1.417(3)
C(26)-C(27)	1.400(4)
C(26)-H(36)	0.9500
C(27)-C(28)	1.385(4)
C(27)-H(37)	0.9500
C(28)-C(29)	1.381(4)
C(28)-H(38)	0.9500
C(29)-C(30)	1.386(3)
C(29)-H(39)	0.9500
C(30)-H(40)	0.9500
C(31)-C(36)	1.396(3)
C(31)-C(32)	1.414(3)
C(32)-C(33)	1.393(3)
C(32)-H(45)	0.9500
C(33)-C(34)	1.382(4)
C(33)-H(44)	0.9500
C(34)-C(35)	1.389(4)
C(34)-H(43)	0.9500
C(35)-C(36)	1.398(3)
C(35)-H(42)	0.9500
C(36)-H(41)	0.9500
C(37)-C(38)	1.401(3)
C(37)-C(42)	1.406(3)
C(38)-C(39)	1.399(3)
C(38)-H(46)	0.9500
C(39)-C(40)	1.378(4)
C(39)-H(47)	0.9500
C(40)-C(41)	1.383(4)
C(40)-H(48)	0.9500

C(41)-C(42)	1.404(3)
C(41)-H(49)	0.9500
C(42)-H(50)	0.9500
C(43)-C(48)	1.388(3)
C(43)-C(44)	1.413(3)
C(44)-C(45)	1.377(4)
C(44)-H(51)	0.9500
C(45)-C(46)	1.395(5)
C(45)-H(52)	0.9500
C(46)-C(47)	1.371(4)
C(46)-H(53)	0.9500
C(47)-C(48)	1.402(3)
C(47)-H(54)	0.9500
C(48)-H(55)	0.9500

N(1)-Co(1)-N(6)	89.93(10)
N(1)-Co(1)-N(4)	88.40(10)
N(6)-Co(1)-N(4)	178.20(10)
N(1)-Co(1)-N(3)	89.17(8)
N(6)-Co(1)-N(3)	91.27(9)
N(4)-Co(1)-N(3)	89.38(9)
N(1)-Co(1)-N(5)	88.18(8)
N(6)-Co(1)-N(5)	88.51(9)
N(4)-Co(1)-N(5)	90.76(8)
N(3)-Co(1)-N(5)	177.34(9)
N(1)-Co(1)-N(2)	179.11(10)
N(6)-Co(1)-N(2)	90.94(10)
N(4)-Co(1)-N(2)	90.73(10)
N(3)-Co(1)-N(2)	90.64(9)
N(5)-Co(1)-N(2)	92.02(9)
O(1)-N(1)-O(2)	121.1(2)
O(1)-N(1)-Co(1)	118.99(18)
O(2)-N(1)-Co(1)	119.87(16)
Co(1)-N(2)-H(1)	109.5
Co(1)-N(2)-H(2)	109.5
H(1)-N(2)-H(2)	109.5
Co(1)-N(2)-H(3)	109.5
H(1)-N(2)-H(3)	109.5
H(2)-N(2)-H(3)	109.5
Co(1)-N(3)-H(4)	109.5
Co(1)-N(3)-H(5)	109.5
H(4)-N(3)-H(5)	109.5
Co(1)-N(3)-H(6)	109.5
H(4)-N(3)-H(6)	109.5
H(5)-N(3)-H(6)	109.5
Co(1)-N(4)-H(7)	109.5
Co(1)-N(4)-H(8)	109.5
H(7)-N(4)-H(8)	109.5
Co(1)-N(4)-H(9)	109.5
H(7)-N(4)-H(9)	109.5
H(8)-N(4)-H(9)	109.5
Co(1)-N(5)-H(10)	109.5
Co(1)-N(5)-H(11)	109.5
H(10)-N(5)-H(11)	109.5
Co(1)-N(5)-H(12)	109.5
H(10)-N(5)-H(12)	109.5
H(11)-N(5)-H(12)	109.5
Co(1)-N(6)-H(13)	109.5
Co(1)-N(6)-H(14)	109.5
H(13)-N(6)-H(14)	109.5
Co(1)-N(6)-H(15)	109.5
H(13)-N(6)-H(15)	109.5

H(14)-N(6)-H(15)	109.5
C(1)-B(1)-C(13)	113.52(17)
C(1)-B(1)-C(7)	109.49(16)
C(13)-B(1)-C(7)	104.20(16)
C(1)-B(1)-C(19)	108.42(16)
C(13)-B(1)-C(19)	111.26(16)
C(7)-B(1)-C(19)	109.88(17)
C(6)-C(1)-C(2)	114.5(2)
C(6)-C(1)-B(1)	126.1(2)
C(2)-C(1)-B(1)	119.18(19)
C(3)-C(2)-C(1)	123.4(2)
C(3)-C(2)-H(16)	118.3
C(1)-C(2)-H(16)	118.3
C(4)-C(3)-C(2)	119.5(2)
C(4)-C(3)-H(17)	120.2
C(2)-C(3)-H(17)	120.2
C(5)-C(4)-C(3)	119.2(2)
C(5)-C(4)-H(18)	120.4
C(3)-C(4)-H(18)	120.4
C(4)-C(5)-C(6)	120.4(2)
C(4)-C(5)-H(19)	119.8
C(6)-C(5)-H(19)	119.8
C(5)-C(6)-C(1)	122.9(2)
C(5)-C(6)-H(20)	118.6
C(1)-C(6)-H(20)	118.6
C(12)-C(7)-C(8)	115.1(2)
C(12)-C(7)-B(1)	124.68(18)
C(8)-C(7)-B(1)	120.17(18)
C(9)-C(8)-C(7)	123.0(2)
C(9)-C(8)-H(21)	118.5
C(7)-C(8)-H(21)	118.5
C(8)-C(9)-C(10)	119.5(2)
C(8)-C(9)-H(22)	120.3
C(10)-C(9)-H(22)	120.3
C(11)-C(10)-C(9)	119.2(2)
C(11)-C(10)-H(23)	120.4
C(9)-C(10)-H(23)	120.4
C(10)-C(11)-C(12)	120.5(2)
C(10)-C(11)-H(24)	119.7
C(12)-C(11)-H(24)	119.7
C(11)-C(12)-C(7)	122.6(2)
C(11)-C(12)-H(25)	118.7
C(7)-C(12)-H(25)	118.7
C(14)-C(13)-C(18)	115.0(2)
C(14)-C(13)-B(1)	123.37(19)
C(18)-C(13)-B(1)	120.85(19)
C(15)-C(14)-C(13)	122.5(2)
C(15)-C(14)-H(26)	118.7
C(13)-C(14)-H(26)	118.7
C(16)-C(15)-C(14)	120.6(3)
C(16)-C(15)-H(27)	119.7
C(14)-C(15)-H(27)	119.7
C(15)-C(16)-C(17)	119.0(2)
C(15)-C(16)-H(28)	120.5
C(17)-C(16)-H(28)	120.5
C(18)-C(17)-C(16)	119.8(2)
C(18)-C(17)-H(29)	120.1
C(16)-C(17)-H(29)	120.1
C(17)-C(18)-C(13)	123.0(2)
C(17)-C(18)-H(30)	118.5
C(13)-C(18)-H(30)	118.5
C(20)-C(19)-C(24)	114.9(2)

C(20)-C(19)-B(1)	123.68(19)
C(24)-C(19)-B(1)	121.41(19)
C(21)-C(20)-C(19)	122.8(2)
C(21)-C(20)-H(31)	118.6
C(19)-C(20)-H(31)	118.6
C(22)-C(21)-C(20)	120.5(3)
C(22)-C(21)-H(32)	119.8
C(20)-C(21)-H(32)	119.8
C(23)-C(22)-C(21)	118.3(2)
C(23)-C(22)-H(33)	120.8
C(21)-C(22)-H(33)	120.8
C(22)-C(23)-C(24)	120.6(2)
C(22)-C(23)-H(34)	119.7
C(24)-C(23)-H(34)	119.7
C(23)-C(24)-C(19)	122.8(2)
C(23)-C(24)-H(35)	118.6
C(19)-C(24)-H(35)	118.6
C(43)-B(2)-C(31)	110.54(17)
C(43)-B(2)-C(37)	112.20(17)
C(31)-B(2)-C(37)	105.65(16)
C(43)-B(2)-C(25)	105.06(17)
C(31)-B(2)-C(25)	112.86(17)
C(37)-B(2)-C(25)	110.70(16)
C(26)-C(25)-C(30)	114.8(2)
C(26)-C(25)-B(2)	125.80(19)
C(30)-C(25)-B(2)	119.29(19)
C(27)-C(26)-C(25)	122.3(2)
C(27)-C(26)-H(36)	118.8
C(25)-C(26)-H(36)	118.8
C(28)-C(27)-C(26)	120.7(2)
C(28)-C(27)-H(37)	119.6
C(26)-C(27)-H(37)	119.6
C(29)-C(28)-C(27)	118.6(2)
C(29)-C(28)-H(38)	120.7
C(27)-C(28)-H(38)	120.7
C(28)-C(29)-C(30)	120.7(2)
C(28)-C(29)-H(39)	119.7
C(30)-C(29)-H(39)	119.7
C(29)-C(30)-C(25)	122.8(2)
C(29)-C(30)-H(40)	118.6
C(25)-C(30)-H(40)	118.6
C(36)-C(31)-C(32)	115.3(2)
C(36)-C(31)-B(2)	122.9(2)
C(32)-C(31)-B(2)	121.74(19)
C(33)-C(32)-C(31)	122.3(2)
C(33)-C(32)-H(45)	118.9
C(31)-C(32)-H(45)	118.9
C(34)-C(33)-C(32)	120.6(2)
C(34)-C(33)-H(44)	119.7
C(32)-C(33)-H(44)	119.7
C(33)-C(34)-C(35)	118.8(2)
C(33)-C(34)-H(43)	120.6
C(35)-C(34)-H(43)	120.6
C(34)-C(35)-C(36)	120.1(2)
C(34)-C(35)-H(42)	120.0
C(36)-C(35)-H(42)	120.0
C(35)-C(36)-C(31)	122.8(2)
C(35)-C(36)-H(41)	118.6
C(31)-C(36)-H(41)	118.6
C(38)-C(37)-C(42)	115.15(19)
C(38)-C(37)-B(2)	122.00(18)
C(42)-C(37)-B(2)	122.71(19)

C(39)-C(38)-C(37)	123.0(2)
C(39)-C(38)-H(46)	118.5
C(37)-C(38)-H(46)	118.5
C(40)-C(39)-C(38)	120.1(2)
C(40)-C(39)-H(47)	120.0
C(38)-C(39)-H(47)	120.0
C(39)-C(40)-C(41)	119.1(2)
C(39)-C(40)-H(48)	120.4
C(41)-C(40)-H(48)	120.4
C(40)-C(41)-C(42)	120.3(2)
C(40)-C(41)-H(49)	119.9
C(42)-C(41)-H(49)	119.9
C(41)-C(42)-C(37)	122.3(2)
C(41)-C(42)-H(50)	118.8
C(37)-C(42)-H(50)	118.8
C(48)-C(43)-C(44)	115.4(2)
C(48)-C(43)-B(2)	123.99(18)
C(44)-C(43)-B(2)	120.4(2)
C(45)-C(44)-C(43)	122.7(3)
C(45)-C(44)-H(51)	118.6
C(43)-C(44)-H(51)	118.6
C(44)-C(45)-C(46)	119.8(3)
C(44)-C(45)-H(52)	120.1
C(46)-C(45)-H(52)	120.1
C(47)-C(46)-C(45)	119.4(2)
C(47)-C(46)-H(53)	120.3
C(45)-C(46)-H(53)	120.3
C(46)-C(47)-C(48)	119.9(3)
C(46)-C(47)-H(54)	120.0
C(48)-C(47)-H(54)	120.0
C(43)-C(48)-C(47)	122.69(19)
C(43)-C(48)-H(55)	118.7
C(47)-C(48)-H(55)	118.7

Symmetry transformations used to generate equivalent atoms:

Table 4. Anisotropic displacement parameters (A^2 x 10^3) for $[Co(NH_3)_5(NO_2)](BPh_4)_2.2H_2O$.
The anisotropic displacement factor exponent takes the form: -2 pi^2 [h^2 a*^2 U11 + ... + 2 h k a* b* U12]

	U11	U22	U33	U23	U13	U12
Co(1)	20(1)	18(1)	23(1)	1(1)	-2(1)	0(1)
N(1)	25(1)	33(1)	33(1)	7(1)	0(1)	2(1)
O(1)	29(1)	62(2)	49(1)	8(1)	-4(1)	-10(1)
O(2)	41(1)	69(2)	49(1)	-13(1)	9(1)	5(1)
N(2)	27(1)	37(1)	38(1)	4(1)	3(1)	5(1)
N(3)	28(1)	30(1)	30(1)	10(1)	-4(1)	0(1)
N(4)	45(1)	26(1)	27(1)	-1(1)	-5(1)	-2(1)
N(5)	29(1)	27(1)	26(1)	1(1)	-4(1)	0(1)
N(6)	38(1)	23(1)	39(1)	-3(1)	-1(1)	-5(1)
B(1)	18(1)	22(1)	21(1)	-2(1)	2(1)	-2(1)
C(1)	21(1)	22(1)	22(1)	-5(1)	-2(1)	-3(1)
C(2)	26(1)	34(1)	41(1)	7(1)	5(1)	-2(1)
C(3)	28(1)	48(2)	48(2)	8(1)	13(1)	-6(1)
C(4)	22(1)	53(2)	58(2)	-5(1)	8(1)	-3(1)
C(5)	28(1)	55(2)	42(2)	1(1)	-2(1)	12(1)
C(6)	29(1)	35(1)	29(1)	-1(1)	0(1)	4(1)
C(7)	21(1)	19(1)	25(1)	0(1)	-3(1)	3(1)

C(8)	22(1)	27(1)	30(1)	-3(1)	1(1)	0(1)
C(9)	25(1)	27(1)	43(1)	0(1)	-8(1)	-2(1)
C(10)	37(1)	24(1)	33(1)	-5(1)	-17(1)	2(1)
C(11)	32(1)	32(1)	24(1)	-4(1)	-5(1)	8(1)
C(12)	22(1)	29(1)	26(1)	-1(1)	-1(1)	5(1)
C(13)	23(1)	24(1)	21(1)	-2(1)	-1(1)	-5(1)
C(14)	29(1)	31(1)	24(1)	0(1)	4(1)	-2(1)
C(15)	33(1)	52(2)	25(1)	4(1)	7(1)	-5(1)
C(16)	34(1)	46(2)	31(1)	12(1)	-1(1)	-12(1)
C(17)	43(1)	28(1)	32(1)	6(1)	-8(1)	-7(1)
C(18)	33(1)	23(1)	29(1)	-2(1)	-2(1)	-1(1)
C(19)	25(1)	23(1)	21(1)	-1(1)	4(1)	0(1)
C(20)	22(1)	29(1)	37(1)	4(1)	0(1)	1(1)
C(21)	28(1)	36(1)	57(2)	12(1)	1(1)	8(1)
C(22)	42(1)	24(1)	56(2)	7(1)	16(1)	9(1)
C(23)	64(2)	20(1)	36(1)	-2(1)	13(1)	-4(1)
C(24)	40(1)	28(1)	26(1)	1(1)	-1(1)	-4(1)
B(2)	22(1)	22(1)	20(1)	2(1)	2(1)	1(1)
C(25)	25(1)	19(1)	23(1)	1(1)	2(1)	-1(1)
C(26)	41(1)	24(1)	29(1)	-2(1)	-3(1)	4(1)
C(27)	57(2)	31(1)	30(1)	-1(1)	-16(1)	-4(1)
C(28)	32(1)	36(1)	42(1)	11(1)	-14(1)	-7(1)
C(29)	27(1)	36(1)	33(1)	9(1)	2(1)	4(1)
C(30)	26(1)	28(1)	25(1)	2(1)	1(1)	0(1)
C(31)	27(1)	22(1)	20(1)	1(1)	3(1)	3(1)
C(32)	31(1)	23(1)	29(1)	2(1)	-1(1)	1(1)
C(33)	45(1)	21(1)	31(1)	-3(1)	-2(1)	2(1)
C(34)	48(1)	30(1)	28(1)	-3(1)	4(1)	13(1)
C(35)	29(1)	36(1)	33(1)	0(1)	6(1)	9(1)
C(36)	28(1)	28(1)	24(1)	-1(1)	1(1)	3(1)
C(37)	20(1)	16(1)	23(1)	-1(1)	3(1)	3(1)
C(38)	26(1)	21(1)	27(1)	2(1)	-1(1)	0(1)
C(39)	37(1)	26(1)	28(1)	0(1)	-6(1)	3(1)
C(40)	42(1)	28(1)	25(1)	5(1)	5(1)	10(1)
C(41)	29(1)	24(1)	34(1)	6(1)	8(1)	3(1)
C(42)	23(1)	19(1)	30(1)	0(1)	1(1)	0(1)
C(43)	19(1)	23(1)	27(1)	5(1)	-1(1)	1(1)
C(44)	31(1)	35(1)	31(1)	8(1)	5(1)	2(1)
C(45)	35(1)	50(2)	46(2)	24(1)	4(1)	-4(1)
C(46)	42(1)	37(1)	64(2)	25(1)	-19(1)	-18(1)
C(47)	45(1)	22(1)	47(2)	6(1)	-21(1)	-5(1)
C(48)	29(1)	22(1)	30(1)	2(1)	-6(1)	1(1)

7.3.6 Crystal Data for Bath 241 - $[Ru(NH_3)_4(SO_2)(H_2O)]_2[(OC_7H_4SO_3)_4].C_2H_5OH.3H_2O$

Table 1. Crystal data and structure refinement for $[Ru(NH_3)_4(SO_2)(H_2O)]_2[(OC_7H_4SO_3)_4].C_2H_5OH.3H_2O$.

Identification code	Bath 24 - $[Ru(NH_3)_4(SO_2)(H_2O)]_2[(OC_7H_4SO_3)_4].C_2H_5OH.3H_2O$	
Empirical formula	$C_{30}\ H_{56}\ N_8\ O_{26}\ Ru_2\ S_6$	
Formula weight	1339.33	
Temperature	150(2) K	
Wavelength	0.71073Å	
Crystal system, space group	Tetragonal, I-4	
Unit cell dimensions	a = 28.029Å	alpha = 90°
	b = 28.029Å	beta = 90°
	c = 13.663Å	gamma = 90°
Volume	10734.0Å^3	
Z, Calculated density	8, 1.658 Mg/m^3	
Absorption coefficient	0.883 mm^{-1}	
F(000)	5472	

Crystal size	0.30 x 0.05 x 0.05 mm
Theta range for data collection	2.30 to 31.70°
Limiting indices	-41<=h<=41, -40<=k<=39, -20<=l<=20
Reflections collected / unique	62795 / 17369 [R(int) = 0.0848]
Completeness to theta = 31.70	98.0 %
Absorption correction	SADABS
Max. and min. transmission	1.0000 and 0.7775
Refinement method	Full-matrix least-squares on F^2
Data / restraints / parameters	17369 / 0 / 672
Goodness-of-fit on F^2	1.002
Final R indices [I>2sigma(I)]	R1 = 0.0608, wR2 = 0.1685
R indices (all data)	R1 = 0.0730, wR2 = 0.1780
Absolute structure parameter	0.04(3)
Largest diff. peak and hole	1.931 and -1.445 e.$Å^{-3}$

Table 2. Atomic coordinates (x 10^4) and equivalent isotropic displacement parameters (A^2 x 10^3) for $[Ru(NH_3)_4(SO_2)(H_2O)]_2[(OC_7H_4SO_3)_4].C_2H_5OH.3H_2O$.
U(eq) is defined as one third of the trace of the orthogonalized Uij tensor.

	x	y	z	U(eq)
Ru(1)	6614(1)	7268(1)	10389(1)	52(1)
S(1)	6187(1)	7870(1)	10247(1)	52(1)
O(1)	5863(2)	7906(2)	9412(3)	72(1)
O(2)	6225(2)	8282(2)	10837(4)	72(1)
O(3)	7056(2)	6668(2)	10520(5)	86(2)
N(1)	6046(2)	6789(3)	10215(7)	98(3)
N(2)	6540(2)	7269(2)	11935(4)	58(1)
N(3)	7256(2)	7640(3)	10646(6)	79(2)
N(4)	6734(2)	7233(3)	8848(4)	71(2)
Ru(2)	6366(1)	5905(1)	5423(1)	43(1)
S(2)	5644(1)	5743(1)	5526(2)	59(1)
O(4)	5331(2)	5780(2)	4689(6)	85(2)
O(5)	5414(2)	5611(2)	6398(5)	80(2)
O(6)	7101(1)	6039(2)	5337(3)	51(1)
N(5)	6386(2)	6123(2)	6909(3)	49(1)
N(6)	6236(2)	6605(2)	4880(4)	56(1)
N(7)	6402(2)	5677(2)	3946(4)	62(1)
N(8)	6595(2)	5224(2)	5909(4)	50(1)
C(1)	9399(2)	5777(2)	7656(3)	34(1)
C(2)	8916(2)	5788(1)	8154(3)	31(1)
C(3)	8560(2)	6066(2)	7762(3)	33(1)
C(4)	8118(2)	6101(2)	8227(3)	32(1)
S(3)	7690(1)	6490(1)	7731(1)	34(1)
O(7)	7663(2)	6393(1)	6685(2)	46(1)
O(8)	7856(1)	6973(1)	7920(3)	43(1)
O(9)	7237(1)	6385(1)	8209(3)	44(1)
C(5)	8031(1)	5856(1)	9097(3)	31(1)
C(6)	8386(2)	5568(1)	9504(3)	32(1)
C(7)	8826(1)	5541(1)	9023(3)	32(1)
O(10)	9176(1)	5257(1)	9435(3)	39(1)
C(8)	8283(1)	5308(2)	10462(3)	35(1)
C(9)	8357(2)	5632(2)	11330(3)	34(1)
C(10)	7972(2)	5874(2)	11746(3)	39(1)
C(11)	8052(2)	6197(2)	12497(3)	41(1)
S(4)	7578(1)	6539(1)	13006(1)	52(1)
O(11)	7648(3)	7023(3)	12617(6)	70(2)
O(12)	7616(2)	6489(3)	14015(4)	60(2)
O(13)	7129(2)	6350(3)	12575(6)	73(2)

O(11')	7269(5)	6199(5)	13544(11)	63(4)
O(13')	7789(5)	6859(6)	13837(11)	64(4)
O(12')	7409(5)	6802(5)	12276(10)	54(3)
C(12)	8499(2)	6275(2)	12854(3)	39(1)
C(13)	8890(2)	6036(2)	12473(3)	34(1)
C(14)	8814(2)	5717(2)	11699(3)	34(1)
O(14)	9199(1)	5474(1)	11334(2)	37(1)
C(15)	9392(2)	6143(2)	12833(3)	35(1)
C(16)	9641(1)	6510(2)	12201(3)	33(1)
C(17)	9535(2)	6991(2)	12332(3)	38(1)
C(18)	9757(2)	7331(2)	11766(3)	38(1)
S(5)	9617(1)	7941(1)	11948(1)	47(1)
O(15)	9673(2)	8176(1)	11013(3)	54(1)
O(16)	9972(2)	8116(2)	12651(4)	66(1)
O(17)	9136(2)	7956(2)	12332(5)	78(2)
C(19)	10093(2)	7204(2)	11070(3)	35(1)
C(20)	10200(1)	6724(2)	10902(3)	32(1)
C(21)	9965(1)	6382(1)	11479(3)	32(1)
O(18)	10060(1)	5906(1)	11281(2)	36(1)
C(22)	10524(2)	6586(2)	10063(3)	34(1)
C(23)	10244(1)	6586(2)	9112(3)	33(1)
C(24)	10207(2)	7005(2)	8562(3)	34(1)
C(25)	9927(2)	7013(2)	7729(3)	37(1)
S(6)	9850(1)	7570(1)	7132(1)	40(1)
O(19)	9461(2)	7806(2)	7663(4)	58(1)
O(20)	10293(1)	7835(1)	7222(3)	43(1)
O(21)	9715(2)	7465(2)	6129(3)	56(1)
C(26)	9684(1)	6622(2)	7427(3)	35(1)
C(27)	9702(2)	6202(2)	7965(3)	34(1)
C(28)	9978(1)	6193(2)	8793(3)	32(1)
O(22)	10002(1)	5768(1)	9336(2)	37(1)
O(23)	8914(3)	6959(3)	9772(6)	106(2)
C(29)	8442(3)	7112(3)	10253(5)	63(2)
C(30)	8178(2)	7447(2)	9657(4)	38(1)
O(24)	4954(3)	6936(3)	9672(6)	106(2)
O(25)	6739(2)	5903(2)	9594(5)	85(2)
O(26)	5824(5)	6305(4)	2574(12)	205(7)

Table 3. Bond lengths [Å] and angles [°] for $[Ru(NH_3)_4(SO_2)(H_2O)]_2[(OC_7H_4SO_3)_4].C_2H_5OH.3H_2O$.

Ru(1)-S(1)	2.0778(15)
Ru(1)-O(3)	2.096(5)
Ru(1)-N(1)	2.097(7)
Ru(1)-N(3)	2.109(6)
Ru(1)-N(2)	2.122(6)
Ru(1)-N(4)	2.135(6)
S(1)-O(2)	1.412(6)
S(1)-O(1)	1.461(5)
N(1)-H(1)	0.9100
N(1)-H(2)	0.9100
N(1)-H(3)	0.9100
N(2)-H(4)	0.9100
N(2)-H(5)	0.9100
N(2)-H(6)	0.9100
N(3)-H(7)	0.9100
N(3)-H(8)	0.9100
N(3)-H(9)	0.9100
N(4)-H(11)	0.9100
N(4)-H(10)	0.9100
N(4)-H(12)	0.9100

Ru(2)-S(2)	2.0809(15)
Ru(2)-O(6)	2.097(4)
Ru(2)-N(8)	2.119(4)
Ru(2)-N(7)	2.119(6)
Ru(2)-N(5)	2.121(5)
Ru(2)-N(6)	2.129(5)
S(2)-O(5)	1.403(7)
S(2)-O(4)	1.444(6)
N(5)-H(13)	0.9100
N(5)-H(14)	0.9100
N(5)-H(15)	0.9100
N(6)-H(16)	0.9100
N(6)-H(17)	0.9100
N(6)-H(18)	0.9100
N(7)-H(19)	0.9100
N(7)-H(20)	0.9100
N(7)-H(21)	0.9100
N(8)-H(22)	0.9100
N(8)-H(23)	0.9100
N(8)-H(24)	0.9100
C(1)-C(2)	1.517(6)
C(1)-C(27)	1.521(6)
C(1)-H(25)	0.9900
C(1)-H(26)	0.9900
C(2)-C(3)	1.374(6)
C(2)-C(7)	1.397(6)
C(3)-C(4)	1.396(6)
C(3)-H(27)	0.9500
C(4)-C(5)	1.396(6)
C(4)-S(3)	1.757(4)
S(3)-O(8)	1.455(4)
S(3)-O(7)	1.456(3)
S(3)-O(9)	1.459(4)
C(5)-C(6)	1.396(5)
C(5)-H(28)	0.9500
C(6)-C(7)	1.398(6)
C(6)-C(8)	1.527(6)
C(7)-O(10)	1.385(5)
C(8)-C(9)	1.508(6)
C(8)-H(29)	0.9900
C(8)-H(30)	0.9900
C(9)-C(10)	1.394(6)
C(9)-C(14)	1.397(6)
C(10)-C(11)	1.387(8)
C(10)-H(31)	0.9500
C(11)-C(12)	1.362(7)
C(11)-S(4)	1.781(5)
S(4)-O(12')	1.329(14)
S(4)-O(12)	1.390(6)
S(4)-O(11)	1.470(8)
S(4)-O(11')	1.482(15)
S(4)-O(13)	1.487(7)
S(4)-O(13')	1.564(16)
C(12)-C(13)	1.385(6)
C(12)-H(32)	0.9500
C(13)-C(14)	1.401(6)
C(13)-C(15)	1.522(6)
C(14)-O(14)	1.370(5)
C(15)-C(16)	1.513(6)
C(15)-H(33)	0.9900
C(15)-H(34)	0.9900
C(16)-C(21)	1.388(6)

C(16)-C(17)	1.394(6)
C(17)-C(18)	1.377(7)
C(17)-H(35)	0.9500
C(18)-C(19)	1.385(6)
C(18)-S(5)	1.772(5)
S(5)-O(15)	1.446(4)
S(5)-O(17)	1.446(4)
S(5)-O(16)	1.466(5)
C(19)-C(20)	1.400(6)
C(19)-H(36)	0.9500
C(20)-C(21)	1.405(6)
C(20)-C(22)	1.512(6)
C(21)-O(18)	1.386(5)
C(22)-C(23)	1.519(6)
C(22)-H(37)	0.9900
C(22)-H(38)	0.9900
C(23)-C(24)	1.398(6)
C(23)-C(28)	1.399(6)
C(24)-C(25)	1.384(6)
C(24)-H(39)	0.9500
C(25)-C(26)	1.354(6)
C(25)-S(6)	1.775(5)
S(6)-O(21)	1.453(4)
S(6)-O(20)	1.453(4)
S(6)-O(19)	1.465(4)
C(26)-C(27)	1.389(6)
C(26)-H(40)	0.9500
C(27)-C(28)	1.371(6)
C(28)-O(22)	1.405(5)
O(23)-C(29)	1.539(10)
O(23)-H(41)	0.8400
C(29)-C(30)	1.446(8)
C(29)-H(42)	0.9900
C(29)-H(43)	0.9900
C(30)-H(44)	0.9800
C(30)-H(45)	0.9800
C(30)-H(46)	0.9800

S(1)-Ru(1)-O(3)	178.9(2)
S(1)-Ru(1)-N(1)	94.1(2)
O(3)-Ru(1)-N(1)	86.8(3)
S(1)-Ru(1)-N(3)	96.1(2)
O(3)-Ru(1)-N(3)	83.0(3)
N(1)-Ru(1)-N(3)	169.5(3)
S(1)-Ru(1)-N(2)	92.02(15)
O(3)-Ru(1)-N(2)	88.5(2)
N(1)-Ru(1)-N(2)	92.2(3)
N(3)-Ru(1)-N(2)	85.2(3)
S(1)-Ru(1)-N(4)	92.06(17)
O(3)-Ru(1)-N(4)	87.4(2)
N(1)-Ru(1)-N(4)	88.8(3)
N(3)-Ru(1)-N(4)	93.0(3)
N(2)-Ru(1)-N(4)	175.7(2)
O(2)-S(1)-O(1)	115.8(3)
O(2)-S(1)-Ru(1)	124.5(2)
O(1)-S(1)-Ru(1)	119.2(2)
Ru(1)-N(1)-H(1)	109.5
Ru(1)-N(1)-H(2)	109.5
H(1)-N(1)-H(2)	109.5
Ru(1)-N(1)-H(3)	109.5
H(1)-N(1)-H(3)	109.5
H(2)-N(1)-H(3)	109.5

Ru(1)-N(2)-H(4)	109.5
Ru(1)-N(2)-H(5)	109.5
H(4)-N(2)-H(5)	109.5
Ru(1)-N(2)-H(6)	109.5
H(4)-N(2)-H(6)	109.5
H(5)-N(2)-H(6)	109.5
Ru(1)-N(3)-H(7)	109.5
Ru(1)-N(3)-H(8)	109.5
H(7)-N(3)-H(8)	109.5
Ru(1)-N(3)-H(9)	109.5
H(7)-N(3)-H(9)	109.5
H(8)-N(3)-H(9)	109.5
Ru(1)-N(4)-H(11)	109.5
Ru(1)-N(4)-H(10)	109.5
H(11)-N(4)-H(10)	109.5
Ru(1)-N(4)-H(12)	109.5
H(11)-N(4)-H(12)	109.5
H(10)-N(4)-H(12)	109.5
S(2)-Ru(2)-O(6)	177.64(13)
S(2)-Ru(2)-N(8)	94.42(14)
O(6)-Ru(2)-N(8)	83.22(18)
S(2)-Ru(2)-N(7)	92.55(17)
O(6)-Ru(2)-N(7)	87.4(2)
N(8)-Ru(2)-N(7)	90.7(2)
S(2)-Ru(2)-N(5)	91.32(14)
O(6)-Ru(2)-N(5)	88.66(17)
N(8)-Ru(2)-N(5)	87.3(2)
N(7)-Ru(2)-N(5)	175.75(19)
S(2)-Ru(2)-N(6)	93.34(16)
O(6)-Ru(2)-N(6)	89.02(19)
N(8)-Ru(2)-N(6)	172.1(2)
N(7)-Ru(2)-N(6)	87.4(2)
N(5)-Ru(2)-N(6)	94.2(2)
O(5)-S(2)-O(4)	114.4(4)
O(5)-S(2)-Ru(2)	124.2(3)
O(4)-S(2)-Ru(2)	121.4(3)
Ru(2)-N(5)-H(13)	109.5
Ru(2)-N(5)-H(14)	109.5
H(13)-N(5)-H(14)	109.5
Ru(2)-N(5)-H(15)	109.5
H(13)-N(5)-H(15)	109.5
H(14)-N(5)-H(15)	109.5
Ru(2)-N(6)-H(16)	109.5
Ru(2)-N(6)-H(17)	109.5
H(16)-N(6)-H(17)	109.5
Ru(2)-N(6)-H(18)	109.5
H(16)-N(6)-H(18)	109.5
H(17)-N(6)-H(18)	109.5
Ru(2)-N(7)-H(19)	109.5
Ru(2)-N(7)-H(20)	109.5
H(19)-N(7)-H(20)	109.5
Ru(2)-N(7)-H(21)	109.5
H(19)-N(7)-H(21)	109.5
H(20)-N(7)-H(21)	109.5
Ru(2)-N(8)-H(22)	109.5
Ru(2)-N(8)-H(23)	109.5
H(22)-N(8)-H(23)	109.5
Ru(2)-N(8)-H(24)	109.5
H(22)-N(8)-H(24)	109.5
H(23)-N(8)-H(24)	109.5
C(2)-C(1)-C(27)	110.9(3)
C(2)-C(1)-H(25)	109.5

C(27)-C(1)-H(25)	109.5
C(2)-C(1)-H(26)	109.5
C(27)-C(1)-H(26)	109.5
H(25)-C(1)-H(26)	108.1
C(3)-C(2)-C(7)	118.7(4)
C(3)-C(2)-C(1)	119.0(4)
C(7)-C(2)-C(1)	122.2(4)
C(2)-C(3)-C(4)	120.4(4)
C(2)-C(3)-H(27)	119.8
C(4)-C(3)-H(27)	119.8
C(5)-C(4)-C(3)	120.6(4)
C(5)-C(4)-S(3)	121.0(3)
C(3)-C(4)-S(3)	118.3(3)
O(8)-S(3)-O(7)	111.4(2)
O(8)-S(3)-O(9)	112.7(2)
O(7)-S(3)-O(9)	110.9(2)
O(8)-S(3)-C(4)	106.9(2)
O(7)-S(3)-C(4)	107.4(2)
O(9)-S(3)-C(4)	107.3(2)
C(4)-C(5)-C(6)	119.9(4)
C(4)-C(5)-H(28)	120.0
C(6)-C(5)-H(28)	120.0
C(5)-C(6)-C(7)	118.2(4)
C(5)-C(6)-C(8)	118.8(4)
C(7)-C(6)-C(8)	123.0(4)
O(10)-C(7)-C(2)	120.2(4)
O(10)-C(7)-C(6)	117.7(4)
C(2)-C(7)-C(6)	122.2(4)
C(9)-C(8)-C(6)	111.1(3)
C(9)-C(8)-H(29)	109.4
C(6)-C(8)-H(29)	109.4
C(9)-C(8)-H(30)	109.4
C(6)-C(8)-H(30)	109.4
H(29)-C(8)-H(30)	108.0
C(10)-C(9)-C(14)	118.6(4)
C(10)-C(9)-C(8)	120.5(4)
C(14)-C(9)-C(8)	120.8(4)
C(11)-C(10)-C(9)	119.6(4)
C(11)-C(10)-H(31)	120.2
C(9)-C(10)-H(31)	120.2
C(12)-C(11)-C(10)	121.3(4)
C(12)-C(11)-S(4)	117.5(4)
C(10)-C(11)-S(4)	121.2(4)
O(12')-S(4)-O(12)	145.8(7)
O(12')-S(4)-O(11)	42.5(6)
O(12)-S(4)-O(11)	116.1(5)
O(12')-S(4)-O(11')	121.5(9)
O(12)-S(4)-O(11')	59.3(7)
O(11)-S(4)-O(11')	148.3(7)
O(12')-S(4)-O(13)	66.3(7)
O(12)-S(4)-O(13)	115.0(5)
O(11)-S(4)-O(13)	107.3(5)
O(11')-S(4)-O(13)	58.3(7)
O(12')-S(4)-O(13')	111.2(8)
O(12)-S(4)-O(13')	46.2(6)
O(11)-S(4)-O(13')	71.4(7)
O(11')-S(4)-O(13')	103.3(8)
O(13)-S(4)-O(13')	144.3(6)
O(12')-S(4)-C(11)	105.8(6)
O(12)-S(4)-C(11)	106.0(3)
O(11)-S(4)-C(11)	104.8(3)
O(11')-S(4)-C(11)	106.5(6)

O(13)-S(4)-C(11)	106.7(3)
O(13')-S(4)-C(11)	108.0(6)
C(11)-C(12)-C(13)	120.9(4)
C(11)-C(12)-H(32)	119.5
C(13)-C(12)-H(32)	119.5
C(12)-C(13)-C(14)	118.2(4)
C(12)-C(13)-C(15)	121.0(4)
C(14)-C(13)-C(15)	120.7(4)
O(14)-C(14)-C(9)	120.4(4)
O(14)-C(14)-C(13)	118.2(4)
C(9)-C(14)-C(13)	121.3(4)
C(16)-C(15)-C(13)	112.0(3)
C(16)-C(15)-H(33)	109.2
C(13)-C(15)-H(33)	109.2
C(16)-C(15)-H(34)	109.2
C(13)-C(15)-H(34)	109.2
H(33)-C(15)-H(34)	107.9
C(21)-C(16)-C(17)	118.7(4)
C(21)-C(16)-C(15)	122.1(4)
C(17)-C(16)-C(15)	119.2(4)
C(18)-C(17)-C(16)	120.1(4)
C(18)-C(17)-H(35)	120.0
C(16)-C(17)-H(35)	120.0
C(17)-C(18)-C(19)	121.1(4)
C(17)-C(18)-S(5)	119.2(4)
C(19)-C(18)-S(5)	119.7(4)
O(15)-S(5)-O(17)	114.1(3)
O(15)-S(5)-O(16)	110.7(3)
O(17)-S(5)-O(16)	112.7(4)
O(15)-S(5)-C(18)	106.9(2)
O(17)-S(5)-C(18)	106.5(2)
O(16)-S(5)-C(18)	105.3(3)
C(18)-C(19)-C(20)	120.3(4)
C(18)-C(19)-H(36)	119.8
C(20)-C(19)-H(36)	119.8
C(19)-C(20)-C(21)	117.6(4)
C(19)-C(20)-C(22)	119.8(4)
C(21)-C(20)-C(22)	122.3(4)
O(18)-C(21)-C(16)	120.8(4)
O(18)-C(21)-C(20)	117.1(4)
C(16)-C(21)-C(20)	122.1(4)
C(20)-C(22)-C(23)	109.7(3)
C(20)-C(22)-H(37)	109.7
C(23)-C(22)-H(37)	109.7
C(20)-C(22)-H(38)	109.7
C(23)-C(22)-H(38)	109.7
H(37)-C(22)-H(38)	108.2
C(24)-C(23)-C(28)	117.0(4)
C(24)-C(23)-C(22)	119.8(4)
C(28)-C(23)-C(22)	122.9(4)
C(25)-C(24)-C(23)	119.9(4)
C(25)-C(24)-H(39)	120.1
C(23)-C(24)-H(39)	120.1
C(26)-C(25)-C(24)	121.4(4)
C(26)-C(25)-S(6)	120.8(3)
C(24)-C(25)-S(6)	117.5(3)
O(21)-S(6)-O(20)	113.9(3)
O(21)-S(6)-O(19)	111.4(3)
O(20)-S(6)-O(19)	111.4(2)
O(21)-S(6)-C(25)	106.6(2)
O(20)-S(6)-C(25)	107.8(2)
O(19)-S(6)-C(25)	105.1(2)

C(25)-C(26)-C(27)	120.6(4)
C(25)-C(26)-H(40)	119.7
C(27)-C(26)-H(40)	119.7
C(28)-C(27)-C(26)	118.1(4)
C(28)-C(27)-C(1)	122.0(4)
C(26)-C(27)-C(1)	119.9(4)
C(27)-C(28)-C(23)	123.0(4)
C(27)-C(28)-O(22)	118.6(4)
C(23)-C(28)-O(22)	118.5(4)
C(29)-O(23)-H(41)	109.5
C(30)-C(29)-O(23)	112.4(6)
C(30)-C(29)-H(42)	109.1
O(23)-C(29)-H(42)	109.1
C(30)-C(29)-H(43)	109.1
O(23)-C(29)-H(43)	109.1
H(42)-C(29)-H(43)	107.9
C(29)-C(30)-H(44)	109.5
C(29)-C(30)-H(45)	109.5
H(44)-C(30)-H(45)	109.5
C(29)-C(30)-H(46)	109.5
H(44)-C(30)-H(46)	109.5
H(45)-C(30)-H(46)	109.5

Symmetry transformations used to generate equivalent atoms:

Table 4. Anisotropic displacement parameters (A^2 x 10^3) for $[Ru(NH_3)_4(SO_2)(H_2O)]_2[(OC_7H_4SO_3)_4].C_2H_5OH.3H_2O$.
The anisotropic displacement factor exponent takes the form:
-2 pi^2 [h^2 a*^2 U11 + ... + 2 h k a* b* U12]

	U11	U22	U33	U23	U13	U12
Ru(1)	38(1)	60(1)	58(1)	-19(1)	-5(1)	13(1)
S(1)	47(1)	66(1)	43(1)	-2(1)	4(1)	12(1)
O(1)	82(3)	99(4)	37(2)	5(2)	5(2)	36(3)
O(2)	60(3)	84(3)	73(3)	-14(3)	10(2)	12(2)
O(3)	64(3)	90(4)	102(4)	-39(3)	-29(3)	40(3)
N(1)	45(3)	128(6)	121(6)	-59(5)	-7(3)	-2(3)
N(2)	55(3)	64(3)	56(3)	-10(2)	-13(2)	7(2)
N(3)	57(3)	81(4)	100(5)	-53(4)	15(3)	-9(3)
N(4)	57(3)	94(4)	61(3)	-29(3)	-1(2)	28(3)
Ru(2)	38(1)	39(1)	52(1)	-8(1)	-9(1)	3(1)
S(2)	39(1)	47(1)	92(1)	-12(1)	-13(1)	5(1)
O(4)	58(3)	61(3)	136(5)	-12(3)	-46(3)	10(2)
O(5)	50(2)	77(3)	113(5)	-18(3)	8(3)	-12(2)
O(6)	42(2)	61(2)	51(2)	-10(2)	-3(2)	0(2)
N(5)	43(2)	53(2)	52(2)	-5(2)	-2(2)	3(2)
N(6)	60(3)	47(2)	61(3)	2(2)	-1(2)	5(2)
N(7)	56(3)	62(3)	69(3)	-22(2)	-21(2)	20(2)
N(8)	43(2)	45(2)	61(3)	-3(2)	-9(2)	3(2)
C(1)	32(2)	36(2)	35(2)	-10(2)	2(1)	-1(1)
C(2)	36(2)	29(2)	27(2)	-7(1)	-2(1)	-5(1)
C(3)	35(2)	36(2)	29(2)	-1(1)	-2(1)	-4(1)
C(4)	37(2)	33(2)	26(2)	-3(1)	-4(1)	0(1)
S(3)	37(1)	33(1)	33(1)	2(1)	-6(1)	3(1)
O(7)	61(2)	46(2)	32(2)	2(1)	-13(1)	7(2)
O(8)	52(2)	34(2)	44(2)	0(1)	-5(1)	4(1)
O(9)	35(2)	43(2)	53(2)	7(1)	-3(1)	4(1)
C(5)	31(2)	30(2)	33(2)	1(1)	-5(1)	-1(1)

C(6)	36(2)	30(2)	31(2)	3(1)	-7(1)	-1(1)
C(7)	32(2)	30(2)	35(2)	-3(1)	-5(1)	-2(1)
O(10)	34(1)	40(2)	44(2)	2(1)	-3(1)	7(1)
C(8)	30(2)	34(2)	42(2)	6(2)	-1(2)	-4(1)
C(9)	35(2)	33(2)	33(2)	10(1)	0(1)	2(1)
C(10)	30(2)	52(3)	37(2)	16(2)	-1(2)	2(2)
C(11)	35(2)	50(2)	37(2)	16(2)	5(2)	8(2)
S(4)	44(1)	68(1)	45(1)	3(1)	5(1)	17(1)
O(11)	69(5)	57(4)	83(5)	8(4)	6(4)	23(3)
O(12)	54(3)	90(5)	35(3)	-1(3)	3(2)	11(3)
O(13)	29(3)	108(6)	81(5)	-24(4)	-10(3)	22(3)
C(12)	46(2)	40(2)	29(2)	6(2)	2(2)	6(2)
C(13)	34(2)	39(2)	28(2)	7(1)	-4(1)	2(2)
C(14)	34(2)	32(2)	36(2)	11(1)	-2(1)	2(1)
O(14)	32(1)	40(2)	40(2)	6(1)	-1(1)	2(1)
C(15)	36(2)	40(2)	29(2)	6(1)	-2(1)	3(2)
C(16)	32(2)	42(2)	24(2)	4(1)	-2(1)	-1(1)
C(17)	34(2)	44(2)	36(2)	-1(2)	-4(2)	1(2)
C(18)	34(2)	42(2)	37(2)	-3(2)	-2(2)	-2(2)
S(5)	47(1)	37(1)	59(1)	-2(1)	12(1)	-1(1)
O(15)	52(2)	43(2)	66(2)	9(2)	8(2)	5(2)
O(16)	81(3)	50(2)	66(3)	-13(2)	2(2)	-15(2)
O(17)	56(2)	42(2)	136(5)	5(2)	48(3)	7(2)
C(19)	33(2)	36(2)	35(2)	0(2)	-1(1)	-5(1)
C(20)	29(2)	39(2)	29(2)	-2(1)	-5(1)	-2(1)
C(21)	32(2)	32(2)	31(2)	1(1)	-7(1)	0(1)
O(18)	35(1)	34(1)	38(2)	-1(1)	-5(1)	4(1)
C(22)	27(2)	41(2)	35(2)	0(2)	-3(1)	-1(2)
C(23)	29(2)	40(2)	31(2)	-1(1)	-1(1)	-4(1)
C(24)	30(2)	37(2)	36(2)	-1(2)	-2(1)	-1(1)
C(25)	35(2)	44(2)	32(2)	0(2)	0(2)	1(2)
S(6)	39(1)	40(1)	42(1)	2(1)	-5(1)	-2(1)
O(19)	52(2)	48(2)	72(3)	2(2)	11(2)	5(2)
O(20)	43(2)	44(2)	42(2)	6(1)	0(1)	-3(1)
O(21)	75(3)	49(2)	44(2)	2(2)	-18(2)	-3(2)
C(26)	29(2)	44(2)	33(2)	-6(2)	-1(1)	0(2)
C(27)	31(2)	43(2)	29(2)	-8(1)	0(1)	-1(2)
C(28)	29(2)	36(2)	29(2)	-5(1)	2(1)	0(1)
O(22)	38(2)	36(2)	37(2)	1(1)	-1(1)	5(1)
O(23)	77(4)	119(6)	123(6)	-36(5)	-14(4)	11(4)
C(29)	70(4)	61(3)	57(3)	-2(3)	3(3)	3(3)
C(30)	31(2)	42(2)	41(2)	-12(2)	3(2)	0(2)
O(24)	106(5)	114(5)	100(5)	-19(4)	-13(4)	-28(4)
O(25)	92(4)	83(4)	79(3)	17(3)	19(3)	6(3)
O(26)	254(14)	97(6)	265(15)	27(8)	-56(12)	102(8)

Table 5. Hydrogen bonds for $[Ru(NH_3)_4(SO_2)(H_2O)]_2[(OC_7H_4SO_3)_4].C_2H_5OH.3H_2O$ [Å and °].

D-H...A	d(D-H)	d(H...A)	d(D...A)	<(DHA)
N(1)-H(3)...O(24)	0.91	2.37	3.178(10)	147.1
N(2)-H(4)...O(8)#1	0.91	2.15	3.030(6)	162.1
N(2)-H(5)...O(13)	0.91	2.28	3.182(10)	170.5
N(2)-H(6)...O(19)#1	0.91	2.08	2.986(7)	171.5
N(4)-H(11)...O(17)#2	0.91	2.36	3.244(8)	162.9
N(4)-H(10)...O(9)	0.91	2.00	2.898(7)	168.3
N(4)-H(12)...O(11)#2	0.91	2.34	3.190(12)	155.8
N(5)-H(13)...O(17)#2	0.91	2.12	3.024(7)	170.2
N(5)-H(14)...O(9)	0.91	2.24	3.063(6)	150.9
N(7)-H(19)...O(15)#3	0.91	2.16	3.053(7)	165.6

N(7)-H(20)...O(13)#4	0.91	2.45	3.350(12)	169.5
N(7)-H(21)...O(26)	0.91	2.34	3.040(12)	133.7
N(8)-H(22)...O(20)#3	0.91	2.30	3.019(6)	135.9
N(8)-H(23)...O(15)#3	0.91	2.23	3.114(7)	164.0

Symmetry transformations used to generate equivalent atoms:
#1 -x+3/2,-y+3/2,z+1/2 #2 -x+3/2,-y+3/2,z-1/2
#3 -y+3/2,x-1/2,-z+3/2 #4 x,y,z-1

7.4 Crystallographic Information Files

Please see the attached compact disc for the final crystallographic information files of the structures reported in this thesis.

7.5 Published Papers

Please see the attached compact disc for the pdf file of the paper published during the course of this thesis.